The effect of herbicides as novel antimalarial drugs on the transcriptome and proteome of *Plasmodium falciparum*

by

Janette Snyman

Submitted in the partial fulfilment of the requirements for the degree
Magister Scientiae

In the Faculty of Natural and Agricultural Sciences
Department of Biochemistry
University of Pretoria
Pretoria 0002
South Africa

SUPERVISOR: Prof. Lyn-Marie Birkholtz
Department of Biochemistry, University of Pretoria, South Africa
CO-SUPERVISOR: Prof. Abraham I Louw
Department of Biochemistry, University of Pretoria, South Africa

2011

I, ... declare that the thesis/dissertation, which I hereby submit for the degree .....at the University of Pretoria, is my own work and has not previously been submitted by me for the degree at this or any other tertiary institution.

SIGNATURE:.....

DATE:.....

PLAGIARISM DECLARATION

Full names of student:..……..

Student number:……

Declaration

1. I understand what plagiarism is and am aware of the University's policy in this regard.

2. I declare that this …… (eg essay, report, project, assignment, dissertation, thesis, etc) is my own original work. Where other people's work has been used (either from a printed source, Internet or any other source), this has been properly acknowledged and referenced in accordance with departmental requirements.

3. I have not used work previously produced by another student or any other person to hand in as my own.

4. I have not allowed, and will not allow, anyone to copy my work with the intention of passing it off as his or her own work.

SIGNATURE STUDENT:.....……....

DATE:.....…….....

ACKNOWLEDGEMENTS

I extend my sincere thanks to my supervisor, Prof Lyn-Marie Birkholtz for her guidance through what has proved to be a fascinating, intellectually stimulating, and challenging project. Thanks to her for being a continuous source of ideas, her inspiration and her patience during this study.

I would like to thank Prof Braam Louw for his insight and input.

I am thankful to Dr Eric Maréchal for hosting me in France, Grenoble, the donation of the compounds tested in this study, his insights, advice and encouragement.

I am forever grateful to Dr Salome Smit for her advice, time, guidance and patience.

I would like to thank Jeff Verlinden for his assistance and design of the Agilent slides.

Thanks must also go to all the members of the Malaria research groups, both past and present.

I am indebted to Sandra van Wyngaardt, for her help and advice, technical and otherwise support.

My deepest thanks to the Lord, for blessing me with this opportunity to learn and grow. Also for His guidance and the strength He gave me every day to complete this study.

I would like to thank the funding bodies (NRF, University of Pretoria post-graduate bursary, SAFeTI and MRC) for the bursaries and funds that enabled me to do this MSc.

Finally, the deepest thanks must go to my mother for her constant love and encouragement, to the rest of my family for believing in me and to Richard, for his patience, love and support throughout my studies.

SUMMARY

The Apicomplexan parasite, *P. falciparum*, is one of the causative agents of the morbidity and mortality in sub-Saharan Africa, especially children under 5 years of age and pregnant women (1). The parasite harbours a non-photosynthetic plastid believed to have been acquired from blue-green algae (2, 3). The presence of this apicoplast in the parasite and its connection to plants opens many doors for to the development of novel antimalarials not harmful to the human host.

In this study, a herbicide-derived compound (A51B1C1_1) with structural similarities to 1,2-diacylglycerol (DAG) was tested against *P. falciparum*. It was anticipated that this herbicide would target similar pathways of the malaria parasite as was shown for *Arabidopsis.* One such pathway is the synthesis of the glycerolipids. Monogalactosyldiacylglycerol (MGDG) and digalactosyldiacylglycerol (DGDG) are the two most studied galactolipids. MGDG is synthesised by MGDG synthase and DGDG is synthesised by DGDG synthase from DAG.

Morphological studies after inhibition of *P. falciparum* parasites with A51B1C1_1 confirmed that the compound does have an effect on the parasites. The determined IC_{50} value, the drug-like properties conforming to Lipinski's rule of five and the specificity of the compound towards the parasite makes A51B1C1_1 a possible antimalarial compound. Transcriptomic data of A51B1C1_1 *P. falciparum* treated parasites revealed 1504 differentially affected transcripts, of which 579 transcripts were unique to this treatment. The differentially affected processes included apicoplast-associated metabolic pathways such as glycerolipid and glycerophospholipid metabolism. These results thus indicated that enzymes involved in glycerolipid synthesis, especially those responsible for the metabolism of DAG, are affected in *P. falciparum* parasites treated with A51B1C1_1.

Proteome analysis indicated that similar processes as shown for the transcriptomic data were affected by the herbicide treatment. At the assay time-point, a total of 276 Plasmodial proteins were uniquely expressed in the A51B1C1_1 treated sample whereas 204 Plasmodial proteins were uniquely expressed in the control sample. Interestingly, the direction of the change in the abundance of these affected proteins did

not necessarily correlate with the change of abundance observed in the transcriptomic data, as seen numerous times before in other reported Plasmodial perturbations.

Global functional genomics aid in the confirmation that compound A51B1C1_1 does affect glycerolipid and glycerophospholipid metabolism in *P. falciparum* as seen in *Arabidopsis* after treatment with the parent compound Galvestine-1. Overall, this study demonstrated the importance of functional genomics in the investigation for potential antimalarial compounds and contributed in the progress of A51B1C1_1 from an early hit to an early lead in the antimalarial drug discovery pipeline.

TABLE OF CONTENT

APPENDICES

LIST OF FIGURES

LIST OF TABLES

LIST OF BOXES

LIST OF EQUATIONS

LIST OF ABBREVIATIONS

2-D	Two-dimensional
2-DE	Two-dimensional gel electrophoresis
ACP	Acyl carrier protein
AIDS	Acquired immune deficiency syndrome
AMA-1	Apical merozoite antigen 1
AOS	ArrayOligoSelecto
BSA	Bovine Serum Albumin
CHAPS	3-[(3-cholamidopropyl) dimethylammonio]-1-propane sulphonate
CoA	Coenzyme A
CSP	Circum sporozoite protein
CV	Coefficient of variation
Da	Daltons
DAG	1,2-diacylglycerol
DDT	Dichloro-diphenyl-trichloroethane
DGD	DGDG synthase
DGDG	Digalactosyldiacylglycerol
DHFR	Dihydrofolate reductase
DHPS	Dihydropteroate synthase
DNA	Deoxyribonucleic acid
DXP	1-deoxy-D-xylulose-5-phosphate
EDTA	Ethylenediamine tetra-acetic acid
EtOH	Ethanol
FabB	β-ketoacyl-ACP synthases I
FabD	Malonyl-CoA:Acyl carrier protein transacylase
FabF	β-ketoacyl-ACP synthase II
FabG	β-oxoacyl-ACP reductase
FabH	β-oxoacyl-ACP synthase III
FabI	Enoyl-ACP reductase
FabZ	β-hydroxyacyl-ACP dehydratase
FC	Fold change
GEO	Gene Expression Omnibus
GO	Gene ontology
HBsAG	Hepatitis B antigen
HIV	Human immunodeficiency virus
hpi	Hours post invasion
h	Hour/s
IC_{50}	Median Inhibitory concentration
IDC	Intra-erythrocytic developmental cycle
IEM	Inner envelope membranes
ITN	Insecticide-treated bed nets
KASIII	β-ketoacyl-ACP synthases III

Kb	Kilobase pair
LDH	Lactate dehydrogenase
LIMMA	Linear Models for Microarray
LSU	Large subunit of ribosome
Mb	Megabase pair
MeOH	Methanol
MGD	MGDG synthase
MGDG	Monogalactosyldiacylglycerol
MIAME	Minimum information about a microarray experiment
min	Minute
MMV	Medicine for Malaria Venture
ms	Milliseconds
MSP-1	Merozoite surface protein
NS	Not sensitive
nt	Nucleotide
OEM	Outer envelope membrane
OMS	Outermost membrane system
PAGE	Polyacrylamide gel electrophoresis
PBS	Phosphate-buffered saline
Pf	*Plasmodium falciparum*
PG	Phosphatidylglycerol
Pr	Prokaryote
PYR	Pyrimethamine
qRT-PCR	Quantitative Real Time Polymerase Chain Reaction
RIN	RNA integrity number
RNA	Ribonucleic acid
rpm	Revolutions per minute
RQI	RNA Quality Indicator
rRNA	Ribosomal RNA
s	Seconds
sp	Specie
SDX	Sulphadoxine
SL	Sulphoquinovosyldiacylglycerol
SSU	Small unit of ribosome
TAG	Triacylglycerol
tetraGDG	Tetra-galactosyldiacylglycerol
Tg	*Toxoplasma gondii*
TLC	Thin layer chromatography
triGDG	Tri-galactosyldiacylglycerol
tRNA	Transfer RNA
Tm	Melting temperature
v/v	Volume per volume
w/v	Weight per volume

CHAPTER 1
INTRODUCTION
LITERATURE REVIEW

'In this, O Nature, yield I pray to me.
I pace and pace, and think and think, and take
The fever'd hands, and note down all I see,
That some distant light may haply break.
The painful faces ask, can we not cure?
We answer, No, not yet; we seek the laws.
O God, revel thro' all this thing obscure
The unseen, small, but million-murdering cause.'
Ronald Ross, 1895

1.1 History of malaria

Malaria, one of the oldest diseases known to mankind, is caused by a protozoal parasite belonging to the *Plasmodium* genus. Initial symptoms of the disease include fever, headaches, diarrhoea, shivers, backaches and vomiting (4). In Egypt, malaria antigens were found in mummies that can be dated back to 3200 BC and notes describing malaria-like symptoms were documented in the Ebers Papyrus (5). In China, evidence of the malaria parasite was found in *Nei Ching* (6), but in 2700 BC the 'disease' was said to be caused by an imbalance of yin and yang because of a lack of knowledge and the strong belief in natural forces (7). Later, the disease was described by Hippocrates, thus proving that Europeans were infected by the parasite around 400 BC. The disease was originally called Roman fever, because infections were found mainly in the Roman Republic's swampy area. A connection between the symptoms of the disease and a source from the environment led to the renaming of the disease to '*mal – aria'* which is the Italian word for 'bad air' (7). The name refers to the warm, humid environment of the parasite's vector, the female *Anopheles* mosquito. The relationship between the parasite and the vector was demonstrated in 1897 by Ronald Ross who was awarded a Noble Prize for this discovery in 1902 (8). Charles Louis Alphonse Laveran, who discovered living, crescent shaped objects in the blood of an Algerian soldier in 1880,

named these parasites *Oscillaria malariae* and received the Nobel Prize in 1906 for his discovery (8). However, the name of the organism was never accepted as *Oscillaria malariae,* because Italian scientists made the same discovery around the same time and named the parasite *Plasmodium malariae.*

1.2 The health and economical risk of malaria

Malaria is currently one of the most lethal diseases, killing almost 800 000 people each year (1). More than half of these mortalities are children in Africa, where 20% of all deaths in children are caused by the parasite. More than 50% of the world's population in 108 countries are at risk of contracting malaria. Children under the age of five, non-immune and semi-immune pregnant women, people living with Human immunodeficiency virus and Acquired immune deficiency syndrome (HIV and AIDS) in sub-Saharan Africa and travellers from non-endemic regions are the most susceptible to malaria. Malaria, caused by *P. falciparum,* is found in Asia, the northern parts of South America and the Middle East as indicated in Figure 1.1 (1).

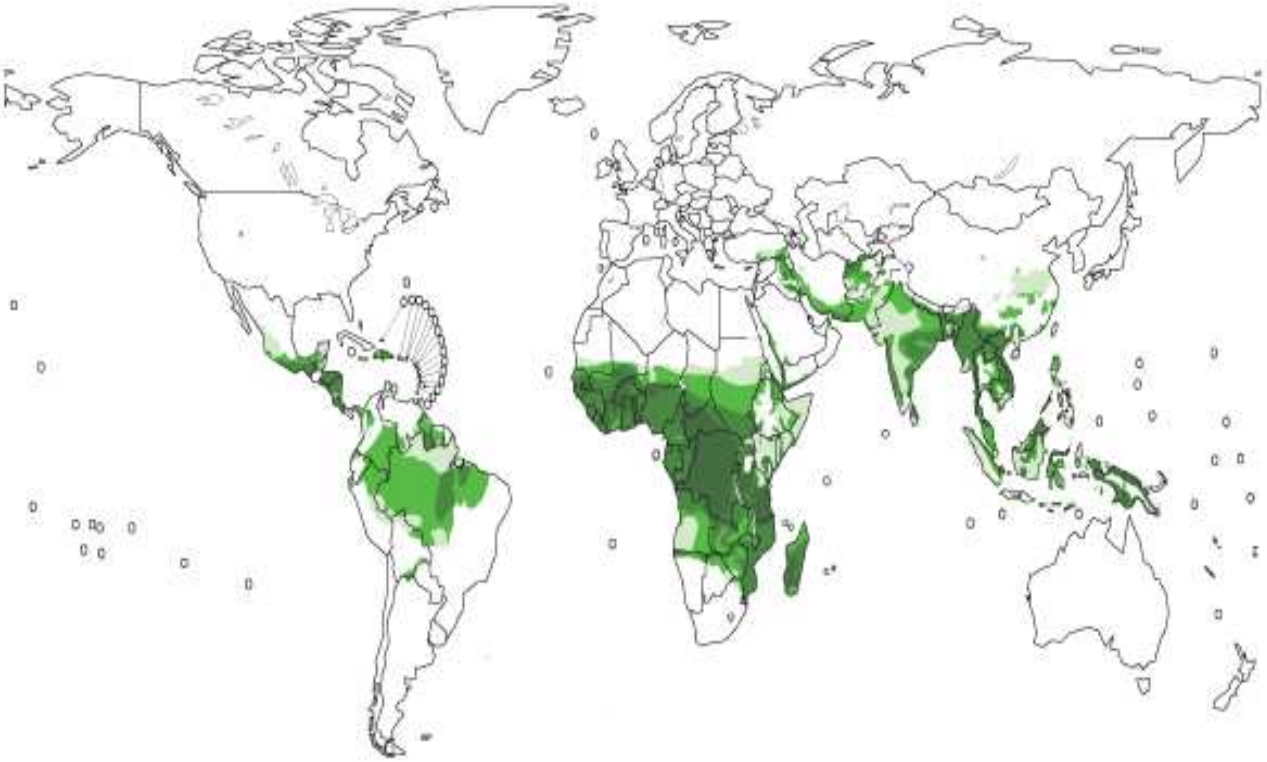

Figure 1.1 Global distributions of *P. falciparum* malaria affected areas (1).
The dark green areas represent endemic locations of malaria. The decrease in intensity of colour indicates a decrease in the number of malaria cases by the reported period (2010).

Each year, almost 250 million people are diagnosed with this life threatening disease, which puts a huge strain on the economies of the countries largest at risk. Malaria

drains the economies of poor countries in Africa annually by decreasing the gross domestic product by 1.3% and using 40% of the public health care funds. Up to 60% of patients visiting clinics and travel clinics in the endemic areas are diagnosed with malaria (1, 9, 10). Burdening factors include increasing parasite drug resistance and insecticide resistance, increase in the number of HIV and AIDS patients contracting malaria and increase in population numbers.

1.3 Etiologic agents of malaria

Five species of the malaria parasites can infect humans; *P. vivax, P. malariae*, *P. ovale, P. knowlesi* and *P. falciparum,* the latter of which is the most lethal (11). The genus *Plasmodium* belongs to the kingdom Protista, the phylum Apicomplexa, the class Hematozoa and the order Haemosporidia (12). These five species belong to a larger group of about 200 *Plasmodium* species that can infect various other hosts such as rodents, birds and even reptiles (13).

Plasmodium parasites are transmitted to humans through the bite of an infected female *Anopheles* mosquito, the invertebrate vector. The parasites undergo sexual reproduction within the insect vector and asexual duplication within the human host (Figure 1.2) (14). *P. falciparum* sporozoites are transmitted through the saliva of the mosquito into the human bloodstream where they circulate until they reach the liver and invade hepatocytes (15). The parasites mature into schizonts and rupture hepatocytes to release up to 30 000 merozoites into the bloodstream that subsequently infect erythrocytes. At this stage, humans become symptomatic of malaria (10 to 15 days after the primary infection). Within the erythrocytes, the parasite will mature from ring stages into metabolically active trophozoites. These then asexually replicate into multi-nucleated schizonts resulting in the release of up to 36 daughter merozoites into the bloodstream to infect new erythrocytes.

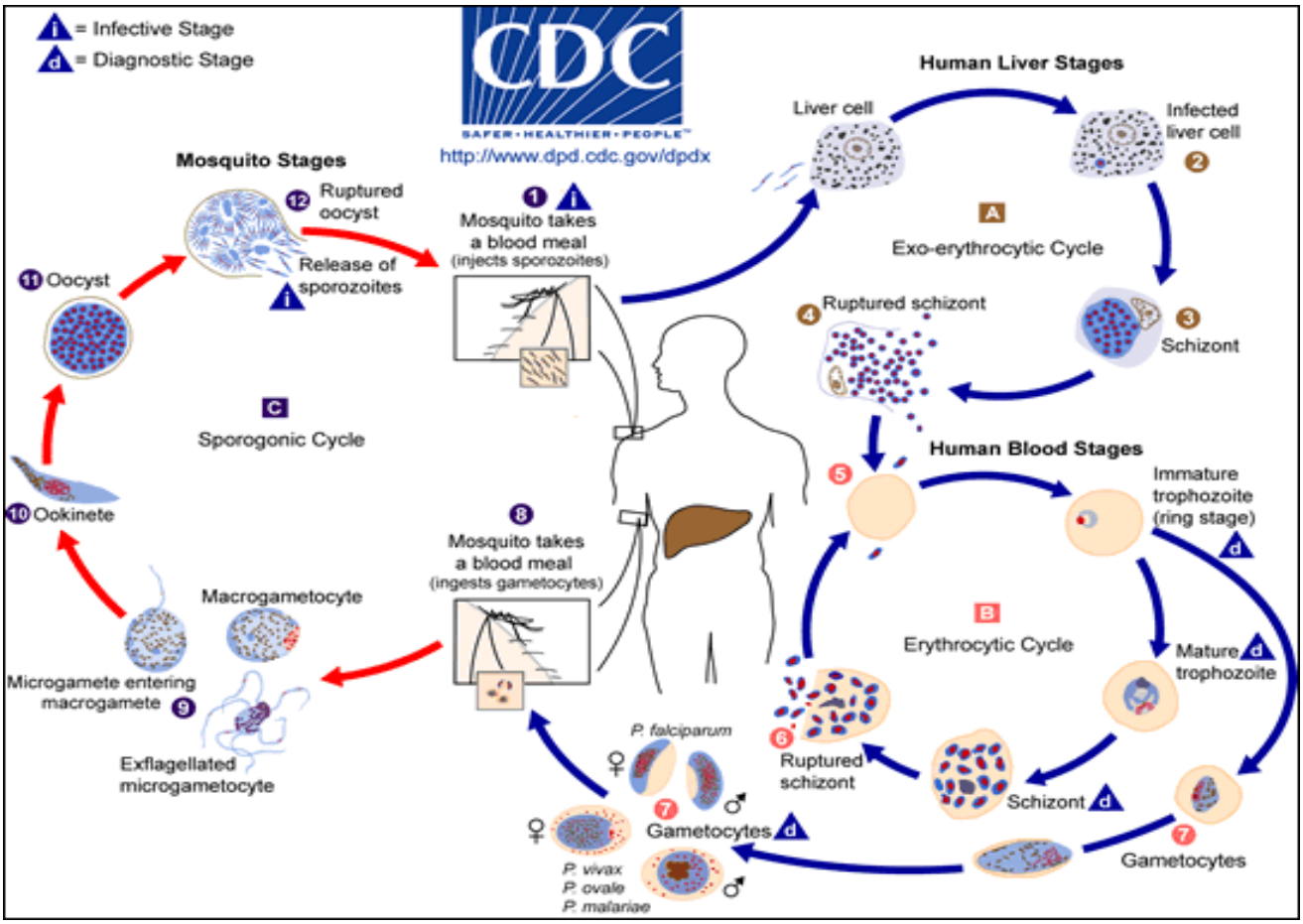

Figure 1.2 The life cycle of the *P. falciparum* malaria parasite.

Anopheles mosquito bites the host (1). The *P. falciparum* sporozoites (from the salivary glands of the mosquito) enter the body and start to circulate within the bloodstream until they reach the liver (2) (15). Inside the liver they mature (3) and merozoites (4) are released from the liver to infect healthy and mature erythrocytes (5). At this stage the human will start to feel symptoms of malaria (2 weeks after the primary infection). The ring form of the parasite will mature into trophozoites and later into schizonts. When erythrocytes burs open, new daughter merozoites will be released into the bloodstream. These merozoites can continue in the asexual cycle by once again infecting erythrocytes. A portion of the asexual parasites will form gametocytes (7) which will be taken up by the next mosquito taking a blood meal from the infected host (8). Inside the midgut of the vector, the gametes will be released from the erythrocytes and will await fertilization (9); after which the ookinetes (10) will penetrate through the wall of the mosquito's stomach, develop into oocysts (11) and then give rise to sporozoites (12). These sporozoites are again injected into the human host's bloodstream during a blood meal and the cycle is repeated (1).

Rupture of the erythrocytes is characterised by cyclical bouts of fever in the human host (every 48 h in the case of *P. falciparum*). A portion of the asexual parasites will develop into sexual macrogametocytes, which are taken up by the next mosquito taking a blood meal from the infected host. Inside the midgut of the vector the macrogametocytes differentiate into gametes (either male or female) and fuse to form an ookinete. The ookinetes penetrate the wall of the mosquito's stomach and develop into oocysts that grow, rupture and release sporozoites. These sporozoites make their way to the

salivary glands from where they are injected into the human host's bloodstream during the mosquito's next blood meal and the cycle is repeated (16).

1.4 Malaria Control

Malaria is a complex disease that links parasite with mosquito, mosquito with human host and human with parasite. Each of these stages should be investigated and targeted to control malaria to eradicate this disease (17).

1.4.1 Vector control

Control of *Anopheles gambiae* mosquitoes can only be achieved if physical numbers of the mosquitoes are decreased, the parasite is eradicated from within the mosquito or if the vector and the human host can be separated permanently (17). Vector control was provided with new opportunities for target discovery with the availability of the complete genome sequence of *A. gambiae* (18). Particularly interesting is the ability to generate genetically modified female mosquitoes that are either fully non-compliant to the parasite (19), or of which genetic modifications are lethal to the mosquito, and thus prevent progeny formation (20). The first insecticide that was used against the vector was dichloro-diphenyl-trichloroethane (DDT). This insecticide was used for indoor spraying of houses and proved successful. However, in the 1970s, DDT was banned because of arguments about the safety of the insecticide to humans (21). This ban was recently lifted and the use of DDT was re-introduced at least in South Africa, due to the occurrence of pyrethroid-resistant (but DDT sensitive) *A. funestus* as major vector in this country (22). An alternative to DDT is the use of insecticide treated bed nets (ITN), which showed reductions in the overall child mortality and cases of malaria in children during the first two years of use (23). Unfortunately, the use of ITNs does have limitations. Firstly, the nets require regular treatment, which has proven difficult because of the large number of nets being utilised. This problem was overcome with the development of long-lasting insecticidal nets that retain the insecticide in the fibres of the net for longer periods (1). The second limitation is the development of pyrethroid resistance as the preferred insecticide used on the ITNs. In addition, large doses of pyrethroids have been shown to have an effect on the nervous system, therefore alternative insecticides are being investigated (24-26). The only way to eliminate the parasite through the eradication of the vector is currently considered to be through obtaining a detailed behavioural knowledge of the vector (27).

1.4.2 Vaccines

The preferable vaccine for the elimination of *P. falciparum* parasites would provide protection to the human host against all stages of the parasite's life cycle, but this has not yet been achieved. Several stages of the parasite's life cycle have been targeted for the development of vaccines. These include the pre-erythrocytic stages (sporozoite invasion of hepatocytes, hepatocytic schizogony and merozoites invasion of erythrocytes) as well as the intra-erythrocytic asexual stages and the sexual stages (28). Most efforts have focused on the pre-erythrocytic stages as this will prevent the invasion of hepatocytes or the destruction of infected hepatocytes. If either is achieved, the patient will be saved from the symptoms of malaria. Desirable properties of the vaccine include ease of synthesis, low production costs, safety and tolerance in small children, pregnant women and immune-compromised people. The most advanced vaccine developed against pre-erythrocytic stage parasites is the RTS,S/AS02A vaccine. This vaccine targets the circum sporozoite protein (CSP) expressed on the surface of sporozoites and results in insufficient binding of the parasites to hepatocytes. The vaccine contains a hybrid of the *P. falciparum* CSP linked to hepatitis B antigen (HBsAG) (29) that is expressed in yeast. The vaccine also contains an adjuvant, AS02A (27). Unfortunately, no long-term protection has been achieved with RTS,S/AS202A. Vaccines that target the blood-stage of the parasite focus mainly on the invasion of the erythrocytes. These targets include merozoite surface protein 1 and apical merozoite antigen 1 (27).

1.4.3 Drugs and drug resistance

Treatment of malaria symptoms already started in the 15th century in Peru through the use of a bitter tasting component of the bark of *Cinchona ledgeriana*. Moreover, Qing Hao (*Artemisia annua*) has been used for more than 2000 years in China (8). Although antimalarials have mainly been used to control *P. falciparum* infections, the resistance this species has developed against most currently available drugs presents a major problem in the control of malaria (1). The antimalarials currently used can be divided into three groups: quinolines (quinine, chloroquine, mefloquine, and primaquine), antifolates [sulphadoxine (SDX) and pyrimethamine (PYR)] and artemisinin derivatives (Table 1.1). Combination therapies have also been used such as sulphadoxine-pyrimethamine (inhibits dihydropteroate synthase (DHPS) and dihydrofolate reductase (DHFR) in folate biosynthesis), atovaquone-proguanil (inhibits mitochondrial

metabolism), dapsone-proguanil (again targeting DHPS and DHFR) and artemether-lumefantrine (inhibits haem metabolism) (30-32).

Table 1.1 Antimalarial drugs currently available (32-34).

Type	Antimalarial	Metabolic pathway target	Restriction and resistance observed
Artemisinin derivatives	Dihydroartemisinin	ER and Membrane of food vacuole	Most effective treatment, costly
	Artemether		
	Arteether		
	Artesunate		
	Artemisinin		
Antifolate	Atovaquone	Membrane of food vacuole and mitochondria	May show resistance; costly
	Pyrimethamine	Cytoplasm	Shows extreme resistance
	Sulphadoxine		
	Proguanil		
Sulpha drugs (Sulphone)	Dapsone		
Quinolines	Quinine	Surface membrane of food vesicle and vacuole	Shows resistance and not safe to use
	Mefloquine	Food vacuole	Shows resistance, safety has not yet been determined and costly
	Halofantrine		Shows resistance, not safe to use and costly
	Piperaquine		
	Amodiaquine		Shows resistance and not safe to use by all
	Lumefantrine		May shows resistance and costly
	Chloroquine		Shows resistance

1.4.4 New antimalarial drug targets

The discovery of a new drug targets in the malaria parasite may overcome the problem of the development of resistance to existing drugs. Several biological processes in the parasite are being investigated to identify novel drug targets. Figure 1.3 demonstrates current antimalarial drug targets and potential new drug targets. The five main subcellular compartments targeted in the *P. falciparum* parasite is the cytosol, food vacuole, parasite membrane, mitochondria and apicoplast of the parasite (35).

Targets in the cytosol are difficult to determine because many of the pathways in this location are evolutionarily conserved and result in similarities between the host and the parasite (35). The most valuable pathway in the cytosol is the folate pathway but increasing resistance to the drugs inhibiting folate biosynthesis is decreasing the efficiency thereof (36, 37).

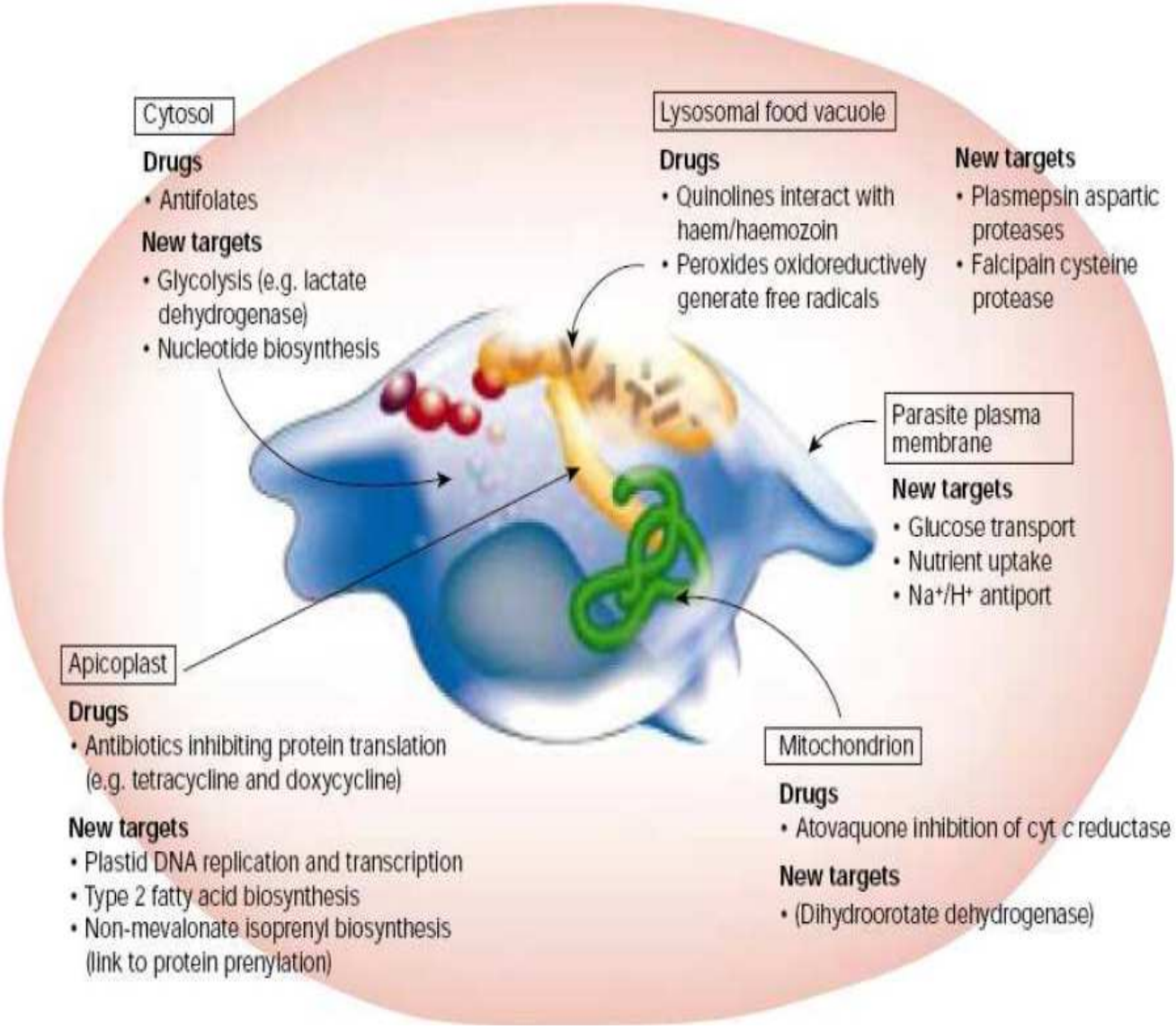

Figure 1.3 An illustration of the available drugs, their targets in the *P. falciparum* parasite and potential new drug targets (32).

The cytosol is the location in the parasite that hosts multiple metabolic pathways, of which the folate pathway, targeted by antifolates, is the most studied (35). New targets include glycolysis and nucleotide biosynthesis. The food vacuole is targeted by the Quinolines and possible new targets include plasmepsin, aspartic proteases and falcipain cysteine protease. Transporters in the parasite plasma membrane are currently investigated as new drug targets. The apicoplast and the mitochondria are also established targets and are targeted by antibiotics and Atovaquone, respectively.

The parasite membrane is the location for parasite-specific unique transporters, which are investigated as new targets for drug development. The choline transporter was identified as a possible target (38). Other transporters include the glucose transporter, different transporters involved in the movement of nutrients across the membrane and multiple ion transporters (35).

Atovaquone targets the mitochondria (Table 1.1) (34) by inhibiting ubiquinol–cytochrome c oxidoreductase (complex III) and results in the collapse of the

mitochondrial membrane potential (39). This is also used in combination with proguanil (an antifolate combination known as Malarone^{TM}) (40).

The food vacuole inside the *P. falciparum* parasite is a specialised proteolytic organelle in which erythrocyte haemoglobin is degraded (41). Large amounts haemoglobin are taken up from the surrounding erythrocytic cytosol and used rapidly (42). Proteases hydrolyse the α- and β-globin chains of the haemoglobin molecule in a complementary manner, resulting in the formation of potentially toxic haem and globin (35, 43, 44). The haem moieties are detoxified into a crystalline pigment known as the haemozoin and provide iron to the parasite during this process (44-46). The globin is broken down into free amino acids to be incorporated in the parasitic proteins (44). The 4-aminoquinoline chloroquine targets the formation of the haemozoin pigment resulting in free toxic haem, which is believed to disrupt the membrane of the vacuole. This non-enzymatic mechanism of action of chloroquine may be the reason for the efficacy of chloroquine (35). New targets currently investigated in the vacuole include the cysteine proteases, which demonstrated potential antimalarial activity when inhibited and the falcipain protease family (47).

Antibiotics show slow antimalarial activity at pharmacological concentrations. The targets and mode of action of these antibiotics differ between prokaryotes and eukaryotes, such as *P. falciparum*. In prokaryotes, tetracyclines, macrolides and lincosamides target the 70S subunit of the ribosome, rifampicin targets RNA polymerases and fluoroquinolones target DNA gyrases (48). In the eukaryotes, such as *P. falciparum*, these antibiotics may target different metabolic activities in a small organelle in the parasite, called the apicoplast (Table 1.2).

The apicoplast is a small plastid-like organelle found in the members of the phylum Apicomplexa. Plastids are colourless non-photosynthetic versions of chloroplast. Chloroplasts, found in plants, contain chlorophyll which is used in photosynthesis to provide the plant with nutrients essential for survival, such as fatty acids and haem. Pathways within the apicoplast may present potential new targets and this organelle is discussed in more detail below (2, 3).

Table 1.2 Drugs proposed to target metabolic activities in the apicoplast (49, 50).

Metabolic activity	Putative Target	Drug	IC_{50}	Comments	Reference used
DNA Replication	Apicoplast DNA gyrase	Ciprofloxacin	*Pf* 8-38 µM *Tg* 30 µM	Confirmed to block apicoplast DNA replication	(51-53)
		Trovafloxacin	*Tg* 0.77-0.98 µg/ml	Causes delayed death *Tg*	(54)
RNA Transcription	Apicoplast RNA polymerase β-subunit	Rifampicin	*Pf* 3 µM *Tg* 3 µM[a]	Confirmed by Northern analysis (*Pf*)	(55, 56)
		Rifabutin	*Tg* 26.5 µg/ml		(57, 58)
Protein Translation	Apicoplast 23S rRNA	Clindamycin	*Pf* 20 nM[a] *Tg* 10 nM[a]	Causes delayed death in *Tg*	(53, 59-61)
		Azithromycin	*Pf* 2 µM[a] *Tg* 2 µM	Causes delayed death in *Tg*	(59-62)
		Spiramycin	*Tg* 40 ng/ml	Causes delayed death in *Tg*	(59, 60)
		Thiostrepton	*Pf* 2 µM *Tg* NS[a]	Drug-target interaction confirmed	(63-66)
		Micrococcin	*Pf* 35 nM		(67)
		Chloramphenicol	*Pf* 10 µM[a] *Tg* 5 µM[a]	Causes delayed death in *Tg*	(60-62, 68)
	Apicoplast 16S rRNA	Doxycycline	*Pf* 11.3 µM	May also target mitochondrion	(68, 69)
		Tetracycline	*Pf* 10 µM *Tg* 20 µM	No delayed death in *Tg* may also target mitochondrion	(61, 62, 68)
	Apicoplast elongation factor TufA	Amythiamicin	*Pf* 10 nM	Inferred by polysome disruption in *Pf*	(70)
Fatty acid biosynthesis	Apicoplast-targeted β -ketoacyl-ACP synthase II and III (FabF and FabH)	Thiolactomycin	*Pf* 50 µM *Tg* 100 µM[a]		(3)
		Thiolactomycin analogues	*Pf* ≥8 µM		(71)
	Apicoplast-targeted enoyl-ACP reductase (FabI)	Triclosan	*Pf* 1 µM	FabI inhibition confirmed	(72, 73)
	Apicoplast-targeted β-ketoacyl-ACP synthase II(FabF)	Cerulenin	*Pf* 11 µM		(71)
	Apicoplast-targeted Acetyl-CoA carboxylase (ACC)	Clodinafop	*Tg* 10 µM	ACC inhibition confirmed	(74, 75)
		Quizalofop	*Tg* 100 µM	ACC inhibition confirmed	(74)
		Haloxyfop	*Tg* 100 µM	ACC inhibition confirmed	(74, 75)
		Fenoxaprop	*Pf* 144 µM		(71)
		Tralkoxydim	*Pf* 181 µM		(71)
		Diclofop	*Pf* 210 µM		(71)
Isoprenoid biosynthesis	Apicoplast-targeted DOXP reducto-isomerase	Fosmidomycin	*Pf* 290-370 nM	DOXP reducto-isomerase inhibition confirmed	(76)
		FR-900098	*Pf* 90-170 nM	DOXP reducto-isomerase inhibition confirmed	(76)
Amino Acid biosynthesis	5-enopyruvyl shikimate3-phosphate synthase(aroA)	Glyphosate	*Pf* 3 mM *Tg* 2 mM	Target enzyme Characterised pathway cytosolic rather than plastidic	(77)

[a] - D. S. Roos unpublished results.
ACP - acyl carrier protein. NS - not sensitive.
Pf: *P. falciparum.*
Tg: Toxoplasma gondii (related protozoan apicomplexan).

1.5 Apicomplexa and the apicoplast

The first Apicomplexan protozoan was observed by Anthony van Leeuwenhoek as oocytes of *Eimeria stiedae* in the gall bladder of a rabbit in 1674. In 1828, the first member of the Apicomplexa was named as *Gregarina ovata* in earwigs by Dufour (78). The phylum now contains thousands of species and these members are responsible for some of the world's most devastating diseases. Members of this phylum include *Toxoplasma gondii,* various *Eimeria* species, *Neospora, Babesia, Theileria, Cryptosporidium* species and *Plasmodium* species. In addition to *Plasmodium* species causing malaria, *Cryptosporidium parvum* have caused many deaths due to water-borne disease outbreaks, *Eimeria* and *Cryptosporidium* are enteric pathogens and *Neospora* and *Theileria* are veterinary pathogens (79). *T. gondii* are transmitted by a variety of animals including mice, cats, sea otters and horses and toxoplasmosis is particularly harmful to pregnant women and cause congenital birth defects (79-81).

1.5.1 Origin and structure of the apicoplast

Plastids originate from endosymbiosis, whereby a prokaryote is engulfed by an eukaryote resulting in a symbiotic partnership (82). There are two theories as to how a once independent bacterium became a small organelle inside Apicomplexan parasites. Firstly, it is thought that a cyanobacterium was engulfed by a phagotrophic eukaryote, which did not consume the cyanobacterium but rather used it to its benefit. Figure 1.4 depicts an algal cell as an eukaryote which contains an internal chloroplast that originated from an engulfed cyanobacterium. The theory postulates that genes were transferred from the chloroplast to the nucleus of the algal cell in conjunction with discarding genes from the algal nucleus. This is known as primary endosymbiosis and examples of these include transfer of plastids such as chloroplasts in plants, green algae and red algae. These plastids are only surrounded by two membranes (83). Apicoplasts are believed to be derived from a secondary endosymbiosis event through the phagotrophic engulfment of a primary endosymbiotic eukaryote (that had already engulfed a cyanobacterium through primary endosymbiosis) by another phagotrophic eukaryote, thus resulting in the apicoplast existing as a small organelle (0.15 – 1.5 µm) within the secondary phagotrophic (Figure 1.4).

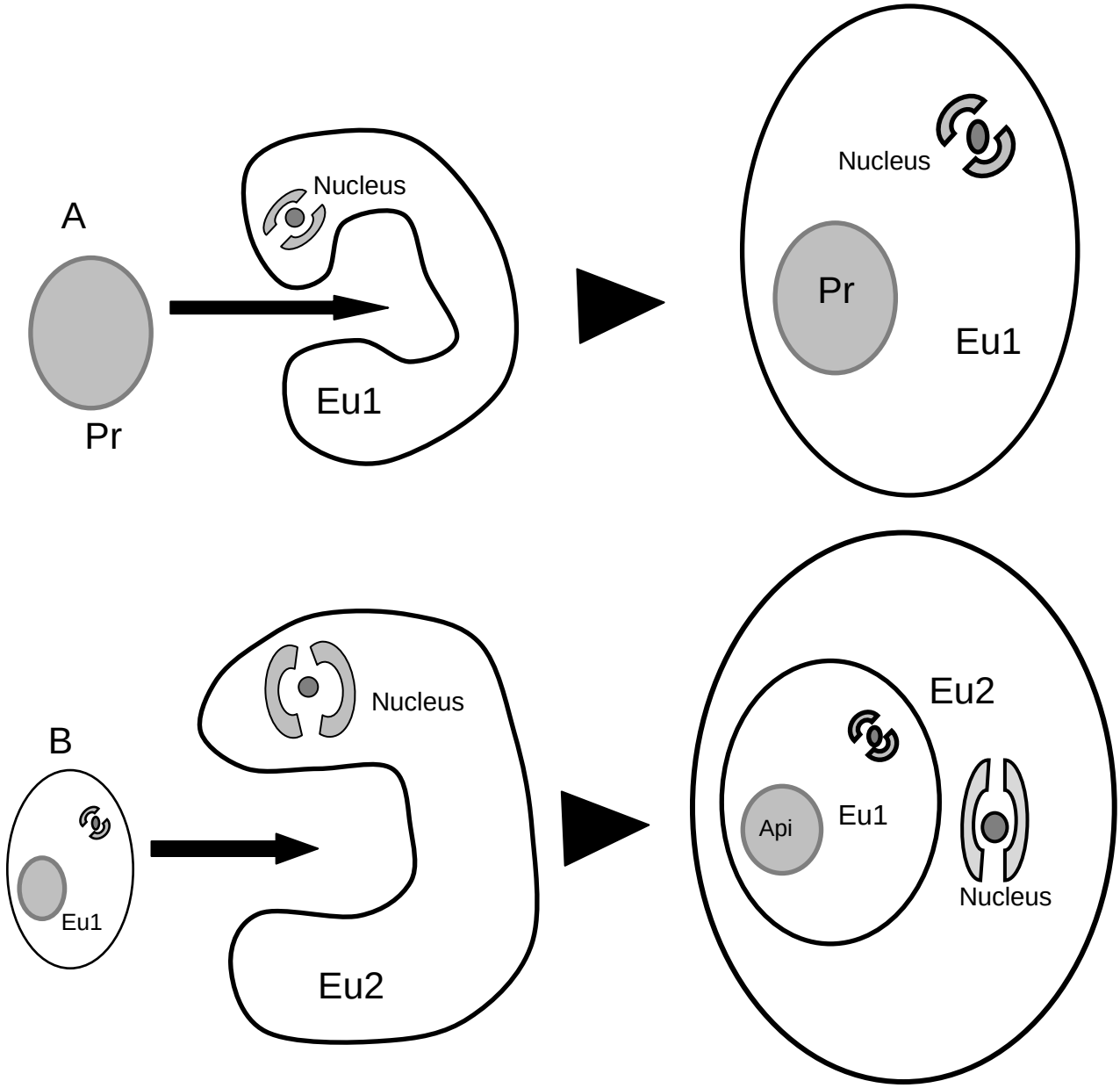

Figure 1.4 Primary and secondary endosymbiosis.
A - Primary endosymbiosis is the product of an engulfed prokaryote (Pr) by an eukaryote (Eu1).
B – Secondary endosymbiosis is then the product of primary endosymbiosis, which is engulfed by a second eukaryote (Eu2). Api – Apicoplast.

Debate is still continuing about the nature of the secondary endosymbiont (84) with support for either green (85, 86) or red (84) algae as origin being favoured. During the secondary endosymbiotic event, genes were once again transferred to the nucleus of the engulfing eukaryote. The apicoplast, though no longer able to photosynthesise, contains its own genome that encodes proteins and prokaryotic-like large and small-subunits rRNAs as well as tRNAs (Figure 1.5).

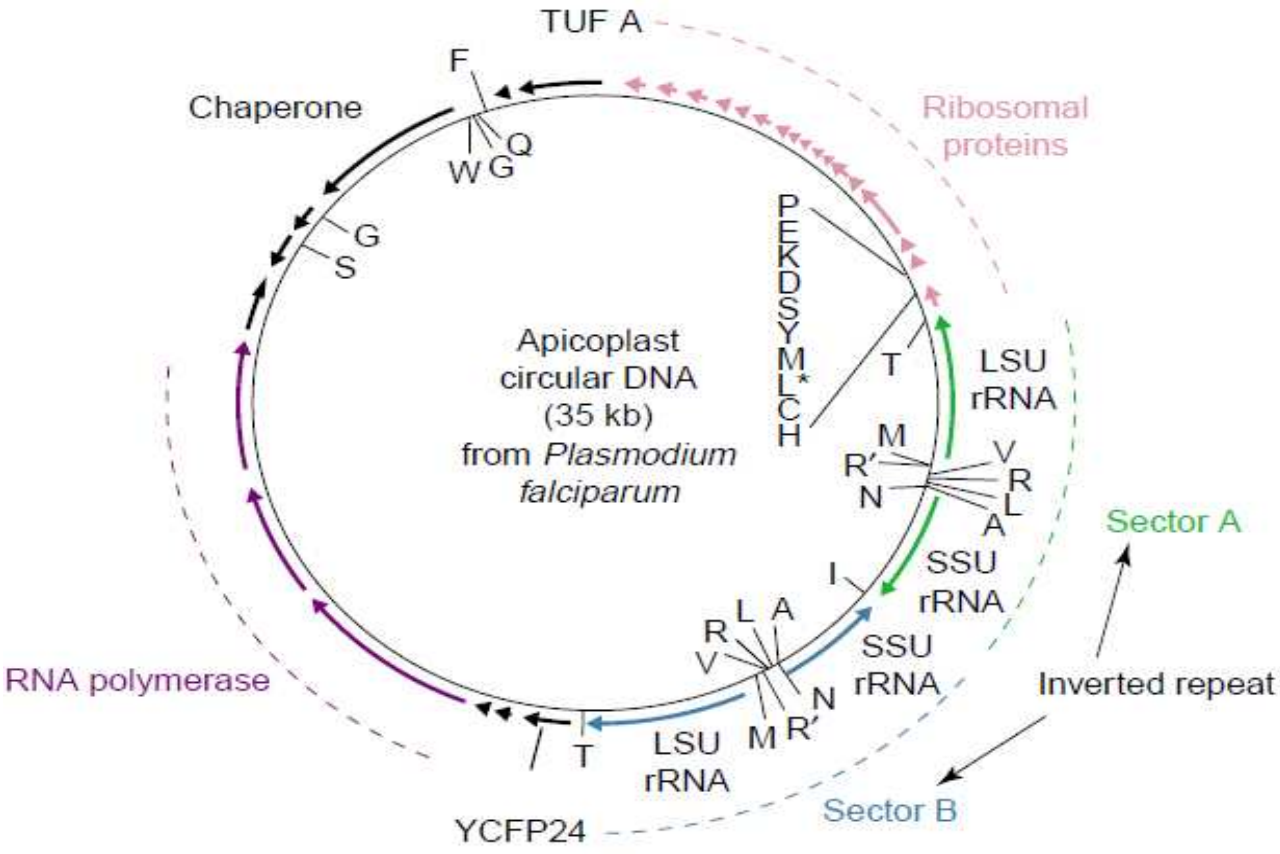

Figure 1.5 The genetic organisation of the apicoplast in the malaria causing *P. falciparum* (82).

The arrows indicate the direction of transcription and the broken lines shows the regions of function. Though this is the sequence for the apicoplast of *P. falciparum* it was found that the other Apicomplexan organisms have similar sequences and size. LSU – Large subunit of ribosome. SSU – Small unit of ribosome. Star – intron. The one letter abbreviations are those of the corresponding amino acids of the specific tRNA. YCFP24 and TUF A are the products of the *ycfp24* and *tufA* genes. Sector A and B are representatives of the two inverted repeats on the apical genome.

A single *P. falciparum* parasite only contains one apicoplast, which is associated with the mitochondrion (87) (Figure 1.6). During the invasion stage of the malaria parasite, the apicoplast is rod shaped and bent because it is pressed against the plasma membrane. The apicoplast is spherical during the parasite's development in the erythrocytes, and increase in size as the parasite matures. The *Plasmodium* parasite's apicoplast is surrounded by a basic set of three to four membranes. The configuration of the outermost membrane of the apicoplast of the *Plasmodium* sp. is a complex extension of flattened cisternae and a myelin sheath-like structure, similar to the thylakoids in plant envelopes, is observed within the stroma. This structure of the apicoplast is the result of tubular whorls of up to six membranes that are rolled-up in such a way to form what is most probably a galactolipid-rich envelope (Figure 1.6).

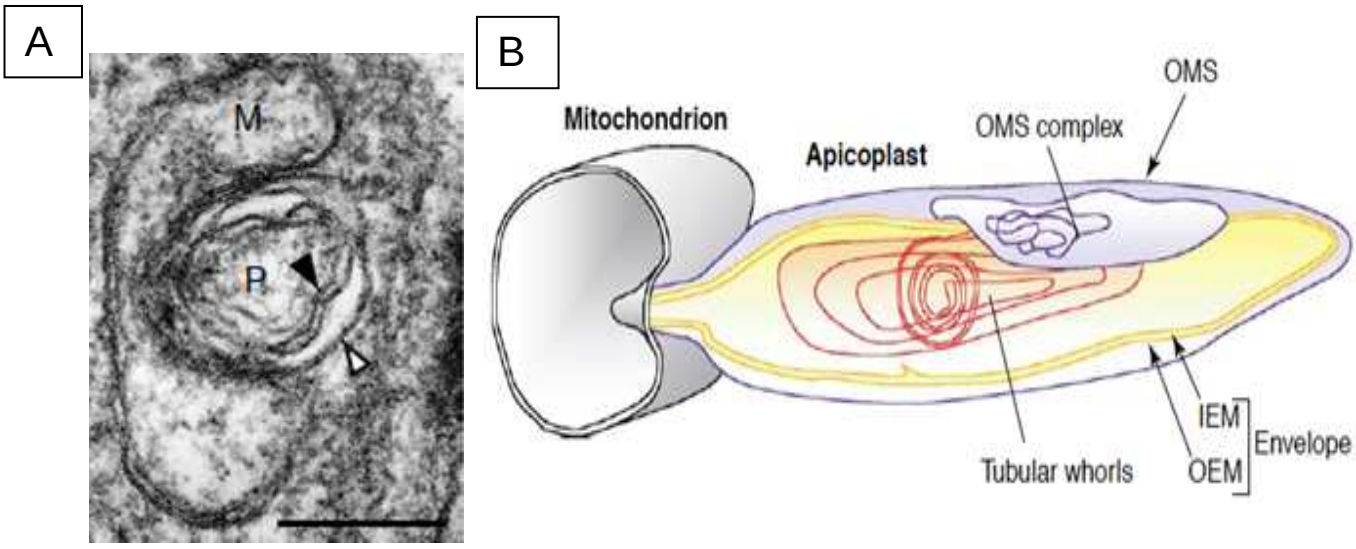

Figure 1.6 The close association of the *Plasmodium* apicoplast and mitochondria (82).
A – The ultrastructure of the apicoplast and the mitochondria. Black arrow heads indicates envelope membranes, White arrow heads indicates outermost membranes. Labels: M, mitochondrion; P, apicoplast. B – Illustration of the three-dimensional reconstitution of *P. falciparum* apicoplast. The apicoplast is ovoid and closely associated with the mitochondria. IEM - Inner envelope membranes, OEM - Outer envelope membrane, OMS - Outermost membrane system. The OMS surface area is expanded because of the complex structures of flattened cisternae, similar to the thylakoids in plant envelopes (observed in the central sections of the apicoplast).

1.5.2 Division mechanism of the apicoplast

The exact mechanism of apicoplast division of *P. falciparum* is not yet fully understood, but because of its endosymbiotic bacterial origin, it is believed that the organelle will divide in a similar way as the division of a bacterial cell (88). In 2000, the first information of apicoplast division in *P. falciparum* was documented (89). The early ring stage of the parasite showed a single crescent shaped apicoplast that becomes round as the parasite develops into the trophozoite stage. The apicoplast increases in size and forms a branched network structure. This structure divides into many daughter plastids as the parasite divides into the multi-nucleated mature schizont such that each merozoite released from the erupted erythrocyte will have a single apicoplast (89). This organelle cannot be formed *de novo* and thus must be present in the newly formed cells before the erythrocytes erupt (90). Nuclear division and plastid division have been proven to be linked as can be seen for *T. gondii* (Figure 1.7 A) (91). The cell division of *T. gondii* differs only slightly from the cell division of *P. falciparum* as it results in only 2 daughter cells, whereas *P. falciparum* results in multiple daughter cells (Figure 1.7 B), but currently, the same principle is considered to apply to both organisms (84).

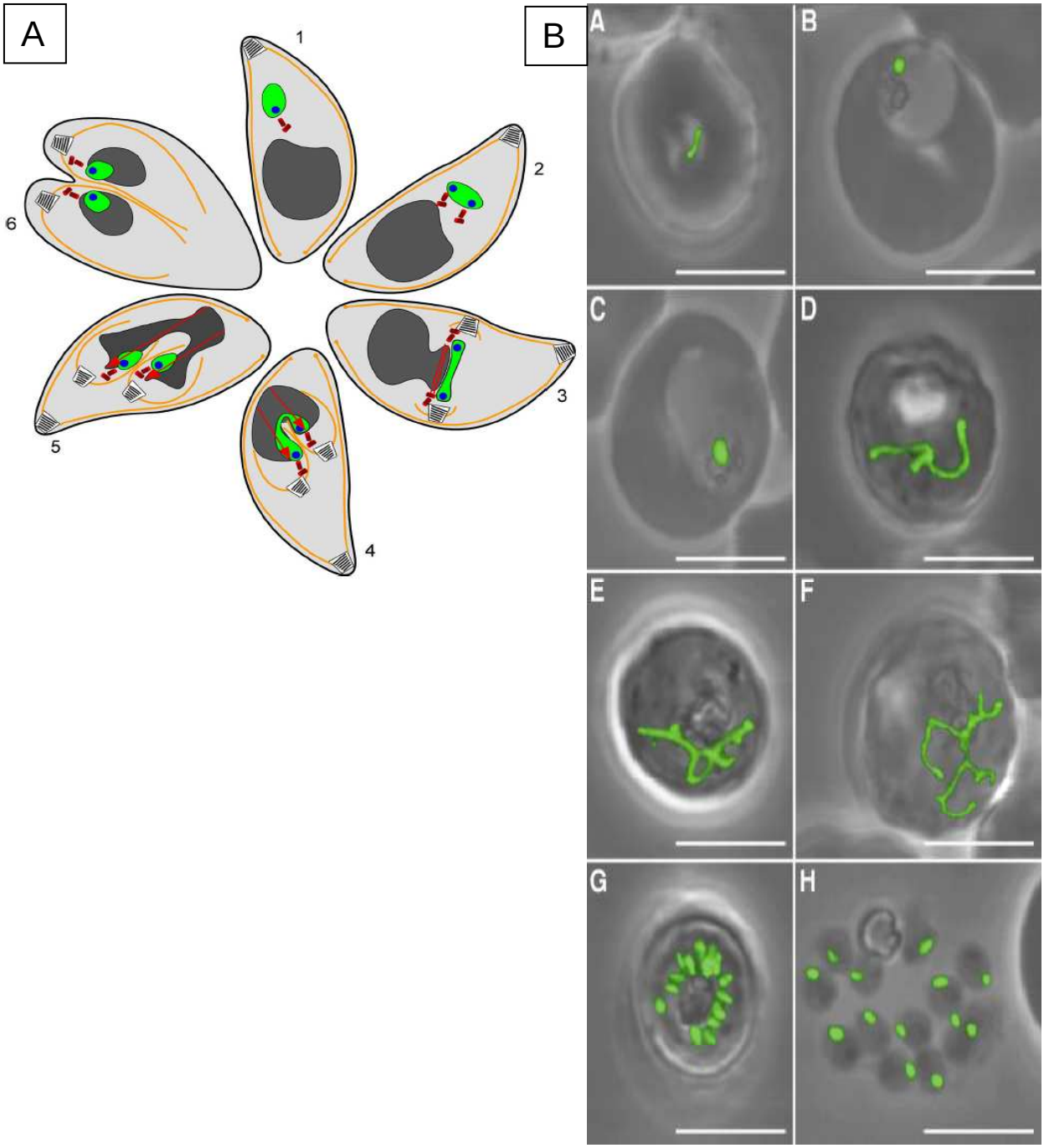

Figure 1.7 The division of apicoplasts in *T. gondii* (91) and *P. falciparum* (89).

A - *T. gondii:* 1 - The ellipsoid plasmid is close to the nucleus, contains many copies of the genome and is associated with the centriole. 2 - Two equal portions of genome are formed. 3 - The dumbbell shape plastid lies on top of the nucleus and the ends of the plastid are associated with the centrioles. 4 - Plastid forms a U-shape and daughter buds grow out. The ends of the U are associated with the centrioles and the middle starts to grow smaller. 5 - Plastid becomes two. Each are bound to its own centriole and together with the divided nucleus, the plastid migrates into the daughter parasite. 6 - The two daughter nuclei are bound in the middle of the parasite after fission. Each newly formed parasite only contains one centriole, one apicoplast and one nucleus.

B - *P. falciparum*: A – ring stage, B – early trophozoite, C – late trophozoite, D – F – early schizonts, G – late schizonts, H – merozoites. During the ring and trophozoite stages the single apicoplast enlarge. During the schizont stages of the parasite the apicoplast forms branched structures which divide during merozoite formation.

1.5.3 Functions of the apicoplast

The apicoplast has been shown to be indispensible to *P. falciparum* parasites and it is impossible to create mutants of these parasites without the plastid, as these are not viable (53, 92-94). The apicoplast is unlikely to be involved in photosynthesis because the complete genome sequence of *P. falciparum* has no genes encoding for products involved in photosynthesis. Furthermore, the apicoplast is located within the parasite that resides within erythrocytes, a nutrient-rich environment and completely in the dark (95). However, the apicoplast plays a definitive role in the synthesis of amino acids (89). It provides mitochondria with haem for respiration within the mitochondria (96), plays a role in fatty acid synthesis (85), plays important role in the synthesis of isoprenoids (76), and it is required for the formation of daughter cell plasma membranes during cytogenesis (97).

1.5.3.1 Isoprenoid biosynthesis

In higher organisms, including mammals, fungi, plants and algae, the biosynthesis of isoprenoids (sterols and ubiquinones) are dependent on the condensation of a variety of different isopentenyl diphosphate units. In mammals, these units are provided by the mevalonate pathway, where three molecules of acetyl coenzyme A (CoA) are converted into 3-hydroxy-3-methylglutaryl CoA. This is then reduced to mevalonate by the enzyme 3-hydroxy-3-methylglutaryl CoA reductase. The next step in the pathway is the conversion of mevalonate to mevalonate-5-posphate and then to isopentenyl diphosphate (98). The apicoplast has low levels of 3-hydroxy-3-methylglutaryl CoA, one of the major molecules in the mammalian isoprenoid pathway, however the enzyme that catalyses the formation of this molecule is not found in the apicoplast (76). This suggests that the mevalonate pathway is not the pathway of isoprenoid synthesis within *P. falciparum*. However, plants and a small selection of eubacteria make use of another pathway to assist in the first few steps of isoprenoid biosynthesis and in higher plants this alternative pathway is responsible for the synthesis of plastidic isoprenoids (99). This pathway is called the 1-deoxy-D-xylulose-5-phosphate (DXP) pathway and results in the conversion of glyceraldehydes-3-phosphate and pyruvate to DXP. The reaction is catalysed by the enzyme DXP synthase. In turn, DXP is converted to 2-C-methyl-D-erythritol-4-phosphate by the enzyme DXP reducto-isomerase. The genes encoding DXP reducto-isomerase was found on chromosome 14 of the *P. falciparum* genome

and was taken as proof that the DXP pathway provided the parasite with isoprenoids (76, 100, 101). An amino terminal signal sequence was found on DXP reducto-isomerase which targets the enzyme to the apicoplast (76).

1.5.3.2 Haem biosynthesis

The *P. falciparum* parasite is capable of producing haem *de novo* (102). In animals the production of haem is the end product of the biosynthesis of tetrapyrrole, which takes place in the mitochondria and cytosol of the cell. In plants, haem synthesis starts in the chloroplast with glutamate and cofactor tRNA and subsequently progress to the mitochondria. The tetrapyrrole biosynthesis pathway forms two branches to form haem and chlorophyll (102). Haem biosynthesis in *P. falciparum* starts in the mitochondria with glycine and succinyl CoA, which are converted to δ-aminolevulinate by the enzyme δ-aminolevulinate synthase. Prediction tools indicated that the successive reactions occur in the apicoplast and cytosol (103, 104). *P. falciparum* has the ability to incorporate radioactively labelled glycine into haem, but cannot do the same with radioactively labelled glutamate (105). Thus it is speculated that enzymes in the haem biosynthesis pathway in *P. falciparum* originated from α-proteobacterial endosymbiosis (106) and the pathway shows similarities to the canonical shemin pathway in the mitochondria of animals and fungi during the initiation stages (107).

The next step in the haem synthesis in plants, animals, fungi and *P. falciparum* is the formation of porphobilinogen catalysed by aminolevulinate dehydratase (HemB). Evidence was found indicating erythrocyte HemB is imported into the cytosol of the parasite (108). This indicates that the porphobilinogen formation occurs in the cytosol (109). The pathway then continues in the apicoplast, as a homologue of the animal and plant HemC, the next enzyme in the haem synthesis pathway, was found to have an apicoplast targeted signal sequence. The rest of the pathway in the *P. falciparum* parasite is of unknown location, but one of the last enzymes in the pathway, a HemH analogue, contains a N-terminal signal sequence and it is thought to be a mitochondrial transit peptide (109). Haem biosynthesis is a clear indication of the close relationship between the parasitic mitochondria and apicoplast (107).

1.5.3.3 Fatty acid biosynthesis

Fatty acids play an indispensable role in living cells, as it mediates cell growth, cell differentiation, membrane formation and act as precursors for energy stores (71). It also plays a role in the maintenance of cell homeostasis. The nuclear encoded enzymes of fatty acid biosynthesis, acyl carrier protein (ACP), enoyl-ACP reductase (FabI), β-ketoacyl-ACP synthases III (KASIII) and I/II (FabB/F) and β-hydroxyacyl-ACP dehydratase is targeted to the apicoplast in *P. falciparum* (3, 72, 73, 89). This provided evidence that type II fatty acid biosynthesis is in fact a function of the apicoplast. The substrate for type II fatty acid biosynthesis is malonyl-CoA that is formed outside the apicoplast from acetyl–CoA by acetyl-CoA carboxylase. Fatty acid elongation consists of rounds of transferring of a malonyl moiety by malonyl-CoA:Acyl carrier protein transacylase (FabD) to ACP to form malonyl-ACP. This is followed by condensation, where the malonyl-ACP molecules are condensed by the enzyme β-oxoacyl-ACP synthase III (FabH) with an acetyl group to form β-oxoacyl-ACP. The acetyl group can be provided by either acetyl-CoA or acetyl-ACP. The next steps are reduction and dehydration reactions that in the end would have added 2 carbons to the growing chain in each cycle. The last step is once again a reduction step by one of the following: β-ketoacyl-ACP I and II [(KAS), FabB/F], β-oxoacyl-ACP reductase (FabG), β-hydroxyacyl-ACP dehydratase (FabZ) or enoyl-ACP reductase (FabI) (110). Type II fatty acid synthesis pathway in the apicoplast of the malaria parasite is essential to the parasite but it is also very different from the cytosolic type I fatty acid biosynthesis of the human host. Thus, it may be a good target for drugs and inhibitors against the malaria parasite (111).

1.5.3.4 Galactolipid synthesis

Biological cell membranes are permeable barriers made up of lipid bilayers (112). Glycerolipids containing a phosphorous head group are the major lipid class in the membranes of animals, yeast and bacteria (113). Phosphatidylglycerol (PG) is the main phospholipid and represent ±10% of thylakoid lipids in chloroplast membranes (114). However, in photosynthetic organisms, such as algae, land plants and cyanobacteria, phosphorous-free galactolipids are the predominant lipid class (115, 116). The envelope of plastids, such as chloroplasts in plants, contains ±80% galactoglycerolipids, mainly monogalactosyldiacylglycerol (MGDG, ±50%) and digalactosyldiacylglycerol

(DGDG, ±30%) (Figure 1.8) (114, 116). MGDG and DGDG can differ in the acyl composition at the sn-1 and the sn-2 position of the glycerol backbone. Two main types of MGDG and DGDG are found in nature. The eukaryotic type contains an 18 carbon fatty acid at the sn-2 site and is found in most land plants. The prokaryotic type, based on cyanobacteria, contains a 16 carbon fatty acid at the sn-2 site. Some plants, such as *Arabidopsis* and spinach, contain both types of MGDG. In most plants, the eukaryotic type DGDG is found (114). Galactolipids can relocate to non-plastid membranes and is considered important in membrane lipid homeostasis (117) and are essential in various processes including photosynthesis, plastid protein import and various other developmental processes (118).

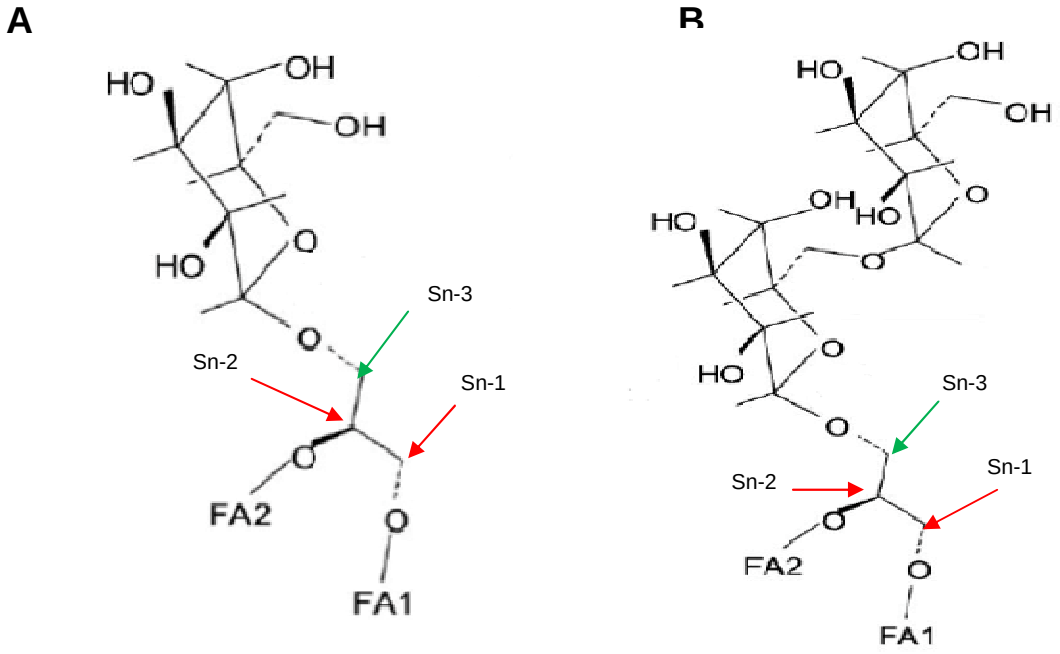

Figure 1.8 The structures of galactolipids. A- Monogalactosyldiacylglycerol (MGDG) and B –Digalactosyldiacylglycerol (DGDG) (119).

Galactolipids can differ in the fatty acid chain at the sn-1 and the sn-2 position of the glycerol backbone (Indicated by red arrows). Two main types of MGDG and DGDG are found in nature. The eukaryotic type contains an 18 carbon fatty acid at the sn-2 site and is found in most land plants. The prokaryotic type, based on cyanobacteria, contains a 16 carbon fatty acid at the sn-2 site (114). A single galactosyl residue is transferred to the sn-3 position of DAG from UDP-galactose (Indicated by green arrows) (120).

MGDG is synthesised in plants by the enzyme MGDG synthase (MGD, EC 2.4.1.46), which is a galactosyltransferase (120). MGD catalyze glycosylation of 1,2-diacylglycerol (DAG) where a single galactosyl residue from UDP-galactose, is transferred to the sn-3 position of DAG (green arrow in Figure 1.8 A). MGD is encoded for by three genes in *Arabidopsis*, *mgd1, mgd2* and *mgd3* (121, 122) resulting in three isoforms that can be grouped phylogenetically into two types. The A-type consists of MGD1, which is responsible for the synthesis of the majority of MGD in the organism (123), whereas

MGD2 and MGD3 are grouped into the B-type. The main differences between the two types are their different functions and substrate specificity (120). As seen in Figure 1.9, the different MGD isoforms are only found in a specific location within the cell, because of the lack of membrane-spanning domains. MDG1 is found in the inner envelope of the chloroplast where it catalyses the reaction of DAG [18 carbon atom fatty acid at sn-1 position and 16-carbon atom fatty acid at sn-2 position $_{(18,\ 16)}$] to MGDG $_{(18,\ 16)}$ (113, 122). MGD2 and MGD3 are associated with the outer membrane of the chloroplast and can catalyse DAG $_{(16,\ 18)}$ and DAG $_{(18,\ 18)}$ to the corresponding MGDG (113, 121).

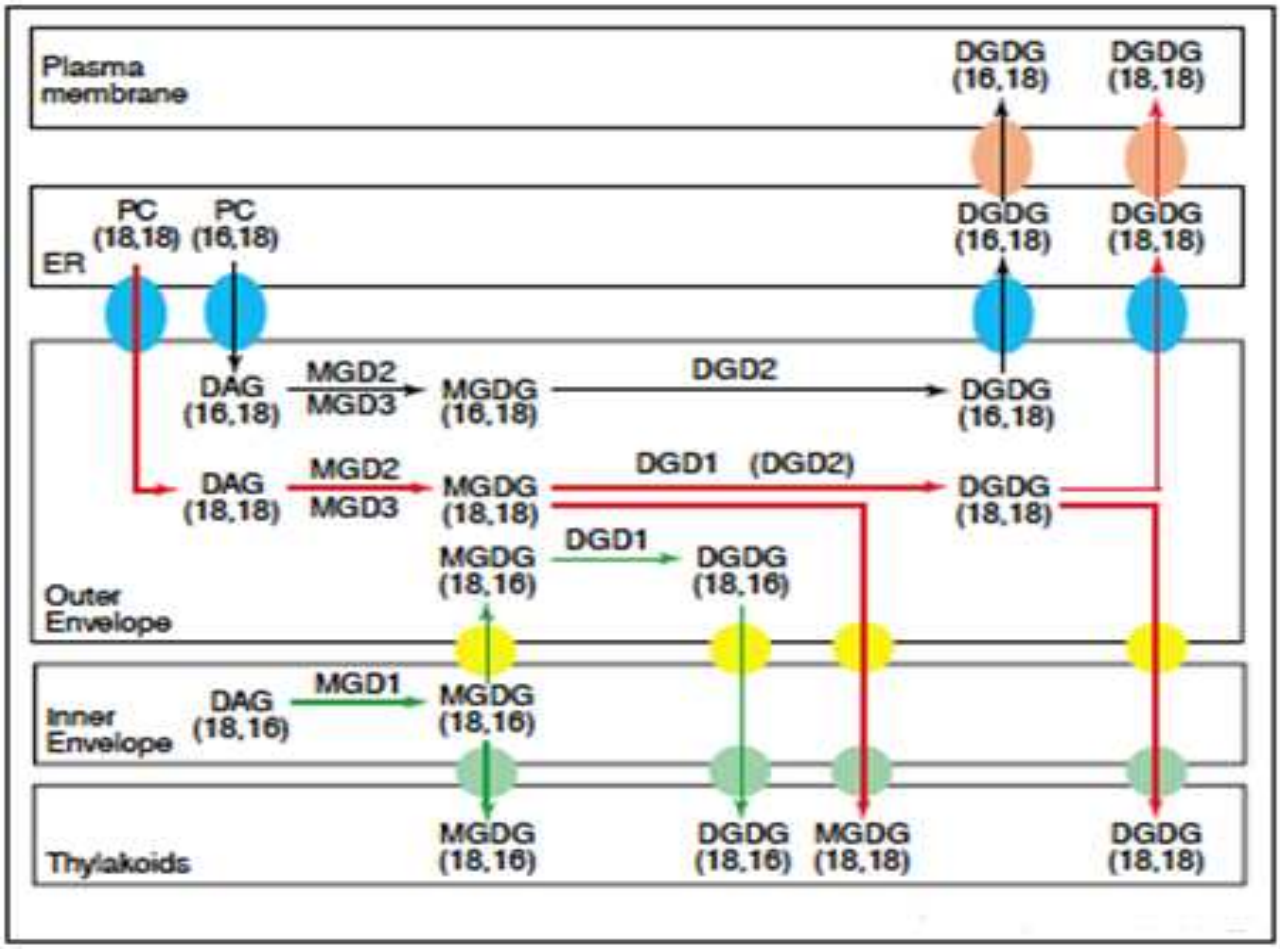

Figure 1.9 Schematic representation of the MGDG and DGDG synthesis of *Arabidopsis* (113).

MGDG synthesis occurs in the envelope of the chloroplast (outer and inner). DGDG synthesis is only located in the outer envelope. Lipid synthesis by prokaryotic pathway: green arrows. Lipid synthesis by eukaryotic pathway: red arrows. DGDG synthesis where DGDG is transported to extraplastidial membranes: black arrows. The number of carbon atoms of fatty acids on the sn-1 and sn-2 positions of the glycerol backbone is indicated in brackets.

DGDG synthesis is catalysed by DGDG synthase (DGD). A second α-galactosyl group is transferred from UDP-galactose to the 6-hydroxyl position of MGDG. The majority of DGDG in *Arabidopsis* is from DGD1 (124). A paralogue of DGD1 is also found in

Arabidopsis, DGD2 (113) with the main difference between DGD1 and DGD2 being that DGD1 consists of both an N-terminal domain for insertion of the protein into the outer envelope of the chloroplast (lacking in DGD2) as well as a C-terminal domain (glycosyltransferase activity) (113, 124, 125).

With *P. falciparum* containing a plant-like plastid apicoplast, the membranes surrounding the apicoplast suggested that glycerolipids that are unique to algae and plant plastids might also be present in the apicoplast membranes. As such, MGDG and DGDG may be present in Apicomplexa like *P. falciparum* and *T. gondii*. Investigations of galactolipid biosynthesis and content in membranes of these Apicomplexa have indicated that radioactively labelled UPD-galactose is incorporated into both MGDG and DGDG. The latter was also immunologically detected in parasite lysates (Figure 1.10). Distinct enzymatic processes or amino acid derivation of the synthases were involved since no clear identification of MGDG or DGDG synthase orthologues could be identified in the *P. falciparum* genome utilising only bioinformatic searches (119).

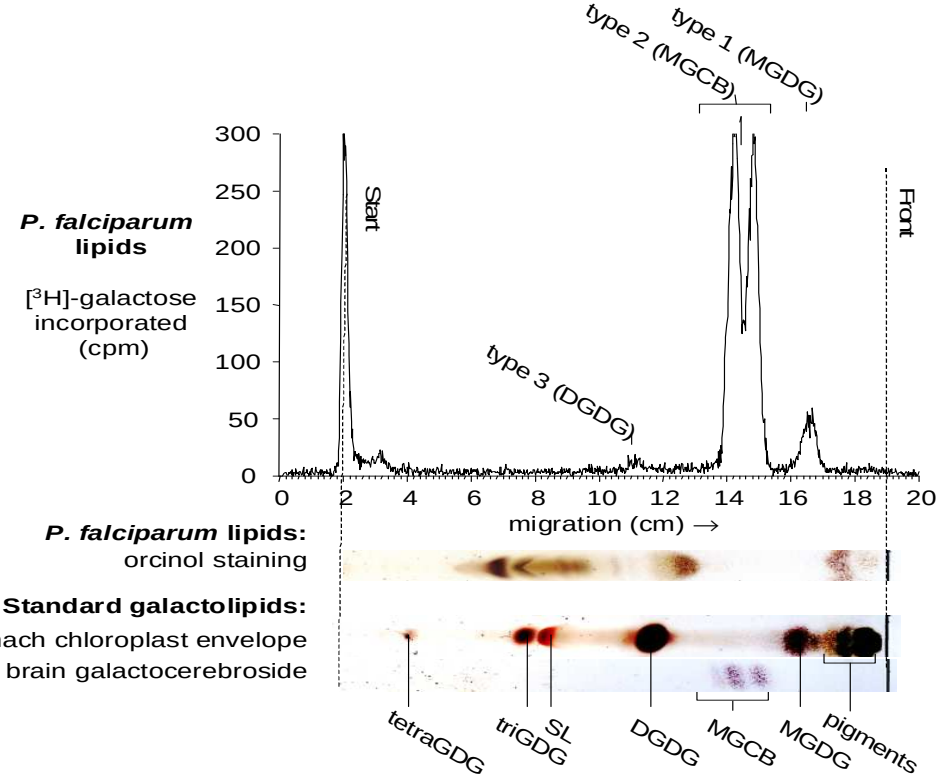

Figure 1.10 Galactolipids synthesised in *P. falciparum* (119).
After the parasites were incubated with tritiated UDP-galactose, the lipid extraction was separated using TLC. Sulfoquinovosyldiacylglycerol (SL), trigalactosyldiacylglycerol (triGDG) and tetragalactosyldiacylglycerol (tetraGDG) as detected in the lipid extraction.

MGDG synthase has been shown to be essential to plant cell growth, with knock-outs of MGD1 in *Arabidopsis* as a member of the multigene MGDG synthase family, leading to a complete lack of chlorophyll, chloroplast ultrastructure disruption and severe plant growth inhibition (118). This data provides support for galactolipid biosynthesis as a valid growth inhibition strategy. As this process is unique in *P. falciparum* and not found in humans, it is an enticing strategy for the development of novel antimalarials.

1.5.4 Apicoplast as drug target in *P. falciparum*

Numerous studies have proven that the targets of antibiotics such as azithromycin, clindamycin, doxycycline, ciprofloxacin, chloramphenicol, tetracycline and rifampicin are different metabolic activities within the apicoplast (Table 1.2), and that these compounds display a phenomenon called 'delayed death' of the malaria parasites (97). Delayed death occurs when the treated parasites do not show signs of growth inhibition in the first life cycle, but the next generation of merozoites following drug intervention cannot invade new erythrocytes and die before a third life cycle (48, 97, 111). It was also found that delayed death only occurs when the house-keeping functions of the parasite's apicoplast are targeted, such as replication, transcription and translation. This will reduce the number of apicoplasts in the next generation, but the remaining apicoplasts enable the parasite population to survive a while longer. This is known as the 'self-sustenance' function of the apicoplast (126). When more essential pathways and functions of the apicoplast, such as fatty acid biosynthesis and haem biosynthesis are targeted by a compound, the growth inhibitory effect is faster resulting in rapid parasite death (126).

Current inhibitors targeting fatty acid biosynthesis include thiolactomycin and triclosan (and analogous) which targets FabB (71). Luteolin-7-*O*-glucoside, a common flavonoid glucoside, targets FabI in the fatty acid biosynthesis pathway, whereas lucteolin and catechin gallate inhibits FabZ, FabG and FabI (127).

1.6 The compound A51B1C1_1

In a study conducted by Botté and Maréchal in 2010 (118), a set of herbicide-derived compounds were tested for activity against *Arabidopsis* to identify novel chemical scaffolds as inhibitors of galactolipid biosynthesis in these plants. A high-throughput screening strategy was followed to screen DAG analogues with inhibitory activity

against recombinantly expressed MGD1 (MGDG synthase family member). The first set of 23360 compounds screened was compiled from the Cerep diversity-based library and only 20 compounds exhibited an apparent inhibition of more than 25%. These 20 compounds, together with 40 additional compounds from the Cerep diversity-based library (not included in the first study) that was selected based on chemical similarities, was tested for their inhibitory properties on MGD1. The inhibition of MGD1 was tested *in vitro* in *Arabidopsis* and two compounds showed MGD1 activity inhibition above 40%, Galvestine-1 and Galvestine-2 (Figure 1.11). These compounds show competitive inhibition with DAG for MGD1.

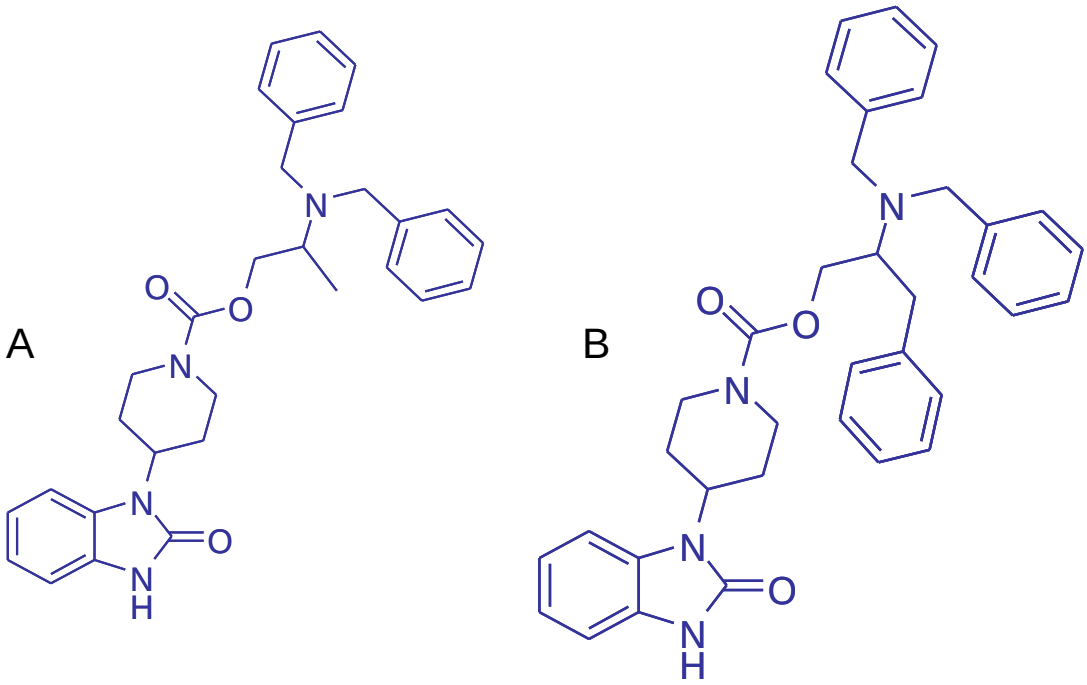

Figure 1.11 The structures of Galvestine-1 (A) and Galvestine-2 (B) (118).

A large set of small molecules were subsequently designed using the structure of Galvestine-1 as scaffold, by changing three active groups on the molecule as shown in Figure 1.12. The linker region (indicated in red) was also exchanged with various possible structures. The resultant Group A molecules included changes to the benzimidazole group on the parent molecule, Group B includes molecules which contained changes to the piperidinyl part and Group C contains changes in the dibenzylamino-ethoxy group. The resultant compounds were therefore named according to the substitution given for each group.

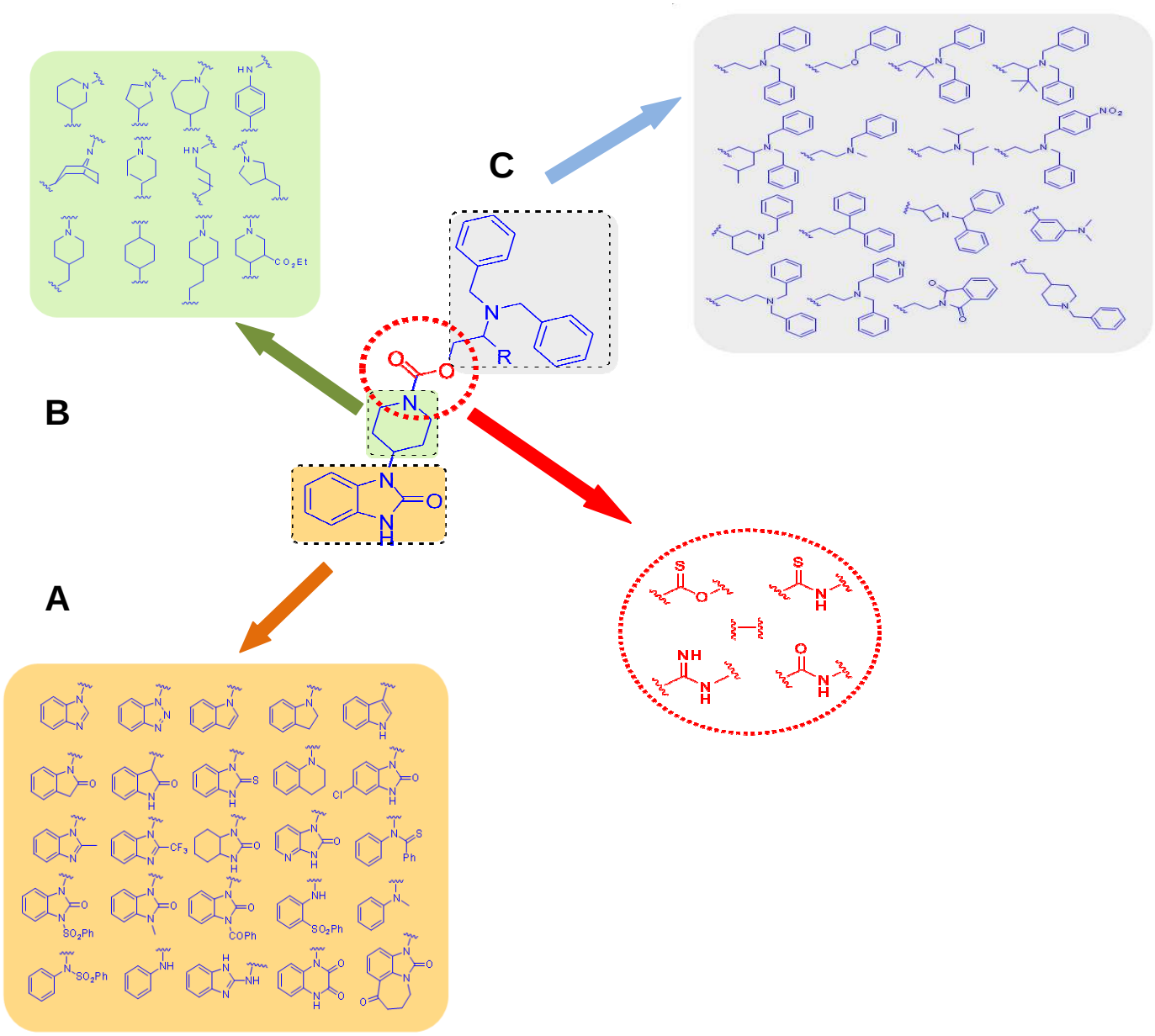

Figure 1.12 The process by which the small molecules were designed, using Galvestine-1 as the guide molecule (118).
Group A - changes to the benzimidazole group, Group B - changes to the piperidinyl part and Group C - changes in the dibenzylamino-ethoxy group.

These molecules were tested for their ability to inhibit MGDG synthesis in the envelope vesicles of chloroplasts that were purified from spinach plants in order to determine their bioavailability in the environment of the membrane. Dose-dependent inhibition of *Arabidopsis* plant growth was observed for Galvestine-1 and -2 as well as some of their derivatives. Moreover, there was a decrease in the production of MGDG and the ratio of MGDG:DGDG was also affected. Galvestine-1 and -2 have *in vitro* growth inhibition IC_{50} values of 10 µM and 12 µM, respectively against *Arabidopsis*. Fifty of the derivatives were found to have IC_{50} values between 200 and 800 µM.

This study therefore showed for the first time that disruption of cellular lipid homeostasis could be affected through targeting MGDG synthases, and this has a dramatic effect on the growth of plants. Due to the presence of MGDG and DGDG in the plant-derived apicoplast of *P. falciparum*, an interesting speculation is that Galvestine-1 and its derivatives might have growth-inhibitory capacity against the malaria parasite by targeting lipid biosynthesis processes in the apicoplast. This study therefore presents the determination of the antimalarial property of one of the lead MGDG synthase inhibitors from the Botté study, A51B1C1_1 (Figure 1.13).

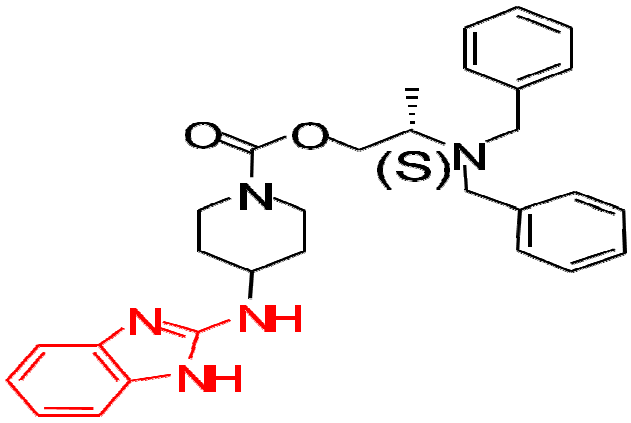

Figure 1.13 The structure of the compound A51B1C1_1 (Personal communication, Eric Maréchal, Pretoria, 2009).

One major advantage of this strategy would be that these compounds are herbicide-derived and could therefore, if they are active against *P. falciparum*, prove to be highly selective to the parasite without targeting any metabolic process in humans. This compound furthermore provides a novel chemical scaffold unrelated to any current antimalarials, which would be a novel action in the parasite compared to currently used antimalarials, and be able to overcome the resistance mechanisms against current antimalarials. Thus, if these compounds prove to be active against the malaria parasite, they may be developed into new antimalarial drugs.

1.7 Research objective and aims

The primary objective of this study was to determine the antimalarial potential of compound A51B1C1_1 as well as the physiological response of *P. falciparum* after treatment with this compound by employing a comprehensive functional genomics approach.

Chapter 2 focuses on determining the antimalarial activity of A51B1C1_1 through morphological investigation of *P. falciparum* after treatment with this compound. This is followed by a complete transcriptome analysis employing DNA microarray to identify responsive transcripts in *P. falciparum* that were differentially regulated upon treatment with this compound.

Chapter 3 introduces the use of higher-level functional genomics analyses of the response of *P. falciparum* to A51B1C1_1 treatment by investigating the proteome of the parasites after perturbation with this herbicide-derived compound.

Chapter 4 is a concluding chapter in which the results and conclusions reached from the above mentioned studies are integrated and future perspectives are presented.

Results from this work were presented in the following instances:

Workshops:

1. J Snyman, J Verlinden, AI Louw, E Maréchal, L Birkholtz. (2009) Functional genomics of a herbicide treated *P. falciparum.* Grenoble, France.

2. J Snyman, J Verlinden, AI Louw, E Maréchal, L Birkholtz. (2011) Transcriptomic profiling of *Plasmodium falciparum* using the Agilent platform. Latest Advances in Microarray Applications and NGS Target Enrichment Technology. Pretoria, South Africa

Conferences:

1. J Snyman, J Verlinden, AI Louw, E Maréchal, L Birkholtz. (2010) Functional genomic investigation of *P. falciparum* treated with herbicide-derived compounds. SASBMB, Bloemfontein, South Africa

Manuscript in preparation:

1. J Snyman, J Verlinden, AI Louw, E Maréchal, L Birkholtz. Exploiting *Plasmodium falciparum*'s plant origins: The discovery of herbicide-derived compounds as new antimalarial drugs.

CHAPTER 2
MORPHOLOGICAL AND TRANSCRIPTOMIC ANALYSES OF THE EFFECT OF A HERBICIDE-DERIVED COMPOUND ON *P. FALCIPARUM* PARASITES

2.1 Introduction

Functional genomics is an essential tool in the development of new drugs against *P. falciparum.* It allows determination of the function of different genes, the mode of action of a novel drug, optimization of drug development, validation of drug targets and identification of new drug targets, amongst others (Box 2.1) (128-130). This contributes to our understanding of gene function and the effect of a specific drug on an organism (128, 131).

Box 2.1 Implementation of functional genomics in drug target discovery in *P. falciparum* (132).

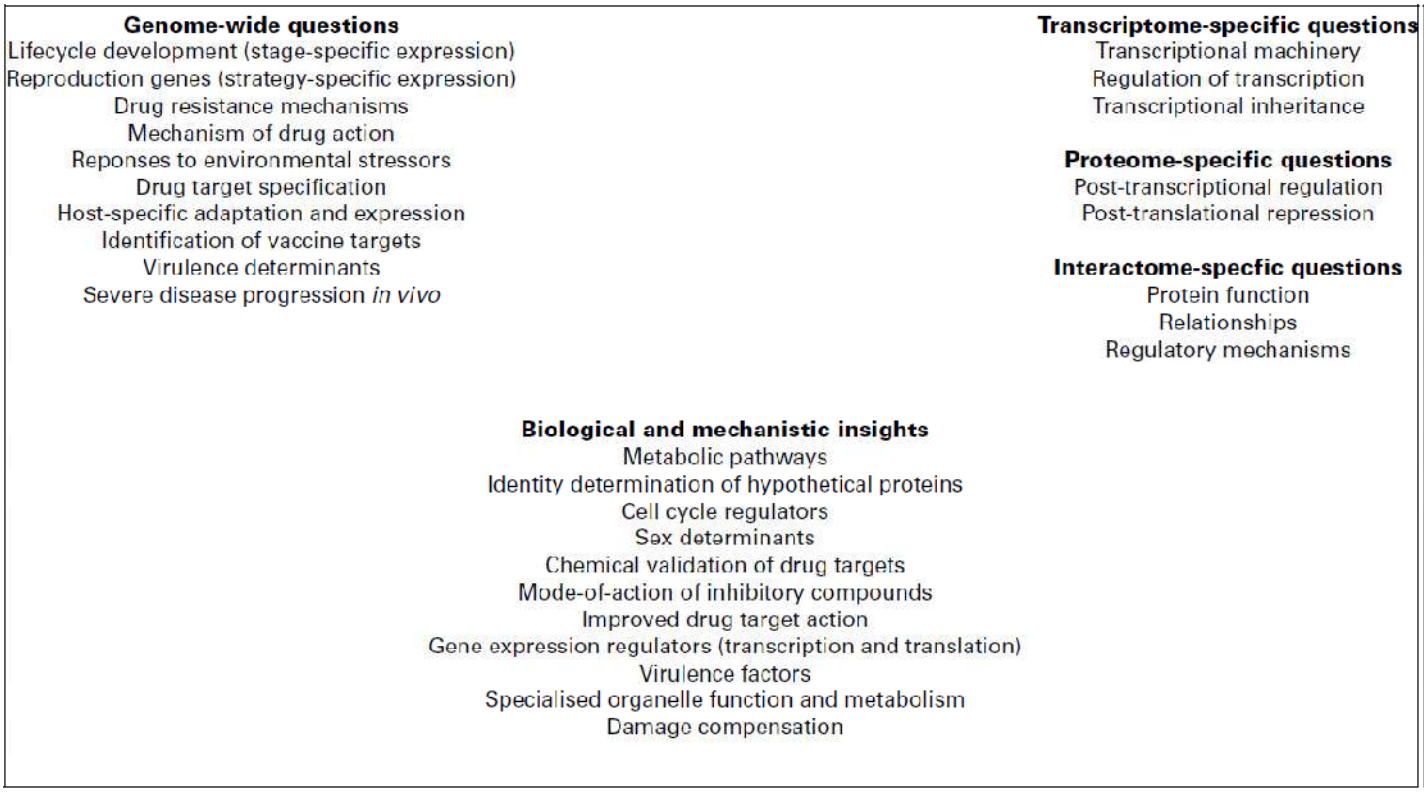

Functional genomics includes multi-level analysis of an organism's complete transcriptome, proteome, interactome, metabolome etc. Transcriptome analysis is usually performed using DNA microarray, which gives a direct quantification of the total mRNA complement in a specific stage of the life cycle of an organism (131). Transcriptomic profiling can be used to determine how cells respond to environmental stress and also allows determination of metabolic pathways, feedback mechanisms and the way the cell buffer itself against induced stress (133).

2.1.1 Transcriptome of *P. falciparum*

By 2002, the genomes of the parasite, *P. falciparum*, the vector, *A. gambiae,* and the host, *Homo sapiens,* were sequenced completely, which allow for the development of new medical treatments and vaccine development (134). The sequences of the genomes of many other *Plasmodium* species: *P. yoelli, P. vivax, P. berghei, P. knowlesi* and *P. gallinaceum* are largely completed (135). The genome of *P. falciparum* is 22.8 Mb in size, which encodes for ~5300 genes on 14 chromosomes ranging between 0.5 – 3.0 Mb in size. The *P. falciparum* genome is A+T-rich (~90% A+T nucleotide content in the intron regions and ~80% on average for the whole genome) (134). The parasite also has a linear mitochondrial genome (~6 kb) (136) and a circular apicoplast genome (~35 kb) (134). The genome of *P. falciparum* is unique and 60% of the predicted 5268 open reading frames show no sequence similarity to genes from other organisms (134). The whole genome transcriptional profiling of the *P. falciparum* has been investigated in 2003 by Bozdech (137, 138) and Le Roch (139) and revealed astonishing peculiarities. Particularly, the transcripts in the parasite are only produced when they are needed during the life cycle of the parasite in a 'just-in-time' fashion (Figure 2.1) (137). This implies that there is a very tight control of transcript production/decay.

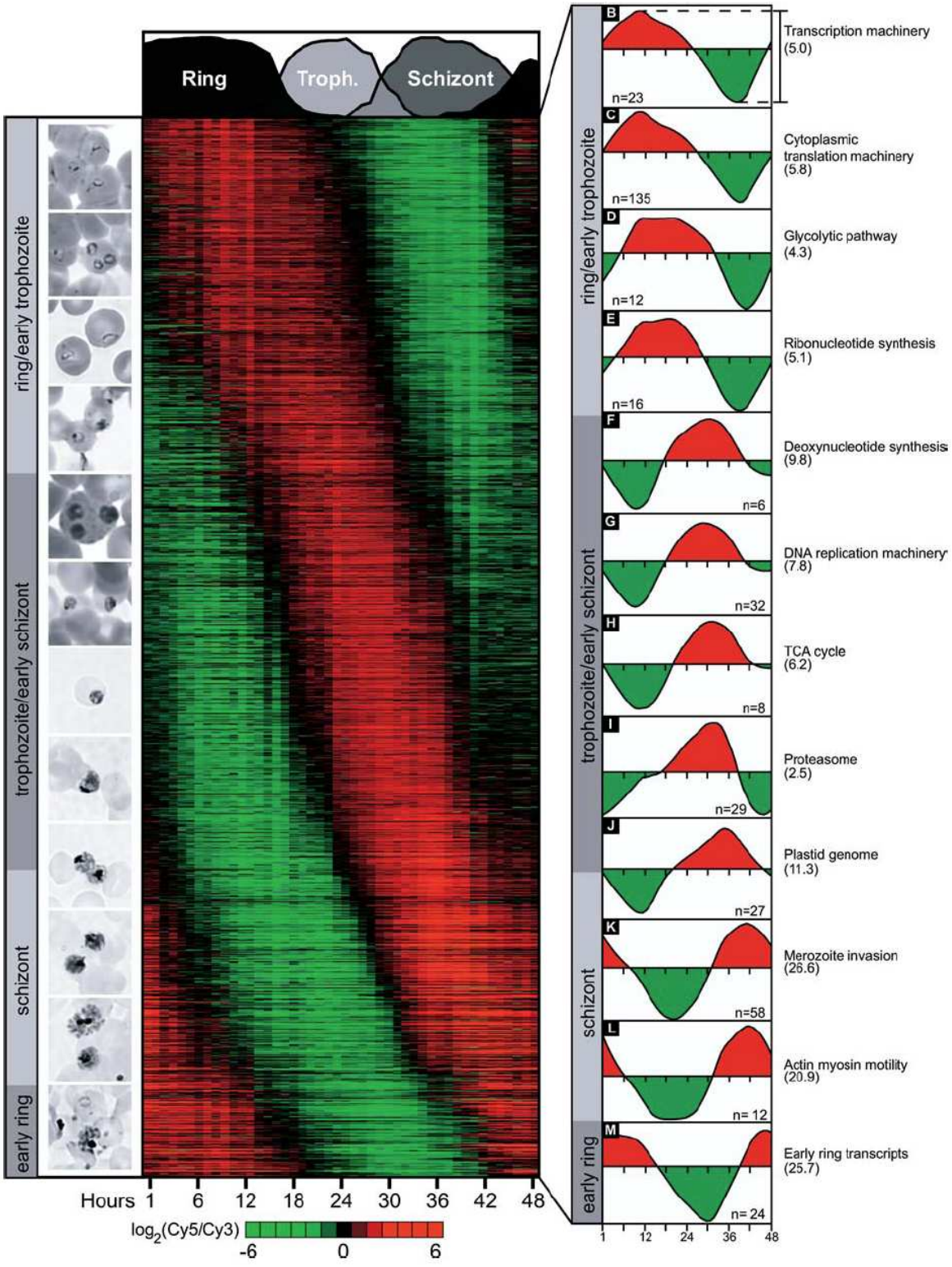

Figure 2.1. The complete transcriptome of *P. falciparum* during the intra-erythrocytic developmental cycle (137).

Transcript production and decay is tightly regulated such that a transcript is only produced (red) during the period in the life cycle state in which it is needed, after which the production is decreased (green).

The factors controlling the *P. falciparum* transcriptome is not clearly elucidated, although a family of transcription factors (ApiAP2) has been implicated to be involved in

parasite-specific transcription control mechanisms (140). However, beyond this tight control of the transcriptome of *P. falciparum* during its intra-erythrocytic developmental cycle (IDC), there is clear evidence that the parasite is able to respond on a transcriptional level to external perturbations. Additionally, Plasmodia use both posttranscriptional and -translational mechanisms to induce differential transcriptome responses to drug treatment (132). Transcriptome-wide analyses has been successfully used to determine the mode of action of known antimalarials e.g. tetracyclines (97) and chloroquine (141) in *P. falciparum,* or to elucidate the functional consequences of treating the parasites with novel, potential antimalarials like difluoromethylornithine (142-144), apicidin (145), cyclohexylamine (146), trichostatin (147) and bisthiazolium compound T4 (148).

In 2006, Dahl *et al.* (97), investigated the effect of tetracycline and its derivatives on the apicoplast in *P. falciparum* parasites. Tetracycline has an inhibitory effect on protein synthesis by these parasites, but only at very high levels. Doxycycline, a derivative of tetracycline, showed morphologically that trophozoite and early schizont stage parasites were more sensitive to treatment by this antibiotic than late schizonts and rings (97). To determine the specific targets of doxycycline, parasites were treated with 1 µM doxycycline and transcriptomics performed on RNA isolated over a 55 h period. Using information from literature (137), Dahl *et al.* (97) calculated the average correlation of expression profiles between the treated and the untreated parasites to be 0.8. This is an indication that the transcriptomic profiles of the treated and the control parasites were similar (Figure 2.2 A). It was found that essentially all the apicoplast genes that were represented on the microarray platform used, were under-expressed relative to other features (Figure 2.2 B). This transcriptome data validated that the site of action of doxycycline was the apicoplast in *P. falciparum* parasites. This under-expression of the apicoplast genes prevents development of the parasites, an effect that was morphologically only visible in the next life cycle even though the apicoplasts of the treated parasites were successfully segregated into the daughter parasites (97).

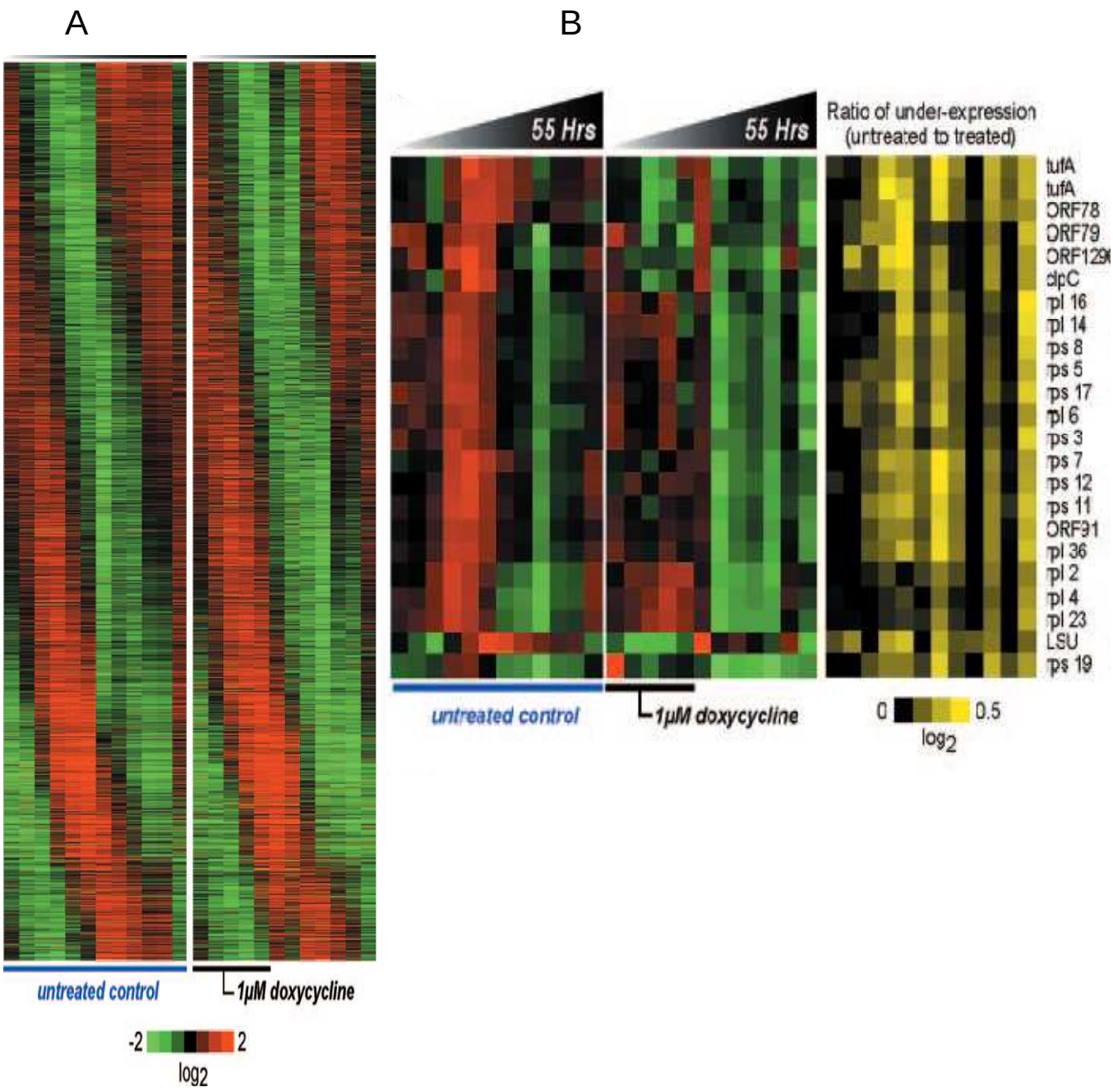

Figure 2.2 The transcriptome profiles of doxycycline treated and control parasites.
A – Expression data of all 3721 oligonucleotide features. These oligonucleotides were plotted on a heat map according to the phase of expression. B –The under-expressed transcript encoding for the apicoplast genes.

2.1.2 Microarray experimental design and data analysis

Various microarray platforms exist each with their own advantages for various applications. Affymetrix quant Gene Chips are synthesised *in situ* using photolithographs combined with solid glass phase on which the 25-mer oligos are produced and are particularly favoured in whole genome analyses (including

untranslated regulatory elements, etc.) (149). NimbleGen uses a digital micromirror system instead of the photolithographs for the *in situ* synthesis of 24 – 70-mers with Ultra density microarrays consisting of 385K up to 2.1 million probes. Operon Biotechnologies produce 70-mer pre-designed arrays or array-ready oligonucleotide sets that can be used for in-house array spotting (150). Eppendorf is known for their Pathway-focused Dual Chips® that are synthesised with long, sense DNA with 200 to 400 nucleotides for maximum signal and minimum background noise for all available arrays (151).

Agilent provides custom printing of 60-mer oligos on a 1 x 3 inch microscope slide in a base-by-base manner by a combination of inkjet technology and phosphoramidite chemistry (152). Phosphoramidite chemistry is efficient for the synthesis of long oligonucleotides *in situ* and is a fast way to produce custom arrays, based on the addition of one nucleotide at a time onto InkJet printed nucleotide precursors (153). This combination ensures uniformed spot shape and size allowing Agilent arrays to be comprised of more differentially expressed genes compared to other systems (154). Additionally, Agilent provides the opportunity for custom designed arrays, which is particularly useful in studying the *P. falciparum* transcriptome.

Microarray experimental design is crucial for accurate data comparison in order to obtain reproducible differential expression profiles. There are two main options for data comparisons: 1) direct comparison of the same transcript between the different sample sets including sequential, loop or mixed designs; or 2) indirect comparison between two different sample sets using a common reference (Figure 2.3). Indirect sample comparisons with a reference design is preferred if the difference in transcripts are analysed over a set time period, as this design allows data to be normalised against a common reference pool and data can be compared across arrays (155). Reference designs additionally have the advantage that all the comparisons that are made occurs with equal efficiency since the samples are always compared to the same reference sample (156). The common reference pool has to be highly representative of all conditions under investigation and may either be an external source of RNA/cDNA or it may be a pooled sample of all the samples included in the experiment, labelled with the Cy3 dye (green channel). In these type of experimental designs, the samples are typically labelled with Cy5 dye (red channel), but dye swopping may be performed.

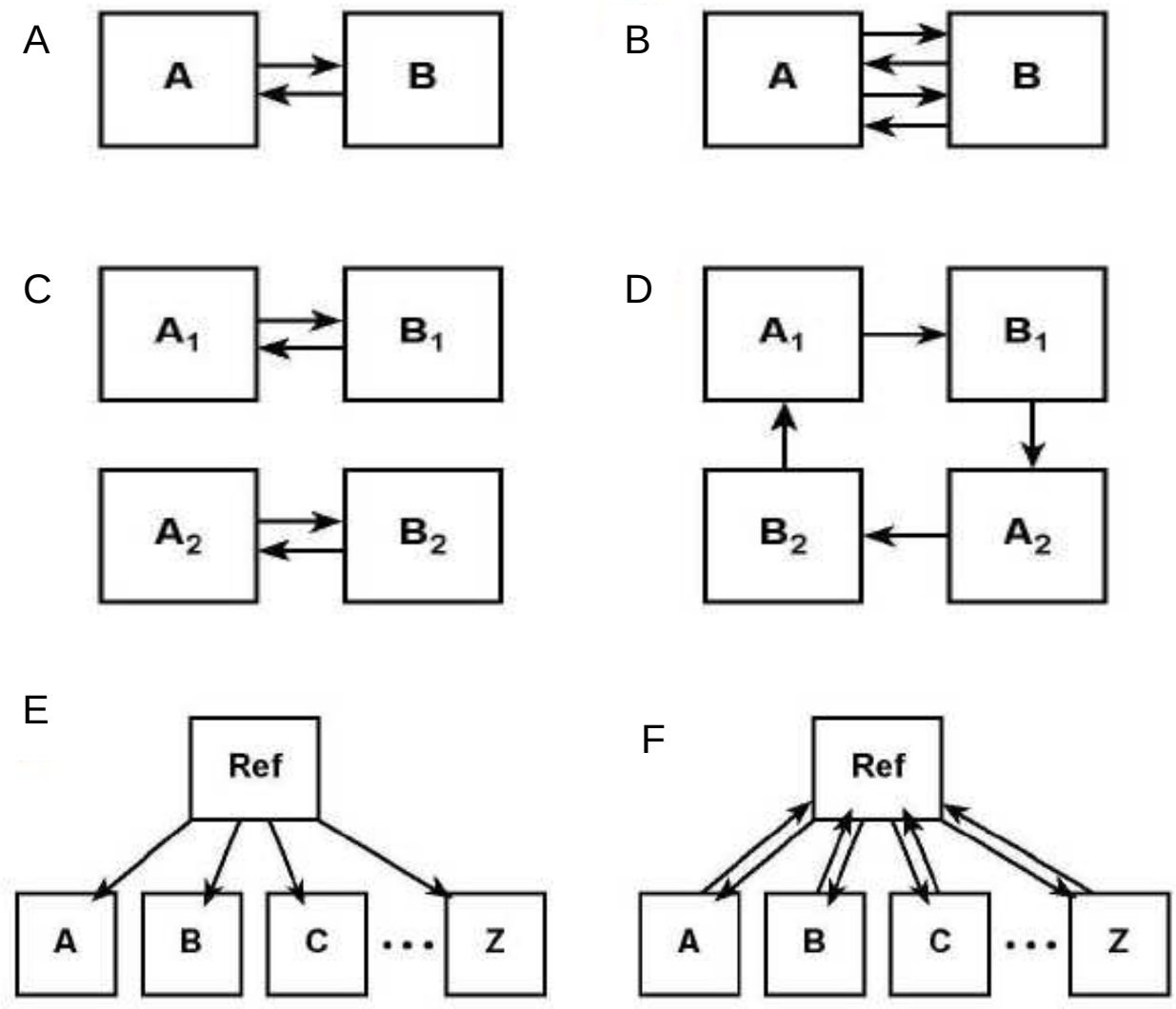

Figure 2.3 Microarray designs for different comparison strategies (156).
A - direct comparison of only one sample set, B - direct comparison of only one sample set with dye swop, C - sequential comparison of replicates and D - loop or mixed design. E and F are examples of reference designs without (E) or with (F) dye swop.

Standardisation of microarray data is extremely important to ensure that equivalent data are available for different microarray experiments to allow comparisons between datasets. The minimum information about a microarray experiment (MIAME) (157) prescribes data standardisation as a pre-requisite for the public release of microarray data into databases such as ArrayExpress (http://www.ebi.ac.uk/microarray-as/ae) and Gene Expression Omnibus (GEO, http://www.ncbi.nlm.nih.gov/geo). This enables analyses across different microarray platforms and comparison between different datasets.

In this chapter, DNA microarray analysis is performed to determine the functional consequences of treating *P. falciparum* with the herbicide-derivative A51B1C1_1. The microarray experiment conformed to MIAME standards and data were deposited in GEO.

2.2 Materials and methods

2.2.1 *In vitro* cultivation of asexual *P. falciparum* parasites

2.2.1.1 Preparation of the erythrocytes

All procedures were performed using aseptic techniques. Blood type O+ was collected from a donor by a medical doctor into a blood bag containing citrate-phosphate-glucose-adenine anticoagulant (Adcock Ingram). The whole blood was left in the bag overnight at 4℃, transferred to sterile 50 ml centrifuge tubes and the unwashed blood stored at 4℃ for 3-4 weeks. The erythrocytes were washed prior to using them in culture to remove white blood cells and serum. Whole blood (50 ml) was centrifuged at 2500*g* for 5 min at room temperature (Hermle Z320 centrifuge) to separate the erythrocytes and buffy-coat. The buffy-coat and serum were aspirated, and the erythrocytes were washed four times with an equal volume of phosphate-buffered saline (PBS) solution (137 mM NaCl, 2.7 mM KCl, 10 mM phosphate, pH 7.4) with centrifugation at 2500*g* for 5 min. Erythrocytes were re-suspended in an equal volume of incomplete culture medium [RPMI-1640 (SIGMA, Missouri, USA), 24 mg/ml gentamycin (SIGMA), 0.4% (w/v) D-glucose (SIGMA), 88 mg/l hypoxanthine, 12 mM HEPES (SIGMA) and 21.4 mM sodium bicarbonate (SIGMA) per litre MilliQ H_2O (distilled, de-ionized, 0.22 µm filter sterilised)] and stored at 4℃ until further use.

2.2.1.2 Thawing of *P. falciparum* parasites

Chloroquine-sensitive *P. falciparum* (3D7 strain, 1 ml) parasites were thawed at 37℃ from liquid nitrogen stocks. NaCl (200 µl, 12% (w/v)) was added drop-wise to the thawed culture to reduce the osmotic potential. Thereafter, 1.8 ml of 0.6% NaCl was added to the thawed culture. Parasite-infected erythrocytes were collected by centrifugation for 5 min at 2500*g*. The supernatant was aspirated and the infected erythrocytes were re-suspended in 30 ml fresh, preheated (37℃) culture medium [incomplete medium supplemented with 0.5% (w/v) Albumax II (purified lipid-rich bovine serum albumin, Invitrogen, Paisley, UK)] to which 1.5 ml washed packed erythrocytes were added to yield a 5% haematocrit culture. Cultures were maintained in 75 cm^2 flasks in an atmosphere of 5% CO_2, 5% O_2 and 90% N_2 (Afrox, Johannesburg, South Africa), with shaking at 58 revolutions per minute (rpm) at 37℃.

Ring-stage *P. falciparum* parasite cultures at a parasitaemia of 5–10% were cryopreserved after centrifugation at 2500*g* for 5 min at room temperature, aspiration of the supernatant and re-suspension of the pellet in an equal volume of freezing medium (28% glycerol in incomplete medium). The resuspended parasites (1 ml) were transferred to cyrovails and stored in liquid nitrogen for future use.

Parasite growth during culturing was monitored morphologically using Giemsa staining and light microscopy of thin blood smears. Blood smears of the cultures were fixed in methanol (MeOH) for 5 s and stained in Giemsa's Azur Eosin methylene blue solution [10% (v/v) Giemsa stock solution (Merck) in PBS] for 3 min. The parasitaemia was determined by counting at least 10 fields of 100 cells each.

2.2.1.3 Synchronisation of *P. falciparum* cultures

A modified method of Lambros and Vanderberg (158) was used for the synchronisation of parasites. The parasites were synchronised in the ring stage every 48 h, for three consecutive cycles with an 8 h staggered time-interval to ensure >97% synchronisation. The parasites were pelleted by centrifugation for 10 min at 2500*g* and re-suspended in three volumes of preheated (37℃) 10% (w/v) sorbitol (SIGMA) and incubated at 37℃ for 10 min. The parasites were washed three times in an equal volume of preheated (37℃) culture medium. The synchronised parasites were re-suspended in 30 ml preheated (37℃) culture medium and fresh erythrocytes were added to obtain a haematocrit of 5%.

2.2.2 IC_{50} determinations of A51B1C1_1

The Malaria SYBR Green I – based fluorescence assay method of Johnson *et al.* (2007) (159) and Smilkstein *et al.* (2004) (160) was followed with some changes. Erythrocytes do not contain DNA, whereas infected erythrocytes contain the DNA of the parasite. SYBR Green I is a fluorescent dye that interacts with DNA, therefore a correlation between DNA content (SYBR Green I signal) and parasitaemia can be used to monitor decrease in parasitaemia due to cell growth inhibition (161). The compound A51B1C1_1 was initially dissolved in DMSO to a concentration of 10 mM. Serial dilutions (1 to 0.0675 mM) of the compound in culture medium were plated out in triplicate in sterile 96-well plates. Early ring stage parasites were examined, counted and added to the pre-dosed 96-well plate to give a final volume of 200 µl at 1%

parasitaemia and 2% haematocrit. Infected erythrocytes were incubated with 0.5 µM chloroquinedisulphate were also included as positive controls whereas parasitised erythrocytes in the absence of any drug or compound served as untreated controls. Parasite cultures were incubated in an atmosphere of 5% CO_2 at 37℃ for 96 h after which, parasites (100 µl each) were transferred into a black fluorescence plate containing100 µl lysis buffer per well (SYBR Green I [2 µl SYBR green I (Invitrogen) in 10 ml of lysis buffer (20 mM Tris (pH 7.5), 5 mM EDTA, 0.008% (w/v) saponin, 0.08% (v/v) Triton X-100)]). Fluorescence was measured after 1 h incubation in the dark at room temperature, with a Fluoroskan Ascent FL Fluorimeter (Thermo LabSystems) at an excitation of 485 nm, emission of 538 nm and integration time of 1000 ms. Data obtained were analysed in Excel 2007 and sigmoidal dose-response curves were plotted using SigmaPlot 9.0.

2.2.3 Morphological monitoring of drug treated parasites

Morphology studies were performed to determine the time points for RNA extraction for the microarray studies and proteomics. *P. falciparum* parasites (3D7, 10% parasitaemia and 5% haematocrit), were treated with 2xIC_{50} A51B1C1_1 dissolved in DMSO (final concentration of DMSO, 0.3%) at the invasion stage of erythrocytes. Control cultures contained DMSO at a final concentration of 0.3% (v/v). Both treated and control cultures were incubated for 72 h at 37℃. Culture medium was replaced every 24 h with drug as appropriate. Morphological monitoring using Giemsa staining and light microscopy of thin blood smears, was performed in triplicate every 3-4 h for a total of 72 h.

2.2.4 Drug treatment for transcriptome analysis

For transcriptome analysis of drug treated parasites, 30 ml synchronised *P. falciparum* cultures (section 2.2.5) with a parasitaemia of 10% and a haematocrit of 5% were used. Two biological replicates of both the treated sample (2xIC_{50} of compound A51B1C1_1) and the control group (0.3% DMSO (v/v)) were included in the experiment. At each specific time point (28 hpi and 36 hpi), 10 ml of culture were removed and centrifuged for 5 min at 2500*g*. The pellet was washed three times with 1xPBS and the infected erythrocytes were snap-cooled in liquid nitrogen and stored at -70℃.

2.2.5 RNA isolation

The isolation of RNA was performed in an RNAse-free environment using RNAse-free equipment and plasticwear. An adapted protocol from Van Brummelen *et al.* (2009) was used (133). To ensure that RNA of high purity was isolated, TRI-Reagent (SIGMA) and the RNeasy kit (Qiagen, Germany) were combined. TRI-reagent was used to isolate the RNA because it contains phenol and guanidine thiocyanate (chaotropic agent) which denature proteins.

Frozen pellets, collected from 30 ml synchronised cultures, were thawed and 600 µl lysis buffer (RLT, proprietary to the RNeasy kit) was added and mixed by vortexing. The mixture was transferred to two QIA-Shredder columns (Qiagen), which consist of biopolymer shredding systems causing physical rupture. The tubes were centrifuged for 2 min at 15700*g* and the flow-through was transferred to a new, clean tube. TRI-Reagent (SIGMA) (600 µl) was added, mixed by vortexing and incubated for 5 min at room temperature. To separate the homogenate, 400 µl chloroform was added to the samples, which was vortexed for 15 s and incubated for 10 min at room temperature. The samples were centrifuged for 15 min at 15700*g*. The upper aqueous phase, which contained the RNA, was removed without transferring the interphase, which contained the DNA, and transferred to a new microfuge tube. The bottom organic phase contained the denatured proteins, and trace amounts of lipids and other cellular components (162). Ethanol (EtOH) [1 volume, 70% (v/v)] was added to increase hydrophobicity and to facilitate binding of the RNA to the column via salt bridges. Two identical samples were pooled and loaded onto an RNeasy column.

The samples were centrifuged for 15 s at 15700*g* and the flow-through was discarded. The columns containing the RNA were washed with 350 µl wash buffer (RW1) and centrifuged for 15 s at 15700*g*. Buffer RDD and DNaseI [27 units (U)] were combined (7:1), added to the columns and incubated at room temperature for 15 min to eliminate any genomic DNA that was transferred from the interphase. The columns containing the RNA were washed with 350 µl RW1, transferred to new collection tubes, 500 µl RPE was added to the samples and centrifuged for 15 min at 15700*g*. The columns were placed in new collection tubes and the RNA was eluted with 30 µl RNase free water by centrifugation at 15700*g* for 1 min. This step was repeated in a new collection tube to ensure that all the RNA had been removed from the columns.

2.2.6 RNA concentration and integrity determination

RNA concentration was determined with a NanoDrop-1000 (Termo) at an absorbance of 260 nm. The purity of the RNA was indicated by the A_{260}:A_{280} ratio (absorbance of nucleic acids to contaminating proteins), which should be greater than 1.8 (163). The RNA samples were also analysed using the Experion automated electrophoresis system (Bio-Rad) to determine the quality and integrity of the RNA. RNA was prepared and processed as described in the manufacturer's instructions. A Lapchip microfluidic separation technology is used by the system, where fluorescent dyes bind to RNA and this is then detected (164). The system defines a RNA integrity number (RIN) or RNA Quality Indicator (RQI), which provide an accurate way of testing the RNA integrity. An advantage of the system is the small amount of sample that is needed per run (163). The RNA samples were stored at -70℃.

2.2.7 cDNA synthesis and clean up

A common reference design was followed in the microarray and a RNA reference pool (Figure 2.4) containing equal amounts (4 µg) of RNA was prepared from all the biological and technical replicates taken at all the time points for both the treated and untreated samples.

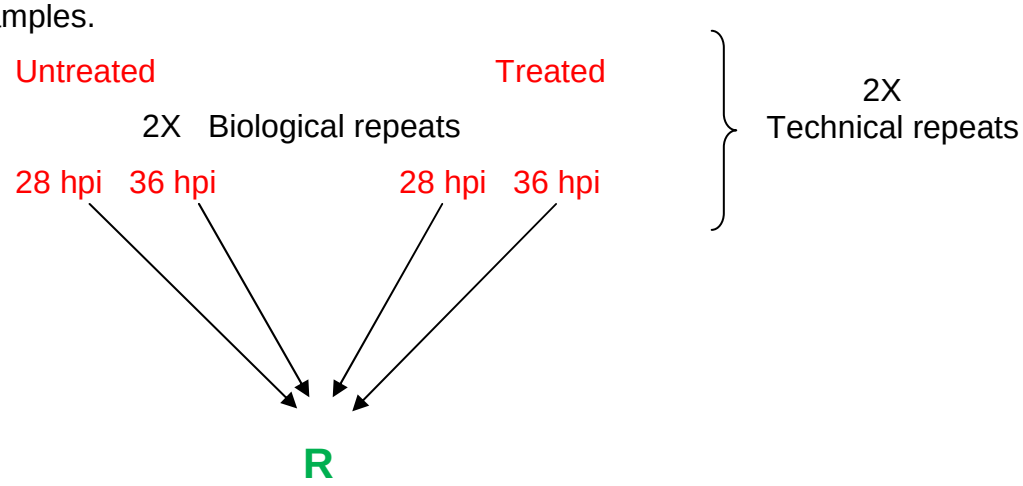

Figure 2.4 Common reference design used for the transcriptome investigation.
The reference (R) was labelled with Cy3 (green) and all the samples were labelled with Cy5 (red).hpi: hours post-infection.

For the synthesis of 1.5 µg of cDNA, 4 µg of RNA were used per sample, to which 775 pmol random nonamer primer (Inqaba) and 250 pmol oligo-dT (dT_{25}) (Inqaba) were added. The reaction was incubated at 70℃ for 10 m in and cooled on ice for 10 min. The protocol by Bozdech *et al.* (2005) (165) was used for the reverse transcription and amino-allyl incorporation with an adaption in the reaction time, as described in Van

Brummelen *et al.* (133). Superscript III RNase H^- reverse transcriptase (Invitrogen, 480 U), 100 mM DTT, 1xSuperscript first-strand buffer, 40 U rRNasin (RNAse Inhibitor, Promega) and dNTPs [1 mM dATP, 500 µM dCTP, 500 µM dGTP, 500 µM dTTP and 500 µM dUTP (Fermentas Life Sciences)] were added to the RNA–primer mixture and RNase-free water added to a final volume of 30 µl with RNase-free water. The mixture contained double the amount of dATPs and dAUP/dATPs because of the A/T rich genome of *P. falciparum*. The reaction was incubated for 20 h at 42℃, after which the RNA was hydrolysed with 0.5 M ethylenediamine tetra-acetic acid (EDTA) and 1 M NaOH for 15 min at 65℃.

The reactions were cleaned using a Nucleo Spin II PCR Clean-Up kit according to the manufacturer's instructions (Macherey-Nagel). A buffer containing salts was added to the DNA to allow binding of the DNA to the silica through electrostatic interactions. The DNA was bound to a silica-based Nucleospin extract II column by centrifugation at 13000*g* for 1 min and the flow-through was discarded. The column was washed three times with an alcohol-based buffer to remove the salts and decrease the ionic strength of the solution. The DNA was subsequently eluted in preheated (37℃) water. The concentration of the DNA was determined using the ss DNA – 33 settings of the NanoDrop-1000 (Thermo).

2.2.8 Cy dye labelling of the cDNA

The fluorescent dyes Cy5 and Cy3 (Amersham Biosciences) were dissolved in DMSO in the dark to a final volume of 13 µl. Newly synthesised cDNA (1.5 µg) was dried under vacuum and then dissolved in 2.5 µl sterile, deionised distilled water. To each sample, 5 µl Na_2CO_3 was added followed by 2.5 µl of the corresponding Cy-dye. The treated and untreated samples were labelled with Cy5 and the reference pool was labelled with Cy3 and incubated at room temperature for 2 h in a dark dessicator to ensure efficient labelling. During cDNA synthesis, the amino allyl-dUTP/UTP is incorporated into the cDNA and thus when adding the Cy-dyes, the N-hydroxysuccinimideester of the monoreactive Cy-dye interacts with the amino group on a 2-carbon spacer that is attached to the methyl group of the dUTP. Excess dye was removed after the labelling step by using the QIAquick PCR purification kit (Qiagen). The kit has the same principles as the Nucleo Spin II PCR Clean-Up kit (Macherey-Nagel) explained in section 2.2.6. The extent of dye incorporation and the concentration of each sample

were determined using the microarray settings of the NanoDrop-1000. The labelling efficiency was determined using the efficiency formula (Equation. 2.1). The labelling efficiency should be at least 10 sufficiently labelled nucleotides out of 1000 nucleotides for successful hybridisation.

$$\text{Labelling efficiency} = \frac{\text{pmol dye} \times 324.5 \text{ pg/mol}}{\text{ng DNA}} \quad \text{.....Equation 2.1}$$

where 324.5 pg/mol is the average mass of a dNTP.

2.2.9 Hybridisation, set up of slides, washing of slides and scanning

The two-colour microarray-based gene expression analysis protocol for an Agilent microarray platform was used for the hybridisation and washing steps. For the hybridisation, 20 pmol of each Cy-dye labelled sample and reference (Section 2.2.7) was used. The sample reference, 1xblocking buffer (Agilent, proprietary mix) and 1xfragmentation buffer (Agilent, proprietary) were mixed and incubated for no longer than 30 min at 60℃. GE hybridisation buffer (2x, Agilent) was added to each sample and mixed by inverting. The samples were loaded onto a SureHyb® gasket slide, which was placed in the slide hybridisation chamber. The Agilent microarray platform was placed onto the loaded SureHyb® gasket slide, with the active side facing the gasket slide. The hybridisation chamber was tightly closed while it was ensured that bubbles in each chamber of the gasket slide were able to move freely when turned. The hybridisation was performed at 65℃ in a hybridisation oven (Agilent) for 17 h at a rotation speed of 10. After the hybridisation, the slide was washed twice with wash buffer 1 (Agilent) for 1 min each, followed by washing using preheated (37℃) wash buffer 2. The slide was dried by centrifugation for 1 min in a slide centrifuge and scanned using an Axon GenePix 4000A scanner (Molecular Devices).

2.2.10 Slide design

The *P. falciparum* Agilent platform, containing 60-mer gene probes, was designed by Mr J.C. Verlinden (166) since it was not commercially available in 2008. The original *P. falciparum* Operon Array contains 8089 70-mer gene probes. All unnecessary oligonucleotide sequences (total of 1085 gene probes) corresponding to the 'NUL' annotations and controls specific to the Operon platform were removed. The remaining

7004 70–mer oligonucleotides were adapted to create the 60-mer Agilent platform by shortening the 70-mer sequences to the 60-mer length. The 10-mer sequence shortening was done in a scanning window (10-mer) from both the 3' and 5' ends. Annealing temperature (Tm) restrictions were applied to keep the annealing temperature close to 65℃ for microarray hybridisat ion, using the following equation.

Tm = 64.9℃ + 41℃ (GC-16.4)/N..... .....Equation 2.2

GC - Number of G and C nucleotides in specific sequence.
N - Total length of the sequence in nucleotides.

Validation of the shortened sequences was done by submitting the target sequence for NBLAST analysis (www.ncbi.nlm.nih.gov/BLAST). All sequences submitted for NBLAST analysis had E-values similar to the 70-mer probes they were derived from and all E-values were below 10^{-6}. Furthermore, the most recent annotated version of *P. falciparum* genome at the time of design (PlasmoDB v 5.4) (www.plasmodb.org) was used to design the 60-mer based Agilent array in addition to the adapted *P. falciparum* Operon Array. This was done to overcome ambiguities in previous annotations used for the Operon array dataset. FASTA files were submitted to ArrayOligoSelector (AOS) which was used to design 60-mer probes from the various target sequences (http://arrayoligosel.sourceforge.net/). The specificity of the 5445 newly designed target sequences to their respective Gene ID and the validation of these sequences were once again done using NBLAST analysis. The resultant in-house designed *P. falciparum* Agilent arrays contained a total of 12468 unique descriptors, which were synthesised and printed by Agilent onto microarray slides (Agilent).

2.2.11 Microarray Data Analysis

Axon GenePix Pro 6.0 software (Molecular Devices) was used for the analysis of the microarray slides. GenePix flagging automated spot detection parameters (Table 2.1) were applied in combination with visual inspection to assess spot quality. The flagged spots received a zero weight value.

Table 2.1 Parameters implemented for spot finding using GenePix.

Parameter	Function[a]	Flag
Circularity of spots	[Circularity] < 40 Or [F Pixels] < 50	Bad
CV of scan channels	[F532 CV] > 400 Or [F635 CV] > 400	Bad
Intensity	[F532 Mean] < 150	Absent
Saturation	[F532 % Sat.] > 20 Or [F635 % Sat.] > 20	Bad
Signal to noise ratio	[SNR 532] < 3 And [SNR 635] < 3	Bad

[a] – The mathematical function used in GenePix.
Circularity – Measure of the shape of spot, F Pixels – Minimum number of pixels for an intensity measure, CV – Coefficient of variation, 532 – 532 nm is the red channel, 635 – 635 nm is the green channel.

The microarray data were further analysed using the Linear Models for Microarray data (LIMMA) algorithm within the program R (http://www.r-project.org/) (167, 168). These packages are freeware from Bioconductor (www.bioconductor.com). Background correction was performed following a spot offset of +50 (169). Each array was normalised using robust spline normalisation, and between-array normalisation was done with Gquantile normalisation due to the common reference design of the experimental set-up (167). The two channels (red and green) must be normalised relative to one another before the interpretation of the data. If this is not done the ratio between these two channels will be biased, and thus the relative expression profiles of the samples will not be correct. The labelling efficiencies may lead to an imbalance between the two dyes, as well as the scanning process and settings. It is best to compare the dyes as a function of the intensities as the difference between the two channels is more complicated than simple scanner settings adjustments. Between-array normalisation is needed where the intensities are normalised with one another to be able to compare all the arrays with one another. Within-array normalisation, in which the M-value ($\log_2$ ratio values) for each array is normalised independently of the other arrays, is also required. The first step in normalisation is the correction of the background making use of the log-ratios of expression (M-value; Equation 2.3) and the overall brightness (A-value; intensity) of the specific spot (Equation 2.4) (167).

$$M = \log_2 R - \log_2 G \quad \text{.....Equation 2.3}$$

$$A = (\log_2 R + \log_2 G) / 2 \quad \text{.....Equation 2.4}$$

Where M (minus) is the $\log_2$ ratio values and A (addition) is the $\log_2$ intensity for each array.

R = Red intensity of spot.

G = Green intensity of spot.

The $\log_2$ are used to indicate a 2 fold change for M and a 2 fold increase for A (167).

Pearson correlation coefficients between the different time points of RNA isolation were determined. Genes with transcript abundance greater than 1.7-fold (log_2 ratio ≥ 0.75 or ≤ -0.75) in either direction, were considered as differentially affected. Transcripts with calculated p-values < 0.05 were regarded as significantly differentially affected. Differentially affected transcripts were submitted to PlasmoDB 6.0 (http://www.plasmodb.org) (170) and their gene ontology (GO) terms were obtained. The biological function and GO terms of each transcript were used for manual clustering. These clusters were submitted to DAVID (http://david.abcc.ncifcrf.gov) (171) and MADIBA (http://www.bi.up.ac.za/MADIBA) (172) to verify the GO terms and to determine the metabolic pathways affected. CLUSTER 2.1.1 (http://rana.stanford.edu.software) was used for hierarchical clustering. Only the transcripts differentially expressed in both Galvestine-2 and A51B1C1_1 datasets were used for clustering. Average linkage clustering and uncentered symmetric correlation were used for the clustering and the data was visualised in TREEVIEW 1.6 (www.EisenSoftware/ClusterTreeView/TreeView).

2.2.12 Inter-species annotation transfers using non-homology based clustering.

Interspecies comparisons of DNA microarray data are not trivial. As such, a comparison method was designed specifically to compare *Arabidopsis* and e.g. *Plasmodium* datasets (Collaborators E Maréchal and L Bréhélin) (173). Because of the low homology of *P. falciparum* transcripts to those of other organisms, non-homologue based methods have been developed. COCO follows the guilt-by-association principle for comparisons of gene expression datasets and functional annotation transfers. Using COCO, comparisons were performed by collaborator L Bréhélin (CNRS, France) between the differential transcriptome datasets of *P. falciparum* treated with A51B1C1_1 and *Arabidopsis* treated with Galvestine-2.

2.2.13 Quantitative qRT-PCR to validate microarray data

The primers used in quantitative Real-Time Polymerase Chain Reaction (qRT-PCR) were designed using the program Oligo 6.7. The primers were designed to have a Tm of about 55℃ (174) and a product length of approxi mately 150 nucleotides (nt) (Table 2.2).

cDNA from 36 hpi samples was used for the qRT-PCR and was diluted to a starting concentration of 0.65 ng/ml. A standard curve was constructed using lactate dehydrogenase (LDH) as household gene. KAPA SYBR Fast qPCR kit was used in 384-well qPCR plates containing 5 µl Kappa mix, 0.1625 ng/µl of template and 5 pmol of each primer. Controls that did not contain any cDNA were included. Each reaction was done in triplicate in a Light Cycler 1.5 (Roche). The reactions were pre-incubated for 10 min at 95℃, followed by 48 amplification cy cles consisting of 95℃ for 10 s (denaturation), 55℃ for 5 s (annealing) and extens ion at 72℃ for 7 s. Melting curve analysis was performed after amplification to exclude primer-dimer interference byincubating the samples at 95℃ for 5 s followed b y 65℃ for 5 s and 95℃. Finally the reaction mixture was cooled down to 40℃ for 30 s. Fold-change comparisons were performed for the treated and untreated samples. Normalisation was done to LDH, the transcript levels of which showed no change in expression levels in any of the time points or between the treated and untreated and may be considered as a household gene. This gene has been used as a housekeeping gene in previous studies as well (175).

Table 2.2 Primers used for the validation of microarray differential transcriptome profiles with qRT-PCR.

Gene	Primers	PlasmoDB ID	Primer Sequence (5' – 3')	Primer length (nt)	Product size (bp)	Tm (℃) [a]
Lactate dehydrogenase	LDHf	PF13_0141	GATTTGGCTGGAGCAGATGTA	21	169	58
	LDHr		CAACAATAATAAAAGCATTTGGACAA	26		55
Cyclophillin	CYCLOf	PFE0505w	AATTCTTTGACCATCTTAATCATTC	25	167	55
	CYCLOr		CAAAACAATTTTACTTCCTTGGGTTA	26		57
Seryl tRNA synthetase	Stsynf	PF07_0073	TTCGGCACATTCTTCCATAA	20	158	53
	Stsyn r		AAGTAGCAGGTCATCGTGGT	21		58
Ca/calmodulin dependent protein kinase2	Ca f	PF1885c	CGCATTGGAAGCATTACA TTCTA	23	154	57
	Ca r		ACATCTCATATTCATTGATGGACTG	25		58
Metacaspase-like protein	Me f	PF14_0363	AACACGAGCAGCAGATAACA	20	172	55
	Me r		AGAAGAATTAAAAGAAAACATACTAC	26		54
1-cys peroxiredoxin	PF08_0131f	PF08_0131	GTTTGTACCACTGAACTTGC	20	152	55
	PF08_0131r		TCCCACTTATCTAGGTTTCC	20		55
Putative transcription factor with AP2 domain	PF07_0126f	PF07_0126	AGATGGCATAATGTATGATG	20	151	51
	PF07_0126r		GAACTCCTGGTTCTAAATG	19		52
Conserved *Plasmodium* protein unknown function	MAL13P1.130f	MAL13P1.13	CGTACTATTTTGATGACCC	19	148	52
	MAL13P1.13rf		CCTTCGGAATGATATACTTC	20		53
Hypothetical protein	PF11_0278f	PF11_0278	TTACATTTTGATGGTCATCC	20	151	51
	PF11_0278r		GATCCGTATCGTAGGCAC	18		56

a -Melting temperature was calculated with the formula: $T_m = 69.3 + (0.41 \times \%GC) - (650/\text{primer length})$ (174). F/f - Forward primer, R/r – Reverse primer.

2.3 Results

2.3.1 IC_{50} determinations

Dose-response curves were established to determine the median inhibitory concentration (IC_{50}) of the herbicide derivative A51B1C1_1 using a fluorescent SYBR Green I assay (MSF assay) on the chloroquine-sensitive *P. falciparum* strain 3D7. The average IC_{50} value of A51B1C1_1 determined in four individual experiments was found to be 447 ±16 nM (Figure 2.5).

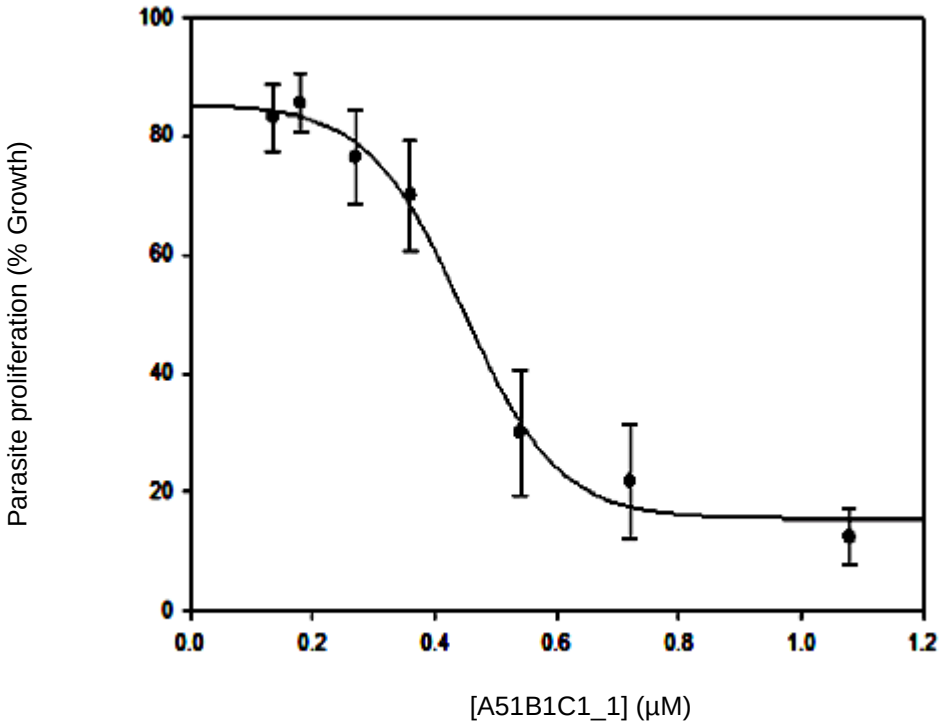

Figure 2.5 Sigmoidal concentration-response curve to calculate the median inhibitory concentration (IC_{50}) of *P. falciparum* (3D7) treated with A51B1C1_1.
Data are representative of 4 independent experiments performed in triplicate, ±SEM.

The morphological impact of A51B1C1_1 on *P. falciparum* parasites was determined next.

2.3.2 Morphology studies

Two independent *P. falciparum* (3D7) parasite cultures were treated at 2xIC_{50} A51B1C1_1 and Galvestine-2 (Data for Galvestine-2 treated *P. falciparum* were obtained from a previous study by Mr J.C. Verlinden (166) and was included in this study as an additional analogue of the Galvestine-1 parent compound) and the effects on the morphology of the parasites were observed for 72 h. The parasites were treated

at the invasion stage (merozoites/early rings) and samples were taken every 2-4 h. The morphology of the treated parasites was compared to that of control parasites (treated with DMSO) as shown in Figure 2.6.

Both treated cultures remained morphologically similar to the control culture up to 12 hpi. However, Galvestine-2 treated parasites showed morphological changes after 24 hpi and after 36 hpi the parasites additionally showed a decrease in the rate of development. At 60 hpi the parasites in the Galvestine-2 treated culture entered the schizont/merozoite stage, whereas the control culture already developed into rings in the subsequent life cycle at the same time point. Although Galvestine-2 had a lagging effect on the parasite's life cycle development, parasites treated with this compound did not show complete life cycle arrest at the concentrations tested, even after 60 hpi.

In contrast *P. falciparum* parasites treated with A51B1C1_1 continued to show similarities to the control culture through the ring stage and early trophozoite stages. However, at 48 hpi, the control untreated parasites entered the merozoite stage, but the A51B1C1_1 treated parasites became pyknotic and remained so for the rest of the life cycle and was unable to progress to a new life cycle. These parasites could not invade new erythrocytes and form new rings, unlike the control culture.

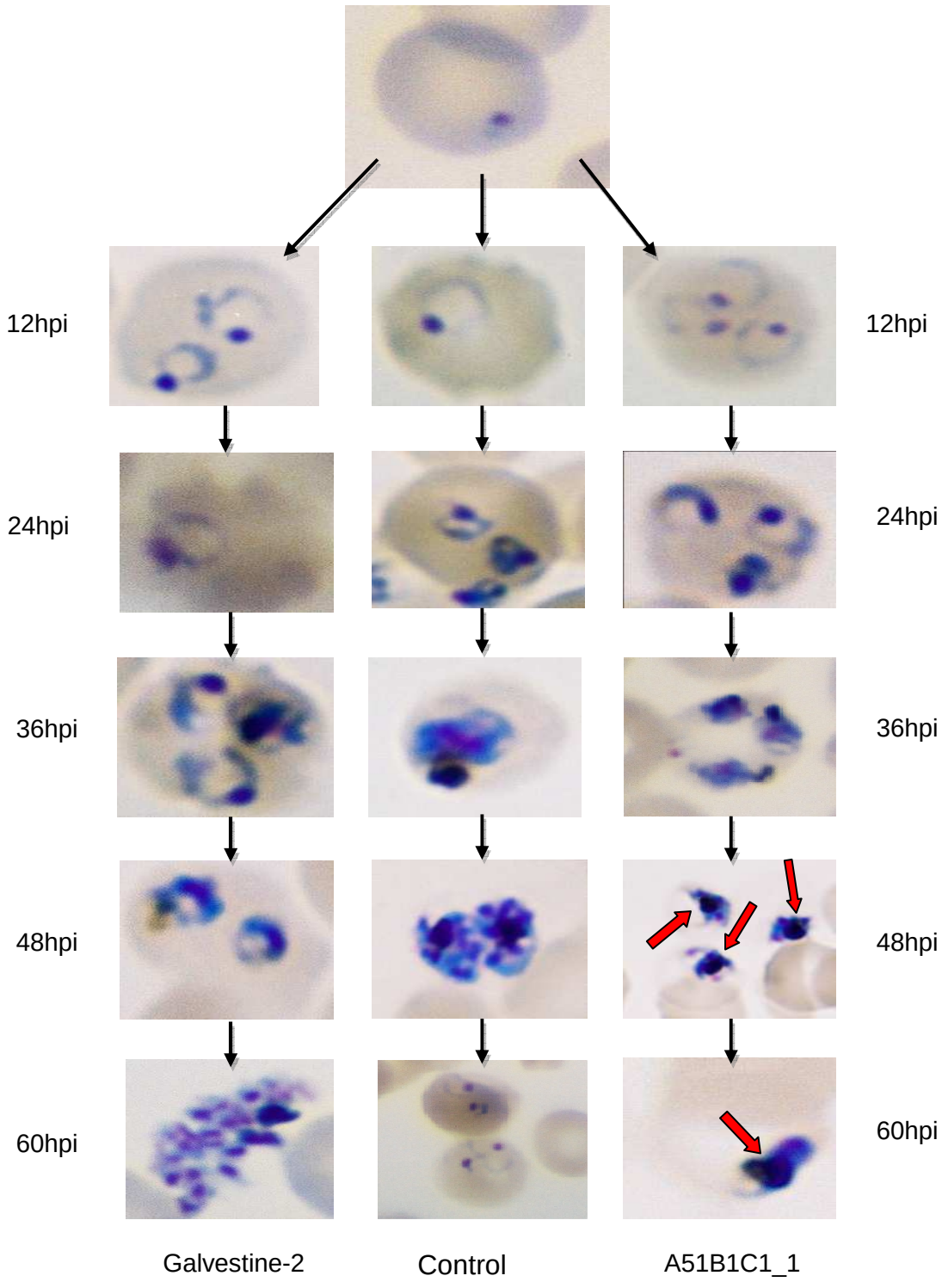

Figure 2.6 Morphological study of *P. falciparum* 3D7 parasites over 72 h after treatment with A51B1C1_1 and Galvestine-2.

After 24 hpi the Galvestine-2 treated culture showed a decrease in the rate of development, but still continued with the life cycle. The Galvestine-2 culture reached the merozoite stage after 60 hpi, whereas the control culture was already at the ring-stage of the next development cycle. The A51B1C1_1 treated culture showed signs of stress after 48 hpi and after prolonged incubation, the stressed parasites became smaller (pyknotic) (red arrows).

The morphological monitoring of the two compounds was repeated in two independent experiments and graphical analyses were used to delineate the time point at which growth inhibition by the compounds occurred (Figure 2.7).

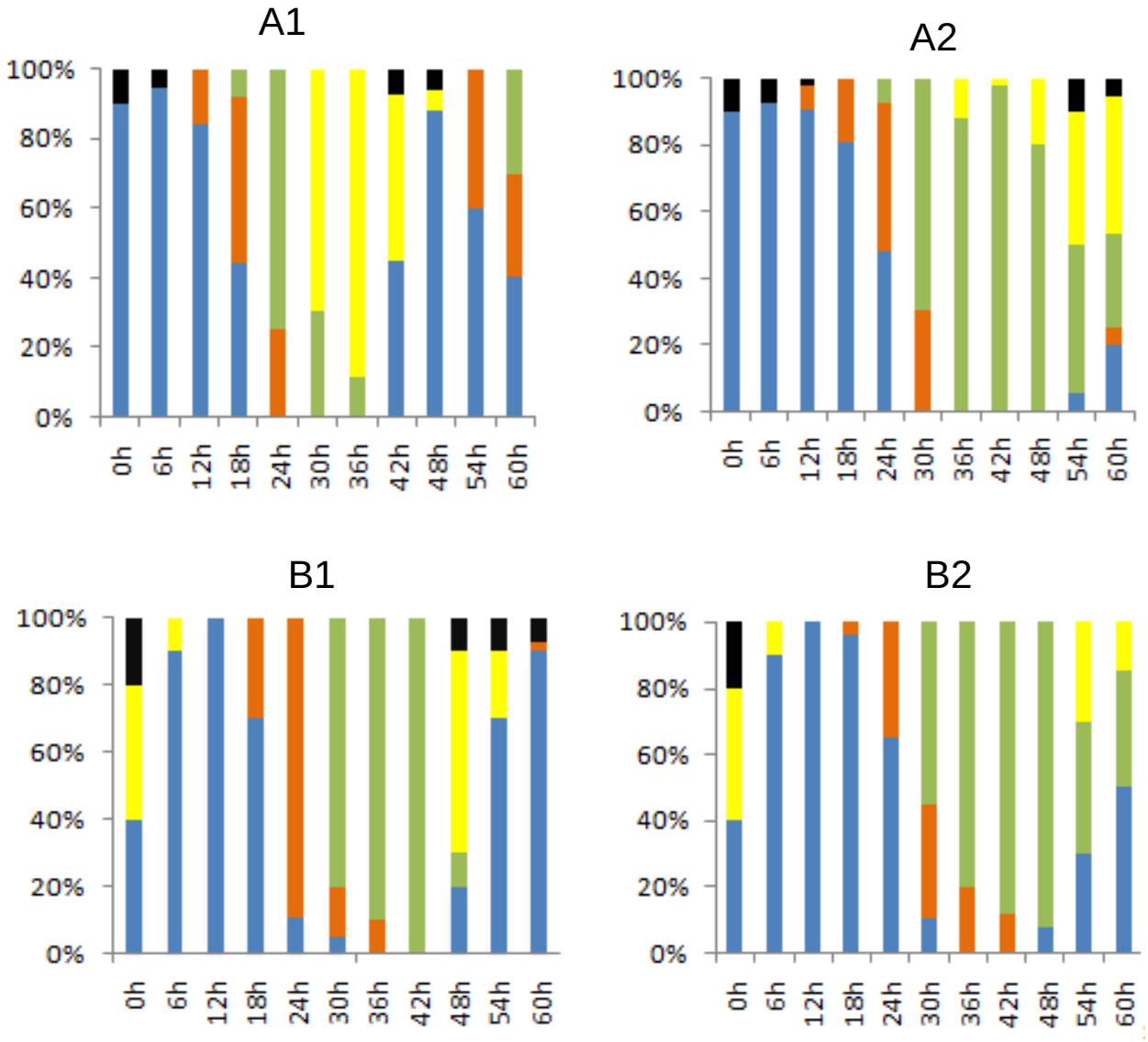

Figure 2.7 Graphical analyses of intra-erythrocytic development of *P. falciparum* (3D7) parasites after treatment with herbicide derivatives.

Untreated parasites (A1 and B1) were morphologically compared to parasites treated with 2xIC_{50} of either Galvestine-2 (A2) or A51B1C1_1 (B2). Parasite cultures were microscopically monitored every 6 h with ring stage parasites characterised as ring shaped single nucleated parasites (blue), trophozoites as dark stained parasites containing prominent haemozoin crystals but without multiple nuclei (Orange: Early Trophozoites, Green: Trophozoites), schizonts contained haemozoin as well as distinct multiple nuclei (Yellow) and merozoites are indicated in black.

The parasites treated with A51B1C1_1 showed a decrease in growth rate after 36-42 hpi. The parasites did continue to grow at this slow rate and schizonts formed only after 54 hpi. However, not all the parasites entered this developmental stage with the majority (40%) remaining as trophozoites. After 48 hpi, the parasites showed clear

stress characteristics, whereas the control culture already had 60% of parasites in the schizont stage after 48 hpi and only 10% trophozoites remained.

For Galvestine-2, the change in parasite morphology was not as noticeable as for compound A51B1C1_1, but the parasites did show a decrease in the rate of growth. Some of the parasites entered the schizont stage at 40 hpi, about ±10 h later than the control culture and the release of merozoites only occurred at 54 h, 12 h later than the control culture.

2.3.3 RNA isolation

After the data from the morphology studies were analysed, two time points were selected: time point 1 at 28 hpi and time point 2 at 36 hpi. Samples of treated and untreated, control *P. falciparum* cultures (10 ml) at 10% parasitaemia and 5% haematocrit were taken at these time points and RNA was isolated. Eight samples were chosen randomly to confirm the integrity and purity of the RNA using the Experion system (Bio-Rad). The virtual gel image is shown in Figure 2.8 (176). The dark bands at about 3500 and 2000 bp (indicated by black arrows) represent the 18S and 28S rRNA units without excessive smears, which would have been indicative of RNA degradation or DNA contamination (177). The small band at 50 bp is the internal standard included in the sample buffer used by the Experion software to align the sample on the virtual gel. The faint band in all the lanes a few bp smaller than 200 bp are the 5S rRNA in each sample.

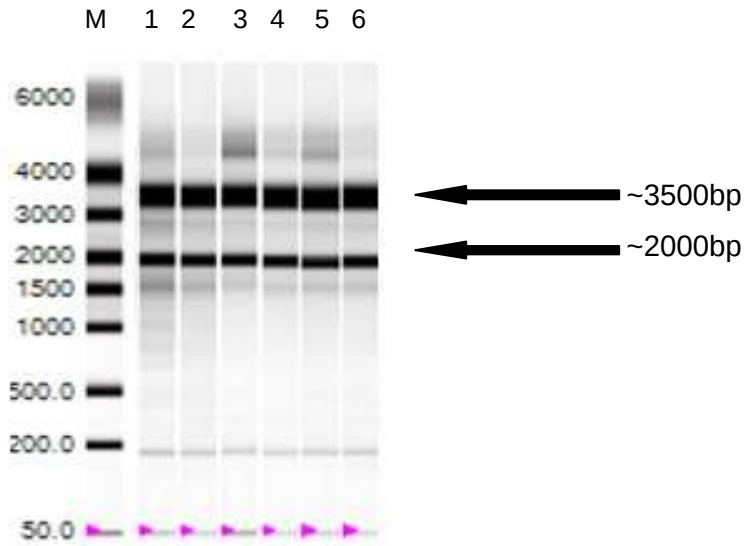

Figure 2.8 The virtual gel image indicating the purity of the RNA.

Lane 1:Control Biological Rep 1 Time point 1 (8.9;1.44), lane 2: Control Biological Rep 1 Time point 2 (9.2;1.5), lane 3: Control Biological Rep 2 Time point 1 (9.7;1.51), lane 4: Control Biological Rep 2 Time point 2 (9.7;1.52), lane 5: Treated Biological Rep 1 Time point 2 (9.6;1.48), lane 6: Treated Biological Rep 2 Time point 2 (9.6;1.58), M is the Molecular marker. The numbers in brackets represent the RQI number and the 28S/18S ratio, respectively. The band at 50 bp is the standard included in the sample buffer supplied by the manufacture. The bands in all the lanes just smaller than 200 bp indicate that trace amounts of 5S rRNA are present in each sample. The 18S and 28S rRNA units are the clear and dark bands at about 3500 and 2000 bp (indicated by black arrows).

The gel image indicates the presence of small amounts of contaminating DNA and RNA degradation products other than the large bands at ~3500 bp and ~2000 bp in lane 1, lane 3 and 5. To determine if the RNA from these samples were still of useful quality, electropherogram data from the Experion system were analysed (Figure 2.9). Peaks representing the 18S and 28S ribosomal RNA (rRNA) units are observed in RNA samples of high purity as most of the 5S rRNA unit has been removed during the RNA isolation with the RNeasy kit (Manual Qiagen 2006). The small peaks/smears before the 18S peak, 20-40 s region (s=running time) are generally indications of RNA degradation. Small peaks between the 18S and 28S peak usually indicate the presence of small amounts of 28S RNA breakdown products. DNA contamination would have been indicated as peaks or smears after the 28S peak if present, which was not the case in these isolations (177).

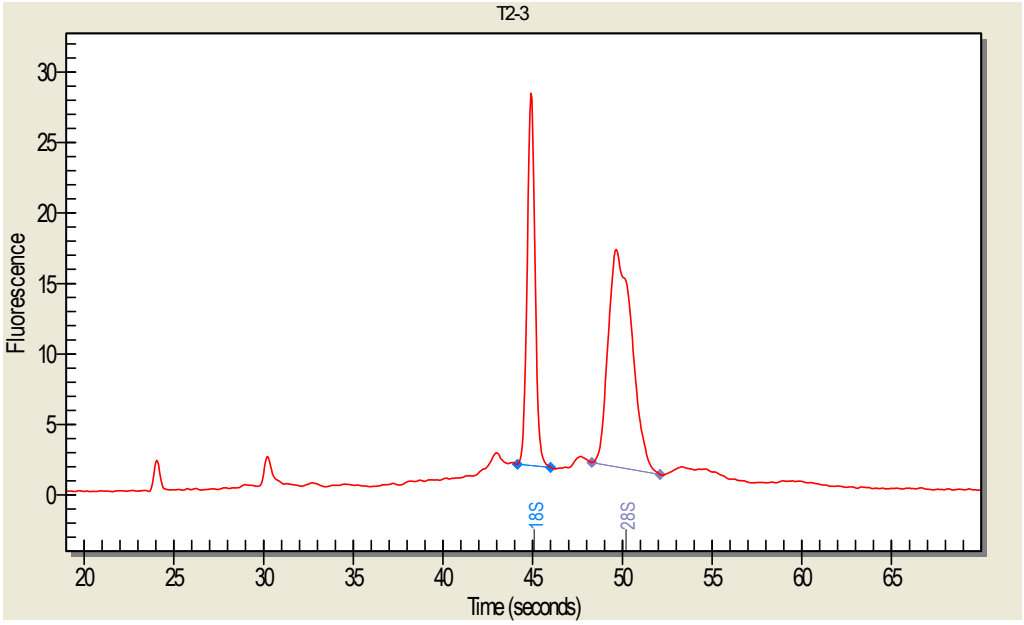

Figure 2.9 The electropherogram as an indication of the purity of the RNA.
Small peaks and smearing between 20-40 seconds (Running time) are degraded RNA. Peaks between the 18S and 28S peaks are products of 28S rRNA degradation. Any peaks and smears after the 28S peak is usually DNA contamination.

The gel image and the electropherogram indicated that the RNA samples are acceptable for use in microarray studies and that degradation is minimal. No DNA contamination is visible as there are no peaks between 55–70 s region. Additionally, an indication of the quality of the RNA can be obtained through RQI values, where a value of 10 refers to RNA of high purity and 1 is an indication of fully degraded RNA. The RQI numbers, 28S/18S ratio and the concentration of the tested RNA samples isolated are indicated in Table 2.3 as a summary.

Table 2.3 The quality and purity of the RNA sample tested on the Experion.

RNA Sample	Lane no.*	28S/18S ratio[a]	RQI number[b]	Concentration ng/µl
Control Biological Rep 1 Time point 1	1	1.44	8.9	248.12
Control Biological Rep 1 Time point 2	2	1.5	9.2	269.55
Control Biological Rep 2 Time point 1	3	1.51	9.7	145.56
Control Biological Rep 2 Time point 2	4	1.52	9.7	249.22
Treated Biological Rep 1 Time point 2	5	1.48	9.6	235.6
Treated Biological Rep 2 Time point 2	6	1.58	9.6	245.52

a - Ratio of the ribosomal bands (28S:18S) which should have a ratio of 2.0 for high quality RNA.
b - RNA Quality Indicator.
*- Corresponding lane numbers to the virtual gel image in Figure 2.11.

The 28S/18S ratio and the RQI number of each RNA sample in Table 2.3 confirm the results in Figure 2.8 and Figure 2.9. The RNA samples all have RQI values of >8, which is an indication of pure, high-quality RNA.

2.3.4 Microarray

Transcriptome profiling of *P. falciparum* 3D7 parasites treated with A51B1C1_1 was performed with the in-house designed 8x15K *Plasmodium* Agilent microarray platform (166). A reference design was used during the microarray experiment, which included a reference pool of all the samples that was hybridised with the various samples. Figure 2.10 provides an example of an Agilent array and the difference between the treated and the control arrays at the same time point (time point 1 at 28 hpi).

The most prominent difference between the arrays of the control and the treated parasites was the overall colour. The treated arrays had a yellowish colour which is associated with the differences in expression of transcripts in the control and treated samples as the parasites progress through their life cycle (133). These differences are visible on the enlarged sections included in Figure 2.10. The majority of the spots on the treated array were either green or yellow, whereas the control array's spots were red, yellow and green. Agilent includes control spots on each corner of the array for quality control and the assessment of the hybridisation of the samples tested. These control spots include dark corners, which act as negative controls and light corners which acts as positive controls (Figure 2.10).

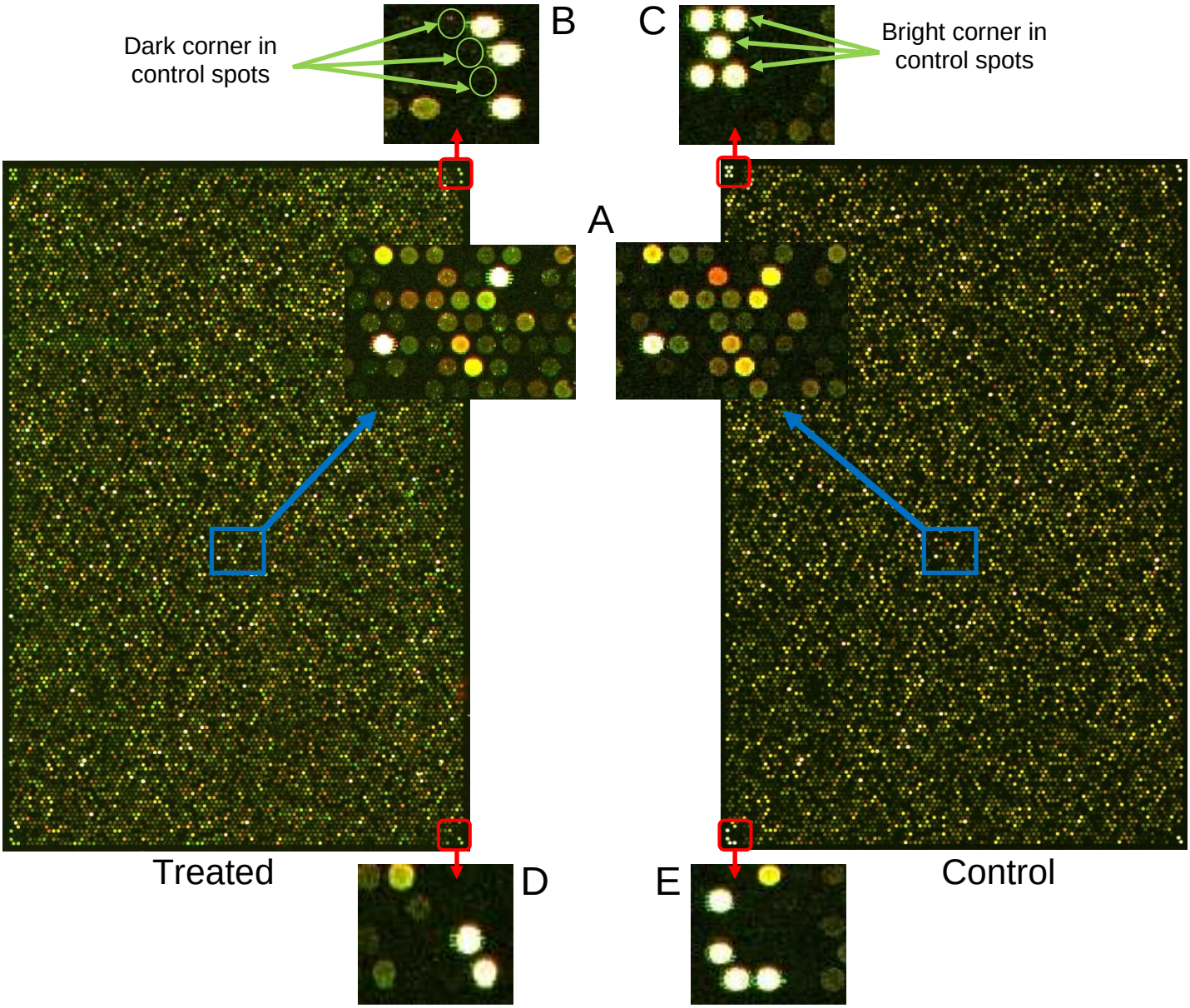

Figure 2.10 Agilent arrays of *P. falciparum* parasites treated with A51B1C1_1.
The overall colour of the treated array (left hand panel) consists of mostly yellow or green spots (enlarged section A). The control array (right hand panel) consists of red, green and yellow spots. This colour difference is because of the differences in transcript abundance between the treated and the control samples. Agilent includes controls on their slides to ensure quality control (enlarged sections B-E). The bright corners act as a positive control and should always be hybridised. The dark corners should always stay dark after hybridisation.

2.3.4.1 Data analysis

Analyses of the arrays were done using GenePix 6.0 and included spot finding and manual checking of the indicated spots. The parameters in Figure 2.11 were entered into GenePix 6.0 and saturated and bad quality spots were removed from the subsequent set of spots.

A

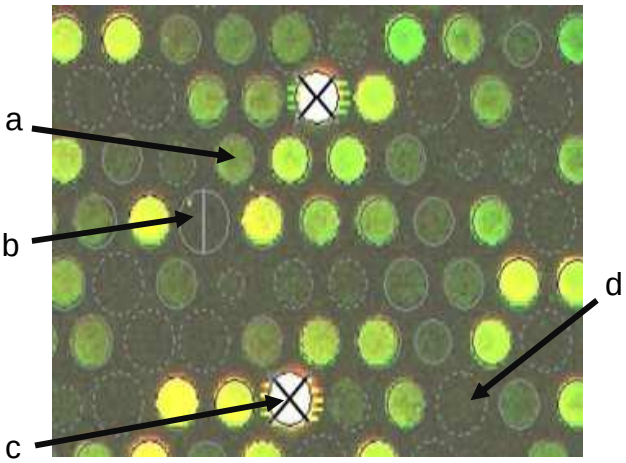

B

Parameter	Flag	% of flagged spots
Circularity of spots	Bad	0
CV of scan channels	Bad	0.1 – 2.5
Intensity	Absent	11.3 – 29.8
Saturation	Bad	0.5 – 2.1
Signal to noise ratio	Bad	15.8 – 36.1

Figure 2.11 The flag parameters used by the automated spot finding in GenePix 6.0.
A: a – Spot that was not flagged by any of the parameters (good spot). b – Spot that was flagged as absent, because of the low intensity. c – Saturated spot. d – Spot that was flagged bad by the signal to noise ratio parameter. B: The parameters set for automated spot detection and the percentage of spots flagged in each parameter.

The remaining spots were used in further analyses. Normalisation (Section 2.3.5.2), Pearson correlations and top table generations were done in R from the Bioconductor package (http://www.bioconductor.org), making use of LIMMA for the normalisation as described below.

2.3.4.2 Normalisation of data

Normalisation of the microarray data ensures that the effects that variation in technology gives to the data, are adjusted for accordingly and that only the true variation in biological samples are represented in the output data. The first step in normalisation is the correction of the background making use of the log-ratios of expression (M-value; Equation 2.3) and the overall brightness (A-value; intensity) of the specific spot (Equation 2.4) (167). Background correction was done for all 12 arrays in this experiment to ensure spots in the more intense background areas are not lost (Figure 2.12). The background intensity was subtracted from the foreground intensity of the different arrays to reduce the noise at an offset of +50.

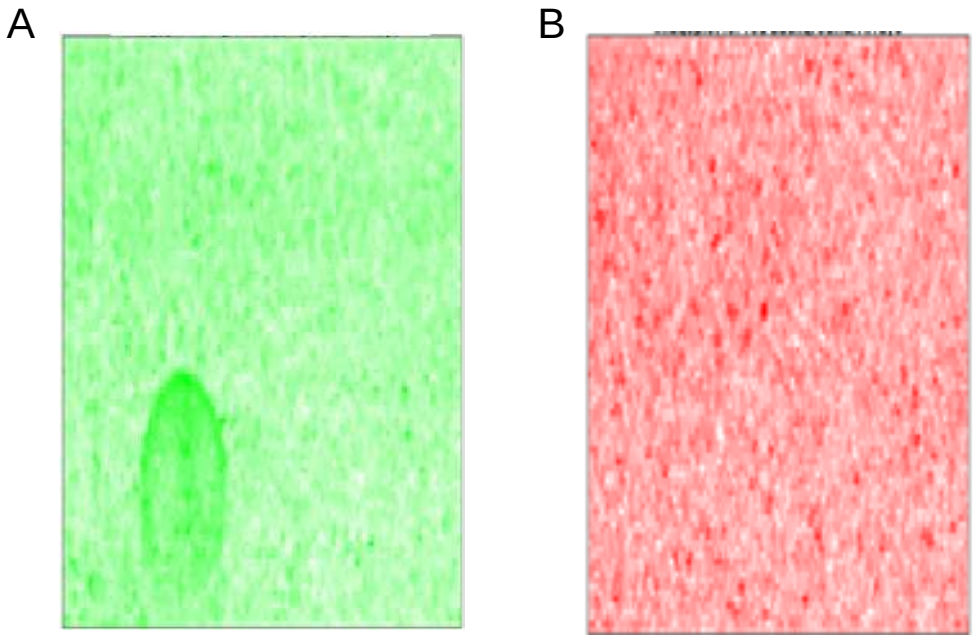

Figure 2.12 The background images of microarray experiment array 5 (treated sample time point 1).

A - The large oval artefact in the green channel only affects that specific channel. B - Speckling is seen in the red channel. The reason for speckling may be inadequate washing.

For within-array normalisation, in which M-values within a single array are normalised to correct for dye effects, either robust spline (empirical compromise between print-tip and global loess normalisation) or global loess (which assumes that the majority of probes are not differentially regulated) normalisation are currently accepted normalisation methods. The normalisation with global loess (Figure 2.13 C) suggested variation in box sizes, which result in an unequal contribution of each box to the overall dataset. The larger boxes have a larger influence on the data than the smaller boxes (167). When the data were normalised with robust spline, the boxes centre all at the same M-value and are similar in size. The outliers in the data are also accounted for without affecting the mean data.

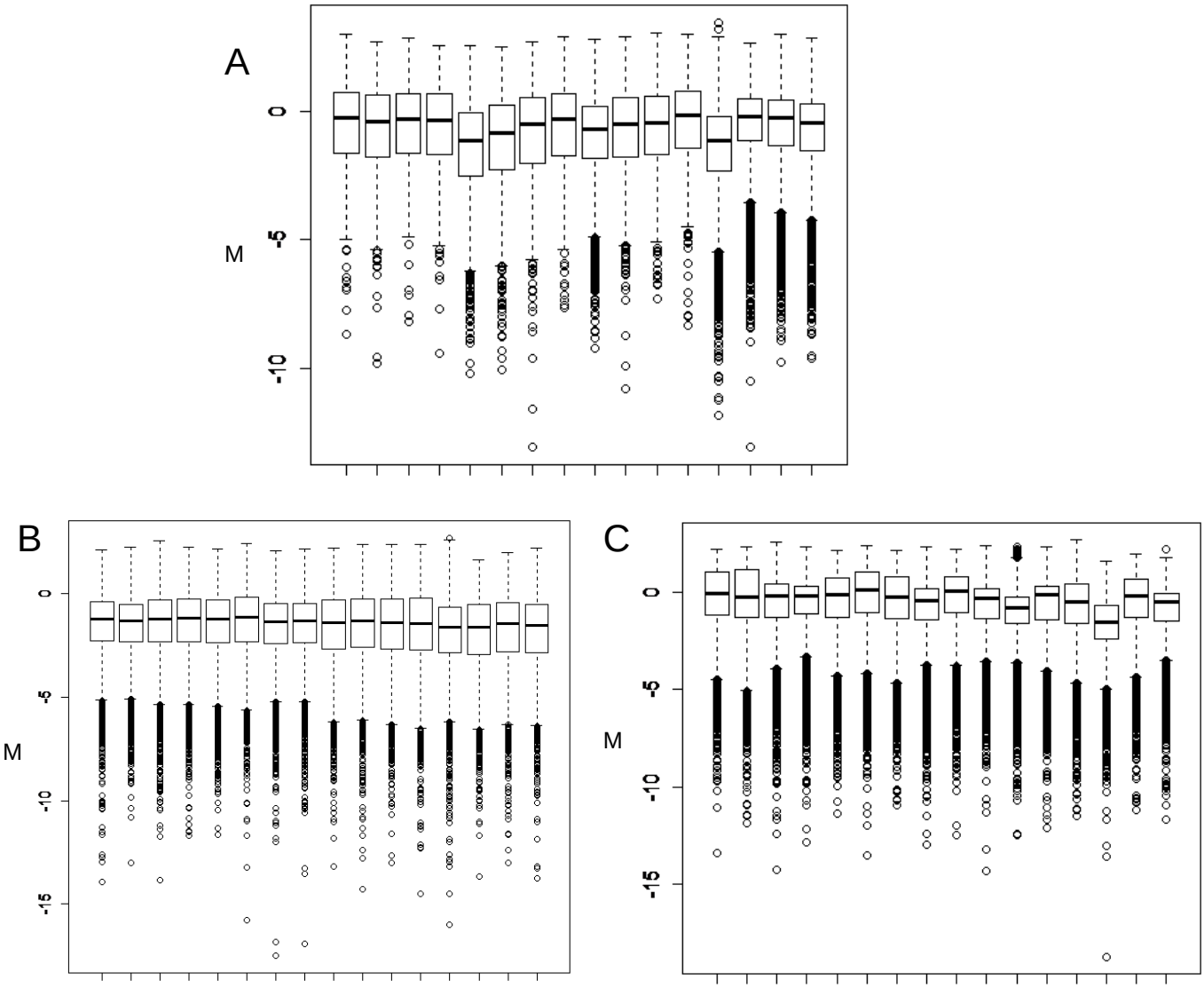

Figure 2.13 The box plots of all the arrays before and after normalisation using both robust spline and global loess.

A – The box plot before normalisation; B – The box plot after normalisation with robust spline and Gquantile; C - The box plot after normalisation with global loess and Gquantile.

Between-array normalisation normalises the individual (red and green) intensity values of the dyes between arrays. For between-array normalisation, Gquantile was used since all the samples were labelled with the same dye (Cy5, red) and the reference pool with Cy3 (green) (Figure 2.14). The density plot before normalisation showed no bias towards any channel, but after normalisation with Gquantile, it is clear that all the arrays were normalised against the reference pool (Cy3, single green line in Figure 2.14, B) which now allow comparison of the Cy5/Cy3 ratio (log_2-ratios). Comparatively, Aquantile normalisation produced the opposite effect.

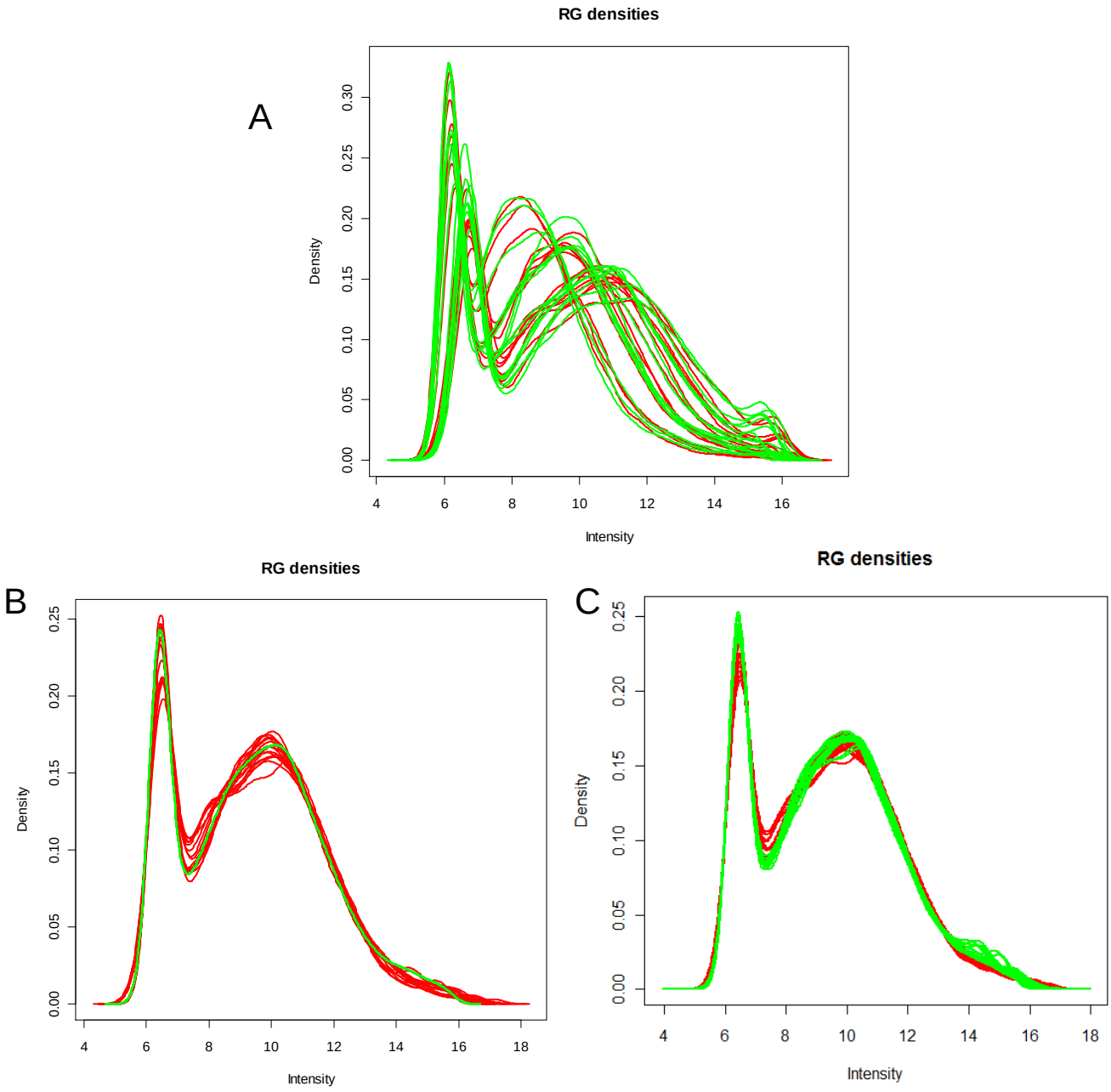

Figure 2.14 The density plots of all the arrays before and after normalisation using both Gquantile and Aquatile.

A – The density plot before normalisation; B – The density plot after normalisation with Gquantile and robust spline; C - The density plot after normalisation with Aquantile and robust spline.

MA-plots were generated (Figure 2.15 A and B) to confirm that the normalisation had the desired effect since the centre of distribution of the $\log_2$ ratios on these plots, should ideally be zero (178).

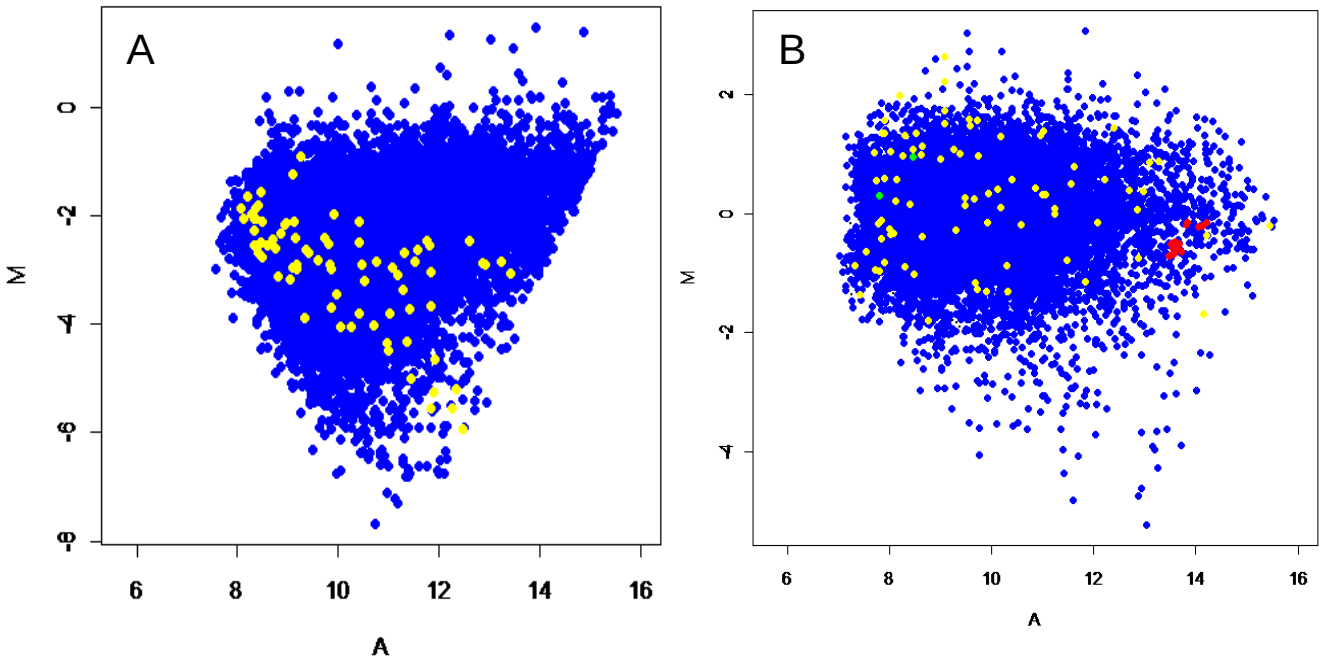

Figure 2.15 MA-plots of an array in the experiment.
A – Before normalisation, B – After normalisation with robust spline and Gquantile. The data post-normalisation fitted the ideal model better. The centre of distribution of the M-values is around zero.

After the necessary intensity distribution was achieved within and between arrays, Pearson correlations were determined for all the samples (Table 2.4). Pearson correlations indicate the relationship between datasets, with r=1 indicating closest fit and therefore where the average gene expression is best correlated with one another.

Table 2.4 The Pearson correlations for the microarray data of the treated and untreated samples of time point 1 (28 hpi) and time point 2 (36 hpi).

Comparison	Correlation (*r*)[a]
Control time point 1 vs. Treated time point 1	0.937
Control time point 1 vs. Control time point 2	0.263
Control time point 1 vs. Treated time point 2	0.338
Treated time point 1 vs. Control time point 2	0.168
Treated time point 1 vs. Treated time point 2	0.271
Control time point 2 vs. Treated time point 2	0.773

[a] – Correlation coefficient.

Each time points' control and treated samples correlated best with one another. Pearson correlation between control time point 1 and treated time point 1 was 0.937, but decreased to 0.773 between control time point 2 and treated time point 2. This decrease in correlation is an indication of the difference in the development between the control parasites and the treated parasites. The correlation between the untreated and untreated parasites at the specific time points allowed their direct comparisons.

2.3.4.3 LIMMA data analysis

LIMMA was used to identify differentially expressed transcripts from the datasets and generated top tables and volcano plots to indicate the distribution of transcripts that showed a change in abundance between the control and the treated parasite transcript sets. The $\log_2$ fold change ($\log_2$ FC) is an indication of the magnitude of change in abundance levels (increased or decreased) of a specific transcript at a specific time point. The cut-off of $\log_2$ FC values for this study was taken as ≥0.75 or ≤-0.75 ($p<0.05$).

The first time point did not show significant changes in the abundance of transcripts, thus further analysis was performed primarily at the 36 hpi time point. A volcano plot of the distribution of all the differentially expressed transcripts (Figure 2.16) indicated that there are a larger number of transcripts with a higher abundance compared to the number of transcripts with a lower abundance. In total, 1504 transcripts out of the 12468 oligonucleotides (12%) on the array were differentially regulated (1.7-fold change in differential expression levels in either direction). Of these, 805 transcripts (54%) showed decreased abundance (maximal decrease of up to $\log_2$ FC=-3.86) and 699 (46%) showed increased abundance (increased to $\log_2$ FC=1.8).

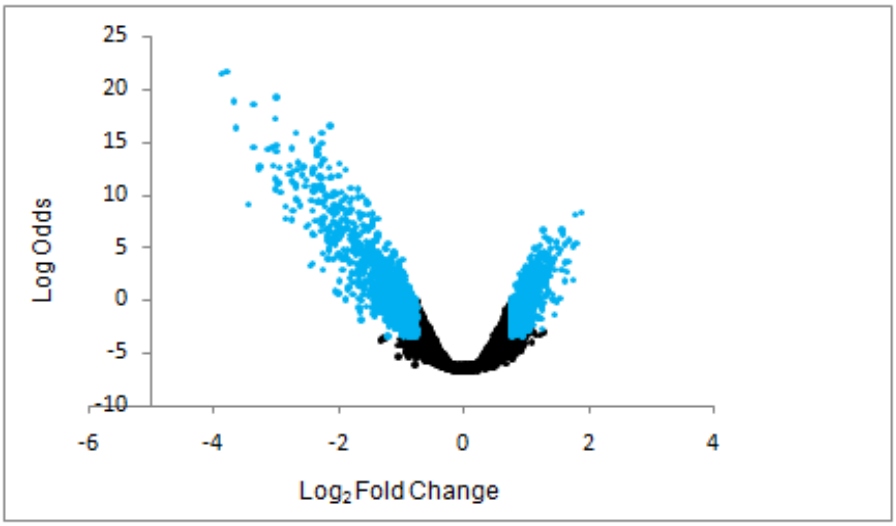

Figure 2.16 Compound A51B1C1_1 showed a high number of differentially expressed transcripts.

Of these transcripts, 805 showed a decrease in abundance and 699 an increase in abundance. The $\log_2$FC is an indication of the fold change in expression (up or down) of a specific transcript (≥0.75 or ≤-0.75; $p<0.05$). The log odds ratio indicates the confidence that the specific transcript is significantly up or down regulated.

A summary of transcripts with the highest differential abundance levels after treatment of *P. falciparum* parasites with A51B1C1_1 is provided in Table 2.5, with complete dataset of the 1506 differentially expressed transcripts provided in Appendix 1.

Table 2.5 Transcripts with highest decrease and increase in abundance (20 each) after treatment of *P. falciparum* parasites with A51B1C1_1.

PlasmoDB ID	Product Description	log_2FC[a]	Adjusted P-value[b]
	Decrease in abundance		
PF13_0173	Hypothetical protein	-3.86306	4.12E-10
PFL1435	Myosin d	-3.78196	4.12E-10
PF10_0344	Glutamate-rich protein	-3.66214	3.63E-09
PF13_0058	Hypothetical protein	-3.64398	2.48E-08
PF14_0102	Rhoptry-associated protein 1, rap1	-3.43429	3.78E-06
PFF1365cd	Hypothetical protein	-3.36262	9.27E-08
MAL13P1.49	Hypothetical protein	-3.35991	4.02E-09
PF14_0337	Hypothetical protein	-3.2534	3.07E-07
PFL2285	Hypothetical protein	-3.12808	9.87E-08
PFF0645	Integral membrane protein	-3.05472	9.27E-08
PF11_0278	Hypothetical protein	-3.01385	1.34E-08
PF14_0607	Hypothetical protein	-3.00148	1.29E-06
MAL13P1.130	Hypothetical protein	-3.00137	5.96E-07
PFC0185w	Hypothetical protein, conserved	-2.99443	9.22E-08
PF08_0035	Hypothetical protein	-2.99283	3.19E-09
PF10_0306	Hypothetical protein	-2.9906	1.07E-07
PF10_0039	Hypothetical protein	-2.96152	8.53E-07
PF10_0119	Hypothetical protein	-2.93718	3.22E-07
PFC0120w	Cytoadherence linked asexual protein, CLAG	-2.92824	1.55E-06
PF11_0373	Hypothetical protein	-2.85528	1.20E-05
	Increase in abundance		
MAL8P1.94	Hypothetical protein	1.450437	0.014454
PF11_0479	Hypothetical protein	1.473504	7.55E-05
PF13_0076	Hypothetical protein	1.491512	0.000101
PF14_0568	Hypothetical protein	1.491768	6.51E-05
MAL13P1.24	Hypothetical protein	1.517027	0.000176
PF07_0126	Hypothetical protein	1.526986	0.003866
PF14_0509	Hypothetical protein	1.540961	2.66E-05
PF11_0259	Hypothetical protein	1.549177	0.000127
PFE1150w	Multidrug resistance protein	1.567055	0.000536
MAL7P1.228	Hypothetical protein	1.576469	3.60E-05
PFB0645c	Ribosomal protein L13, putative	1.58619	2.66E-05
PFE1100	Hypothetical protein	1.61043	0.001052
MAL8P1.45	Hypothetical protein	1.617669	0.000299
PFE1095w	Hypothetical protein	1.622853	7.67E-05
PF13_0109	N2,N2-dimethylguanosine tRNA methyltransferase	1.663046	0.000312
PF11_0165	Falcipain 2 precursor	1.675169	5.75E-05
PF13_0011	*Plasmodium falciparum* gamete antigen 27/25	1.7377	0.00105
PFB0650w	Hypothetical protein	1.747555	9.62E-05
PFD1170	RESA-like protein, truncated	1.797368	7.38E-05
PFE1245w	Zinc finger protein, putative	1.87245	6.81E-06

[a] -The cut off of the log_2 FC $\geq$0.75 or $\leq$-0.75.

[b] - Adjusted p-value is an indication of the significance of transcripts statistically determined by LIMMA. A cut off of p<0.05 was used to avoid false positives.

2.3.4.4 Biological processes in which the differentially expressed transcripts are involved in.

For the further identification of the function of the differentially regulated transcripts, the dataset obtained from LIMMA (www.bioconductor.com) was compared to the information in web-based annotation programs including MADIBA (http://www.bi.up.ac.za/MADIBA), DAVID (http://david.abcc.ncifcrf.gov) and PlasmoDB (http://www.plasmodb.org). The transcripts were grouped according to their function in a specific biological process (Figure 2.17).

The largest clusters formed by the transcripts that decrease in abundance were the parasite-host interaction (50 transcripts), post-translational modifications (32 transcripts), transport (26 transcripts), proteolysis (24 transcripts) and lipid biosynthesis (7 transcripts). The largest clusters formed by the transcripts that increased in abundance were the RNA metabolism (63 transcripts), translation (40 transcripts), primary metabolism (37 transcripts) and post-translational modifications (32 transcripts). There were transcripts involved in lipid biosynthesis that showed a decrease in abundance as well (3 transcripts). The large number of transcripts with unknown function corresponds to the *P. falciparum* genome, where ~60% of the genes encode proteins with unknown function (137).

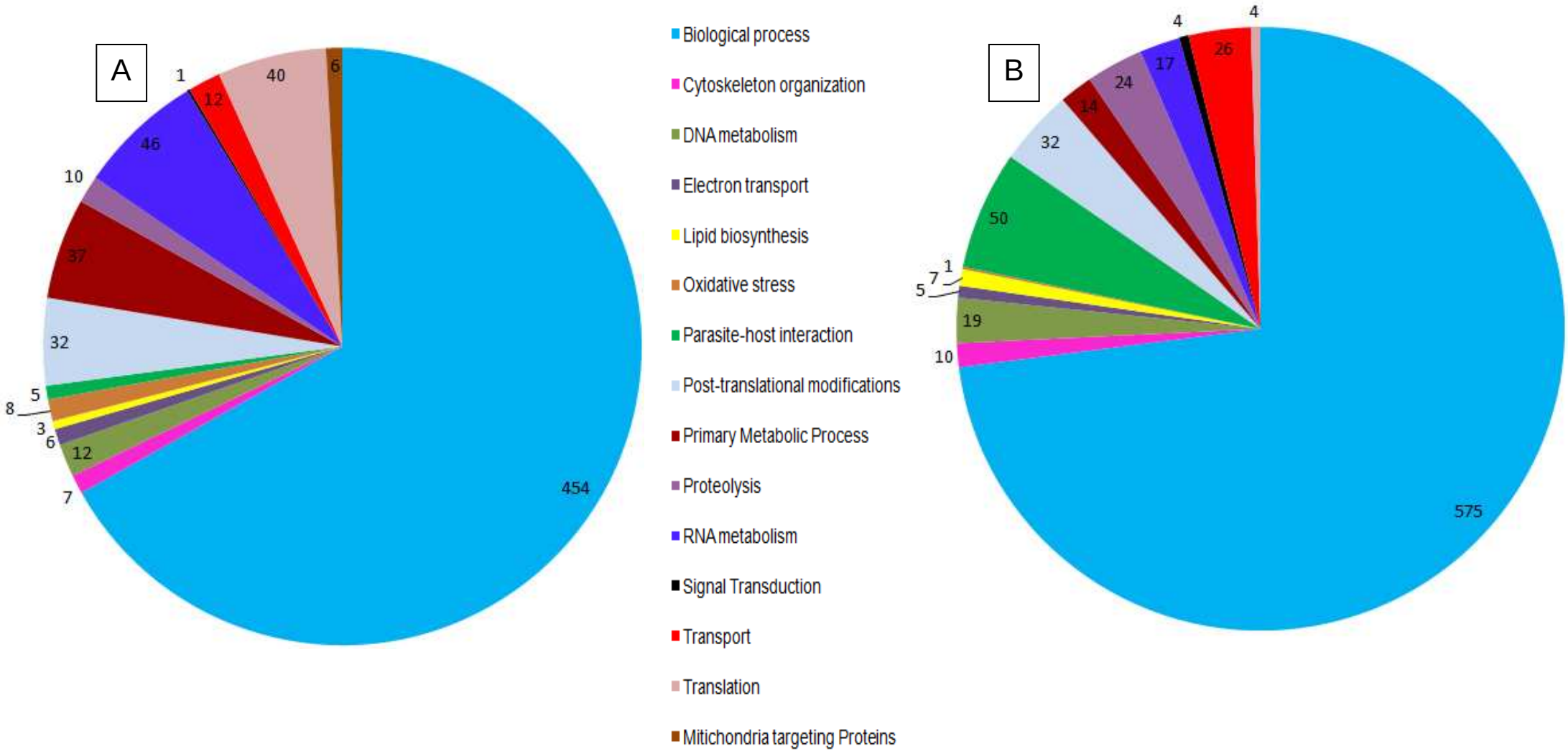

Figure 2.17 Gene ontology annotation of the differentially abundant transcripts after treatment of *P. falciparum* with A51B1C1_1.

A – The GO annotation clustering for the 805 transcripts that decreased in abundance. B – The GO annotation clustering for the 699 transcripts that increased in abundance.

Lipid, fatty acid and glycerophospholipid metabolism were included in the list of transcripts that showed changes in abundance (Table 2.6). The transcripts PFF0290w (long chain polyunsaturated fatty acid elongation enzyme), PF10_0016 (acyl CoA binding protein), PFL0415w (Acyl carrier protein) and PFC0050 (long chain fatty acid ligase) are involved in fatty acid biosynthesis. PFI1370c (phosphatidylserine decarboxylase), PFC0995c (DAG O-acyltransferase), PFI1485 (DAG kinase) and PF14_0097 (cytidine diphosphate-diacylglycerol synthase) are involved in glycerophospholipid metabolism. PF14_0020 and PFL1125 are transcripts that play a part in lipid biosynthesis.

Table 2.6 Differentially expressed transcripts involved in lipid, fatty acid and glycerophospholipid metabolism after treatment of *P. falciparum* parasites with A51B1C1_1.

PlasmoDB ID	Description	log_2FC[a]	Adjusted P value[b]	GO term[c]	GO cluster
Decrease in abundance					
PFF0290w	Long chain polyunsaturated fatty acid elongation enzyme, putative	-1.4	0.00257	GO:0019368	Fatty acid elongation,unsaturated fatty acid
PFI1370c	Phosphatidylserine decarboxylase	-1.2	0.00389	GO:0008654	Phospholipid biosynthetic process
PFC0050	Long chain fatty acid ligase, putative	-1.2	0.00378	GO:0019368	Fatty acid elongation
PFC0995c	DAG O-acyltransferase, putative	-1.1	0.00250	GO:0019432	Triacylglycerol biosynthetic process
PFI1485	DAG kinase, putative	-1.0	0.00638	GO:0019432	Triacylglycerol biosynthetic process
PF14_0020	Choline kinase, putative	-1.0	0.01102	GO:0006629	Lipid metabolic process
PFL1125	Phospholipid-transporting ATPase, putative	-0.8	0.00462	GO:0006629	Lipid metabolic process
Increase in abundance					
PF10_0016	Acyl CoA binding protein, putative	1.2	0.01128	GO:0006631	Fatty acid metabolic process
PFL0415w	Acyl carrier protein, mitochondrial precursor, putative	1.2	0.00159	GO:0006633	Fatty acid biosynthetic process
PF14_0097	Cytidine diphosphate-diacylglycerol synthase	1.3	0.00057	GO:0008654	Phospholipid biosynthetic process

[a] - The cut off of the log_2 FC ≥ 0.75 or ≤ -0.75.
[b] - Adjusted p-value is an indication of the significance of transcripts statistically determined by LIMMA. A cut off of $p<0.05$ was used to avoid false positives.
[c] – Gene annotations (GO) assigned by MADIBA (http://www.bi.up.ac.za/MADIBA).

2.3.4.5 Comparison of the A51B1C1_1 dataset with other *P. falciparum* perturbation data

The 1504 transcripts from the A51B1C1_1 inhibition transcriptome dataset were compared to other published perturbation studies. The datasets included from literature

was the Hu *et al*. dataset, which analysed the response of the parasite to treatment with 20 different compounds including known antimalarials as well as Febrifugine, Colchicine, $NaOV_3$, E64, Leupeptine, Retinol A, Quinine, Chloroquine, Artemisinin, FK506, Cyclosporine A, Roscovitine, Kn93, W-7, ML-7, Staurosporine, PMSF, Apicidine, Trichostatin A and EGTA (179). Additionally, transcriptome analyses of *P. falciparum* parasites after artesunuate treatment (180), antifolate treatment (181), chloroquine treatment (141, 182) and febrile temperature changes (183) were also included. This was done to determine which transcripts of *P. falciparum* parasites are uniquely affected by treatment withA51B1C_1. Comparison of the A51B1C1_1 dataset with the Hu *et al*. perturbations (179) indicated that 727 transcripts were shared between these datasets (Figure 2.18). Comparison to parasites treated with chloroquine showed that 30 transcripts were uniquely shared (141), whilst only 16 transcripts were shared when the parasites were treated with either A51B1C1_1 or exposed to febrile temperature changes (183). Between the artesunuate treatment (180) and the A51B1C1_1 treatment, 14 transcripts were shared only between these datasets, whereas the inhibition of antifolates (181) compared to the inhibition with A51B1C1_1 showed only one uniquely shared transcript affected by both studies.

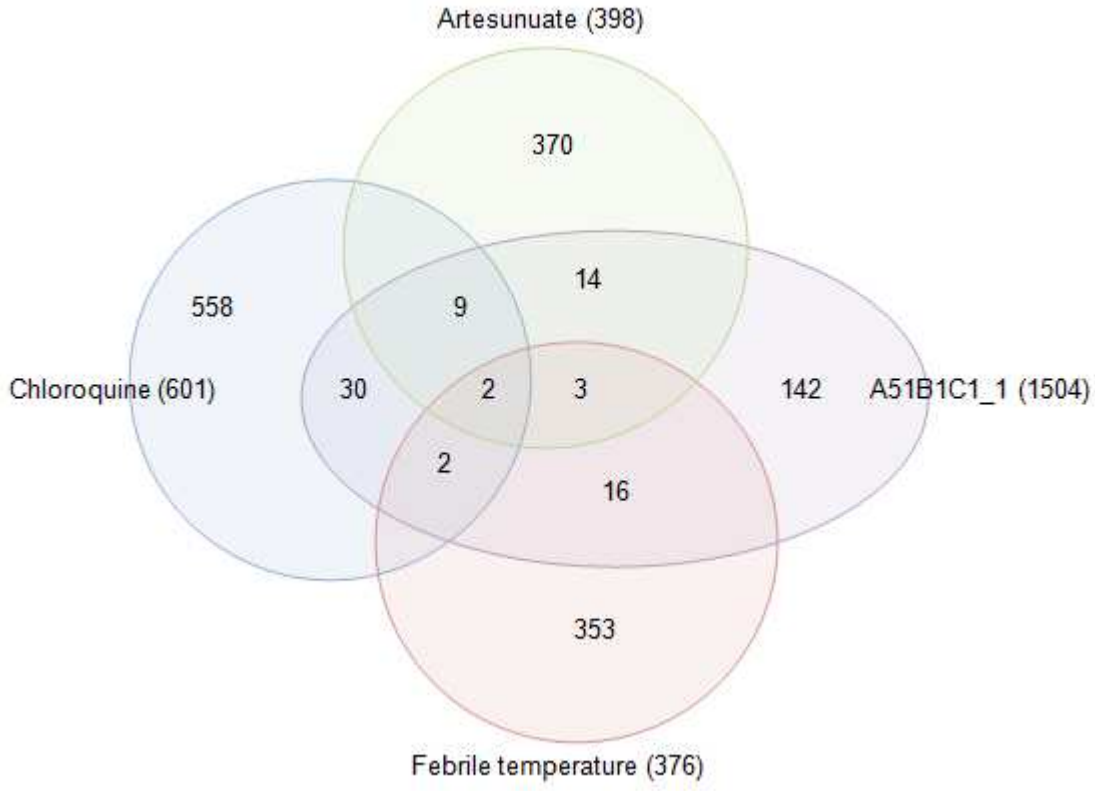

Figure 2.18 A bubble graph of shared and unique transcripts in the *P. falciparum* transcriptome after various perturbations.

The number of transcripts differentially regulated after treatment of *P .falciparum* parasites with either artesunuate, chloroquine, or A51B1C1_1 or by changes in febrile temperature.

Comparisons of the differentially regulated transcriptome of *P. falciparum* parasites treated with A51B1C1_1 (1504 differentially affected transcripts) to the 5 datasets described above show that 579 transcripts are uniquely due to the treatment of the parasite with the herbicide-derived compound (Table 2.7). A complete list of unique transcripts is presented in Appendix 2.

Table 2.7 The 10 transcripts with the highest increased and decreased abundance from the complete set of 579 unique transcripts found only after treatment of *P. falciparum* parasites with A51B1C1_1.

PlasmoDB ID	PlasmoDB annotations	Log_2FC	Adj.P.Val
Decrease in abundance			
MAL13P1.49	Hypothetical protein	-3.4	4.02E-09
PF14_0337	Hypothetical protein	-3.3	3.07E-07
PFL2280	Hypothetical protein	-3.1	9.87E-08
PFC0150	Hypothetical protein, conserved	-3.0	9.22E-08
PF10_0119	Hypothetical protein	-2.9	3.22E-07
PF10_0248	Hypothetical protein	-2.8	4.76E-07
PFF0705	Hypothetical protein, conserved	-2.7	9.27E-08
PFF1000	Hypothetical protein, conserved	-2.7	1.14E-06
PF11_0193	Hypothetical protein	-2.7	2.88E-06
PFD1100	Hypothetical protein	-2.7	3.41E-07
Increase in abundance			
PFI0805	Hypothetical protein, conserved	0.8	0.010283
PFC0300	Hypothetical protein	0.8	0.006049
PFD0385	Hypothetical protein	0.8	0.017936
PFA0220	Ubiquitin carboxyl-terminal hydrolase, putative	0.8	0.00786
PF10_0225	Orotidine-monophosphate-decarboxylase, putative	0.8	0.006059
PFL1150	GTP cyclohydrolase I	0.8	0.006286
PFD0955w	ROI kinase-like protein	0.8	0.013944
PFL1870	Calcium/calmodulin-dependent protein kinase 2, putative	0.8	0.017242
PFC0510	Hypothetical protein	0.8	0.01964
PFI0575	Hypothetical protein	0.8	0.031453

2.3.4.6 Comparison of the A51B1C1_1 dataset with the expression data from Galvestine-2 and other datasets

A51B1C1_1 and Galvestine-2 are similar in structure but the observed morphologies of the parasites treated with the two compounds, were different. It was thus decided to compare the transcriptomics results of *P. falciparum* parasites treated with these two

compounds to each other (Table 2.8). Treatment of *P. falciparum* parasites with A51B1C1_1 revealed a larger number of differentially expressed transcripts (1504) compared to the parasites treated with Galvestine-2 (704). However, the distribution of processes affected between the datasets show some similarity, particularly for general metabolic and biochemical processes including parasite-host interaction, translation, DNA metabolic process, post-translational modifications, transport, proteolysis, and lipid biosynthesis (Table 2.8).

Table 2.8 Metabolic annotation of the largest clusters (excluding hypothetical proteins) that was shared in both the Galvestine-2 and the A51B1C1_1 datasets.

Cluster	Galvestine-2		A51B1C1_1	
	Nr of transcripts[a]	Percentage[b]	Nr of transcripts[a]	Percentage[b]
DNA metabolic process	17	2.4	31	2.1
Parasite-Host interaction	18	2.6	55	3.7
Lipid Biosynthesis	11	1.6	10	0.7
Post-translational modification	40	5.7	64	4.3
Proteolysis	11	1.6	34	2.3
Translation	20	2.9	18	1.2
Transport[c]	14	2.0	66	4.4

[a] – The number of transcripts affected by the corresponding treatment.
[b] – The percentage of transcripts in the specific cluster out of total transcripts.
[c] – Transcripts in the transport cluster include general transport and electron transport.

When the datasets were compared, 239 transcripts were found to be shared. These 239 transcripts were compared to various other published perturbations studies of the parasite. Hierarchical clustering of these transcripts with those differentially regulated after 20 different perturbations (Hu *et al*. as described above), was performed using Cluster (http://rana.stanford.edu.software) and TreeView (www.EisenSoftware/ClusterTreeView/TreeView) (Figure 2.19).

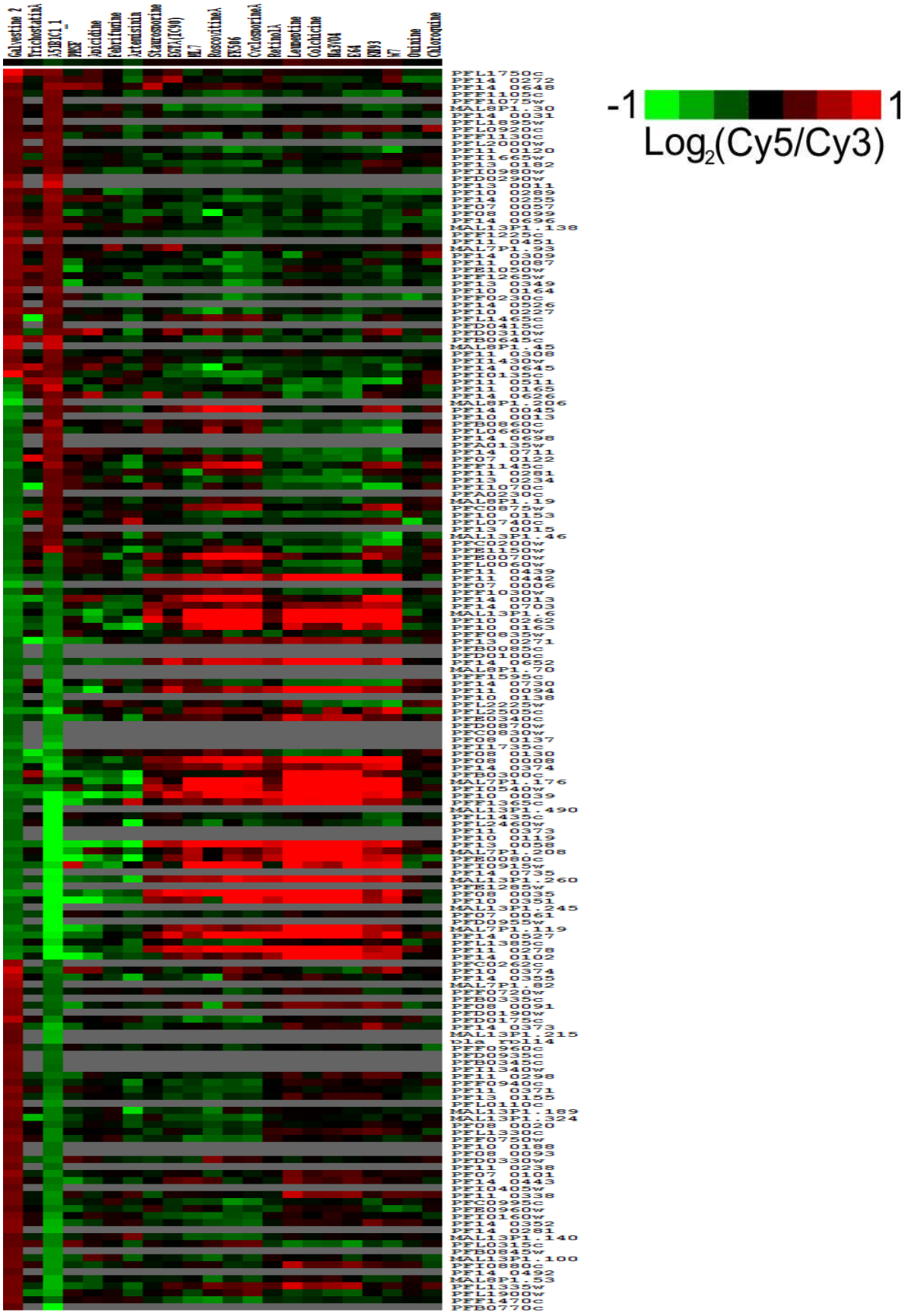

Figure 2.19 A heat map representation of the comparison between the transcriptional data of the 20 compounds of the Hu *et al.* study (179) and the 239 transcripts found in both Galvestine-2 and A51B1C1_1 datasets.

The green indicates decrease of abundance and red increased abundance of transcripts. Grey indicates the absence of the gene in the correlating treatment.

The heat map (Figure 2.19) shows areas in grey, which indicated transcripts that were only present in the 239 shared transcripts of the A51B1C1_1 and Galvestine-2 datasets. In total, 50 of the transcripts shared between the Galvestine-2 and A51B1C1_1 datasets are unique to the treatment with these two compounds (Table 2.9). Besides the largest cluster within these 50 transcripts belonging to hypothetically annotated proteins, the second most abundant cluster contained transcripts of proteins involved in membrane transport processes.

2.3.5 Comparison of *P. falciparum* transcripts after treatment with A51B1C1_1 to transcripts of *Arabidopsis* treated with Galvestine-2

Compound A51B1C1_1 is a derivative of Galvestine-1, which is a herbicide. All 1504 transcripts that showed differential abundance after treatment of *P. falciparum* parasites with A51B1C1_1 was compared to the differentially expressed transcript dataset obtained for *Arabidopsis* treated with Galvestine-1 (118) (Table 2.10, complete comparative dataset provided in Appendix 3). Many of the clusters of co-regulated transcripts between these organisms were identified to have transcripts involved in membrane associated processes and lipid metabolism and to be located in the apicoplast.

Table 2.9 The 50 transcripts which are unique to the perturbation of *P. falciparum* with either Galvestine 2 orA51B1C1_1.

PlasmoDB ID	PlasmoDB annotation Go Process	PlasmoDB annotation Go Cellular component	PlasmoDB annotation GO Function	Log Fold change
PFF1595c	Antigenic variation	Host cell plasma membrane, infected host cell surface knob, integral to membrane, outer membrane	Cell adhesion molecule binding, receptor activity	-1.0
PFD0955w	Attachment of GPI anchor to protein	Hypothetical	Hypothetical	-2.1
PF11_0373	Attachment of GPI anchor to protein	Membrane	Hypothetical	-2.9
PF10_0188	Cation transport	Integral to membrane	ATP binding,	-0.9
PFB0770c	Cholesterol metabolic process, endocytosis, lipid transport	Coated pit, integral to membrane	Calcium ion binding, lipid transporter activity, receptor activity	-2.3
MAL7P1.82	Hypothetical	Integral to membrane, membrane	Hydrolase activity, transferase activity	-0.8
PFI1340w	Hypothetical	Hypothetical	Hydro-lyase activity	-0.8
PFA0135w	Hypothetical	Hypothetical	Hypothetical	0.9
PFA0230c	Hypothetical	Hypothetical	Hypothetical	0.9
PFC0262c	Hypothetical	Cytoplasm	Hypothetical	-0.8
PFC0830w	Hypothetical	Hypothetical	Hypothetical	-1.1
PFD0100c	Hypothetical	Hypothetical	Hypothetical	-1.0
PFD0190w	Hypothetical	Hypothetical	Hypothetical	-0.8
PFD0290w	Hypothetical	Hypothetical	Hypothetical	1.3
PFD0415c	Hypothetical	Hypothetical	Hypothetical	0.8
PFD0870w	Hypothetical	Hypothetical	Hypothetical	-1.2
PFE1285w	Hypothetical	Hypothetical	Hypothetical	-2.1
PF07_0006	Hypothetical	Cell surface	Hypothetical	-1.2
PF08_0137	Hypothetical	Apicoplast, nucleus	Hypothetical	-1.3
MAL8P1.45	Hypothetical	Hypothetical	Hypothetical	1.6
MAL8P1.206	Hypothetical	Hypothetical	Hypothetical	1.1
PFI0405w	Hypothetical	Apicoplast	Hypothetical	-1.0
PFI0980w	Hypothetical	Integral to membrane	Hypothetical	1.0
PFI1735c	Hypothetical	Cytoplasm, host cell cytoplasm, host cell	Hypothetical	-1.6

		membrane		
PF10_0013	Hypothetical	Maurer's cleft, apicoplast	Hypothetical	0.9
PF10_0119	Hypothetical	Apicoplast, membrane, nucleus	Hypothetical	-2.9
PF10_0138	Hypothetical	Apicoplast, membrane	Hypothetical	-1.1
PF10_0164	Hypothetical	Membrane	Hypothetical	1.1
PF11_0238	Hypothetical	Apicoplast, membrane	Hypothetical	-0.9
PF13_0015	Hypothetical	Hypothetical	Hypothetical	0.8
MAL13P1.215	Hypothetical	Hypothetical	Hypothetical	-1.4
MAL13P1.245	Hypothetical	Cytoplasm	Hypothetical	-2.0
MAL13P1.490	Hypothetical	Hypothetical	Hypothetical	-3.4
PF14_0526	Hypothetical	Hypothetical	Hypothetical	0.8
PF14_0698	Hypothetical	Membrane	Hypothetical	1.1
MAL8P1.70	Hypothetical	Hypothetical	Nucleic acid binding, zinc ion binding	-1.1
PF11_0451	Hypothetical	Cytoplasm, intracellular, membrane	Nucleotide binding	1.1
PF13_0011	Hypothetical	Hypothetical	RNA binding, SH3 domain binding, protein dimerisation activity	1.7
PFB0335c	Immunoglobulin production,	Symbiont-containing vacuole	Cysteine-type peptidase activity	-0.9
PFB0345c	Immunoglobulin production,	Symbiont-containing vacuole	Cysteine-type peptidase activity	-0.9
PF14_0492	Protein amino acid dephosphorylation	Calcineurin complex	Calcium ion binding, calcium-dependent protein serine/threonine phosphatase regulator activity	-1.2
PFB0085c	Protein folding	Host cell part	Heat shock protein binding, unfolded protein binding	-1.0
PF14_0735	Protein folding, response to stress	Membrane	ATP binding, unfolded protein binding	-2.1
PF14_0281	Proteolysis	Hypothetical	Aspartic-type endopeptidase activity	-1.5
PFD0935c	RNA-protein covalent cross-linking, proteolysis, transcription, RNA-dependent	Cytoplasm, cytoplasmic vesicle, membrane	ATP binding, RNA binding, RNA helicase activity	-0.9
PFL1895w	Translation	Intracellular, mitochondrion, ribosome	Structural constituent of ribosome	1.0
PF08_0093	Transport	Membrane	Binding	-0.9
PFL0110c	Transport	Mitochondrial inner membrane, mitochondrion	Binding	-1.2
PFB0845w	Transport	Integral to membrane	Hydrolase activity, metal ion binding, nucleotide binding	-1.2
PFF1075w	Vacuolar transport, vacuole fusion	Endoplasmic reticulum, integral to membrane	Hypothetical	0.9

Table 2.10 Guilt-by-association clustering of the transcripts found in both *P. falciparum* and *Arabidopsis* datasets after treatment with A51B1C1_1 and Galvestine-1, respectively. Data obtained from collaborator L Bréhélin.

PlasmoDB annotation	PlasmoDB ID	*Arabidopsis* gene ID
Cluster1		
Conserved *Plasmodium* protein, unknown function	MAL7P1.157	AT1G13220
Inositol phosphatase, putative	MAL8P1.151	AT1G17340
Cg3 protein	PF07_0034	AT3G08950
Mitochondrial ribosomal protein L22/L43, putative	PF10_0097	AT3G59650
Transcription factor with AP2 domain(s), putative	PF14_0471	AT4G09630
ERCC1 nucleotide excision repair protein, putative	PFB0160w	AT3G05210
Conserved *Plasmodium* protein, unknown function	PFB0250w	AT4G33920
Serine repeat antigen 2	PFB0355c	AT3G19400
Phospholipase A2, putative	PFB0410c	AT1G61850
Tubulin-tyrosine ligase, putative	PFE0700c	AT1G77550
S-adenosyl-methyltransferase, putative	PFL1775c	AT5G10910
Conserved *Plasmodium* membrane protein, unknown function	PFL2170c	AT2G35330
Cluster 2		
Acyl CoA:DAG acyltransferase, putative	MAL13P1.285	AT1G61850
Lysophospholipase, putative	PF07_0040	AT1G18360
DAG O-acyltransferase	PFC0995c	AT2G19450
Patatin-like phospholipase, putative	PFI1560c	AT4G33700
Cluster 3		
Apicoplast ribosomal protein L36e precursor, putative	PF11_0106	AT2G37600
Small nuclear ribonucleoprotein D1, putative	PF11_0266	AT4G02840
Aspartyl-tRNA synthetase	PFA0145c	AT4G26870
Plasmodium exported protein (hyp9), unknown function	PFB0930w	AT4G02500
Eukaryotic translation initiation factor, putative	PFE0885w	AT5G25780
Karyopherin beta	PFE1195w	AT5G19820
Small nuclear ribonucleoprotein (snRNP), putative	PFI0475w	AT1G76300
RNA polymerase subunit 8c, putative	PFL0665c	AT1G54250
Cytoplasmic translation machinery associated protein, putative	PFL2150c	AT2G20280
Cluster 4		
Glideosome associated protein with multiple membrane spans 3, putative	PF14_0065	AT2G32040
Rhoptry-associated protein 2	PFE0080c	AT5G65410

2.3.6 Validation of microarray data with qRT-PCR

The use of quantitative qRT-PCR is an accepted method for validation of microarray data. A house keeping gene, LDH, which did not show change in fold change between the treated and the control samples and does not show differential regulation during the microarray experiment, was included (175). Three transcripts that showed increased

abundance in the microarray dataset as well as three transcripts with decreased abundance were compared to LDH transcripts (Table 2.11).

Table 2.11 Validation of the microarray dataset with qRT-PCR for six selected differentially expressed transcripts after treatment of *P. falciparum* with compound A51B1C1_1.

Name of gene	qRT – PCR results log_2FC	Microarray Results log_2FC
MAL13P1.130	-6.4	-3.0
PF07_0126	1.9	1.53
PF08_0131	0.9	1.36
PF11_0278	-9.3	-3.21
PFL1885c	0.9	0.75
PF14_0363	-3.7	-1.55
LDH (House hold)	1	-

All six transcripts showed the same direction of change in abundance that was observed in the microarray experiment, thereby independently validating the results obtained in the microarray experiment. However, it is also evident that the numeric values in fold change between the microarray experiment and the qRT-PCR, are not necessarily in the same range.

2.4 Discussion

The resistance that *P. falciparum* parasites have developed against current antimalarials implies an urgent need to identify novel drug targets and to develop new drugs. Relatively little attention has been focused on the apicoplast of *P. falciparum* parasites. However, there is an evolutionary relationship between the multi-membrane apicoplast of these parasites and the photosynthetic chloroplast of plants (2), therefore it is hypothesised that compounds that inhibit the growth of plants, may also inhibit the development of the parasite (118).

Galvestine-2 and A51B1C1_1 are modified from Galvestine-1 as parent compound, which is a herbicide derivative. In *Arabidopsis*, Galvestine-1 inhibits the activity of MGD1 in membrane vesicles and also in the released micelles (118). This indicated the potency of the compound and potentially its derivatives as galactolipid synthesis inhibitors. Kinetic analyses of the enzymatic (MGD1) inhibition on mixed micelles, showed that Galvestine-1 competes with the binding of DAG, the substrate for MGDG and DGDG synthesis (184). DGDG-like epitopes have been detected in the plasma membrane and inner membrane complex of *P. falciparum* but not in the apicoplast as found in *Arabidopsis* (Personal communication, Eric Maréchal, Pretoria, 2009). *Arabidopsis* treatment with Galvestine-1 triggered an *in vivo* inhibition of MGDG synthase activity and resulted in the overall reduction of the galactolipids, especially MGDG. The effect was seen mainly on the chloroplast, with a decrease in the membrane expansion of the chloroplast resulting in a decrease in the overall size of the chloroplasts. No other subcellular structure was affected by the treatment. Transcriptomic effects after treatment of *Arabidopsis* with Galvestine-1 indicated a decrease in abundance of gene transcripts involved in galactolipid synthesis (118).

One method for the determination of the IC_{50} for potential antimalarials *in vitro* is the measurement of ^{3}H-hypoxanthine incorporation (185). However, this assay is expensive and the use of radioactive materials poses safety hazards and disposal problems (186). Enzymatic reactions and antibodies are also used as alternative methods to detect the presence of lactate dehydrogenase (187), and histidine-rich protein II, respectively (188) which indicate the number of viable parasites after treatment. These assays are not suited for high-throughput antimalarial drug screening as they are time consuming (189). Non-radioactive DNA stains, such as SYBR Green I

(160) and PICO green® (190) are safe and cost-effective methods to determine the IC_{50}s of anti-*Plasmodium* compounds, compared to other published methods. The IC_{50} of compound A51B1C1_1 determined in a preliminary study in Grenoble, France (collaborator E. Maréchal), using the ^{3}H-hypoxanthine incorporation method, was found to be 180 nM (Personal communication, Eric Maréchal, Pretoria, 2009). The IC_{50} value determined in this study using the SYBR Green I method was shown to be 447 ±16 nM. The different values may be due to the techniques used to determine the IC_{50} as was previously observed (186, 191, 192). Values below 1 µM comply with the MMV requirements (www.mmv.org) and are an indication that a compound may have potential against *P. falciparum*. .

Delayed death is a phenomenon where the perturbation only causes the death of the parasite in the next life cycle. Examples are the effects seen after treatment of *P. falciparum* parasites with drugs such as tetracycline (97, 111, 126) and macrolides (48, 193, 194) which are both translation inhibitions and Gyrase inhibition caused by ciprofloxacin (48, 111, 195). The reason for the delayed death was found to be the transfer of non-functional apicoplasts to the progeny and thus lack of apicoplast protein production (196). In contrast, drugs affecting non-housekeeping processes in the apicoplast of *P. falciparum* have been shown to not display delayed death phenomena (126). These drugs result in visible stress symptoms and growth arrest of the parasites within the first life cycle after exposure. Analyses of *P. falciparum* parasites treated with the herbicide derivative A51B1C1_1 ($2xIC_{50}$) revealed morphological signs of stress in the form of pyknotic parasites within the first 48 h. The formation of pyknotic bodies was also seen by Deponte and Becker in 2004 (197) in a study where they treated either *P. falciparum* parasites with antimalarials followed by exposure to oxidant stress or left to starve. These parasites showed signs of programmed cell death, with cell shrinkage (pyknotic bodies), membrane blebbing and nuclear fragmentation visible (197). Stressed forms of *P. falciparum* parasites under A51B1C1_1 pressure could indicate that either 1) this compound targets non-housekeeping processes of the apicoplast with no delayed death phenotype; or 2) the compound targets another biological process in the parasite not associated with the apicoplast.

Morphological monitoring of *P. falciparum* parasites under A51B1C1_1 pressure revealed that the parasites' life cycle development was slowed down to a point where the life cycle was halted within the first life cycle. Whereas untreated parasites were at

the mature schizont stage after 48 h, A51B1C1_1 treated *P. falciparum* were present as stressed (possibly dead) trophozoites with only a few maturing to merozoites for invasion of new erythrocytes. In contrast to this, Galvestine-2 affected the parasites to a lesser degree. After the first life cycle (48 h), the Galvestine-2 treated parasites were in the late trophozoite stage with a few schizonts with no morphological signs of stress and slightly delayed life cycle of the parasite, rather than causing pyknotic parasites (death) as observed for A51B1C1_1 treatment.

DNA microarray allows global analyses of the complete transcriptome of an organism, at any moment in its lifecycle, in a single experiment (198). This holds a challenge for the analysis to make sense of the large amount of high-quality raw data. The Plasmodial Agilent platform was chosen because the overall spot quality of this platform is a significant improvement on previously Plasmodial arrays used in our lab (133, 166, 199). The higher quality in the microarray data results allows higher confidence in the analysis of the data (133, 200). The A+T richness of the genome of *P. falciparum* causes difficulties in the PCR reaction to generate more starting material (201) and one advantage of the Agilent platform is that it needs less starting material than other methods.

Using the information obtained from the morphological studies, the microarray study was designed and two time points were selected for the extraction of RNA from synchronised parasites. The background noise from multiple life stages is reduced in synchronised cultures enabling the detection of abundance differences in transcript levels above the normal levels in the IDC (158). Small changes on transcriptomic level may have been missed if the cultures used in this study were not synchronised. Synchronised cultures have been used in previous studies for the above mentioned reason and these authors were able to detect perturbation induced transcriptional changes, independent of the normal transcript production due to life cycle development (158, 180, 202, 203). There have been reports on *P. falciparum* studies using non-synchronised cultures (139, 141) however, in most of these studies the authors failed to notice transcriptional responses to perturbation. The time points selected for the sampling of RNA was 28 hpi and 36 hpi, which covers the life stages in which a morphological effect is seen after treatment with A51B1C1_1.

For confidence and statistical analysis, the experiment included two biological and two technical replicates. A reference design for the microarray set up was performed on the Plasmodial Agilent platform, which allow for the simultaneous analysis of the samples. This design also enables easy comparison between the samples. The reference is a pool of all the samples (treated and control) in equal amounts to ensure a representative sample. The quality of the data resulting from the Agilent arrays was of high standard (200). The statistical significance of transcripts showing a change in abundance levels was calculated with t-test (167, 168) and only the transcripts with at least a $\log_2$-ratio ≥ 0.75 or ≤ -0.75 (fold change of 1.7) with 95% confidence were regarded as differentially expressed.

Normalisation, data correction and local background subtraction are essential processes in DNA microarray data analyses to allow for correction of variation between technical and biological replicates and accurate identification of differentially expressed transcripts between two sample sets. Various algorithms are available for the correction of variation between spots on the same array in an intensity-dependent manner. In this study two methods were tested to determine which gives the best normalisation. Global loess makes the assumption that most of the genes are not expressed differentially, which cannot be assumed in this study and resulted in box plots of different sizes and outliers that influenced the results, which are an indication of the success of the normalisation (167). Robust spline was used in the experiments as it uses 5 parameter regression splines instead of curves as in loess and was designed to deal with outliers is such a way that it does not affect the mean (167, 178). This resulted in boxes of similar size and around the same M value (Figure 2.13). The same box size is an indication of equal contribution of the samples and the same M-value proves successful normalisation of the intensity of the different arrays.

For between-array normalisation both Aqualtile and Gqualtile were tested. Aquantile was designed for experiments where the samples are labelled with Cy3 and the reference with Cy5 (149). This resulted in a density plot with multiple green lines, representing the reference. Gquantile normalisation was used in this study as this was designed for Cy3 labelling of the common reference. Gquantile was used for the correction of background effects between arrays, which enables the comparison across the different arrays and resulted in acceptable normalisation of the A51B1C1_1 datasets. The Agilent platform and reference design microarray strategy has been

previously used, and in these instances, success was achieved with Gquantile normalisation. (166, 199). Fulfilment of all the set criteria and thorough analyses resulted in valid, high quality data sets, which are reproducible and reliable (198).

Pearson correlations indicated that the time points chosen for sampling of RNA from *P. falciparum* parasites after treatment with A51B1C1_1 for the microarray were early enough to enable direct comparison between the treated and the control parasites at a specific time point and identification of differentially expressed transcripts (Table 2.4). The same direct comparison was used by Dahl *et al.* (2006) after 55 h treatment with doxycycline because of the little variation between the treated and the control samples (97). Since transcripts in the *P. falciparum* IDC are only produced once needed (137), it is essential that comparisons between parasite populations only detect drug-specific responses and not normal life stage specific responses (133). In the case where direct comparisons of treated and control parasites are not possible, the use of a t_0 strategy was developed to determine the point of transcriptional arrest and using that point as the reference to make comparisons between the treated and control samples (133).

In this study, the steady state levels of the affected transcripts at a specific time point were determined. A total of 1504 transcripts (Appendix 1) were affected by treatment with compound A51B1C1_1 of which 805 decreased in abundance and 699 increased in abundance. The larger number of transcripts with decreased abundance correlates to other perturbation studies done on *P. falciparum* (133, 199). Additionally, the range of fold changes of the transcripts detected is between 1.9 (increased abundance) and -3.9 (decreased abundance), and is in agreement with previous transcriptomic reports (97). The transcripts with decreased abundance showed a much higher level of confidence and the fold of decrease was also higher than the fold of increase, similar to published data (133, 141, 199). However, the number of transcripts affected is much higher (in most cases, more than double the number of transcripts) than for most other reported studies (97, 133, 183, 199, 202).

A paradoxical effect is seen after treatment of *P. falciparum* parasites with A51B1C1_1. The treatment caused both an increase and a decrease in abundance of transcripts representing the same biological process (cluster). This is not uncommon in treated *P. falciparum* and has been seen numerous times with methionine and polyamine metabolism inhibition (133, 199). Both the 699 transcripts with increased abundance

and the 805 transcripts with decreased abundance were clustered into the same 14 functional groups (transcripts with decreased abundance contained an extra cluster) (Figure 2.17) using GO annotations obtained from PlasmoDB and MADIBA. The largest clusters of affected transcripts with an increase in abundance were RNA metabolic processes (9%), translation (6%), primary metabolism (5%) and post-translational modifications (5%). Transcripts with a decrease in abundance are involved in parasite-host interactions (6%), post-translational modifications (4%), transport (3%) and proteolysis (3%). As seen in previous studies, the clusters consist of transcripts with increased abundance, as well as transcripts with decreased abundance (133, 166, 199).

The 1504 transcript data set includes ten transcripts (three with increased abundance and seven with decreased abundance, Table 2.6) involved in lipid biosynthesis or fatty acid biosynthesis. The presence of these transcripts (all have Log_2 FC of about 1) in the data set indicates the effect of the treatment on lipid biosynthesis (three in glycerophospholipid metabolism, Figure 2.20, and two in glycerolipid metabolism, Figure 2.21). In glycerophospholipid metabolism, three transcripts were affected of which one increased in abundance (PF14_0097, EC 2.7.7.41 – Cytidine-diphosphate-DAG synthase) and two with decreased abundance (PFI 1370, EC 4.1.1.65 – Phosphatidyl serine-decarboxylase and PF14_0020, EC 2.7.1.32 – Choline kinase) (Figure 2.20). In glycerolipid metabolism two transcripts (PFC0995c, EC 2.3.1.20 – DAG O-acyltransferase and PFI 1485, EC 2.7.1.107 – DAG kinase) both decreased in abundance (Figure 2.21). DAG O-acyltransferase is the enzyme that convert DAG into triacylglycerol (TAG), one of the lipids proven by Maréchal *et al.* (2002) to be present in the *P. falciparum* parasite (119). The *P. falciparum* genome was found to only have one open reading frame for the enzyme DAG O-acyltransferase (204). The function of this enzyme in the IDC is still under debate (204), but reports show an increase in TAG levels in mature forms of the parasites (205) and TAG metabolism and trafficking in *P. falciparum* infected erythrocytes is stage-specific (206). In other organisms, TAG serves as highly reduced store of oxidisable energy (206) and also plays a vital role in the homeostasis of the organism (207). The enzyme DAG kinase is responsible for the conversion of DAG to 1,2-diacyl-sn-glycerol-3-phosphate.

A comparison between the transcriptomic data obtained after treatment with A51B1C1_1 and other Plasmodial perturbation studies was done to determine the level of specificity of the A51B1C1_1 inhibited transcriptome dataset and to identify

transcripts due to the natural stress response by the parasite. These studies included treatment of *P. falciparum* with chloroquine, artemisinin, antifolates and effects of high temperatures together with the 20 perturbations investigated by Hu *et al.* (179). From these comparisons 579 transcripts were identified as unique to the transcriptomic profile of the parasites treated with the herbicide-derived compound A51B1C1_1 (Table 2.7). Two transcripts involved in fatty acid or lipid synthesis were among the 579 unique transcripts (PFC0050 - long chain fatty acid ligase and PFI 1485 –DAG kinase.

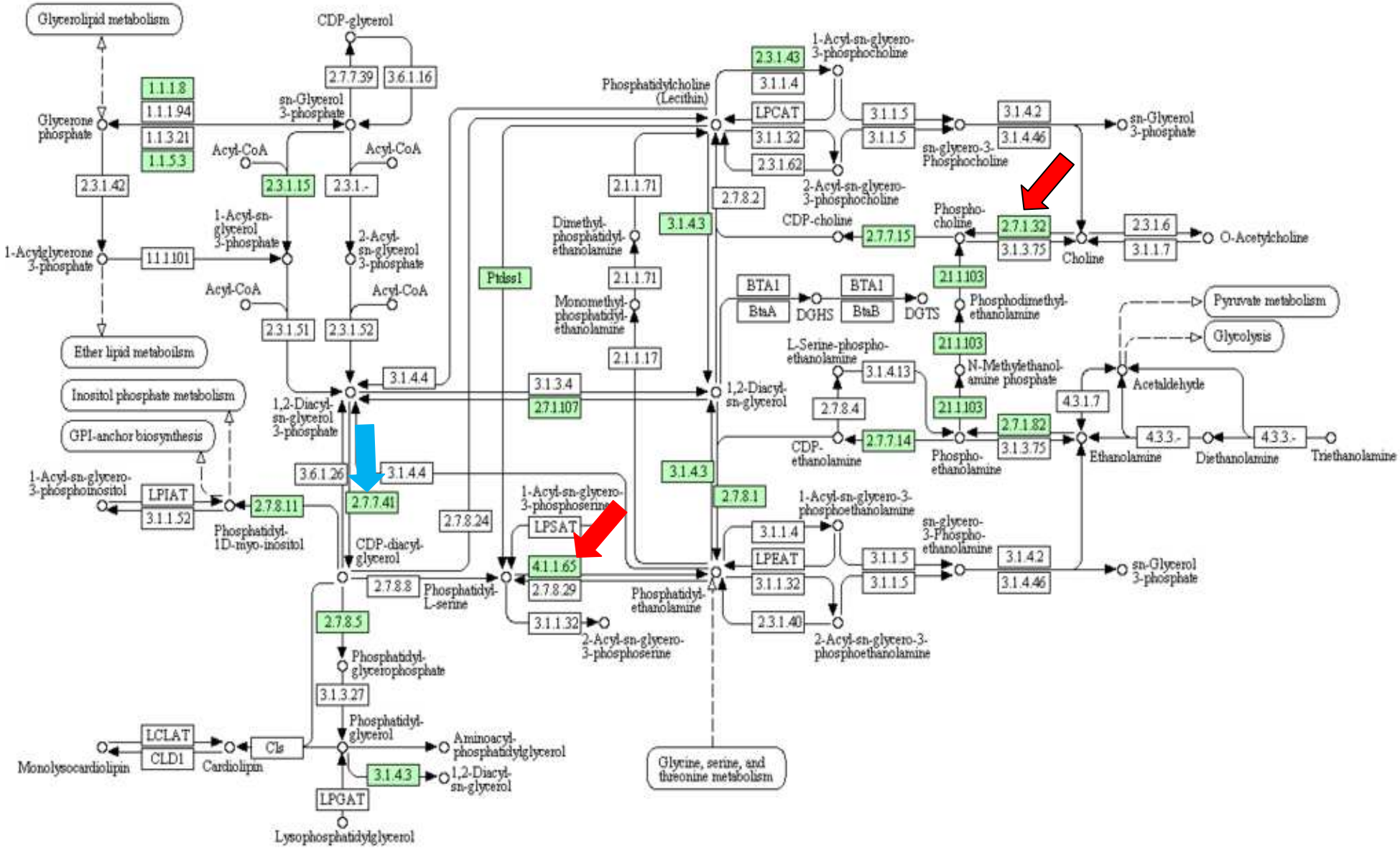

Figure 2.20 Glycerophospholipid metabolism as presented by KEGG (208).

Green blocks indicates the enzymes present in the pathway of *P. falciparum* parasites. Red arrows indicate the transcripts with decreased abundance and blue arrow indicates transcript with increase in abundance. EC 2.7.7.41 – Cytidine-diphosphate-DAG synthase (PF14_0097), EC 4.1.1.65 – Phosphatidyl serine-decarboxylase (PFI 1370), EC 2.7.1.32 – Choline kinase (PF14_0020).

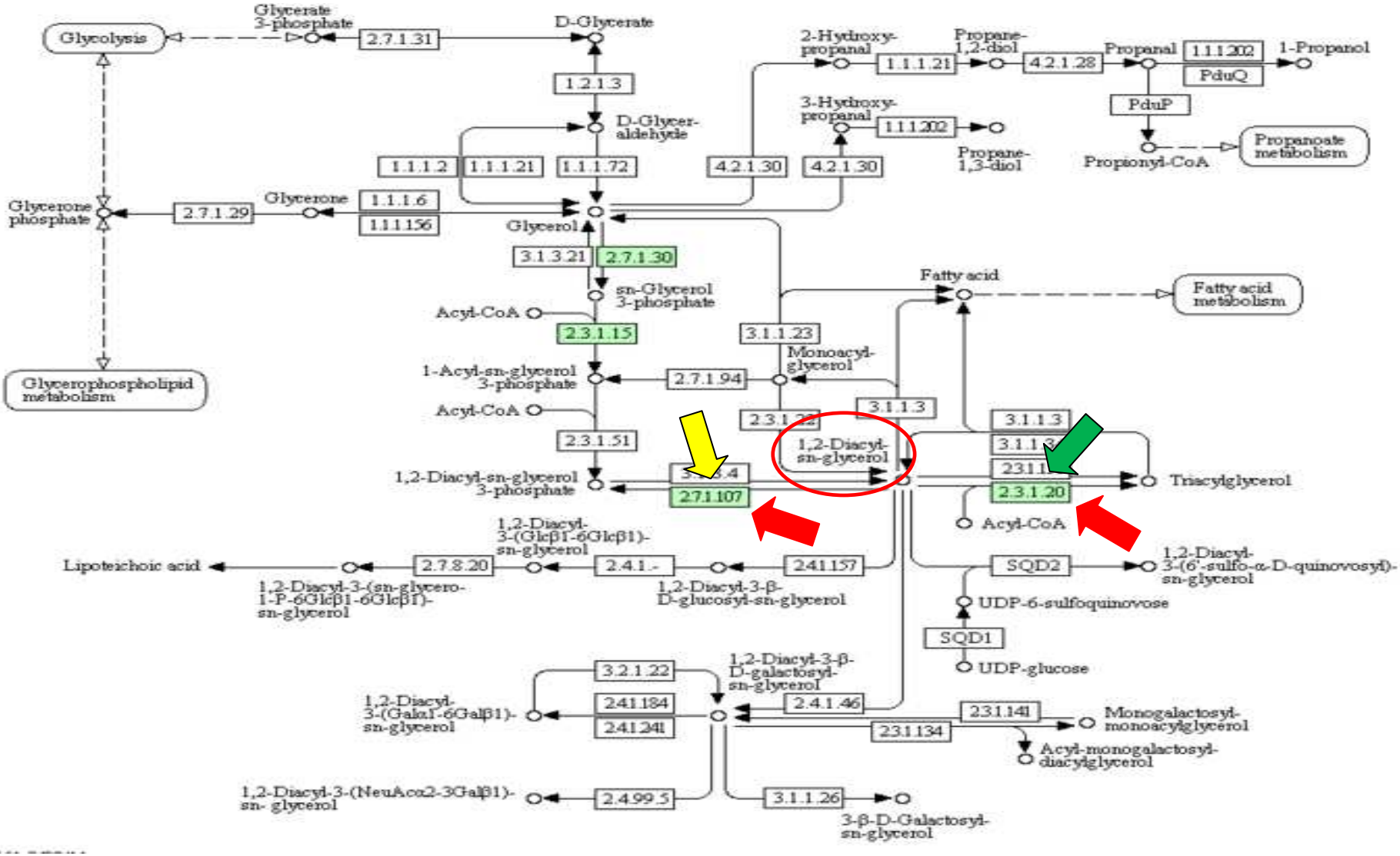

Figure 2.21 Glycerolipid metabolism as presented by KEGG (208).

Green blocks indicate the enzymes present in the pathway of *P. falciparum.* Red arrows indicate the transcripts with decreased abundance, yellow arrow indicates transcript in the unique dataset (579 transcripts), green arrow indicates the transcript affected in both *Arabidopsis* and *P. falciparum* after treatment with respectively Galvestine-2 and A51B1C1_1. Diacylglycerol (DAG) is encircled in red. EC 2.3.1.20 – DAG O-acyltransferase (PFC0995c), EC 2.7.1.107 – DAG kinase (PFI 1485).

The only structural difference between A51B1C1_1 and Galvestine-1 is on the benzimidazole group where Galvestine-1 has an extra oxygen group (Figure 1.12 and Figure 1.14). Between A51B1C1_1 and Galvestine-2, there are two structural differences. The benzimidazole group of Galvestine-2 has an extra oxygen group and the dibenzylamino-ethoxy group of Galvestine-2 contains 3 benzyl groups, whereas A51B1C1_1 only contains 2 benzyl groups (Personal communication, Eric Maréchal, Pretoria, 2009). These similarities in the structures of Galvestine-2 and A51B1C1_1 may lead to similar effects on the parasite. Comparing the transcriptional datasets after treatment with either Galvestine-2 (166) or A51B1C1_1 and finding the similarities between the two datasets, may help to determine the mode of action of these herbicide derived compounds. The shared transcripts (239 transcripts) showed lipid biosynthesis to be affected by both treatments (Galvestine-2, 1.6% and A51C1B1_1, 0.7%). To determine if the 239 shared transcripts (between A51B1C1_1 and Galvestine-2) were unique to the herbicide derived treatment, these transcripts were compared to the results found in the study conducted by Hu *et al.*(179). Of the shared transcripts, 50 were found to be unique to herbicide treatments, which include five transcripts unique to the apicoplast (PF08_0137, PFI0405w, PF10_0119, PF10_0138 and PF11_0238, Table 2.8) as well as PFB0770c as part of lipid transport processes (decreased abundance in the A51B1C1_1 dataset and increased abundance in the Galvestine-2 dataset). These results indicate that the differences in the structures in the two compounds may result in slight difference in potency for each compound. This is not uncommon in studies with different structural derivatives (209-212). Comparative studies between Galvestine-2 treated *Arabidopsis* and A51B1C1_1 treated *P. falciparum* did reveal transcripts that are involved in lipid biosynthesis such as MAL13P1.285 (Acyl CoA:DAG acyltransferase) and PFC0995c (DAG O-acyltransferase, indicated with a green arrow in Figure 2.21).

In this chapter the transcriptomic response to a herbicide derived compound, A51B1C1_1 on the *P. falciparum* parasite was investigated. Evidence was also provided that of the 1504 differentially regulated transcripts after treatment with A51B1C1_1, a total of 579 transcripts were drug-specific. The data showed apicoplast associated metabolic systems are affected. *P. falciparum* does synthesise galactolipids (which would be the target of Galvestine-1), however, no sequence homologues have been found in the *P. falciparum* genome database with statistically reliable similarities to chloroplast envelope MGDG synthase or DGDG synthase multigenic families (119).

The results indicate that enzymes involved in glycerolipid synthesis that are responsible for the conversion of DAG are affected in *P. falciparum* parasites treated with A51B1C1_1. Fatty acid synthesis is also affected by the treatment; however the transcripts involved in this process showed an increase in abundance. In the following chapter the effect of treating these parasites with the herbicide-derived compound on the proteome of the parasites are investigated.

CHAPTER 3

INVESTIGATION OF THE PROTEOMIC RESPONSE OF *P. FALCIPARUM* TREATED WITH A HERBICIDE-DERIVED COMPOUND

3.1 Introduction

The complex life cycle of *P. falciparum* is tightly controlled with a unique flow of gene regulation (137). This result in a 'just-in-time' transcription of genes involved in related biological processes and in the majority of cases the production of the related proteins without delay (137, 213). The *P. falciparum* proteome is complex due to the stage-specific expression of proteins associated with the biological and metabolic changes during the IDC of the parasite (214). Regulation of proteins is achieved by PTM's to ensure the proteins are active in the correct life cycle stage of the parasite (215). Certain proteins are predicted to act as control centres that are interconnected to others resulting therefore in a specialised interactome (132, 216). Few studies attempted to describe the Plasmodial proteome, which is predicted to have about 5300 proteins of which ~60% are hypothetical and un-annotated (137, 217-219).

The >80% A+T-richness of the Plasmodial genome (134) translate to long hydrophobic stretches and amino acid repeats (lysine and asparagine) in the proteome. The proteins are comparatively large, non-homologous and more charged compared to their orthologues with multiple isoforms of proteins being present (220). These properties have made it difficult to analyse the Plasmodial proteome and to recombinantly express Plasmodial proteins (221, 222).

Comparison of the *P. falciparum* genome to that of other free-living eukaryotes indicated that the parasite has fewer proposed enzymes and transporter proteins but has instead a large number of genes coding for proteins involved in immune evasion and specific host–parasite interactions (134). The proteins that are responsible for immune evasion, such as the *var* and *rif* genes, are specific to the sporozoite stage and are found in large amounts at this blood life-cycle stage (223). Proteins of each life stage of the parasite are unique to that specific life cycle stage. In sporozoites, 49% of the proteins are

unique and only 25% of these proteins are shared with other life cycle stages (223). The trophozoite, merozoite and gametocyte stages all have between 20 and 33% unique proteins and 39 – 56% of their proteins are shared with other life cycle stages. Only 6% (152 proteins) of the parasite's proteins are shared between all the life stages of the parasite. The distribution of function of the proteins in each life stage of the *P. falciparum* parasite is shown in Figure 3.1 (223).

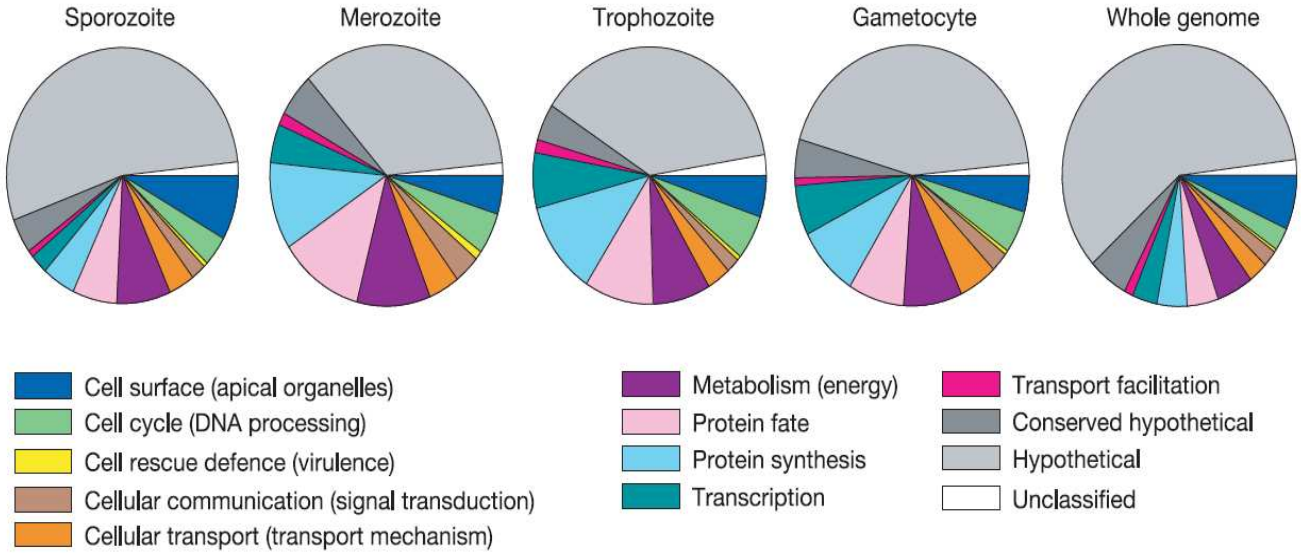

Figure 3.1 The proteins in each stage of the life cycle of the *P. falciparum* differ from one another.
Only 6% of the parasites proteins are found in all the life stages (223).

Some *P. falciparum* proteins encoded by the nucleus are post-translationally targeted to the apicoplast. The 35 kb genome of the apicoplast encodes for ~30 proteins, but 551 nuclear-encoded proteins are found to function within the apicoplast. Proteins that are targeted to the apicoplast have bipartite N-terminal extensions that contain a signal peptide and a transit peptide (224). The transit peptide has a positive charge and it contains mainly lysine, asparagine and isoleucine residues (224). The signal peptide, which is a classical secretory signal peptide, directs the co-translational insertion of proteins into the endomembrane system (89).

Currently, there are multiple techniques available for the investigation of the proteome of an organism. The use of two-dimensional gel electrophoresis (2-DE) followed by mass spectrometry (MS) to identify proteins are predominantly used. Two-dimensional electrophoresis (2-DE) was first introduced in the 1970's by O'Farrell and is still used to assess proteomes of various organisms in proteome mapping as well as to study

differentially regulated proteins and for the detection of PTM's. 2-DE has been used in the proteomic investigations of *P. falciparum* and allowed the characterisation of the proteome at different life stages of the parasite (225). In the first dimension of separation, proteins are separated based on their iso-electric point (pI). The proteins are then separated based on their molecular weight (Mr) during the second dimension. The advantages of 2-DE technology include high resolution of abundant proteins, semi-quantitative analysis, monitoring of PTMs and the approximation of pI and molecular weight values (226). The disadvantages are that the technique is limited to high abundance proteins and has a bias towards soluble proteins and mid-range molecular weight and pI proteins.

Multistage liquid chromatography mass spectrometry (LC-MS) has the ability to analyse complex peptide mixtures and allows for differential labeling of samples via chemical tagging of proteins/peptides with stable isotopes known as isotope coded affinity tags (ICAT) (227). ICAT depends on the cysteine residues in the proteins, thus making this method not ideal for *P. falciparum* because of the low number of cysteine residues in the Plasmodial proteome (214, 215). Another labelling method, isobaric tags (iTRAQ), employs a specific amine reactive tag on the lysine side chains of peptides and at the N-terminus for the quantitative analysis of differentially expressed proteins (228). iTRAQ have a slight bias towards the more acidic proteins (less arginine and lysine residues) but can be used for all types of proteins (228). These labelled peptides (isobaric) cannot be distinguished with MS, but ions are produced with a noticeable signature during fragmentation with tandem MS (MS/MS) (229). MS and MS/MS are the most commonly used methods for the identification of proteins. By measuring the mass/charge ratio of each protein digestion or fragment and using the information available on the proteome and genome of an organism (databases with the mass/charge ratios and peak intensities of known peptides) (230), proteins can be identified.

Other techniques includes protein microarrays that have been developed for the identification and quantification of proteins (231) and surface-enhanced laser desorption/ionisation-time-of-flight/ionisation-time-of-flight/mass spectrometry (SELDI-TOF/MS) that can separate proteins based on the biophysical properties (SELDI) followed by the identification of the proteins (TOF/MS) (232). Matrix assisted laser

desorption/ionisation (MALDI) and electrospray ionisation (ESI) is soft ionisation techniques which enable volatilisation of biological molecules (230).

As with the microarray data, proteomic data have to comply with specific standards. The minimum information about a proteomics experiment (MIAPE) was established to avoid discrepancies in data reporting (233) and to ensure that data are sufficient for the reader to understand and that experiments are repeatable by most laboratories (233).

For the validation of the transcriptomic data (Chapter 2), *P. falciparum* parasites were treated with A51B1C1_1 and 2-DE based proteomics were performed.

3.2 Methods and Materials

3.2.1 Culturing *P. falciparum* for proteomics

Synchronised *P. falciparum* 3D7 cultures (60 ml, Section 2.2.1.3) at 8% parasitaemia and 5% haematocrit were used for each gel. Compound A51B1C1_1 was received at a concentration of 10 mM and diluted using DMSO (0.3% DMSO (v/v) at a final volume) to a final concentration in the culture at twice the IC_{50}. Samples from the last time point of the microarray experiment (36 hpi) were used for the proteomics. A control culture containing DMSO was included as well as four biological replicates. Saponin (SIGMA) dissolved in 1xPBS was added to a final concentration of 0.01% (v/v), to each culture and the cultures were incubated on ice for 5 min to lyse erythrocytes and release the parasites. The lysed erythrocytes were centrifuged for 15 min at 2500*g* and the supernatants were discarded. The pellets were washed four times with PBS, or until the PBS was clear, with centrifugation for 1 min at 4℃ at 2500*g* between each wash step. The pellets were stored at -70℃ for a maximum of 3 0 days.

3.2.2 Isolation of proteins

The protocol of Smit *et al.* (225) was followed for the isolation of the proteins and the identification thereof. The parasite pellets were thawed on ice and 250 µl rehydration buffer [8 M urea, 2 M thiourea, 2% (w/v) 3-[(3-cholamidopropyl) dimethylammonio]-1-propanesulphonate] (CHAPS) containing 32 mM DTT (Pharmacia Biotech) and 0.7% (v/v) ampholytes (GE Healthcare)] were added. The four biological replicates were pooled. The samples were pulse-sonicated using the Branson Sonifier 450 with microtip for 10 pulses (1 s pulse followed by 1 s rest) at 40% duty cycle and an output control of three to lyse the parasites and release the proteins. Between each set of pulsing (4 in total), the samples were placed on ice to prevent foaming (indication of denaturation) and to inhibit carbamylation of the samples. Samples were centrifuged for 60 min at 16000*g* at 4℃ and supernatants were transferred to a clea n, sterile microfuge tubes and kept on ice.

3.2.3 Protein concentration determination

The 2D Quant kit (GE Healthcare) was used for the quantification of proteins according to manufacturer's instructions with minor modifications. The proteins were precipitated

quantitatively to remove interfering substances such as the ampholytes, thiourea and urea which were left in the aspirated supernatant. The principle of the 2D Quant kit is based on the specific binding of copper ions to proteins. The precipitated proteins are resuspended in a solution containing free copper ions and the unbound copper is measured with a colorimetric agent at 480 nm. The intensity of the colour is inversely proportional to the protein concentration.

A standard curve was constructed using 6 dilutions (0, 10, 20, 30, 40, 50 µg) (225) of the 2 mg/ml BSA stock solution. Different volumes of the *Plasmodium* proteins (0.5, 1, 2, 5 µl) were included for protein determination. Precipitant solution (500 µl) was added to each sample, mixed by vortexing and incubated for 3 min at room temperature, after which 500 µl of co-precipitant solution was added. The samples were vortexed and centrifuged at 16000*g* for 15 min at 4℃. The supernatants were discarde d and the pellets were centrifuged again for 3 min as above. The remaining supernatant was carefully removed by pipetting. To the pellets, 100 µl copper solution and 400 µl MilliQ water were added and mixed by vortexing. Working solution (1 ml) was added to a sample, which was mixed immediately by inversion, before proceeding to the next sample. Triplicate samples were incubated at room temperature for 20 min before transferring 300 µl of each sample to the wells of a 96 well plate. The absorbencies of the samples were measured at 492 nm with a Multiskan Ascent spectrophotometer (Thermo Labsysytems).

3.2.4 Iso-electric focusing (IEF)

Iso-electric focussing was done in quadruplicate with 400 µg of isolated protein from each individual sample. The protein concentrations determined in section 3.2.3 were used to calculate the correct volumes of protein isolations to be diluted in rehydration buffer containing 0.5% (w/v) DTT (Pharmacia Biotach), 0.7% (v/v) ampholytes (IPG buffer for pH3-10 Linear). The prepared samples (340 µl) were added to ceramic chambers (Amersham Biosciences) before the 18 cm Immobiline DryStrips, pH 3-10 Linear (Amersham Biosciences), were placed into the chamber with the gel side directed to the bottom. Air bubbles were removed and the strips were covered with oil (GE Healthcare) to ensure insulation from air, which would dry out the strip and result in crystallisation of the urea. The Etthan IPGphor II iso-electric focusing system (Amersham Bioscience) was run starting with a 10 h active rehydration step at 30 V and

20℃ (step 1, Table 3.1). The voltage was gradually increased in a step-and-hold fashion (Equation 3.1 represent gradient Vh, volt hours), to 8000 V (steps 2–8, Table 3.1) and kept at 8000 V (step 9, Table 3.1) for 24000 Vh (Equation 3.2 represent step Vh). When a total of 35000 Vh was reached the run was terminated.

$$Vh = h \times [(V_{step(n-1)} + V_{step\ n}) / 2] \quad \text{.....Equation 3.1}$$

$$Vh = h \times Volts \quad \text{.....Equation 3.2}$$

Where Vh is the volt hours, h is hours, V is the volts and n is the current step.

Table 3.1 Summary of the IEF step-and-hold program used for the 18 cm Immobiline DryStrip, pH 3-10 Linear.

Step	Type of run	Volts	Time
1	Step and hold	30 V	10 h
2	Gradient	200 V	0.10 h
3	Step and hold	200 V	0.20 h
4	Gradient	500 V	0.20 h
5	Step and hold	500 V	0.20 h
6	Gradient	2000 V	0.20 h
7	Step and hold	2000 V	0.45 h
8	Gradient	8000 V	1.40 h
9	Step and hold	8000V	**24000Vh**
TOTAL		**35000 Vh**	

3.2.5 Two-dimensional polyacrylamide gel electrophoresis (2D-GE)

The IEF strips were rinsed with MilliQ water, followed by three equilibration steps of 10 min each. Fresh equilibration buffer [50 mM Tris-HCl, pH 6.8, 6 M urea, 30% (v/v) glycerol, 2% (w/v) SDS, 0.002% (w/v) bromophenol blue] was used in the first two steps. In the first step, 2% (w/v) DTT (Pharmacia Biotach) was added, and in the second step, 2.5% (w/v) iodoacetamide (Sigma) was added to the equilibration buffer. In the third step, SDS running buffer (0.25 M Tris-HCl, pH 8.3, 0.1% SDS, 192 mM glycine) was used. Strips were placed back into the ceramic chamber and incubated at 20℃ with shaking. Between each step, the strips were rinsed with MilliQ water. Vertical 10% SDS-polyacrylamide gels [10% (w/v) acrylamide stock (30% (w/v) acrylamide, 0.8% (w/v) bisacrylamide), 1.5 M Tris-HCl pH 8.8, 0.1% (w/v) SDS, 0.05% (w/v) ammonium persulphate, 0.0003% (v/v)*N,N,N,N* -tetramethyl-ethylenediamine] were used for the second dimension separation in the Hoefer SE 600 system. The IPG strips were placed on top of the gel and sealed with 1% (w/v) agarose dissolved in SDS

running buffer. The gels were run in SDS running buffer at 80 mA at 20℃ until the bromophenol blue front reached the bottom of the glass (about 4 h).

3.2.6 Flamingo Pink staining of gels

The gels were gently removed from the glass plates and placed in a glass bowl containing fixing solution [40% (v/v) EtOH and 10% (v/v) acetic acid in MilliQ water]. The gels were fixed for 2 h with slight agitation at 20℃. After removing the fixing solution, the gels were stained for 16 h in 100 ml per gel Flamingo Pink fluorescent gel stain (Bio-Rad, Dalifornia, USA) in the dark. Flamingo Pink dye is a fluorescent dye that only fluoresces when it binds with denatured proteins. After the incubation period, the gels were blocked with 0.1% (w/v) Tween-20 for 30 min, washed twice with MilliQ water and scanned.

3.2.7 Scanning of gels and data analysis

VersaDoc 3000 (Bio-Rad) was used for the imaging of the gels and the images were analysed using the PD Quest 8.0.1 software package (Bio-Rad). The three best gels for the control and treated sets were chosen to be analysed. The gels were cropped to the same size and dimensions and filtered to remove most of the speckles caused by dust (salt setting) and the background and the horizontal and vertical streaks (filter wizard). Automatic spot detection (spot detection wizard) was performed to detect the centres of the potential spots on one gel and the same number of spots was detected on other gels. Normalisation was performed using the total density setting, because of the presence of saturated spots. A master gel was created and each spot was manually verified. Spots were added to and deleted from master gel to ensure maximum precision of the master gel.

3.2.8 Identification of spots using Plasmo2D

The master image generated in PD Quest 8.0.1, was loaded onto the software Plasmo2D (http://144.16.89.25/Plasmo2D.zip) (234). All proteins in the *P. falciparum* data base (PlasmoDB) on a pI versus MW scale were used to analyse the virtual 2-DE images that have been generated for the identification of protein. The proteins on the physical 2-DE gel are identified by comparing the position of migration of the spot on both the pI and MW axis to that position on the virtual 2-DE gel.

Making use of the molecular marker and 2-DE gel images of *P. falciparum* the gel was aligned (Figure 3.2) according to the molecular weight of the marker and the pI (133, 225).

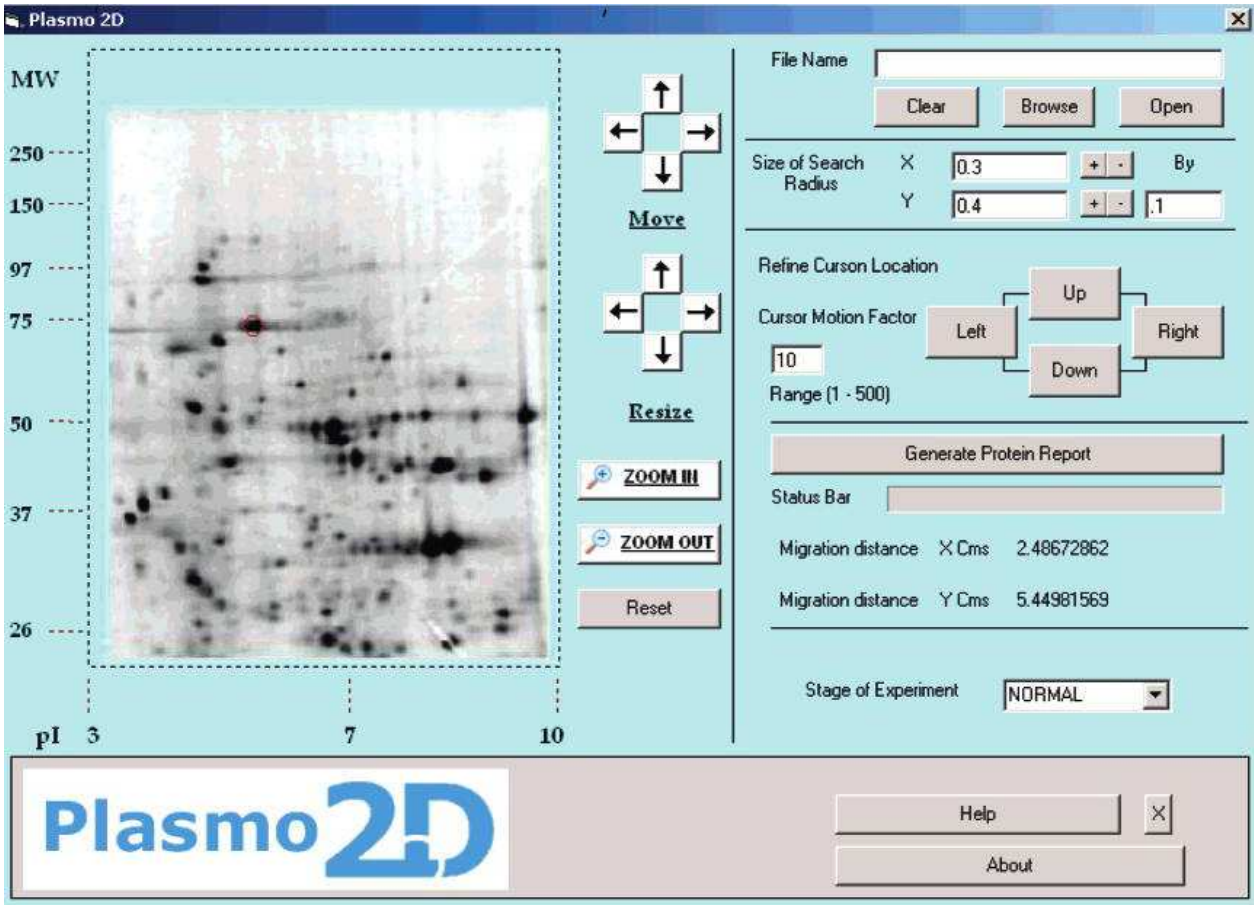

Figure 3.2 The program Plasmo2D (234).
The program uses the annotations in PlasmoDB to generate a virtual image that is compared to the physical 2-DEgel to identify spots.

The spot of interest is encircled by clicking on it and the program generates a protein report (Generate protein report button) in which the potential proteins for that spot are listed. Each protein is assigned a score that is an indication of the probability that that specific protein is the protein on the loaded 2-DE image.

3.2.9 Identification of proteins by mass spectrometry

Identification of proteins after treatment with A51B1C1_1 was confirmed using LC-MS. This was done by Dr Salome Smit at the University of Stellenbosch using the Linear ion trap Orbitrap Velos (LTQ Orbitrap).

3.3 Results

3.3.1 Protein concentration determination

Protein extraction was performed on both A51B1C1_1 treated and control *P. falciparum* parasites. The total protein concentration was subsequently determined as a measure of the efficacy of the extraction method. Standard curves were established with BSA standards for both the treated and untreated samples (Figure 3.3). Because the protein concentrations were determined on separate days for the two samples, a standard curve was generated for each sample to ensure accuracy in determining protein concentration.

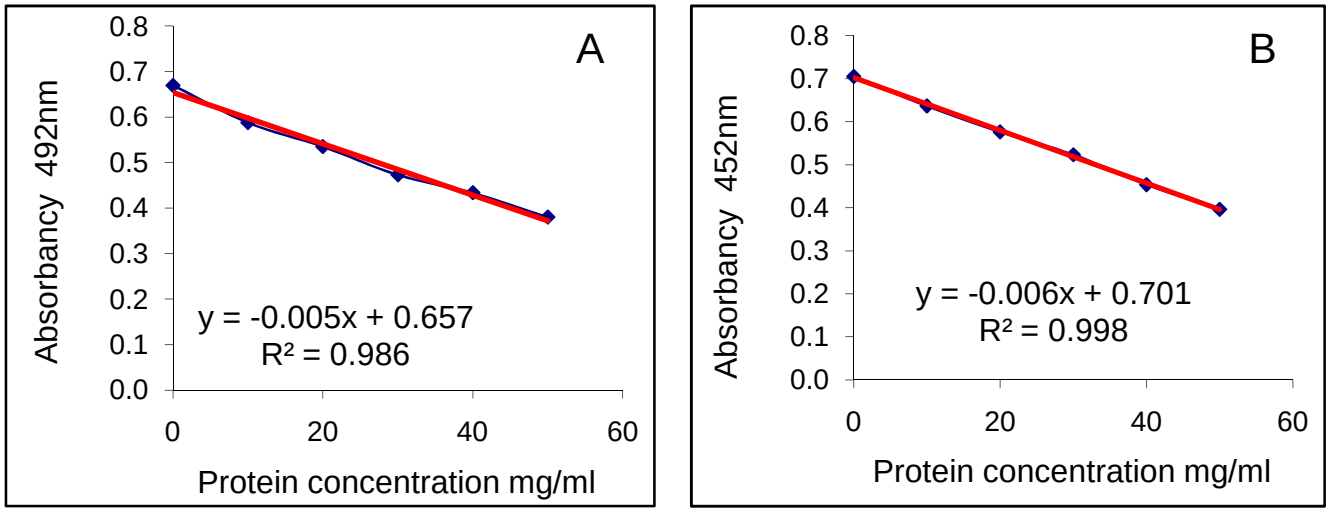

Figure 3.3 Standard curves established with BSA.
The concentration determination curve for the A –Proteins isolated from *P. falciparum* parasites treated with A51B1C1_1 and B-control parasite culture.

Both graphs showed good correlations with R^2 values at 0.986 and 0.998 (Figure 3.3). Calculations of the total protein concentrations in the treated and untreated samples (using equations obtained from the standard curves in Figure. 3.1) indicated concentrations of 10.8 and 18.1 mg/ml, respectively.

3.3.2 2-DE analysis of A51B1C1_1 treated *P. falciparum* parasites

The protein concentrations determined in section 3.3.1 were used to determine the volume of samples to be used for loading 400 µg of protein onto the IPG strip. It is important that the same concentration of protein is loaded for both the treated and the control sample to ensure reliable comparative analysis. After the proteins separated on basis of pH, the strips were loaded onto a SDS-PAGE. The proteins were now

separated according to MW. After staining of the gels with Flamigo Pink stain, the gels were scanned to obtain gel images for further analysis.

The program PD Quest 8.0.1 was used to normalise and analyse the data obtained from the 2-DE gels. PD Quest distinguishes between speckles caused by dust and actual protein spots (Figure 3.4).

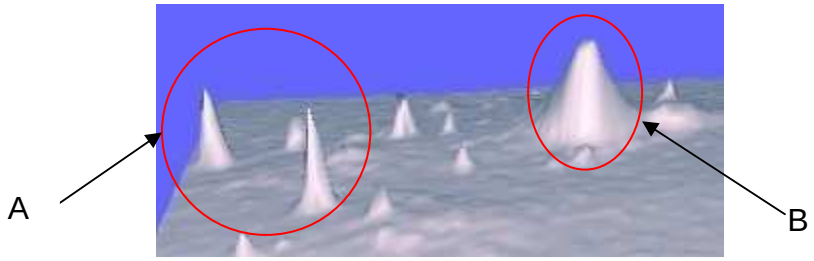

Figure 3.4 The 3D view to distinguish between a speckle and a protein spot.
A: Dust speckles. B: Protein spot.

This information was then used to identify spots. The three best gels for both the treated and the control protein samples were subsequently used for the detection of spots. The spot detection wizard within PD Quest detected all possible spots, which were then manually checked. Missed spots were manually added and false positives, caused by undetected remaining speckles, were removed. All the spots on all the six gels were used to generate a master image (Figure 3.5).

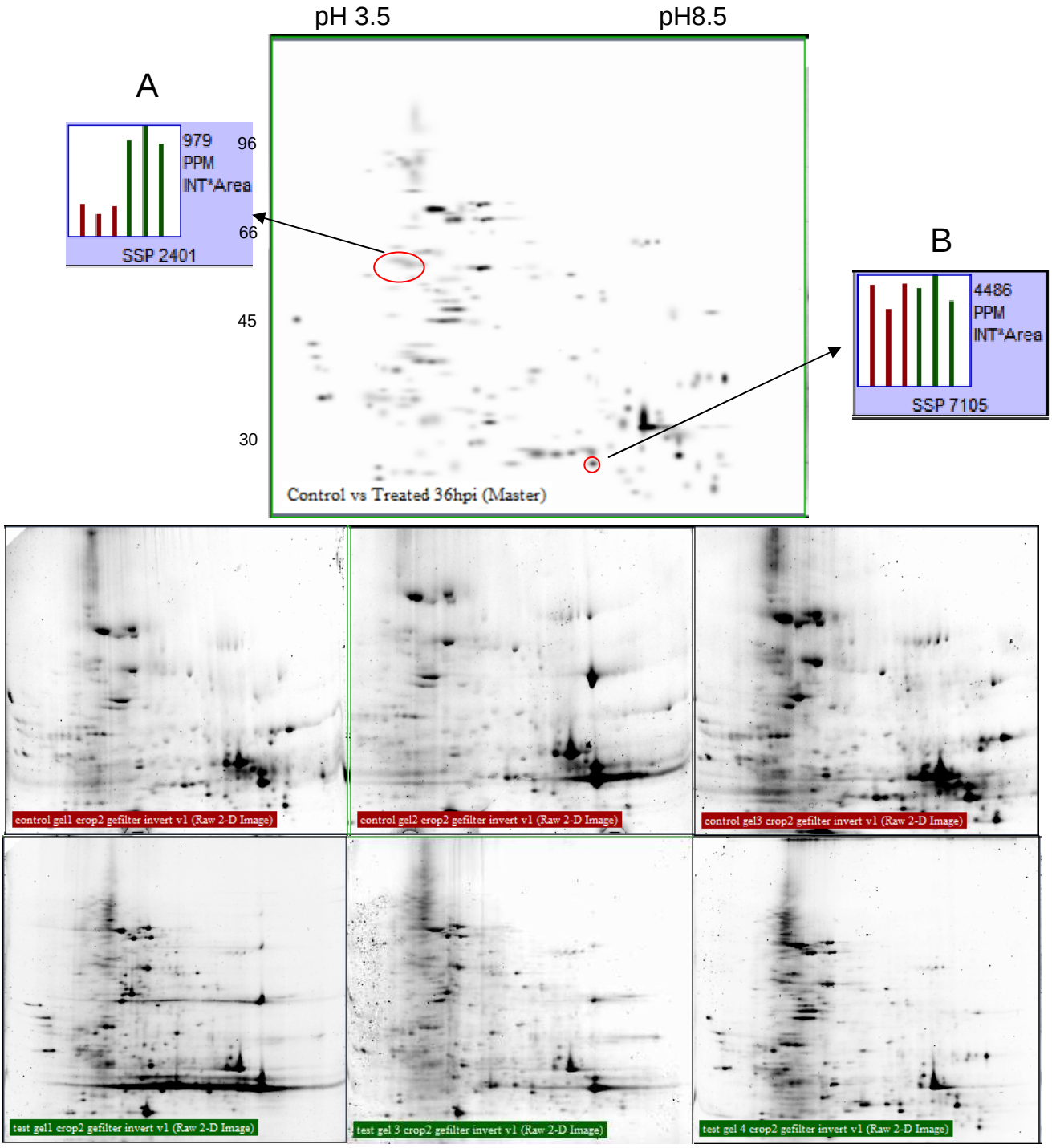

Figure 3.5 The three gels for the treated (green) and the three control gels (red) were combined to give a master image from which all the spot information can be obtained.

After the master image is created, all the spots on the image represent all the spots on the six original gels. The spot review function in PD Quest can be used to obtain the information on a specific spot, thus obtaining the information of that spot on all the individual gels. A: an example of a change in abundance between the treated and the control parasite cultures, red is the control samples and green is the treated samples. B: Example of a protein that did not show any change in abundance between the treated and the control parasite samples.

The master image is a virtual gel image that contains the combined spot information (from all 6 gels) for a single spot and all the information on that specific spot from all the

gels is represented in a spot review graph (Figure 3.5). These graphs indicate the protein levels and allow for a graphical representation of the abundance levels of proteins within specific spots in all the gels. The control spots are indicated in red bars and the treated spots are indicated in green bars. A summary of the data obtained from PD Quest for both treated and control samples are shown in Table 3.2. The overall match rate (number of spots matched for each individual gel) was on average 97% and the master match rate (number of spots of each individual gel to the number of spots on the master image) was 72%. The master image contained 185 uniquely identified spots present on at least 2 of either the control or treated group of gels, thus included into the master image.

Table 3.2 Data obtained after spot detection for the treated and control gels.

Condition	Data obtained
Master image spot count	185
Control vs. treated correlation coefficient	0.713
Average match rate per gel	97%±0.9[a]
Average master match rate	72% ±14.7[a]
Average spots per gel	144
Spots matching all gels	54

[a] – The average match rate per gel and average master match rate are averages of the six gels with standard deviation.

PD Quest analysis, through the master image, allowed the analysis of differential protein expression of the 185 uniquely identified spots present. To determine the differentially affected protein spots (p-value<0.05), the average change in abundance is taken. The significance difference between the protein spots in the treated and the control group is then determined. Differentially expressed proteins were both graphically and quantitatively represented for any single spot as indicated in Figure 3.6.

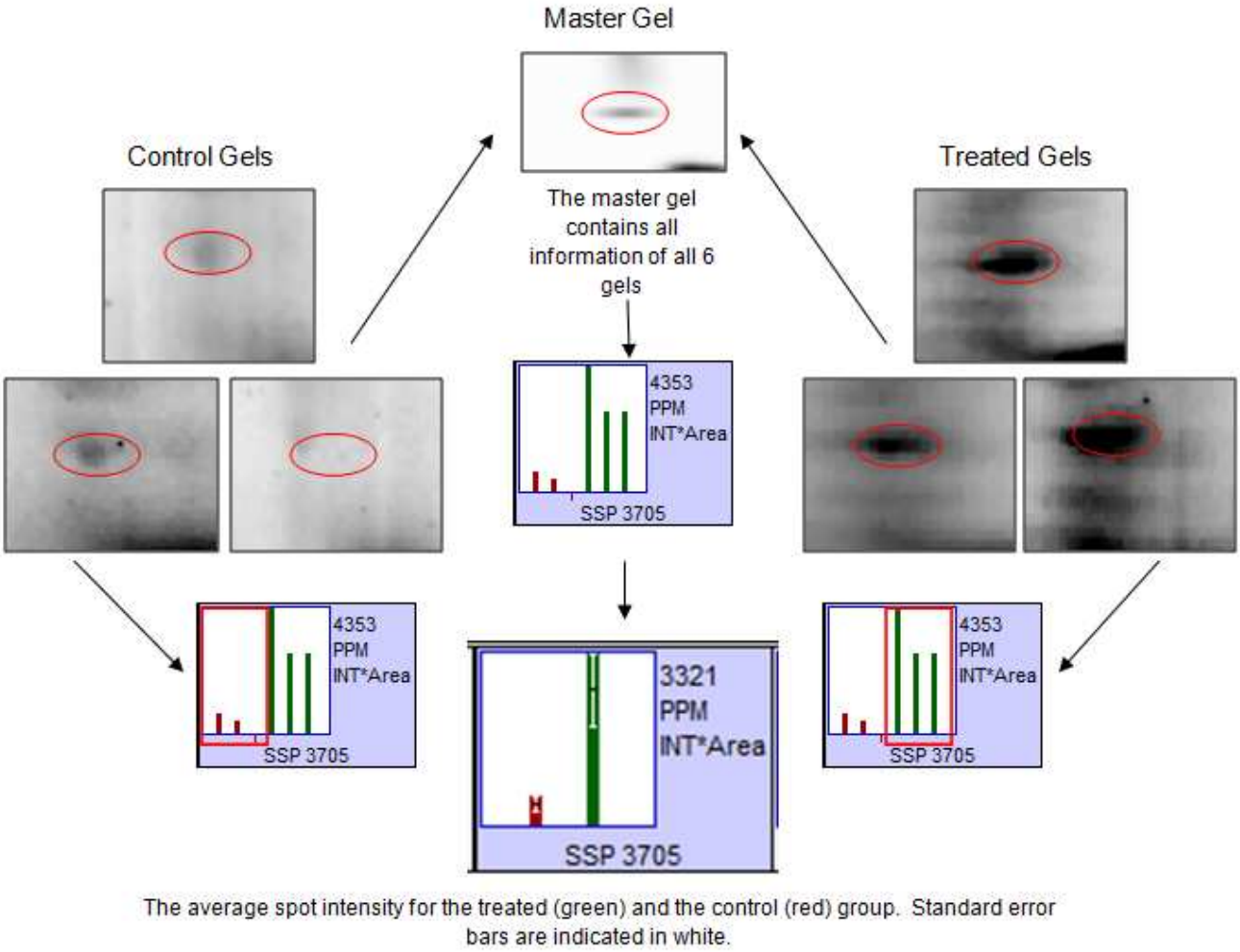

Figure 3.6 The process in PD Quest to determine the differentially affected protein spots.

The three gels from the treated and the three gels from the control group are combined to generate the master image. The master image contains all the information of all the gels in a single gel image. Using the master image the difference in abundance in protein between the treated and control samples can be determined. Each spot on each gel is also represented as a bar graph, which can be combined to calculate the average of the three gels in each group (treated or control). The white error bar is also included in the average bar graph.

Of the 185 protein spots analysed 21 showed an increase in abundance and 11 decreased in abundance (Figure 3.7) after treatment of *P. falciparum* parasites with the compound A51B1C1_1. Figure 3.7 indicated that the majority of proteins with increased abundance were more acidic (pI below 6) and had large MWs (mostly above 35 kDa). The proteins that showed a decrease in abundance had pI values above 5.5 and were smaller in MW (mostly below 30 kDa).

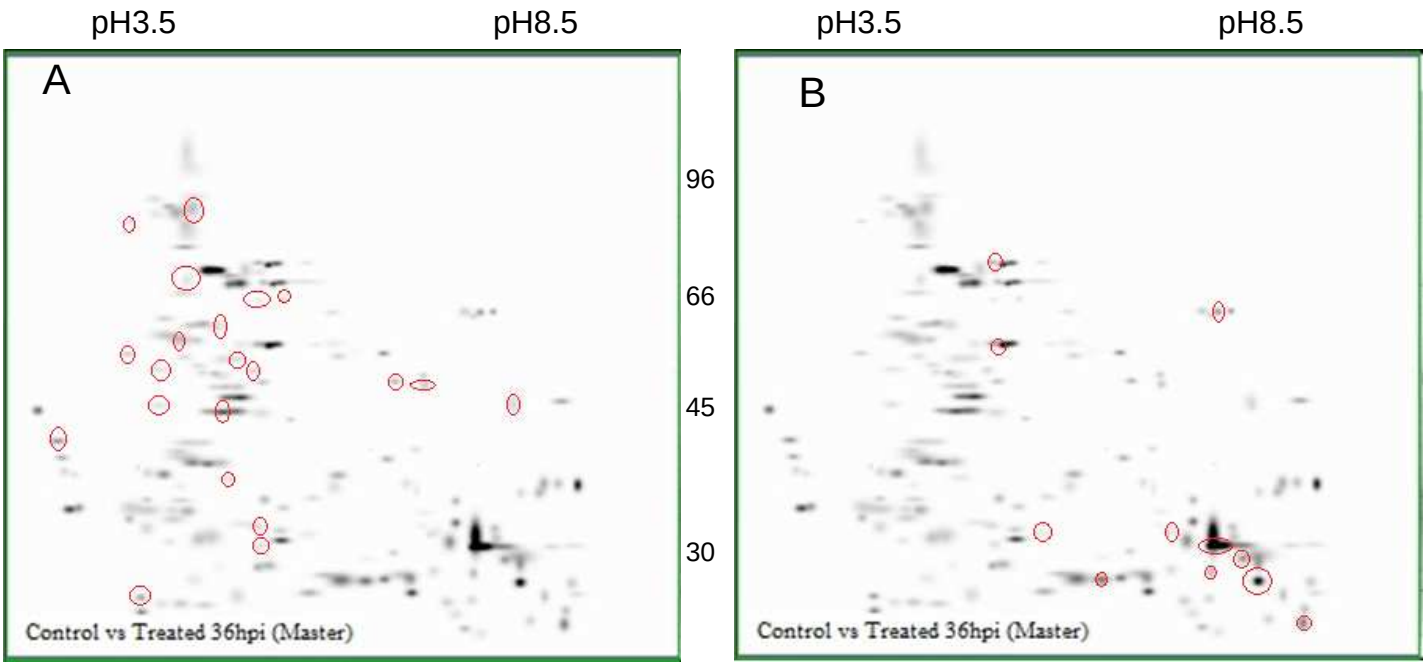

Figure 3.7 The master image generated in PD Quest indicating all the proteins with differential abundance levels.

A - Proteins with increased abundance; B – Proteins with decreased abundance. $p<0.05$. Molecular weight is in kDa. Red circles indicate the proteins spots with difference in abundance.

3.3.3 Identification of the differentially expressed proteins in A51B1C1_1-treated *P. falciparum* parasites

In an attempt to identify the 32 protein spots (21 with increased abundance and 11 with decreased abundance) that were indicated with 2-DE to be differentially expressed in the *P. falciparum* proteome after treatment with A51B1C1_1, Plasmo2D was employed (http://144.16.89.25/Plasmo2D.zip) (234). Plasmo2D contains a complete virtual map of the 2-DE proteome of *P. falciparum* with all proteins in the proteome annotated and positioned according to their pI and molecular weight and confirmed by mass spectrometry analysis. As such, the localisation of proteins within a newly studied *P. falciparum* proteome is correlated to the Plasmo2D map and the identity of the specific protein in a spot is inferred.

Therefore, differentially regulated protein spots identified within the 2-DE maps of the *P. falciparum* proteome obtained above, were analysed with Plasmo2D. Table 3.3 indicates the inferred identities of the differentially regulated proteins after treatment of *P. falciparum* with A51B1C1_1.

Table 3.3 The protein spots indicated by PD Quest to have an increase or decrease in abundance as annotated by Plasmo2D.

Number[a]	ID[b]	Description	pI	MW	Score[c]
Spots with increased abundance					
8403	PF14_0436	Helicase, truncated, putative	8.92	39868.27	37
4406	PF10_0289	Adenosine deaminase, putative	5.42	42465.43	4
1301	MAL8P1.95	Hypothetical protein	4.13	37499.69	65
3803	PF08_0054	Heatshock 70kDa protein	5.51	73914.18	404
3502	PF14_0077	Plasmepsin 2 precursor	5.36	51480.3	77
7403	PF14_0261	Proliferation- associated protein2g4	7.92	42640.65	62
5404	PF10_0155	Enolase	6.22	48677.16	50
6404	PFC0285c	T-complex protein betasubunit	6	62529.24	34
5609	MAL13P1.28	TCP1 chaperonin delta subunit	6.1	57971.82	33
2005	Out of range				
3603	PFE1600w	Hypothetical protein	4.93	30187.75	82
4503	MAL8P1.17	Disulphide isomerise precursor	5.57	55500.74	414
2004	PFA0400c	Beta3 proteasome subunit, putative	5.08	23080.27	4
5103	MAL13P1.27	Proteasome subunit, putative	6.18	27228.05	16
4504	PF14_0655	RNA helicase-1, putative	5.49	45309.66	24
2501	PFE1370w	Hsp70 interacting protein, putative	4.67	51125.11	18
5201	PF10_0264	40S ribosomal protein, putative	5.92	29855.91	101
2401	PFL2215w	Actin	5.21	41870.23	41
4304	MAL8P1.83	-	5.98	31023.57	27
2705	PF07_0029	Heatshock protein 86	4.94	86165.48	303
7401	MAL13P1.23	Hypothetical protein	7.15	42159.23	97
Spots with decreased abundance					
8106	PFL0595c	Glutathioneperoxidase	8..99	23952.48	9
8101	PF11_0208	Phosphoglyceratemutase, putative	8.3	28769.82	30
8004	Out of range				
5502	PFB0445c	Helicase, putative	5.69	52223.16	63
7107	PFA0335w	*P. falciparum* GTP bindingproteinRAB5	6.91	24328	0
7206	PF10_0121	Hypoxanthine phosphorbosyl transferase	7.6	26362.2	11
8104	PF07_0008	Hypothetical protein	8.55	27672.77	4
5701	PF08_0081	Hypothetical protein	5.95	65609.12	54
8102	PFC0635c	Translation initiation factor E4, putative	8.39	26947.48	3
8602	PF14_0078	HAPprotein	8.04	51692.76	123
6206	PF10_0210	Deoxyribose-phosphatealdolase	6.85	28979.43	1

a – The number is assigned by PD Quest to each spot on the master image.
b – PlasmoDB identification.
c – The score is assigned by Plasmo2D as the probability that the annotation of the specific spot is correct, the higher score indicates a higher probability.

These identified proteins were subsequently used to obtain GO annotations with PlasmoDB as an indication of the broad biological processes that were affected (Table 3.4).

Table 3.4 The biological functions assigned to the recognized genes encoding for the proteins differentially regulated.

Gene ID	Biological function	GO term	GO clustering
Increased abundance			
PF14_0436	Biological Process	GO:0008150	Biological process
MAL8P1.83	Hypothetical Protein	GO:0006412	Biological process
PFA0400c	Beta3 Proteasome Subunit, Putative	GO:0006511	Biological process
MAL8P1.95	Hypothetical Protein	-	Biological process
MAL13P1.28	TCP1 chaperonin delta subunit	-	Biological process
PFE1600w	Hypothetical Protein	-	Biological process
MAL13P1.27	Proteasome Subunit, Putative	-	Biological process
PFE1370w	Hsp70 interacting protein, putative	-	Biological process
PF14_0261	Cell Cycle Arrest	GO:0007050	Primary metabolism
PFL2215w	Cytoskeleton Organisation And Biogenesis	GO:0007010	Primary metabolism
PF10_0155	Gluconeogenesis	GO:0006094	Primary metabolism
PF14_0077	Hemoglobin Catabolic Process	GO:0042540	Primary metabolism
PF10_0289	Purine Ribonucleoside Monophosphate Biosynthetic	GO:0009168	Primary metabolism
PFC0285c	Protein Folding	GO:0006457	Protein folding
MAL8P1.17	Protein Folding	GO:0006457	Protein folding
PF08_0054	Response To Unfolded Protein	GO:0006986	Protein folding
PF07_0029	Response To Unfolded Protein	GO:0006986	Protein folding
PF14_0655	Regulation Of Translational Initiation	GO:0006446	Translation
PF10_0264	Translation	GO:0006412	Translation
MAL13P1.23	Metal Ion Transport	GO:0030001	Transport
Decreased abundance			
PFL0595c	Response To Oxidative Stress	GO:0006979	Oxidative stress
PFB0445c	Biological_Process	GO:0008150	Biological process
PF07_0008	Hypothetical Protein	-	Biological process
PF08_0081	Hypothetical Protein	-	Biological process
PF10_0210	Deoxyribonucleotide Catabolic Process	GO:0009264	Primary metabolism
PF11_0208	Glysolysis	GO:0006096	Primary metabolism
PF10_0121	Purine Ribonucleoside Salvage	GO:0006166	Primary metabolism
PF14_0078	Proteolysis	GO:0006508	Proteolysis
PFA0335w	Small GTPase Mediated Signal Transduction	GO:0007264	Signal transduction
PFC0635c	Translational Initiation	GO:0006413	Translation

3.3.4 Identification of the differentially expressed proteins in A51B1C1_1-treated *P. falciparum* parasites with mass spectrometry

(At time of submitting only the proteins identified to be unique to the treated or control sample were available. The remaining data will be included in the article)

Samples of the control and the A51B1C1_1 treated parasites were separated with SDS-PAGE and the differentially affected proteins were identified by Dr Salome Smit at the University of Stellenbosch. The analysis was done on the LTQ Orbitrap instrument. The ions are accumulated in the linear ion trap and passed on to the analyser, resulting in high resolution MS measurements (235). A total of 276 Plasmodial proteins were only present in the treated A51B1C1_1 sample (Appendix 4) and 204 Plasmodial proteins were only present in the control sample (Appendix 5). The proteins from the control and treated were clustered separately using PlasmoDB and MADIBA into 12 clusters (Figure 3.8). Three proteins involved in lipid biosynthesis were identified uniquely to the treated samples and three proteins involved in the same process were unique to the control sample (Table 3.5).

Table 3.5 Proteins unique to either the treated or the untreated sample.

PlasmoDB ID	Description	GO term	GO Cluster
Proteins only found in the treated sample			
PFI1180w	Hypothetical Protein	GO:0006629	Lipid metabolism
PF07_0040	Lysophospholipase-Like Protein	GO:0006644	Lipid metabolism
PF11_0257	Ethanolamine Kinase	GO:0006646	Lipid metabolism
Proteins only found in the control sample			
PF14_0664	Biotin Carboxylase Subunit Of Acetyl CoA Carboxylase	GO:0006633	Lipid metabolism
PF14_0250	Hypothetical Protein	GO:0006629	Lipid metabolism
PFF0410w	Hypothetical Protein	GO:0006629	Lipid metabolism

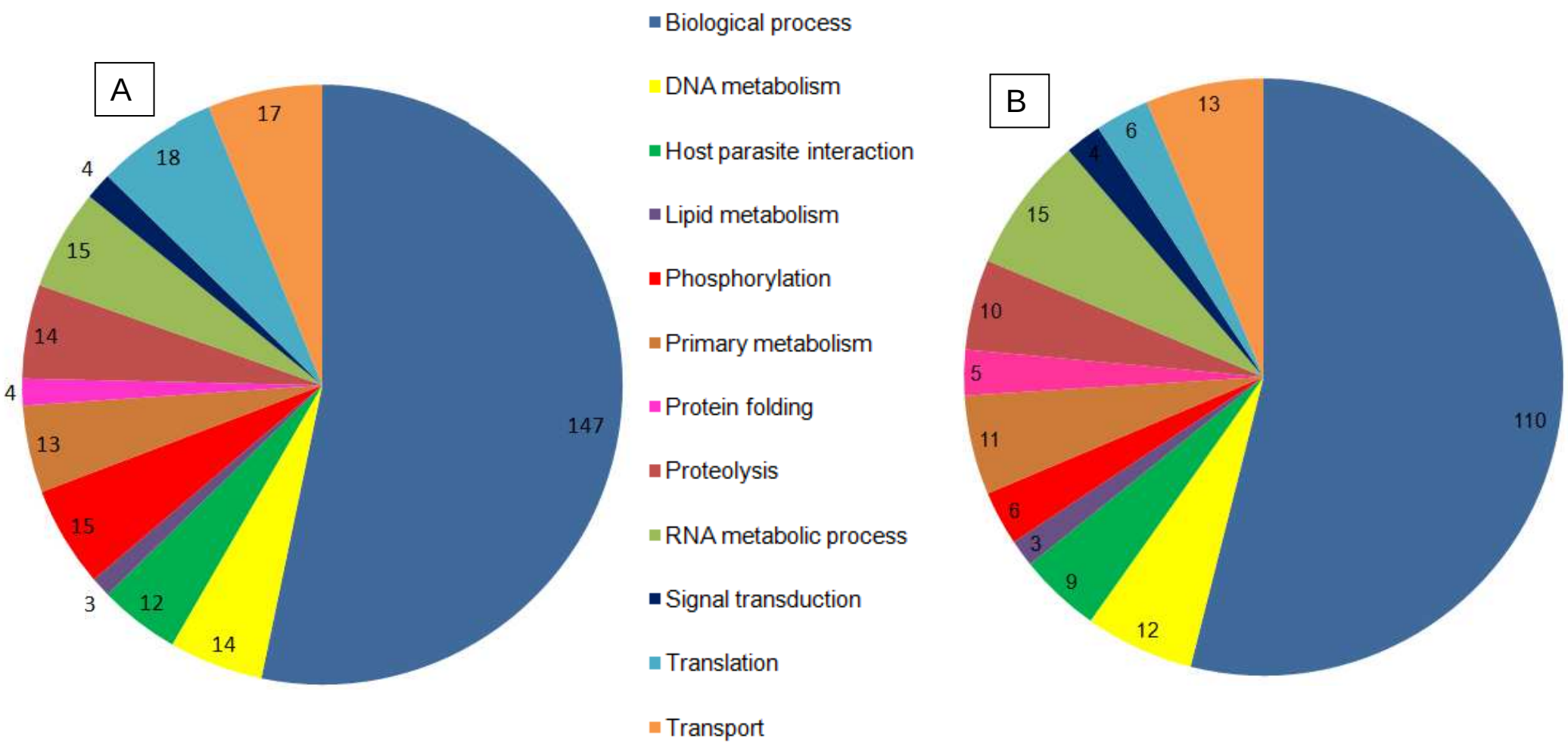

Figure 3.8 Gene ontology annotation of the affected proteins after treatment of *P. falciparum* with A51B1C1_1.

A – The GO annotation clustering for the proteins only found in the treated sample. B – The GO annotation clustering for proteins only in the control sample.

3.4 Discussion

P. falciparum is a multistage organism with specialised gene regulation resulting in a 'just-in-time' production of transcripts involved in the biological processes of the specific life cycle stage of the parasite (137). Proteins are thus produced from the corresponding transcript mainly without delay and are expressed between 0.75 and 1.5 times of a life cycle in the parasite (137, 213). This study used both 2-DE gel-based and MS methods for the determination of differentially regulated proteins after A51B1C1_1 treatment.

The ability of 2-DE to capture this production of proteins has proven to be valuable to the study of a multistage organism, such as the malaria parasite. The technique is used to investigate the proteome of the organism through the detection of PTM's and the study of the differentially regulated proteins after treatment. When the results of 2-DE analysis of other protozoan parasites were compared to that of *P. falciparum*, there was a definite need for improvement of the method because of the low number of spots that could be detected with the protocols used at that time (218, 219, 236). Although, 2-DE has been hampered by numerous technical constraints in the past including low protein coverage mainly because of protein solubility constraints (223) and exclusion of proteins due to extreme pI and MW (237), the methodology used in this study has subsequently been successfully optimised to provide ~80% coverage of the *P. falciparum* trophozoite proteome (225).

General methods of protein staining after 2-DE include the use of SYPRO Ruby, Flamingo Pink, Colloidal Coomassie and silver staining. The most sensitive stains are SYPRO Ruby and Flamingo Pink, which can detect up to 1 ng of protein and have a linear range (199). Silver stain can detect a minimum of 10 ng of protein but has a poor linear range. The least sensitive stain is Colloidal Coomassie, with a detection limit of 25 ng of protein and also have a poor linear range (225). In context of the *P. falciparum* proteome, with its specific properties including large protein size, pI, hydrophobicity etc. (220), Flamingo Pink stain was shown to have the best MS/MS identification rates and good linear range (199, 225). Because of the multiple advantages of Flamingo Pink shown by Smit *et al.* (2010), this fluorescent dye was used to aid in the investigation of the proteome of the A51B1C1_1 treated parasites.

After inhibition with A51B1C1_1, 32 spots were identified on the 2-DE gels as spots that had a change in the abundance between the treated and the control samples using PD Quest. The optimisations in the proteomic protocol resulted in the absence of haemoglobin on the 2-DE gels and an increase in spot detection, especially the proteins in the pH 8-9 range with low abundance. The majority of these proteins also have MWs below 30 kDa. The proteins with increased abundance had pI values below 6 and were larger in size. In previous studies the overall distribution of spots (high and low abundance spots) on the gels have been more random and grouping of spots seen on the 2-DE gels of results in this study has not yet been noticed in other studies (225). Of the 32 protein spots identified by PD Quest to be differentially regulated, 21 protein spots indicated an increased in abundance and 11 proteins showed a decrease in abundance.

In sillico analyses of proteome data is a useful predictor of the identity of differentially expressed proteins. Particularly for the *P. falciparum* proteome, analysis of 2-DE gels can also be done by the virtual 2-DE generator, Plasmo2D (234). Plasmo2D provides rapid identification of the *P. falciparum* parasites' proteome based on genome data and proteome characteristics including protein pI and MW data. Plasmo2D was validated by comparing western blotting and MALDI-TOF MS to protein identification done by Plasmo2D (234). The advantage of this analysis tool is that it aids in the identification and analysis of stage specific expression of even low abundance proteins in protein complexes and subcellular organelle fractions (234). Analysis of the 32 differentially regulated protein spots in the proteome of *P. falciparum* parasites treated with A51B1C1_1 with Plasmo2D allowed identification and clustering of the proteins based on GO annotations. Besides the expected proteins involved in the cluster biological processes, proteins involved in primary metabolism (including lipid metabolism) were also affected. It was decided to confirm the preliminary data obtained from Plasmo2D by MS/MS.

Proteins uniquely found to be present in the control *P. falciparum* parasites or those treated with A51B1C1_1 were subsequently identified with MS. In each of these datasets, 3 proteins were uniquely identified to be involved in lipid biosynthesis. Besides the unannotated proteins in these datasets, PF11_0257 (2.7.1.32, Ethanolamine kinase) and PF07_0040 (3.1.1.15, Lysophospholipase-like protein) was unique to the treated sample (Figure3.9). Ethanolamine kinase is also known as

choline kinase (PFI1485) and was also present in the transcriptome dataset (Chapter 2), where the transcript for this protein showed a decrease in abundance. This difference between the transcriptomic and the proteomic data is not uncommon and have been seen in previous studies (199) and it has been reported that the parasite is able to differentially regulate protein and transcripts levels (238). Ethanolamine kinase is the enzyme responsible for the conversion of choline to phosphocholine (239, 240). Phosphocholine is the precursor for the major membrane phospholipid, phosphatidylcholine (PC) (241). The parasite is also capable of synthesising phosphocholine from serine via a *de novo* pathway (242). Both ethanolamine kinase and lysophosholipase-like protein are involved in glycerophospholipid metabolism (Figure 3.9). PF14_0664 - Biotin carboxylase subunit of acetyl CoA carboxylase plays a role in fatty acid metabolism and is unique to the control sample and decreased in abundance after treatment to the point where it is not detectable with MS. The enzyme acetyl CoA carboxylase is the first enzyme of the *de novo* fatty acid synthesis, the carboxylation of acetyl-CoA, to produce malonyl-CoA by using bicarbonate as a source of the carboxyl group, biotin as a cofactor, and ATP as a source of energy. It also provides malonyl-CoA for the synthesis of very long chain fatty acids and for secondary metabolism (110, 243). Zuther *et al.* (1999) treated *T. gondii* with a herbicide and also proved a decrease in the abundance of the enzyme acetyl CoA carboxylase (74). In Chapter 2, PF10_0016 (Acyl CoA binding protein) and PFL0415w (Acyl carrier protein) are both transcripts involved in fatty acid biosynthesis. Both these transcripts showed an increase in abundance during the transcriptomics in the treated sample. The increase of these two transcripts may by a compensational mechanism of the parasite to counteract the effect of the treatment on acetyl CoA carboxylase.

In this chapter, the proteomic response to A51B1C1_1 treatment was investigated. In this investigation perturbation-specific response were determined in the transcriptome and in the proteome as well as correlation between the transcript and the proteins. It seems that treatment of *P. falciparum* parasites with A51B1C1_1 did have an effect on the conversion of DAG into TAG and fatty acid biosynthesis. After transcriptome-wide analyses and proteome investigation of parasites treated with this herbicide-derived compound, it was found that similar processes are affected, although the effect itself may differ between the proteome ad transcriptome at the given time.

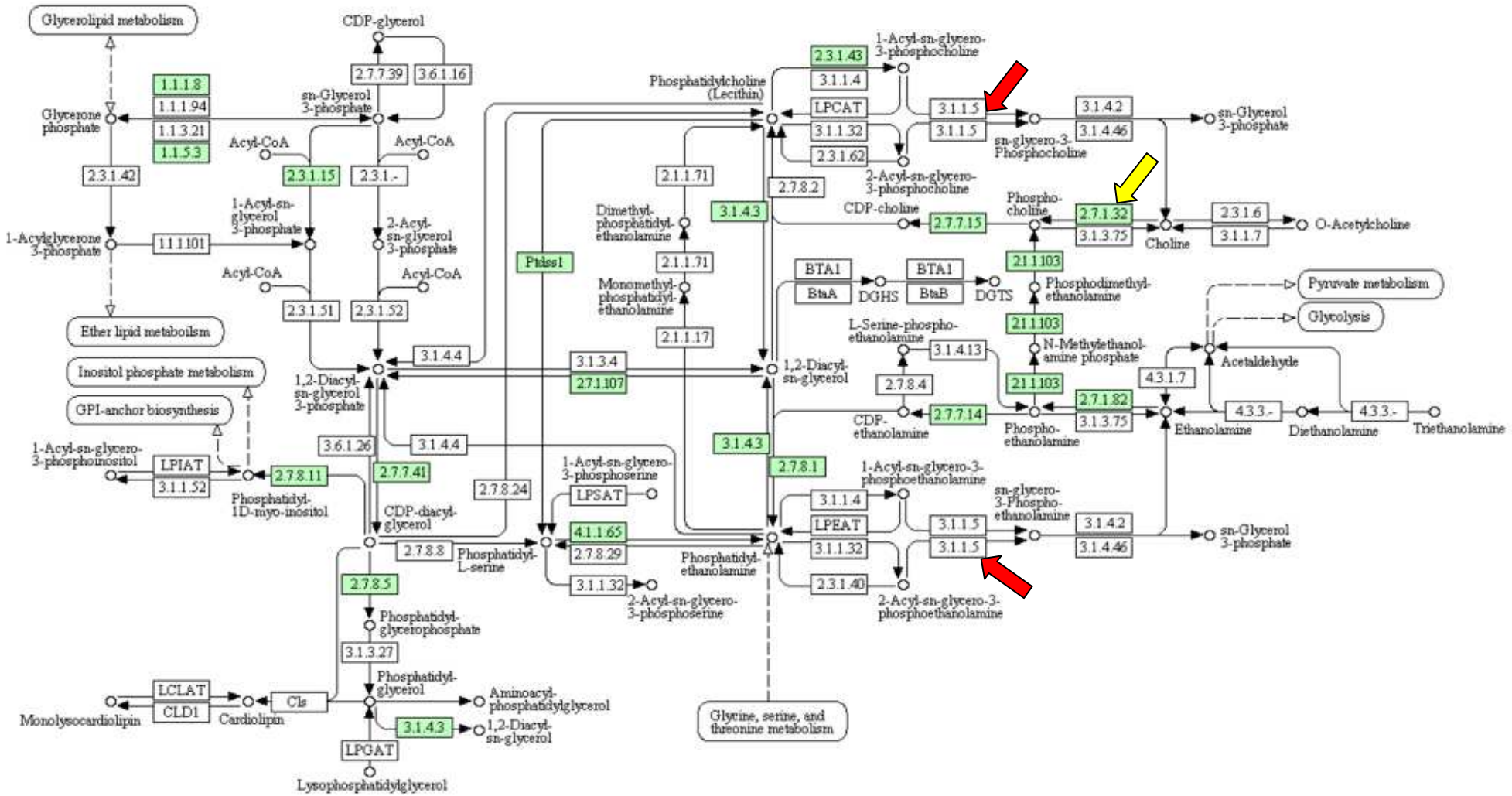

Figure 3.9 Glycerophospholipid metabolism as presented by KEGG (208).

Green blocks indicate the enzymes present in the pathway of *P. falciparum.* Red arrows indicate PF07_0040 (EC 3.1.1.15, Lysophospholipase-Like Protein) and yellow arrow PF11_0257 (EC 2.7.1.32, Ethanolamine Kinase).

CHAPTER 4
CONCLUDING DISCUSSION

4.1 Rational of the study

Malaria is one of the most fatal diseases, caused by a protozoal parasite (4). *P. falciparum* is developing resistance against currently available antimalarial drugs (1) and therefore, there is an urgent need for the development of new drugs and the discovery of new drug targets (35). One potential new drug target is the apicoplast and its associated metabolic processes that are essential to parasite survival (3). The apicoplast is closely related to the chloroplasts within plants and therefore it is deemed possible to apply highly selective herbicide-derived compounds to the malaria parasite and affect its death (3).

The evolutionary relationship of *P. falciparum* with plants motivated the investigation if a herbicide derived compound may be a novel antimalarial drug. Galactolipid synthesis within the apicoplast may be a possible pathway to inhibit within the apicoplast of the parasite (119). MGDG and DGDG, the two major galactolipids, are not found in the human host of the malaria parasite. In plants it is localised in the membrane of the chloroplast (50, 95). No homologues of MGDG and DGDG synthase could be identified in the genome of *P. falciparum* but a DGDG-like epitope was detected in the plasma membrane and the inner membrane in several stages in the life cycle of the parasite (119). Thus compounds developed to inhibit the galactolipid synthesis in plants, may kill the *P. falciparum* parasite. This study investigated the effect of one such compound, A51B1C1_1 on the transcriptome and the proteome of the parasite (118). The compound A51B1C1_1 was derived from Galvestine-1, a competitive inhibitor of DAG, the substrate for MGDG and DGDG synthesis.

The development of new antimalarials has been standardised globally by the compound progression criteria initiated by the Medicine for Malaria Venture (MMV) (244). The MMV standardisation ensures that all potential antimalarials screened as early leads are safe through *in vitro* investigation before the compounds proceeding to *in vivo* studies (early hits). These criteria include the determination of 1) the biological activity of new compounds, which should possess an IC_{50} of < 1 µM when tested against various *P.*

falciparum strains, 2) the selectivity, 3) the chemistry of the compound ('drug-ability') and 4) indication of the physiological response (mode of action) of the compounds in the parasite.

The general objective of this study was to determine the response the parasite will have to treatment with A51B1C1_1 using transcriptomics and proteomics.

4.2 Summary of the findings

In vitro whole cell activity of compound A51B1C1_1 against *P. falciparum* (strain 3D7) showed an IC_{50} value of 447 ±16 nM, indicating the potential sensitivity of this compound against the parasite. Galvestine-1 and Galvestine-2 showed IC_{50} values at 6.12 µM and 1.45 µM respectively. The difference in the IC_{50} values is an indication that the small variations in structure between these compounds do have an effect on the activity of the compound on *P. falciparum*. The IC_{50} of A51B1C1_1 compares well with other well known antimalarials commercially available such as chloroquine (50 nM) (182), Artemisinin (100 nM) (245), Artesunate (3.4 nM) (180) and Eurartesim® (3 nM) (246), and is well under the cut-off limit 1 µM stipulated by the MMV. The biggest problem currently with compounds targeting the apicoplast in the malaria parasite is the phenomena 'delayed death'. This is due to slow acting compounds because the effect is only seen in the next life cycle after treatment. However, the compound, A51B1C1_1 is fast acting and demonstrates effecting parasite growth inhibition within the first life cycle and thereby overcoming the limitations that drugs with a 'delayed death' phenotype would pose in an antimalarial treatment regime.

Compound A51B1C1_1 is originally derived from a herbicide; therefore it may prove to be highly selective to the apicoplast of *P. falciparum* without targeting any metabolic process in the human host. The compound was tested on human erythroblasts (K-562) and showed an IC_{50} of 13.3 µM (Personal communication, Eric Maréchal, Pretoria, 2009). This shows a selectivity almost 25-fold larger towards the *P. falciparum* parasites and thus comply with the MMV standards on selectivity. The selectivity of the compound against HepG2 cells (human liver hepatocellular carcinoma cell line) must show a larger than 10-fold selectivity toward the parasites (MMV criteria). HepG2 cells are the work-horse of selectivity testing because of its mammalian origin and the liver cells are responsible for the metabolism of toxic compounds. Therefore, the effect seen

of any compound tested on HepG2 cells is a very close approximation of the true effect on the human body. The compound should therefore be investigated on HepG2 cells in addition to determining off target effects in the host.

The chemistry of the compound includes determination of the solubility of the compound in PBS, the compliance to Lipinski's rule of five and the synthesis process of the compound, which should be environmentally-friendly, easy and cost efficient. The chemical scaffold of compound A51B1C1_1 is unrelated to any current antimalarials and may therefore have a novel action on the parasite. Additionally, this may imply that there should not be a rapid development of resistance against the compound since the parasite has not been exposed to this chemotype. Compound A51B1C1_1 conforms to all the properties required of a novel drug lead according to Lipinski's rule of five (247). Particularly, the compound shows only one minor regression with a log P value at 5.58 compared to the other descriptors falling into the expected '5' value cut off: hydrogen bond acceptors = 4; hydrogen bond donors = 2 and molecular Weight = 497. These drug-like properties of the A51B1C1_1 compound are a good indication of the possibility of drug activity of the compound, according to the MMV.

4.3 Implication and limitations of findings

The functional genomics investigation proved to be of immense value in the investigations of the effect of drug perturbations on *P. falciparum.* This allowed the global determination of the physiological response of the parasite to treatment with A51B1C1_1, and therefore this contributes to describing a possible mode of action. In this transcriptomic microarray study, the A51B1C1_1 treatment specific response was seen above the tight 'just-in-time' control of transcripts in the parasite. Moreover, both the transcriptome and the proteome indicated highly unique responses in *P. falciparum* parasites after treatment with the herbicide derived compound that has not been previously described with other perturbations. From the results of the proteomic and transcriptomic studies, there are evidence that lipid biosynthesis is affected by the treatment. Particularly, glycerophospholipid metabolism, glycerolipid metabolism and fatty acid metabolism was affected. Both transcriptomics and proteomics gave evidence that the target in glycerophospholipids metabolism is the formation of TAG from the substrate DAG.

The compound A51B1C1_1 was derived from Galvestine-1, a competitive inhibitor of DAG, the substrate for MGDG and DGDG synthesis in *Arabidopsis*. Although no sequence homologues have been found in the *P. falciparum* genome database with statistically reliable similarities to chloroplast envelope MGDG synthase or DGDG synthase multigenic families, it has been determined that *P. falciparum* does synthesise galactolipids (which would be the target of Galvestine-1 (119)) and from the data in this study it is evident that A51B1C1_1 could compete for the binding of DAG in *P. falciparum*. The compound A51B1C1_1 and the parent compound Galvestine-1 only have one structural difference and that is at the benzimidazole group. Between A51B1C1_1 and Galvestine-2 there are two structural differences, at the benzimidazole group and dibenzylamino-ethoxy group. However, even with these differences in structure between A51B1C1_1 and Galvestine-2, comparative transcriptome analyses showed possible shared interference with membrane associated processes as well as potential apicoplast associated metabolic systems. Therefore, the unique structures of these herbicide derived compounds, never tested on the parasite before, show a clear preliminary structure-activity relationship.

4.4 Future directions

Based on the above, compound A51B1C1_1 shows the potential to be an anti-malarial because of its high sensitivity and selectivity and also its novel drug like properties, according to MMV requirements. Functional genomics has proven to be a vital tool in this investigation and provide a global view of the effect of the treatment. The unique transcript and protein response of the parasite to the compound confirms that A51B1C1_1 is a good early lead in the MMV pipeline. It is important to determine the mode of action of the compound A51B1C1_1 to prevent drug resistance as seen in chloroquine, which mode of action is still unknown. In this study insight was obtained about the effect of the compound A51B1C1_1 on the *Plasmodium* parasite. The MMV requirements for the further development of A51B1C1_1 as a potential anti-malarial, is that *in vivo* efficacy of the compound must be investigated. The first step will be testing the compound on a rodent malaria model (248). The work done in this study contributed in the progress of A51B1C1_1 from an early hit to an early lead in the MMV pipeline and future studies can now be done on the compound to develop a novel, non-resistant and efficient anti-malarial.

REFERENCES

1. (2010) World Malaria Report 2010.
2. Ralph, S. A., D'Ombrain, M. C., and McFadden, G. I. (2001) The apicoplast as an antimalarial drug target, *Drug Resist Updat* **4**, 145-151.
3. Waller, R. F., Keeling, P. J., Donald, R. G., Striepen, B., Handman, E., Lang-Unnasch, N., Cowman, A. F., Besra, G. S., Roos, D. S., and McFadden, G. I. (1998) Nuclear-encoded proteins target to the plastid in *Toxoplasma gondii* and *Plasmodium falciparum*, *Proc Natl Acad Sci U S A* **95**, 12352-12357.
4. Garnham, P. C. (1945) Malaria Epidemics at Exceptionally High Altitudes, *Br Med J* **2**, 45-47.
5. Miller, R. L., Ikram, S., Armelagos, G. J., Walker, R., Harer, W. B., Shiff, C. J., Baggett, D., Carrigan, M., and Maret, S. M. (1994) Diagnosis of *Plasmodium falciparum* infections in mummies using the rapid manual ParaSight-F test, *Trans R Soc Trop Med Hyg* **88**, 31-32.
6. Man, W. (1950) Nei Ching, the Chinese canon of medicine, *Chin Med J* **68**, 1-33.
7. Trenholme, K. A., and Gardine, D. L. (2004) A sticky problem in malaria, *Biologist* **51**, 37-40.
8. Lewison, G., and Srivastava, D. (2008) Malaria research, 1980-2004, and the burden of disease, *Acta Trop* **106**, 96-103.
9. Barnes, K. I., and White, N. J. (2005) Population biology and antimalarial resistance: The transmission of antimalarial drug resistance in *Plasmodium falciparum*, *Acta Trop* **94**, 230-240.
10. Gallup, J. L., and Sachs, J. D. (2001) The economic burden of malaria, *Am J Trop Med Hyg* **64**, 85-96.
11. Gunther, S., Storm, J., and Muller, S. (2009) *Plasmodium falciparum*: organelle-specific acquisition of lipoic acid, *Int J Biochem Cell Biol* **41**, 748-752.
12. Morrison, D. A., and Ellis, J. T. (1997) Effects of nucleotide sequence alignment on phylogeny estimation: a case study of 18S rDNAs of apicomplexa, *Mol Biol Evol* **14**, 428-441.
13. Trenholme, K. A., and Gardiner, D. L. (2004) A sticky problem in malaria, *Biologist* **51**, 37-40.
14. Baton, L. A., and Ranford-Cartwright, L. C. (2005) Spreading the seeds of million-murdering death: metamorphoses of malaria in the mosquito, *Trends Parasitol* **21**, 573-580.
15. Ono, T., Cabrita-Santos, L., Leitao, R., Bettiol, E., Purcell, L. A., Diaz-Pulido, O., Andrews, L. B., Tadakuma, T., Bhanot, P., Mota, M. M., and Rodriguez, A. (2008) Adenylyl cyclase alpha and cAMP signaling mediate Plasmodium sporozoite apical regulated exocytosis and hepatocyte infection, *PLoS Pathog* **4**, e1000008.
16. Barillas-Mury, C., and Kumar, S. (2005) Plasmodium-mosquito interactions: a tale of dangerous liaisons, *Cell Microbiol* **7**, 1539-1545.
17. Tripathi, R. P., Mishra, R. C., Dwivedi, N., Tewari, N., and Verma, S. S. (2005) Current status of malaria control, *Curr Med Chem* **12**, 2643-2659.
18. Brey, P. T. (2003) *Anopheles gambiae* genome: perspectives for malaria control, *Mol Cells* **15**, 133-138.
19. Coleman, P. G., and Alphey, L. (2004) Genetic control of vector populations: an imminent prospect, *Trop Med Int Health* **9**, 433-437.
20. Alphey, L., Beard, C. B., Billingsley, P., Coetzee, M., Crisanti, A., Curtis, C., Eggleston, P., Godfray, C., Hemingway, J., Jacobs-Lorena, M., James, A. A., Kafatos, F. C., Mukwaya, L. G., Paton, M., Powell, J. R., Schneider, W., Scott, T. W., Sina, B., Sinden, R., Sinkins, S., Spielman, A., Toure, Y., and Collins, F. H. (2002) Malaria control with genetically manipulated insect vectors, *Science* **298**, 119-121.
21. Roberts, D. R., Manguin, S., and Mouchet, J. (2000) DDT house spraying and re-emerging malaria, *Lancet* **356**, 330-332.

22. Maharaj, R., Mthembu, D. J., and Sharp, B. L. (2005) Impact of DDT re-introduction on malaria transmission in KwaZulu-Natal, *S Afr Med J* **95**, 871-874.
23. Mabaso, M. L., Sharp, B., and Lengeler, C. (2004) Historical review of malarial control in southern African with emphasis on the use of indoor residual house-spraying, *Trop Med Int Health* **9**, 846-856.
24. Toure, Y. T., Oduola, A. M., and Morel, C. M. (2004) The *Anopheles gambiae* genome: next steps for malaria vector control, *Trends Parasitol* **20**, 142-149.
25. Hemingway, J., Beaty, B. J., Rowland, M., Scott, T. W., and Sharp, B. L. (2006) The Innovative Vector Control Consortium: improved control of mosquito-borne diseases, *Trends Parasitol* **22**, 308-312.
26. Zaim, M., and Guillet, P. (2002) Alternative insecticides: an urgent need, *Trends Parasitol* **18**, 161-163.
27. Greenwood, B. M., Bojang, K., Whitty, C. J., and Targett, G. A. (2005) Malaria, *Lancet* **365**, 1487-1498.
28. Richie, T. L., and Saul, A. (2002) Progress and challenges for malaria vaccines, *Nature* **415**, 694-701.
29. Stoute, J. A., Slaoui, M., Heppner, D. G., Momin, P., Kester, K. E., Desmons, P., Wellde, B. T., Garcon, N., Krzych, U., and Marchand, M. (1997) A preliminary evaluation of a recombinant circumsporozoite protein vaccine against *Plasmodium falciparum* malaria. RTS,S Malaria Vaccine Evaluation Group, *N Engl J Med* **336**, 86-91.
30. Yeh, I., and Altman, R. B. (2006) Drug Targets for *Plasmodium falciparum*: a post-genomic review/survey, *Mini Rev Med Chem* **6**, 177-202.
31. Vallely, A., Vallely, L., Changalucha, J., Greenwood, B., and Chandramohan, D. (2007) Intermittent preventive treatment for malaria in pregnancy in Africa: what's new, what's needed?, *Malar J* **6**, 16.
32. Ridley, R. G. (2002) Medical need, scientific opportunity and the drive for antimalarial drugs, *Nature* **415**, 686-693.
33. Muller, I. B., and Hyde, J. E. (2010) Antimalarial drugs: modes of action and mechanisms of parasite resistance, *Future Microbiol* **5**, 1857-1873.
34. Srivastava, I. K., Rottenberg, H., and Vaidya, A. B. (1997) Atovaquone, a broad spectrum antiparasitic drug, collapses mitochondrial membrane potential in a malarial parasite, *J Biol Chem* **272**, 3961-3966.
35. Rosenthal, P. J. (2003) Antimalarial drug discovery: old and new approaches, *J Exp Biol* **206**, 3735-3744.
36. Nzila, A. M., Nduati, E., Mberu, E. K., Hopkins Sibley, C., Monks, S. A., Winstanley, P. A., and Watkins, W. M. (2000) Molecular evidence of greater selective pressure for drug resistance exerted by the long-acting antifolate Pyrimethamine/Sulfadoxine compared with the shorter-acting chlorproguanil/dapsone on Kenyan *Plasmodium falciparum*, *J Infect Dis* **181**, 2023-2028.
37. Mutabingwa, T., Nzila, A., Mberu, E., Nduati, E., Winstanley, P., Hills, E., and Watkins, W. (2001) Chlorproguanil-dapsone for treatment of drug-resistant falciparum malaria in Tanzania, *Lancet* **358**, 1218-1223.
38. Calas, M., Ancelin, M. L., Cordina, G., Portefaix, P., Piquet, G., Vidal-Sailhan, V., and Vial, H. (2000) Antimalarial activity of compounds interfering with *Plasmodium falciparum* phospholipid metabolism: comparison between mono- and bisquaternary ammonium salts, *J Med Chem* **43**, 505-516.
39. Vaidya, A. B., and Mather, M. W. (2000) Atovaquone resistance in malaria parasites, *Drug Resist Updat* **3**, 283-287.
40. Radloff, P. D., Philipps, J., Nkeyi, M., Hutchinson, D., and Kremsner, P. G. (1996) Atovaquone and proguanil for *Plasmodium falciparum* malaria, *Lancet* **347**, 1511-1514.
41. Rudzinska, M. A., Trager, W., and Bray, R. S. (1965) Pinocytotic uptake and the digestion of hemoglobin in malaria parasites, *J Protozool* **12**, 563-576.
42. Banerjee, R., Liu, J., Beatty, W., Pelosof, L., Klemba, M., and Goldberg, D. E. (2002) Four plasmepsins are active in the *Plasmodium falciparum* food vacuole, including a protease with an active-site histidine, *Proc Natl Acad Sci U S A* **99**, 990-995.

43. Ragheb, D., Dalal, S., Bompiani, K. M., Ray, W. K., and Klemba, M. (2011) Distribution and biochemical properties of an M1-family aminopeptidase in *Plasmodium falciparum* indicate a role in vacuolar hemoglobin catabolism, *J Biol Chem*.
44. Rosenthal, P. J., and Meshnick, S. R. (1996) Hemoglobin catabolism and iron utilization by malaria parasites, *Mol Biochem Parasitol* **83**, 131-139.
45. Sherman, I. W. (1979) Biochemistry of Plasmodium (malarial parasites), *Microbiol Rev* **43**, 453-495.
46. Goldberg, D. E., Slater, A. F., Cerami, A., and Henderson, G. B. (1990) Hemoglobin degradation in the malaria parasite *Plasmodium falciparum*: an ordered process in a unique organelle, *Proc Natl Acad Sci U S A* **87**, 2931-2935.
47. Rosenthal, P. J. (2011) Falcipains and other cysteine proteases of malaria parasites, *Adv Exp Med Biol* **712**, 30-48.
48. Dahl, E. L., and Rosenthal, P. J. (2007) Multiple antibiotics exert delayed effects against the *Plasmodium falciparum* apicoplast, *Antimicrob Agents Chemother* **51**, 3485-3490.
49. Waller, R. F., and McFadden, G. I. (2005) The apicoplast: a review of the derived plastid of apicomplexan parasites, *Curr Issues Mol Biol* **7**, 57-79.
50. McFadden, G. I., and Roos, D. S. (1999) Apicomplexan plastids as drug targets, *Trends Microbiol* **7**, 328-333.
51. Divo, A. A., Sartorelli, A. C., Patton, C. L., and Bia, F. J. (1988) Activity of fluoroquinolone antibiotics against *Plasmodium falciparum* in vitro, *Antimicrob Agents Chemother* **32**, 1182-1186.
52. Weissig, V., Vetro-Widenhouse, T. S., and Rowe, T. C. (1997) Topoisomerase II inhibitors induce cleavage of nuclear and 35-kb plastid DNAs in the malarial parasite *Plasmodium falciparum*, *DNA Cell Biol* **16**, 1483-1492.
53. Fichera, M. E., and Roos, D. S. (1997) A plastid organelle as a drug target in apicomplexan parasites, *Nature* **390**, 407-409.
54. Khan, A. A., Slifer, T., Araujo, F. G., and Remington, J. S. (1996) Trovafloxacin is active against *Toxoplasma gondii*, *Antimicrob Agents Chemother* **40**, 1855-1859.
55. Strath, M., Scott-Finnigan, T., Gardner, M., Williamson, D., and Wilson, I. (1993) Antimalarial activity of rifampicin in vitro and in rodent models, *Trans R Soc Trop Med Hyg* **87**, 211-216.
56. Pukrittayakamee, S., Viravan, C., Charoenlarp, P., Yeamput, C., Wilson, R. J., and White, N. J. (1994) Antimalarial effects of rifampin in Plasmodium vivax malaria, *Antimicrob Agents Chemother* **38**, 511-514.
57. Araujo, F. G., Slifer, T., and Remington, J. S. (1994) Rifabutin is active in murine models of toxoplasmosis, *Antimicrob Agents Chemother* **38**, 570-575.
58. Olliaro, P., Gorini, G., Jabes, D., Regazzetti, A., Rossi, R., Marchetti, A., Tinelli, C., and Della Bruna, C. (1994) In-vitro and in-vivo activity of rifabutin against *Toxoplasma gondii*, *J Antimicrob Chemother* **34**, 649-657.
59. Pfefferkorn, E. R., and Borotz, S. E. (1994) Comparison of mutants of *Toxoplasma gondii* selected for resistance to azithromycin, spiramycin, or clindamycin, *Antimicrob Agents Chemother* **38**, 31-37.
60. Fichera, M. E., Bhopale, M. K., and Roos, D. S. (1995) In vitro assays elucidate peculiar kinetics of clindamycin action against *Toxoplasma gondii*, *Antimicrob Agents Chemother* **39**, 1530-1537.
61. Woods, K. M., Nesterenko, M. V., and Upton, S. J. (1996) Efficacy of 101 antimicrobials and other agents on the development of Cryptosporidium parvum in vitro, *Ann Trop Med Parasitol* **90**, 603-615.
62. Beckers, C. J., Roos, D. S., Donald, R. G., Luft, B. J., Schwab, J. C., Cao, Y., and Joiner, K. A. (1995) Inhibition of cytoplasmic and organellar protein synthesis in *Toxoplasma gondii*. Implications for the target of macrolide antibiotics, *J Clin Invest* **95**, 367-376.
63. Clough, B., Strath, M., Preiser, P., Denny, P., and Wilson, I. R. (1997) Thiostrepton binds to malarial plastid rRNA, *FEBS Lett* **406**, 123-125.

64. McConkey, G. A., Rogers, M. J., and McCutchan, T. F. (1997) Inhibition of *Plasmodium falciparum* protein synthesis. Targeting the plastid-like organelle with thiostrepton, *J Biol Chem* **272**, 2046-2049.
65. Rogers, M. J., Bukhman, Y. V., McCutchan, T. F., and Draper, D. E. (1997) Interaction of thiostrepton with an RNA fragment derived from the plastid-encoded ribosomal RNA of the malaria parasite, *RNA* **3**, 815-820.
66. Sullivan, M., Li, J., Kumar, S., Rogers, M. J., and McCutchan, T. F. (2000) Effects of interruption of apicoplast function on malaria infection, development, and transmission, *Mol Biochem Parasitol* **109**, 17-23.
67. Rogers, M. J., Cundliffe, E., and McCutchan, T. F. (1998) The antibiotic micrococcin is a potent inhibitor of growth and protein synthesis in the malaria parasite, *Antimicrob Agents Chemother* **42**, 715-716.
68. Budimulja, A. S., Syafruddin, Tapchaisri, P., Wilairat, P., and Marzuki, S. (1997) The sensitivity of Plasmodium protein synthesis to prokaryotic ribosomal inhibitors, *Mol Biochem Parasitol* **84**, 137-141.
69. Pradines, B., Spiegel, A., Rogier, C., Tall, A., Mosnier, J., Fusai, T., Trape, J. F., and Parzy, D. (2000) Antibiotics for prophylaxis of *Plasmodium falciparum* infections: in vitro activity of doxycycline against Senegalese isolates, *Am J Trop Med Hyg* **62**, 82-85.
70. Clough, B., Rangachari, K., Strath, M., Preiser, P. R., and Wilson, R. J. (1999) Antibiotic inhibitors of organellar protein synthesis in *Plasmodium falciparum*, *Protist* **150**, 189-195.
71. Waller, R. F., Ralph, S. A., Reed, M. B., Su, V., Douglas, J. D., Minnikin, D. E., Cowman, A. F., Besra, G. S., and McFadden, G. I. (2003) A type II pathway for fatty acid biosynthesis presents drug targets in *Plasmodium falciparum*, *Antimicrob Agents Chemother* **47**, 297-301.
72. Surolia, N., and Surolia, A. (2001) Triclosan offers protection against blood stages of malaria by inhibiting enoyl-ACP reductase of *Plasmodium falciparum*, *Nat Med* **7**, 167-173.
73. McLeod, R., Muench, S. P., Rafferty, J. B., Kyle, D. E., Mui, E. J., Kirisits, M. J., Mack, D. G., Roberts, C. W., Samuel, B. U., Lyons, R. E., Dorris, M., Milhous, W. K., and Rice, D. W. (2001) Triclosan inhibits the growth of *Plasmodium falciparum* and *Toxoplasma gondii* by inhibition of apicomplexan Fab I, *Int J Parasitol* **31**, 109-113.
74. Zuther, E., Johnson, J. J., Haselkorn, R., McLeod, R., and Gornicki, P. (1999) Growth of *Toxoplasma gondii* is inhibited by aryloxyphenoxypropionate herbicides targeting acetyl-CoA carboxylase, *Proc Natl Acad Sci U S A* **96**, 13387-13392.
75. Zagnitko, O., Jelenska, J., Tevzadze, G., Haselkorn, R., and Gornicki, P. (2001) An isoleucine/leucine residue in the carboxyltransferase domain of acetyl-CoA carboxylase is critical for interaction with aryloxyphenoxypropionate and cyclohexanedione inhibitors, *Proc Natl Acad Sci U S A* **98**, 6617-6622.
76. Jomaa, H., Wiesner, J., Sanderbrand, S., Altincicek, B., Weidemeyer, C., Hintz, M., Turbachova, I., Eberl, M., Zeidler, J., Lichtenthaler, H. K., Soldati, D., and Beck, E. (1999) Inhibitors of the nonmevalonate pathway of isoprenoid biosynthesis as antimalarial drugs, *Science* **285**, 1573-1576.
77. Roberts, F., Roberts, C. W., Johnson, J. J., Kyle, D. E., Krell, T., Coggins, J. R., Coombs, G. H., Milhous, W. K., Tzipori, S., Ferguson, D. J., Chakrabarti, D., and McLeod, R. (1998) Evidence for the shikimate pathway in apicomplexan parasites, *Nature* **393**, 801-805.
78. Levine, N. D. (1988) Progress in taxonomy of the Apicomplexan protozoa, *J Protozool* **35**, 518-520.
79. Kim, K., and Weiss, L. M. (2004) *Toxoplasma gondii*: the model apicomplexan, *Int J Parasitol* **34**, 423-432.
80. Gibson, A. K., Raverty, S., Lambourn, D. M., Huggins, J., Magargal, S. L., and Grigg, M. E. (2011) Polyparasitism is associated with increased disease severity in *Toxoplasma gondii*-infected marine sentinel species, *PLoS Negl Trop Dis* **5**, e1142.
81. Anazi, A. D., and Alyousif, M. S. (2011) Prevalence of antibodies to *Toxoplasma gondii* in horses in Riyadh province , Saudi Arabia, *J Parasitol*.

82. Marechal, E., and Cesbron-Delauw, M. F. (2001) The apicoplast: a new member of the plastid family, *Trends Plant Sci* **6**, 200-205.
83. Huang, J., Mullapudi, N., Sicheritz-Ponten, T., and Kissinger, J. C. (2004) A first glimpse into the pattern and scale of gene transfer in Apicomplexa, *Int J Parasitol* **34**, 265-274.
84. Lim, L., and McFadden, G. I. (2010) The evolution, metabolism and functions of the apicoplast, *Philos Trans R Soc Lond B Biol Sci* **365**, 749-763.
85. Kohler, S., Delwiche, C. F., Denny, P. W., Tilney, L. G., Webster, P., Wilson, R. J., Palmer, J. D., and Roos, D. S. (1997) A plastid of probable green algal origin in Apicomplexan parasites, *Science* **275**, 1485-1489.
86. Funes, S., Davidson, E., Reyes-Prieto, A., Magallon, S., Herion, P., King, M. P., and Gonzalez-Halphen, D. (2002) A green algal apicoplast ancestor, *Science* **298**, 2155.
87. Kobayashi, T., Sato, S., Takamiya, S., Komaki-Yasuda, K., Yano, K., Hirata, A., Onitsuka, I., Hata, M., Mi-ichi, F., Tanaka, T., Hase, T., Miyajima, A., Kawazu, S., Watanabe, Y., and Kita, K. (2007) Mitochondria and apicoplast of *Plasmodium falciparum*: behaviour on subcellular fractionation and the implication, *Mitochondrion* **7**, 125-132.
88. Foth, B. J., and McFadden, G. I. (2003) The apicoplast: a plastid in *Plasmodium falciparum* and other Apicomplexan parasites, *Int Rev Cytol* **224**, 57-110.
89. Waller, R. F., Reed, M. B., Cowman, A. F., and McFadden, G. I. (2000) Protein trafficking to the plastid of *Plasmodium falciparum* is via the secretory pathway, *EMBO J* **19**, 1794-1802.
90. Stanway, R. R., Witt, T., Zobiak, B., Aepfelbacher, M., and Heussler, V. T. (2009) GFP-targeting allows visualization of the apicoplast throughout the life cycle of live malaria parasites, *Biol Cell* **101**, 415-430, 415 p following 430.
91. Striepen, B., Crawford, M. J., Shaw, M. K., Tilney, L. G., Seeber, F., and Roos, D. S. (2000) The plastid of *Toxoplasma gondii* is divided by association with the centrosomes, *J Cell Biol* **151**, 1423-1434.
92. McFadden, G. I., and Waller, R. F. (1997) Plastids in parasites of humans, *Bioessays* **19**, 1033-1040.
93. Law, A. E., Mullineaux, C. W., Hirst, E. M., Saldanha, J., and Wilson, R. J. (2000) Bacterial orthologues indicate the malarial plastid gene ycf24 is essential, *Protist* **151**, 317-327.
94. He, C. Y., Shaw, M. K., Pletcher, C. H., Striepen, B., Tilney, L. G., and Roos, D. S. (2001) A plastid segregation defect in the protozoan parasite *Toxoplasma gondii*, *EMBO J* **20**, 330-339.
95. Escalante, A. A., and Ayala, F. J. (1995) Evolutionary origin of Plasmodium and other Apicomplexa based on rRNA genes, *Proc Natl Acad Sci U S A* **92**, 5793-5797.
96. Wilson, R. J., Gardner, M. J., Feagin, J. E., and Williamson, D. H. (1991) Have malaria parasites three genomes?, *Parasitol Today* **7**, 134-136.
97. Dahl, E. L., Shock, J. L., Shenai, B. R., Gut, J., DeRisi, J. L., and Rosenthal, P. J. (2006) Tetracyclines specifically target the apicoplast of the malaria parasite *Plasmodium falciparum*, *Antimicrob Agents Chemother* **50**, 3124-3131.
98. Goldstein, J. L., and Brown, M. S. (1990) Regulation of the mevalonate pathway, *Nature* **343**, 425-430.
99. Koppisch, A. T., Fox, D. T., Blagg, B. S., and Poulter, C. D. (2002) E. coli MEP synthase: steady-state kinetic analysis and substrate binding, *Biochemistry* **41**, 236-243.
100. Cassera, M. B., Gozzo, F. C., D'Alexandri, F. L., Merino, E. F., del Portillo, H. A., Peres, V. J., Almeida, I. C., Eberlin, M. N., Wunderlich, G., Wiesner, J., Jomaa, H., Kimura, E. A., and Katzin, A. M. (2004) The methylerythritol phosphate pathway is functionally active in all intraerythrocytic stages of *Plasmodium falciparum*, *J Biol Chem* **279**, 51749-51759.
101. Odom, A. R., and Van Voorhis, W. C. (2010) Functional genetic analysis of the *Plasmodium falciparum* deoxyxylulose 5-phosphate reductoisomerase gene, *Mol Biochem Parasitol* **170**, 108-111.

102. Kannangara, C. G., Gough, S. P., Bruyant, P., Hoober, J. K., Kahn, A., and von Wettstein, D. (1988) tRNA(Glu) as a cofactor in delta-aminolevulinate biosynthesis: steps that regulate chlorophyll synthesis, *Trends Biochem Sci* **13**, 139-143.
103. Varadharajan, S., Dhanasekaran, S., Bonday, Z. Q., Rangarajan, P. N., and Padmanaban, G. (2002) Involvement of delta-aminolaevulinate synthase encoded by the parasite gene in de novo haem synthesis by *Plasmodium falciparum*, *Biochem J* **367**, 321-327.
104. Wilson, C. M., Smith, A. B., and Baylon, R. V. (1996) Characterization of the delta-aminolevulinate synthase gene homologue in P. falciparum, *Mol Biochem Parasitol* **79**, 135-140.
105. Surolia, N., and Padmanaban, G. (1992) de novo biosynthesis of heme offers a new chemotherapeutic target in the human malarial parasite, *Biochem Biophys Res Commun* **187**, 744-750.
106. Panek, H., and O'Brian, M. R. (2002) A whole genome view of prokaryotic haem biosynthesis, *Microbiology* **148**, 2273-2282.
107. Ralph, S. A., van Dooren, G. G., Waller, R. F., Crawford, M. J., Fraunholz, M. J., Foth, B. J., Tonkin, C. J., Roos, D. S., and McFadden, G. I. (2004) Tropical infectious diseases: metabolic maps and functions of the *Plasmodium falciparum* apicoplast, *Nat Rev Microbiol* **2**, 203-216.
108. Bonday, Z. Q., Taketani, S., Gupta, P. D., and Padmanaban, G. (1997) Heme biosynthesis by the malarial parasite. Import of delta-aminolevulinate dehydrase from the host red cell, *J Biol Chem* **272**, 21839-21846.
109. Bonday, Z. Q., Dhanasekaran, S., Rangarajan, P. N., and Padmanaban, G. (2000) Import of host delta-aminolevulinate dehydratase into the malarial parasite: identification of a new drug target, *Nat Med* **6**, 898-903.
110. Magnuson, K., Jackowski, S., Rock, C. O., and Cronan, J. E., Jr. (1993) Regulation of fatty acid biosynthesis in Escherichia coli, *Microbiol Rev* **57**, 522-542.
111. Goodman, C. D., Su, V., and McFadden, G. I. (2007) The effects of anti-bacterials on the malaria parasite *Plasmodium falciparum*, *Mol Biochem Parasitol* **152**, 181-191.
112. Singer, S. J., and Nicolson, G. L. (1972) The fluid mosaic model of the structure of cell membranes, *Science* **175**, 720-731.
113. Kelly, A. A., and Dormann, P. (2004) Green light for galactolipid trafficking, *Curr Opin Plant Biol* **7**, 262-269.
114. Dubots, E., Audry, M., Yamaryo, Y., Bastien, O., Ohta, H., Breton, C., Marechal, E., and Block, M. A. (2010) Activation of the chloroplast monogalactosyldiacylglycerol synthase MGD1 by phosphatidic acid and phosphatidylglycerol, *J Biol Chem* **285**, 6003-6011.
115. Dormann, P., and Benning, C. (2002) Galactolipids rule in seed plants, *Trends Plant Sci* **7**, 112-118.
116. Douce, R. (1974) Site of biosynthesis of galactolipids in spinach chloroplasts, *Science* **183**, 852-853.
117. Hartel, H., Dormann, P., and Benning, C. (2000) DGD1-independent biosynthesis of extraplastidic galactolipids after phosphate deprivation in Arabidopsis, *Proc Natl Acad Sci U S A* **97**, 10649-10654.
118. Botté, C. Y., Deligny, M., Roccia, A., Bonneau, A., Saïdani, N., Hardré, H., Aci, S., Yamaryo-Botté, Y., Jouhet, J., Dubots, E., Loizeau, K., Bastien, O., Brehelin, L., Joyard, J., Cintrat, J., Falconet, D., Block, M. A., Rousseau, B., Lopez, R., and Marechal, E. (2011) Chemical inhibitors of monogalactosyldiacylglycerol synthases in Arabidopsis thaliana.
119. Marechal, E., Azzouz, N., de Macedo, C. S., Block, M. A., Feagin, J. E., Schwarz, R. T., and Joyard, J. (2002) Synthesis of chloroplast galactolipids in apicomplexan parasites, *Eukaryot Cell* **1**, 653-656.
120. Benning, C., and Ohta, H. (2005) Three enzyme systems for galactoglycerolipid biosynthesis are coordinately regulated in plants, *J Biol Chem* **280**, 2397-2400.
121. Awai, K., Marechal, E., Block, M. A., Brun, D., Masuda, T., Shimada, H., Takamiya, K., Ohta, H., and Joyard, J. (2001) Two types of MGDG synthase genes, found widely in both 16:3 and 18:3 plants, differentially mediate galactolipid syntheses in photosynthetic

and nonphotosynthetic tissues in Arabidopsis thaliana, *Proc Natl Acad Sci U S A* **98**, 10960-10965.
122. Miege, C., Marechal, E., Shimojima, M., Awai, K., Block, M. A., Ohta, H., Takamiya, K., Douce, R., and Joyard, J. (1999) Biochemical and topological properties of type A MGDG synthase, a spinach chloroplast envelope enzyme catalyzing the synthesis of both prokaryotic and eukaryotic MGDG, *Eur J Biochem* **265**, 990-1001.
123. Jarvis, P., Dormann, P., Peto, C. A., Lutes, J., Benning, C., and Chory, J. (2000) Galactolipid deficiency and abnormal chloroplast development in the Arabidopsis MGD synthase 1 mutant, *Proc Natl Acad Sci U S A* **97**, 8175-8179.
124. Dormann, P., Balbo, I., and Benning, C. (1999) Arabidopsis galactolipid biosynthesis and lipid trafficking mediated by DGD1, *Science* **284**, 2181-2184.
125. Froehlich, J. E., Benning, C., and Dormann, P. (2001) The digalactosyldiacylglycerol (DGDG) synthase DGD1 is inserted into the outer envelope membrane of chloroplasts in a manner independent of the general import pathway and does not depend on direct interaction with monogalactosyldiacylglycerol synthase for DGDG biosynthesis, *J Biol Chem* **276**, 31806-31812.
126. Ramya, T. N., Mishra, S., Karmodiya, K., Surolia, N., and Surolia, A. (2007) Inhibitors of nonhousekeeping functions of the apicoplast defy delayed death in *Plasmodium falciparum*, *Antimicrob Agents Chemother* **51**, 307-316.
127. Tasdemir, D., Lack, G., Brun, R., Ruedi, P., Scapozza, L., and Perozzo, R. (2006) Inhibition of *Plasmodium falciparum* fatty acid biosynthesis: evaluation of FabG, FabZ, and FabI as drug targets for flavonoids, *J Med Chem* **49**, 3345-3353.
128. Brotz-Oesterhelt, H., Bandow, J. E., and Labischinski, H. (2005) Bacterial proteomics and its role in antibacterial drug discovery, *Mass Spectrom Rev* **24**, 549-565.
129. Birkholtz, L. M., Bastien, O., Wells, G., Grando, D., Joubert, F., Kasam, V., Zimmermann, M., Ortet, P., Jacq, N., Saidani, N., Roy, S., Hofmann-Apitius, M., Breton, V., Louw, A. I., and Marechal, E. (2006) Integration and mining of malaria molecular, functional and pharmacological data: how far are we from a chemogenomic knowledge space?, *Malar J* **5**, 110.
130. Ohlstein, E. H., Ruffolo, R. R., Jr., and Elliott, J. D. (2000) Drug discovery in the next millennium, *Annu Rev Pharmacol Toxicol* **40**, 177-191.
131. Freiberg, C., and Brotz-Oesterhelt, H. (2005) Functional genomics in antibacterial drug discovery, *Drug Discov Today* **10**, 927-935.
132. Birkholtz, L., van Brummelen, A. C., Clark, K., Niemand, J., Marechal, E., Llinas, M., and Louw, A. I. (2008) Exploring functional genomics for drug target and therapeutics discovery in Plasmodia, *Acta Trop* **105**, 113-123.
133. van Brummelen, A. C., Olszewski, K. L., Wilinski, D., Llinas, M., Louw, A. I., and Birkholtz, L. M. (2009) Co-inhibition of *Plasmodium falciparum* S-adenosylmethionine decarboxylase/ornithine decarboxylase reveals perturbation-specific compensatory mechanisms by transcriptome, proteome, and metabolome analyses, *J Biol Chem* **284**, 4635-4646.
134. Gardner, M. J., Hall, N., Fung, E., White, O., Berriman, M., Hyman, R. W., Carlton, J. M., Pain, A., Nelson, K. E., Bowman, S., Paulsen, I. T., James, K., Eisen, J. A., Rutherford, K., Salzberg, S. L., Craig, A., Kyes, S., Chan, M. S., Nene, V., Shallom, S. J., Suh, B., Peterson, J., Angiuoli, S., Pertea, M., Allen, J., Selengut, J., Haft, D., Mather, M. W., Vaidya, A. B., Martin, D. M., Fairlamb, A. H., Fraunholz, M. J., Roos, D. S., Ralph, S. A., McFadden, G. I., Cummings, L. M., Subramanian, G. M., Mungall, C., Venter, J. C., Carucci, D. J., Hoffman, S. L., Newbold, C., Davis, R. W., Fraser, C. M., and Barrell, B. (2002) Genome sequence of the human malaria parasite *Plasmodium falciparum*, *Nature* **419**, 498-511.
135. Carucci, D. J., Horrocks, P., and Gardner, M. J. (2002) Purification of chromosomes from *Plasmodium falciparum*, *Methods Mol Med* **72**, 235-240.
136. Painter, H. J., Morrisey, J. M., Mather, M. W., and Vaidya, A. B. (2007) Specific role of mitochondrial electron transport in blood-stage *Plasmodium falciparum*, *Nature* **446**, 88-91.

137. Bozdech, Z., Llinas, M., Pulliam, B. L., Wong, E. D., Zhu, J., and DeRisi, J. L. (2003) The transcriptome of the intraerythrocytic developmental cycle of *Plasmodium falciparum*, *PLoS Biol* **1**, E5.
138. Bozdech, Z., Zhu, J., Joachimiak, M. P., Cohen, F. E., Pulliam, B., and DeRisi, J. L. (2003) Expression profiling of the schizont and trophozoite stages of *Plasmodium falciparum* with a long-oligonucleotide microarray, *Genome Biol* **4**, R9.
139. Le Roch, K. G., Zhou, Y., Blair, P. L., Grainger, M., Moch, J. K., Haynes, J. D., De La Vega, P., Holder, A. A., Batalov, S., Carucci, D. J., and Winzeler, E. A. (2003) Discovery of gene function by expression profiling of the malaria parasite life cycle, *Science* **301**, 1503-1508.
140. Balaji, S., Babu, M. M., Iyer, L. M., and Aravind, L. (2005) Discovery of the principal specific transcription factors of Apicomplexa and their implication for the evolution of the AP2-integrase DNA binding domains, *Nucleic Acids Res* **33**, 3994-4006.
141. Gunasekera, A. M., Myrick, A., Le Roch, K., Winzeler, E., and Wirth, D. F. (2007) *Plasmodium falciparum*: genome wide perturbations in transcript profiles among mixed stage cultures after chloroquine treatment, *Exp Parasitol* **117**, 87-92.
142. Clark, K., Niemand, J., Reeksting, S., Smit, S., van Brummelen, A. C., Williams, M., Louw, A. I., and Birkholtz, L. (2010) Functional consequences of perturbing polyamine metabolism in the malaria parasite, *Plasmodium falciparum*, *Amino Acids* **38**, 633-644.
143. Clark, K., Dhoogra, M., Louw, A. I., and Birkholtz, L. M. (2008) Transcriptional responses of *Plasmodium falciparum* to alpha-difluoromethylornithine-induced polyamine depletion, *Biol Chem* **389**, 111-125.
144. Assaraf, Y. G., Golenser, J., Spira, D. T., Messer, G., and Bachrach, U. (1987) Cytostatic effect of DL-alpha-difluoromethylornithine against *Plasmodium falciparum* and its reversal by diamines and spermidine, *Parasitol Res* **73**, 313-318.
145. Andrews, K. T., Walduck, A., Kelso, M. J., Fairlie, D. P., Saul, A., and Parsons, P. G. (2000) Anti-malarial effect of histone deacetylation inhibitors and mammalian tumour cytodifferentiating agents, *Int J Parasitol* **30**, 761-768.
146. Becker, J. V., Mtwisha, L., Crampton, B. G., Stoychev, S., van Brummelen, A. C., Reeksting, S., Louw, A. I., Birkholtz, L. M., and Mancama, D. T. (2010) *Plasmodium falciparum* spermidine synthase inhibition results in unique perturbation-specific effects observed on transcript, protein and metabolite levels, *BMC Genomics* **11**, 235.
147. Riggs, M. G., Whittaker, R. G., Neumann, J. R., and Ingram, V. M. (1977) n-Butyrate causes histone modification in HeLa and Friend erythroleukaemia cells, *Nature* **268**, 462-464.
148. Le Roch, K. G., Johnson, J. R., Ahiboh, H., Chung, D. W., Prudhomme, J., Plouffe, D., Henson, K., Zhou, Y., Witola, W., Yates, J. R., Mamoun, C. B., Winzeler, E. A., and Vial, H. (2008) A systematic approach to understand the mechanism of action of the bisthiazolium compound T4 on the human malaria parasite, *Plasmodium falciparum*, *BMC Genomics* **9**, 513.
149. Kreil, D. P., and Russell, R. R. (2005) There is no silver bullet--a guide to low-level data transforms and normalisation methods for microarray data, *Brief Bioinform* **6**, 86-97.
150. Hardiman, G. (2004) Microarray platforms--comparisons and contrasts, *Pharmacogenomics* **5**, 487-502.
151. Systems, E. B. Microarray Systems, In *www.eppendorf.com* (AG, E., Ed.), Eppendorf AGEppendorf AG, Hamburg, Germany.
152. Wolber, P. K., Collins, P. J., Lucas, A. B., De Witte, A., and Shannon, K. W. (2006) The agilent in situ-synthesized microarray platform, *DNA Microarrays Part A: Array Platforms and Wet-Bench Protocols* **410**, 28-57.
153. Wolber, P. K., Collins, P. J., Lucas, A. B., De Witte, A., and Shannon, K. W. (2006) The Agilent in situ-synthesized microarray platform, *Methods Enzymol* **410**, 28-57.
154. Hockley, S. L., Mathijs, K., Staal, Y. C. M., Brewer, D., Giddings, I., van Delft, J. H. M., and Phillips, D. H. (2009) Interlaboratory and Interplatform Comparison of Microarray Gene Expression Analysis of HepG2 Cells Exposed to Benzo(a)pyrene, *OMICS* **13**, 115-125.

155. Yang, Y. H., and Speed, T. (2002) Design issues for cDNA microarray experiments, *Nat Rev Genet* **3**, 579-588.
156. Churchill, G. A. (2002) Fundamentals of experimental design for cDNA microarrays, *Nat Genet* **32 Suppl**, 490-495.
157. Brazma, A., Hingamp, P., Quackenbush, J., Sherlock, G., Spellman, P., Stoeckert, C., Aach, J., Ansorge, W., Ball, C. A., Causton, H. C., Gaasterland, T., Glenisson, P., Holstege, F. C., Kim, I. F., Markowitz, V., Matese, J. C., Parkinson, H., Robinson, A., Sarkans, U., Schulze-Kremer, S., Stewart, J., Taylor, R., Vilo, J., and Vingron, M. (2001) Minimum information about a microarray experiment (MIAME)-toward standards for microarray data, *Nat Genet* **29**, 365-371.
158. Lambros, C., and Vanderberg, J. P. (1979) Synchronization of *Plasmodium falciparum* erythrocytic stages in culture, *J Parasitol* **65**, 418-420.
159. Johnson, J. D., Dennull, R. A., Gerena, L., Lopez-Sanchez, M., Roncal, N. E., and Waters, N. C. (2007) Assessment and continued validation of the malaria SYBR green I-based fluorescence assay for use in malaria drug screening, *Antimicrob Agents Chemother* **51**, 1926-1933.
160. Smilkstein, M., Sriwilaijaroen, N., Kelly, J. X., Wilairat, P., and Riscoe, M. (2004) Simple and inexpensive fluorescence-based technique for high-throughput antimalarial drug screening, *Antimicrob Agents Chemother* **48**, 1803-1806.
161. Bennett, T. N., Paguio, M., Gligorijevic, B., Seudieu, C., Kosar, A. D., Davidson, E., and Roepe, P. D. (2004) Novel, rapid, and inexpensive cell-based quantification of antimalarial drug efficacy, *Antimicrob Agents Chemother* **48**, 1807-1810.
162. Rio, D. C., Ares, M., Jr., Hannon, G. J., and Nilsen, T. W. (2010) Purification of RNA using TRIzol (TRI reagent), *Cold Spring Harb Protoc* **2010**, pdb prot5439.
163. Imbeaud, S., Graudens, E., Boulanger, V., Barlet, X., Zaborski, P., Eveno, E., Mueller, O., Schroeder, A., and Auffray, C. (2005) Towards standardization of RNA quality assessment using user-independent classifiers of microcapillary electrophoresis traces, *Nucleic Acids Res* **33**, e56.
164. Delibato, E., Gattuso, A., Minucci, A., Auricchio, B., De Medici, D., Toti, L., Castagnola, M., Capoluongo, E., and Gianfranceschi, M. V. (2009) PCR experion automated electrophoresis system to detect Listeria monocytogenes in foods, *J Sep Sci* **32**, 3817-3821.
165. Bozdech, Z., and Ginsburg, H. (2005) Data mining of the transcriptome of *Plasmodium falciparum*: the pentose phosphate pathway and ancillary processes, *Malar J* **4**, 17.
166. Verlinden, J. C. (In preparation) Functional genomics investigation of drug challenged *Plasmodium falciparum* and the role of herbicides as antimalarial drugs, In *Biochemistry*, University of Pretoria, Pretoria.
167. Smyth, G. K., and Speed, T. (2003) Normalization of cDNA microarray data, *Methods* **31**, 265-273.
168. Smyth, G. K. (2004) Linear models and empirical bayes methods for assessing differential expression in microarray experiments, *Stat Appl Genet Mol Biol* **3**, Article3.
169. Ritchie, M. E., Silver, J., Oshlack, A., Holmes, M., Diyagama, D., Holloway, A., and Smyth, G. K. (2007) A comparison of background correction methods for two-colour microarrays, *Bioinformatics* **23**, 2700-2707.
170. Stoeckert, C. J., Jr., Fischer, S., Kissinger, J. C., Heiges, M., Aurrecoechea, C., Gajria, B., and Roos, D. S. (2006) PlasmoDB v5: new looks, new genomes, *Trends Parasitol* **22**, 543-546.
171. Dennis, G., Jr., Sherman, B. T., Hosack, D. A., Yang, J., Gao, W., Lane, H. C., and Lempicki, R. A. (2003) DAVID: Database for Annotation, Visualization, and Integrated Discovery, *Genome Biol* **4**, P3.
172. Law, P. J., Claudel-Renard, C., Joubert, F., Louw, A. I., and Berger, D. K. (2008) MADIBA: a web server toolkit for biological interpretation of Plasmodium and plant gene clusters, *BMC Genomics* **9**, 105.
173. Brehelin, L., Florent, I., Gascuel, O., and Marechal, E. (2010) Assessing functional annotation transfers with inter-species conserved coexpression: application to *Plasmodium falciparum*, *BMC Genomics* **11**, 35.

174. Rychlik, W., Spencer, W. J., and Rhoads, R. E. (1990) Optimization of the annealing temperature for DNA amplification in vitro, *Nucleic Acids Res* **18**, 6409-6412.
175. Tanabe, K., Sakihama, N., Hattori, T., Ranford-Cartwright, L., Goldman, I., Escalante, A. A., and Lal, A. A. (2004) Genetic distance in housekeeping genes between *Plasmodium falciparum* and Plasmodium reichenowi and within P. falciparum, *J Mol Evol* **59**, 687-694.
176. Denisov, V., Strong, W., Walder, M., Gingrich, J., and Wintz, H. (2008) Development and validation of RQI: An RNA quality indicator for the Experion Automated Electrophoresis System, In *Technical Note 5761* (BioRad Laboratories, I., Ed.) Bulletin 5761 ed.
177. Copois, V., Bibeau, F., Bascoul-Mollevi, C., Salvetat, N., Chalbos, P., Bareil, C., Candeil, L., Fraslon, C., Conseiller, E., Granci, V., Maziere, P., Kramar, A., Ychou, M., Pau, B., Martineau, P., Molina, F., and Del Rio, M. (2007) Impact of RNA degradation on gene expression profiles: assessment of different methods to reliably determine RNA quality, *J Biotechnol* **127**, 549-559.
178. Leung, Y. F., and Cavalieri, D. (2003) Fundamentals of cDNA microarray data analysis, *Trends Genet* **19**, 649-659.
179. Hu, G., Cabrera, A., Kono, M., Mok, S., Chaal, B. K., Haase, S., Engelberg, K., Cheemadan, S., Spielmann, T., Preiser, P. R., Gilberger, T. W., and Bozdech, Z. (2010) Transcriptional profiling of growth perturbations of the human malaria parasite *Plasmodium falciparum*, *Nat Biotechnol* **28**, 91-98.
180. Natalang, O., Bischoff, E., Deplaine, G., Proux, C., Dillies, M. A., Sismeiro, O., Guigon, G., Bonnefoy, S., Patarapotikul, J., Mercereau-Puijalon, O., Coppee, J. Y., and David, P. H. (2008) Dynamic RNA profiling in *Plasmodium falciparum* synchronized blood stages exposed to lethal doses of artesunate, *BMC Genomics* **9**, 388.
181. Ganesan, K., Ponmee, N., Jiang, L., Fowble, J. W., White, J., Kamchonwongpaisan, S., Yuthavong, Y., Wilairat, P., and Rathod, P. K. (2008) A genetically hard-wired metabolic transcriptome in *Plasmodium falciparum* fails to mount protective responses to lethal antifolates, *PLoS Pathog* **4**, e1000214.
182. Gunasekera, A. M., Patankar, S., Schug, J., Eisen, G., and Wirth, D. F. (2003) Drug-induced alterations in gene expression of the asexual blood forms of *Plasmodium falciparum*, *Mol Microbiol* **50**, 1229-1239.
183. Oakley, M. S., Kumar, S., Anantharaman, V., Zheng, H., Mahajan, B., Haynes, J. D., Moch, J. K., Fairhurst, R., McCutchan, T. F., and Aravind, L. (2007) Molecular factors and biochemical pathways induced by febrile temperature in intraerythrocytic *Plasmodium falciparum* parasites, *Infect Immun* **75**, 2012-2025.
184. Benning, C. (2009) Mechanisms of lipid transport involved in organelle biogenesis in plant cells, *Annu Rev Cell Dev Biol* **25**, 71-91.
185. Desjardins, R. E., Canfield, C. J., Haynes, J. D., and Chulay, J. D. (1979) Quantitative assessment of antimalarial activity in vitro by a semiautomated microdilution technique, *Antimicrob Agents Chemother* **16**, 710-718.
186. Abiodun, O. O., Gbotosho, G. O., Ajaiyeoba, E. O., Happi, C. T., Hofer, S., Wittlin, S., Sowunmi, A., Brun, R., and Oduola, A. M. (2010) Comparison of SYBR Green I-, PicoGreen-, and [3H]-hypoxanthine-based assays for in vitro antimalarial screening of plants from Nigerian ethnomedicine, *Parasitol Res* **106**, 933-939.
187. Makler, M. T., and Hinrichs, D. J. (1993) Measurement of the lactate dehydrogenase activity of *Plasmodium falciparum* as an assessment of parasitemia, *Am J Trop Med Hyg* **48**, 205-210.
188. Noedl, H., Wernsdorfer, W. H., Miller, R. S., and Wongsrichanalai, C. (2002) Histidine-rich protein II: a novel approach to malaria drug sensitivity testing, *Antimicrob Agents Chemother* **46**, 1658-1664.
189. Druilhe, P., Moreno, A., Blanc, C., Brasseur, P. H., and Jacquier, P. (2001) A colorimetric in vitro drug sensitivity assay for *Plasmodium falciparum* based on a highly sensitive double-site lactate dehydrogenase antigen-capture enzyme-linked immunosorbent assay, *Am J Trop Med Hyg* **64**, 233-241.

190. Corbett, Y., Herrera, L., Gonzalez, J., Cubilla, L., Capson, T. L., Coley, P. D., Kursar, T. A., Romero, L. I., and Ortega-Barria, E. (2004) A novel DNA-based microfluorimetric method to evaluate antimalarial drug activity, *Am J Trop Med Hyg* **70**, 119-124.
191. Singh, S., Srivastava, R. K., Srivastava, M., Puri, S. K., and Srivastava, K. (2011) In-vitro culture of *Plasmodium falciparum*: utility of modified (RPNI) medium for drug-sensitivity studies using SYBR Green I assay, *Exp Parasitol* **127**, 318-321.
192. Wein, S., Maynadier, M., Tran Van Ba, C., Cerdan, R., Peyrottes, S., Fraisse, L., and Vial, H. (2010) Reliability of antimalarial sensitivity tests depends on drug mechanisms of action, *J Clin Microbiol* **48**, 1651-1660.
193. Yeo, A. E., and Rieckmann, K. H. (1995) Increased antimalarial activity of azithromycin during prolonged exposure of *Plasmodium falciparum* in vitro, *Int J Parasitol* **25**, 531-532.
194. Sidhu, A. B., Sun, Q., Nkrumah, L. J., Dunne, M. W., Sacchettini, J. C., and Fidock, D. A. (2007) In vitro efficacy, resistance selection, and structural modeling studies implicate the malarial parasite apicoplast as the target of azithromycin, *J Biol Chem* **282**, 2494-2504.
195. Krishna, S., Davis, T. M., Chan, P. C., Wells, R. A., and Robson, K. J. (1988) Ciprofloxacin and malaria, *Lancet* **1**, 1231-1232.
196. Dahl, E. L., and Rosenthal, P. J. (2008) Apicoplast translation, transcription and genome replication: targets for antimalarial antibiotics, *Trends Parasitol* **24**, 279-284.
197. Deponte, M., and Becker, K. (2004) *Plasmodium falciparum*--do killers commit suicide?, *Trends Parasitol* **20**, 165-169.
198. Shi, L., Perkins, R. G., Fang, H., and Tong, W. (2008) Reproducible and reliable microarray results through quality control: good laboratory proficiency and appropriate data analysis practices are essential, *Curr Opin Biotechnol* **19**, 10-18.
199. Smit, S. (2010) Functional consequences of the inhibition of Malaria S-adenosylmethionine decarboxylase as a key regulator of polyamine and methionine metabolism, In *Biochemistry*, University of Pretoria, Pretoria.
200. Hester, S. D., Reid, L., Nowak, N., Jones, W. D., Parker, J. S., Knudtson, K., Ward, W., Tiesman, J., and Denslow, N. D. (2009) Comparison of comparative genomic hybridization technologies across microarray platforms, *J Biomol Tech* **20**, 135-151.
201. Hayward, R. E., Derisi, J. L., Alfadhli, S., Kaslow, D. C., Brown, P. O., and Rathod, P. K. (2000) Shotgun DNA microarrays and stage-specific gene expression in *Plasmodium falciparum* malaria, *Mol Microbiol* **35**, 6-14.
202. Kritsiriwuthinan, K., Chaotheing, S., Shaw, P. J., Wongsombat, C., Chavalitshewinkoon-Petmitr, P., and Kamchonwongpaisan, S. (2011) Global gene expression profiling of *Plasmodium falciparum* in response to the anti-malarial drug pyronaridine, *Malar J* **10**, 242.
203. Tamez, P. A., Bhattacharjee, S., van Ooij, C., Hiller, N. L., Llinas, M., Balu, B., Adams, J. H., and Haldar, K. (2008) An erythrocyte vesicle protein exported by the malaria parasite promotes tubovesicular lipid import from the host cell surface, *PLoS Pathog* **4**, e1000118.
204. Palacpac, N. M., Hiramine, Y., Seto, S., Hiramatsu, R., Horii, T., and Mitamura, T. (2004) Evidence that *Plasmodium falciparum* diacylglycerol acyltransferase is essential for intraerythrocytic proliferation, *Biochem Biophys Res Commun* **321**, 1062-1068.
205. Beach, D. H., Sherman, I. W., and Holz, G. G., Jr. (1977) Lipids of Plasmodium lophurae, and of erythrocytes and plasma of normal and P. lophurae-infected Pekin ducklings, *J Parasitol* **63**, 62-75.
206. Palacpac, N. M., Hiramine, Y., Mi-ichi, F., Torii, M., Kita, K., Hiramatsu, R., Horii, T., and Mitamura, T. (2004) Developmental-stage-specific triacylglycerol biosynthesis, degradation and trafficking as lipid bodies in *Plasmodium falciparum*-infected erythrocytes, *J Cell Sci* **117**, 1469-1480.
207. Coleman, R. A., and Lee, D. P. (2004) Enzymes of triacylglycerol synthesis and their regulation, *Prog Lipid Res* **43**, 134-176.
208. (2011) www.genome.jp/kegg/pathway.html.

209. Held, J., Soomro, S. A., Kremsner, P. G., Jansen, F. H., and Mordmuller, B. (2011) In vitro activity of new artemisinin derivatives against *Plasmodium falciparum* clinical isolates from Gabon, *Int J Antimicrob Agents* **37**, 485-488.
210. Ramalhete, C., Lopes, D., Molnar, J., Mulhovo, S., Rosario, V. E., and Ferreira, M. J. (2011) Karavilagenin C derivatives as antimalarials, *Bioorg Med Chem* **19**, 330-338.
211. Olmo, E. D., Barboza, B., Chiaradia, L. D., Moreno, A., Carrero-Lerida, J., Gonzalez-Pacanowska, D., Munoz, V., Lopez-Perez, J. L., Gimenez, A., Benito, A., Martinez, A. R., Ruiz-Perez, L. M., and San Feliciano, A. (2011) Antimalarial activity of imidazo[2,1-a]isoindol-5-ol derivatives and related compounds, *Eur J Med Chem*.
212. Verlinden, B. K., Niemand, J., Snyman, J., Sharma, S. K., Beattie, R. J., Woster, P. M., and Birkholtz, L. M. (2011) Discovery of Novel Alkylated (bis)Urea and (bis)Thiourea Polyamine Analogues with Potent Antimalarial Activities, *J Med Chem* **54**, 6624-6633.
213. Le Roch, K. G., Johnson, J. R., Florens, L., Zhou, Y., Santrosyan, A., Grainger, M., Yan, S. F., Williamson, K. C., Holder, A. A., Carucci, D. J., Yates, J. R., 3rd, and Winzeler, E. A. (2004) Global analysis of transcript and protein levels across the *Plasmodium falciparum* life cycle, *Genome Res* **14**, 2308-2318.
214. Sims, P. F., and Hyde, J. E. (2006) Proteomics of the human malaria parasite *Plasmodium falciparum*, *Expert Rev Proteomics* **3**, 87-95.
215. Nirmalan, N., Sims, P. F., and Hyde, J. E. (2004) Quantitative proteomics of the human malaria parasite *Plasmodium falciparum* and its application to studies of development and inhibition, *Mol Microbiol* **52**, 1187-1199.
216. Wuchty, S., Adams, J. H., and Ferdig, M. T. (2009) A comprehensive *Plasmodium falciparum* protein interaction map reveals a distinct architecture of a core interactome, *Proteomics* **9**, 1841-1849.
217. Foth, B. J., Zhang, N., Mok, S., Preiser, P. R., and Bozdech, Z. (2008) Quantitative protein expression profiling reveals extensive post-transcriptional regulation and post-translational modifications in schizont-stage malaria parasites, *Genome Biol* **9**, R177.
218. Gelhaus, C., Fritsch, J., Krause, E., and Leippe, M. (2005) Fractionation and identification of proteins by 2-DE and MS: towards a proteomic analysis of *Plasmodium falciparum*, *Proteomics* **5**, 4213-4222.
219. Makanga, M., Bray, P. G., Horrocks, P., and Ward, S. A. (2005) Towards a proteomic definition of CoArtem action in *Plasmodium falciparum* malaria, *Proteomics* **5**, 1849-1858.
220. Birkholtz, L. M., Blatch, G., Coetzer, T. L., Hoppe, H. C., Human, E., Morris, E. J., Ngcete, Z., Oldfield, L., Roth, R., Shonhai, A., Stephens, L., and Louw, A. I. (2008) Heterologous expression of plasmodial proteins for structural studies and functional annotation, *Malar J* **7**, 197.
221. Mehlin, C., Boni, E., Buckner, F. S., Engel, L., Feist, T., Gelb, M. H., Haji, L., Kim, D., Liu, C., Mueller, N., Myler, P. J., Reddy, J. T., Sampson, J. N., Subramanian, E., Van Voorhis, W. C., Worthey, E., Zucker, F., and Hol, W. G. (2006) Heterologous expression of proteins from *Plasmodium falciparum*: results from 1000 genes, *Mol Biochem Parasitol* **148**, 144-160.
222. Vedadi, M., Lew, J., Artz, J., Amani, M., Zhao, Y., Dong, A., Wasney, G. A., Gao, M., Hills, T., Brokx, S., Qiu, W., Sharma, S., Diassiti, A., Alam, Z., Melone, M., Mulichak, A., Wernimont, A., Bray, J., Loppnau, P., Plotnikova, O., Newberry, K., Sundararajan, E., Houston, S., Walker, J., Tempel, W., Bochkarev, A., Kozieradzki, I., Edwards, A., Arrowsmith, C., Roos, D., Kain, K., and Hui, R. (2007) Genome-scale protein expression and structural biology of *Plasmodium falciparum* and related Apicomplexan organisms, *Mol Biochem Parasitol* **151**, 100-110.
223. Florens, L., Washburn, M. P., Raine, J. D., Anthony, R. M., Grainger, M., Haynes, J. D., Moch, J. K., Muster, N., Sacci, J. B., Tabb, D. L., Witney, A. A., Wolters, D., Wu, Y., Gardner, M. J., Holder, A. A., Sinden, R. E., Yates, J. R., and Carucci, D. J. (2002) A proteomic view of the *Plasmodium falciparum* life cycle, *Nature* **419**, 520-526.
224. Zuegge, J., Ralph, S., Schmuker, M., McFadden, G. I., and Schneider, G. (2001) Deciphering apicoplast targeting signals--feature extraction from nuclear-encoded precursors of *Plasmodium falciparum* apicoplast proteins, *Gene* **280**, 19-26.

225. Smit, S., Stoychev, S., Louw, A. I., and Birkholtz, L. M. (2010) Proteomic profiling of *Plasmodium falciparum* through improved, semiquantitative two-dimensional gel electrophoresis, *J Proteome Res* **9**, 2170-2181.
226. Lopez, M. F. (2000) Better approaches to finding the needle in a haystack: optimizing proteome analysis through automation, *Electrophoresis* **21**, 1082-1093.
227. Shiio, Y., and Aebersold, R. (2006) Quantitative proteome analysis using isotope-coded affinity tags and mass spectrometry, *Nat Protoc* **1**, 139-145.
228. Aggarwal, K., Choe, L. H., and Lee, K. H. (2006) Shotgun proteomics using the iTRAQ isobaric tags, *Brief Funct Genomic Proteomic* **5**, 112-120.
229. Wu, Y., and Craig, A. (2006) Comparative proteomic analysis of metabolically labelled proteins from *Plasmodium falciparum* isolates with different adhesion properties, *Malar J* **5**, 67.
230. Wysocki, V. H., Resing, K. A., Zhang, Q., and Cheng, G. (2005) Mass spectrometry of peptides and proteins, *Methods* **35**, 211-222.
231. MacBeath, G. (2002) Protein microarrays and proteomics, *Nat Genet* **32 Suppl**, 526-532.
232. Merchant, M., and Weinberger, S. R. (2000) Recent advancements in surface-enhanced laser desorption/ionization-time of flight-mass spectrometry, *Electrophoresis* **21**, 1164-1177.
233. Taylor, C. F., Paton, N. W., Lilley, K. S., Binz, P. A., Julian, R. K., Jr., Jones, A. R., Zhu, W., Apweiler, R., Aebersold, R., Deutsch, E. W., Dunn, M. J., Heck, A. J., Leitner, A., Macht, M., Mann, M., Martens, L., Neubert, T. A., Patterson, S. D., Ping, P., Seymour, S. L., Souda, P., Tsugita, A., Vandekerckhove, J., Vondriska, T. M., Whitelegge, J. P., Wilkins, M. R., Xenarios, I., Yates, J. R., 3rd, and Hermjakob, H. (2007) The minimum information about a proteomics experiment (MIAPE), *Nat Biotechnol* **25**, 887-893.
234. Khachane, A., Kumar, R., Jain, S., Banumathy, G., Singh, V., Nagpal, S., and Tatu, U. (2005) "Plasmo2D": an ancillary proteomic tool to aid identification of proteins from *Plasmodium falciparum*, *J Proteome Res* **4**, 2369-2374.
235. Olsen, J. V., Schwartz, J. C., Griep-Raming, J., Nielsen, M. L., Damoc, E., Denisov, E., Lange, O., Remes, P., Taylor, D., Splendore, M., Wouters, E. R., Senko, M., Makarov, A., Mann, M., and Horning, S. (2009) A dual pressure linear ion trap Orbitrap instrument with very high sequencing speed, *Mol Cell Proteomics* **8**, 2759-2769.
236. Radfar, A., Diez, A., and Bautista, J. M. (2008) Chloroquine mediates specific proteome oxidative damage across the erythrocytic cycle of resistant *Plasmodium falciparum*, *Free Radic Biol Med* **44**, 2034-2042.
237. Carrette, O., Burkhard, P. R., Sanchez, J. C., and Hochstrasser, D. F. (2006) State-of-the-art two-dimensional gel electrophoresis: a key tool of proteomics research, *Nat Protoc* **1**, 812-823.
238. Gygi, S. P., Rochon, Y., Franza, B. R., and Aebersold, R. (1999) Correlation between protein and mRNA abundance in yeast, *Mol Cell Biol* **19**, 1720-1730.
239. Choubey, V., Maity, P., Guha, M., Kumar, S., Srivastava, K., Puri, S. K., and Bandyopadhyay, U. (2007) Inhibition of *Plasmodium falciparum* choline kinase by hexadecyltrimethylammonium bromide: a possible antimalarial mechanism, *Antimicrob Agents Chemother* **51**, 696-706.
240. Choubey, V., Guha, M., Maity, P., Kumar, S., Raghunandan, R., Maulik, P. R., Mitra, K., Halder, U. C., and Bandyopadhyay, U. (2006) Molecular characterization and localization of *Plasmodium falciparum* choline kinase, *Biochim Biophys Acta* **1760**, 1027-1038.
241. Larvor, M. P., Cerdan, R., Gumila, C., Maurin, L., Seta, P., Roustan, C., and Vial, H. (2003) Characterization of the lipid-binding domain of the *Plasmodium falciparum* CTP:phosphocholine cytidylyltransferase through synthetic-peptide studies, *Biochem J* **375**, 653-661.
242. Pessi, G., Kociubinski, G., and Mamoun, C. B. (2004) A pathway for phosphatidylcholine biosynthesis in *Plasmodium falciparum* involving phosphoethanolamine methylation, *Proc Natl Acad Sci U S A* **101**, 6206-6211.

243. Jelenska, J., Crawford, M. J., Harb, O. S., Zuther, E., Haselkorn, R., Roos, D. S., and Gornicki, P. (2001) Subcellular localization of acetyl-CoA carboxylase in the apicomplexan parasite *Toxoplasma gondii*, *Proc Natl Acad Sci U S A* **98**, 2723-2728.
244. (2008) http://www.mmv.org.
245. White, N. J. (2008) Qinghaosu (Artemisinin): The Price of Success, *Science* **320**, 330-334.
246. Muangnoicharoen, S., Johnson, D. J., Looareesuwan, S., Krudsood, S., and Ward, S. A. (2009) Role of known molecular markers of resistance in the antimalarial potency of piperaquine and dihydroartemisinin in vitro, *Antimicrob Agents Chemother* **53**, 1362-1366.
247. Lipinski, C. A., Lombardo, F., Dominy, B. W., and Feeney, P. J. (2001) Experimental and computational approaches to estimate solubility and permeability in drug discovery and development settings, *Adv Drug Deliv Rev* **46**, 3-26.
248. Burrows, J. N., Leroy, D., Lotharius, J., and Waterson, D. (2011) Challenges in antimalarial drug discovery, *Future Med Chem* **3**, 1401-1412.

APPENDICES

The full appendices 1, 2, 4 and 5 can be viewed on the CD provided with this dissertation. The tables for appendices 1, 2, 4 and 5 provided in the printed version of the dissertation do not include the hypothetical transcripts. All other appendices in this dissertation are complete in the printed version.

APPENDIX 1

Differentially affected transcripts of *P. falciparum* after inhibition with A51B1C1_1

PlasmoDB ID	PlasmoDB Product description	LogFC	Adj. P-value	GO ID	Annotated GO Process
Cytoskeleton organization					
MAL7P1.161	Dynein light chain, putative	-1.0631	0.0009	GO:0007017	Microtubule-based process
MAL8P1.132	Kinesin-like protein, putative	0.8434	0.0030	GO:0007018	Microtubule-based movement
PF07_0104	Kinesin-like protein, putative	-0.7846	0.0097	GO:0007017	Microtubule-based process
PF08_0125	Tubulin gamma chain	1.0106	0.0324	GO:0007017	Microtubule-based process
PF10_0368	Dynamin protein, putative	-1.9909	0.0002	GO:0007017	Microtubule-based process
PF11_0114	Actin, putative	-1.1689	0.0108	GO:0007010	Cytoskeleton organization and biogenesis
PF11_0465	Dynamin-like protein	-0.7987	0.0267	GO:0007017	Microtubule-based process
PF14_0124	Actin II	0.7995	0.0338	GO:0007010	Cytoskeleton organization and biogenesis
PF14_0243	Dynein-associated protein, putative	-1.2867	0.0017	GO:0007018	Microtubule-based movement
PF14_0626	Dynein beta chain, putative	0.9285	0.0170	GO:0007018	Microtubule-based movement
PFA0190	Actin	-1.2348	0.0012		Null
PFF1480	Microtubule-associated protein ytm1 homologue, putative	0.9016	0.0080		Null
PFL0660w	Dynein light chain 1, putative	0.9921	0.0247	GO:0007017	Microtubule-based process
PFL1435	Myosin d	-3.7820	0.0000		Null
PFL2215	Actin	-1.3431	0.0074		Null
DNA metabolism					
MAL13P1.22	DNA ligase 1	-0.7877	0.0324	GO:0006266	DNA ligation
MAL13P1.301	Guanylyl cyclase	-1.0597	0.0006	GO:0009190	Cyclic nucleotide biosynthetic process
MAL13P1.96	Chromosome segregation protein, putative	-1.0683	0.0005	GO:0006259	DNA metabolic process
MAL8P1.150	Hypothetical protein	-2.2544	0.0000	GO:0009190	Cyclic nucleotide biosynthetic process
MAL8P1.32	Nucleoside transporter, putative	0.8986	0.0015	GO:0015858	Nucleoside transport
PF10_0232	Chromodomain-helicase-DNA-binding protien 1 homolog, putative	-0.9102	0.0320	GO:0006333	Chromatin assembly or disassembly
PF10_0289	Adenosine deaminase, putative	1.0586	0.0004	GO:0009168	Purine ribonucleoside monullphosphate biosynthetic process
PF10_0369	Helicase, putative	-1.1376	0.0203	GO:0006281	DNA repair
PF11_0083	Nucleic acid binding factor, putative	-0.9746	0.0125	GO:0006139	Nucleobase, nucleoside,nucleotide and

					nucleic acid metabolic process
PF11_0087	Rad51 homolog, putative	0.9268	0.0054	GO:0006259	DNA metabolic process
PF11_0395	Guanylyl cyclase	-1.5888	0.0004	GO:0006182	cGMP biosynthetic process
PF13_0080	Hypothetical protein	0.9373	0.0072	GO:0006278	RNA-dependent DNA replication
PF13_0143	Phosphoribosylpyrophosphate synthetase	0.9434	0.0041	GO:0009116	Nucleoside metabolic process
PF13_0176	Apurinic/apyrimidinic endonuclease Apn1	-1.0874	0.0031	GO:0006281	DNA repair
PF13_0291	Replication licensing factor, putative	-0.8594	0.0240	GO:0006270	DNA replication initiation
PF13_0308	DNA helicase	-0.7560	0.0064		null
PF14_0314	Chromatin assembly factor 1 p55 subunit, putative	-1.4095	0.0012	GO:0006334	Nucleosome assembly
PF14_0352	Ribonucleoside-diphosphate reductase, large subunit	-1.4269	0.0014	GO:0006260	DNA replication
PF14_0639	DNA-3-methyladenine glycosylase, putative	-0.9570	0.0007	GO:0006284	Base-excision repair
PFA0520c	Chromatin assembly factor 1 protein WD40 domain, putative	0.8384	0.0257	GO:0006334	Nucleosome assembly
PFA0555c	UMP-CMP kinase, putative	-1.8010	0.0000	GO:0006221	Pyrimidine nucleotide biosynthetic process
PFC0340w	DNA polymerase delta small subunit, putative	0.7936	0.0059	GO:0006260	DNA replication
PFE0675c	deoxyribodipyrimidine photolyase (photoreactivating enzyme, DNA photolyase), putative	0.8394	0.0301	GO:0006281	DNA repair
PFE0730c	Ribose 5-phosphate epimerase, putative	1.1966	0.0021	GO:0009052	Pentose-phosphate shunt
PFF0865w	Histone h3	-0.8094	0.0332	GO:0007001	Chromosome organization and biogenesis
PFF1225c	DNA polymerase 1, putative	0.7922	0.0188	GO:0006260	DNA replication
PFF1410c	Hypothetical protein, conserved	0.9283	0.0265	GO:0019363	Pyridine nucleotide biosynthetic process
PFF1470c	DNA polymerase epsilon, catalytic subunit a, putative	-0.8425	0.0081	GO:0006260	DNA replication
PFL1005c	Chromodomain protein	-0.8063	0.0136	GO:0006333	Chromatin assembly or disassembly
Electron transport					
MAL13P1.225	Thioredoxin, putative	1.1157	0.0058	GO:0006118	Electron transport
MAL7P1.75	Mitochondrial ATP synthase F1, epsilon subunit, putative	0.8210	0.0275	GO:0015986	ATP synthesis coupled proton transport
PF07_0034	Cg3 protein	0.8983	0.0222	GO:0006118	Electron transport
PF07_0085	Ferrodoxin reductase-like protein	1.0916	0.0116	GO:0006118	Electron transport
PF11_0485	Mitochondrial ATP-synthase, delta subunit putative	-1.1162	0.0070	GO:0015986	ATP synthesis coupled proton transport
PF14_0038	Cytochrome c, putative	1.0742	0.0007	GO:0006118	Electron transport
PF14_0288	Cytochrome c oxidase subunit II precursor, putative	-0.9067	0.0130	GO:0006118	Electron transport

PF14_0373	Ubiquinol cytochrome c oxidoreductase, putative	-1.4926	0.0019	GO:0006118	Electron transport
PFL0180w	Cytochrome c1 heme lyase, putative	0.9546	0.0005	GO:0006118	Electron transport
PFL1700c	Vacuolar-type H+-translocating inorganic pyrophosphatase	-1.4587	0.0028	GO:0015992	Proton transport
Lipid biosynthesis					
PF10_0016	Acyl CoA binding protein, putative	1.1583	0.0113	GO:0006631	Fatty acid metabolic process
PF14_0020	Choline kinase, putative	-0.9606	0.0110	GO:0006629	Lipid metabolic process
PF14_0097	Cytidine diphosphate-diacylglycerol synthase	1.3080	0.0006	GO:0008654	Phospholipid biosynthetic process
PFC0995c	Diacylglycerol O-acyltransferase, putative	-1.1307	0.0025	GO:0019432	Triacylglycerol biosynthetic process
PFF0290w	Long chain polyunsaturated fatty acid elongation enzyme, putative	-1.4463	0.0026	GO:0019368	Fatty acid elongation,unsaturated fatty acid
PFI1370c	Phosphatidylserine decarboxylase	-1.2267	0.0039	GO:0008654	Phospholipid biosynthetic process
PFL0415w	Acyl carrier protein, mitochondrial precursor, putative	1.2257	0.0016	GO:0006633	Fatty acid biosynthetic process
PFL0885w	Hypothetical protein	-1.1777	0.0003	GO:0006886	Intracellular protein transport
Mitochondria targeting Proteins					
PF10_0153	Hsp60	0.8565	0.0046	GO:0006626	Protein targeting to mitochondrion
PF11_0265	Mitochondrial import inner membrane translocase, putative	1.2517	0.0073	GO:0006626	Protein targeting to mitochondrion
PF13_0358	Mitochondrial import inner membrane translocase, putative	1.2963	0.0011	GO:0006626	Protein targeting to mitochondrion
PF14_0208	Hypothetical protein, conserved	0.9255	0.0205	GO:0045039	Protein targeting to mitochondrion inner membrane
PF14_0328	Mitochondrial import inner membrane translocase subunit tim17, putative	1.2223	0.0011	GO:0006626	Protein targeting to mitochondrion
PFL0430w	Tim10 homologue, putative	1.0625	0.0061	GO:0006626	Protein targeting to mitochondrion
Oxidative stress					
MAL7P1.27	Chloroquine resistance transporter, putative	1.1414	0.0011	GO:0042493	Response to drug
PF07_0030	Heat shock protein 86 family protein	0.9091	0.0161	GO:0009408	Response to heat
PF07_0036	Cg6 protein	0.8314	0.0075	GO:0045454	Cell redox homeostasis
PF08_0131	1-cys peroxidoxin	1.3645	0.0003	GO:0006979	Response to oxidative stress
PF13_0021	Small heat shock protein, putative	1.2023	0.0009	GO:0009408	Response to heat
PF14_0048	Hypothetical protein	-0.9625	0.0099	GO:0006801	Superoxide metabolic process
PFE0605c	Glutathione synthetase	0.9734	0.0211	GO:0006979	Response to oxidative stress
PFE1150w	Multidrug resistance protein	1.5671	0.0005	GO:0042493	Response to drug
PFF1130c	Fe-superoxide dismutase	0.9918	0.0022	GO:0019430	Removal of superoxide radicals

Parasite-host interaction					
MAL13P1.1	Erythrocyte membrane protein 1 (PfEMP1)	-1.2199	0.0004	GO:0009405	Pathogenesis
MAL13P1.356	Erythrocyte membrane protein 1 (PfEMP1)	-0.9336	0.0049	GO:0009405	Pathogenesis
MAL13P1.49	Rifin	-3.3599	0.0000		Null
MAL13P1.53	Rifin	0.8834	0.0297		Null
MAL13P1.60	Erythrocyte binding antigen 140	-0.9041	0.0043	GO:0009405	Pathogenesis
MAL7P1.176	Erythrocyte binding antigen	-0.8306	0.0297	GO:0009405	Pathogenesis
MAL7P1.212	Erythrocyte membrane protein1 (PfEMP1)	-0.8283	0.0061	GO:0009405	Pathogenesis
MAL7P1.213	Rifin	-1.6573	0.0001		Null
MAL7P1.50	Erythrocyte membrane protein 1 (PfEMP1)	-1.0475	0.0003	GO:0020033	Antigenic variation
PF08_0104	Rifin	-0.7500	0.0409	GO:0020033	Antigenic variation
PF08_0142	Erythrocyte membrane protein 1 (PfEMP1)	-2.2805	0.0000	GO:0020033	Antigenic variation
PF10_0002	Rifin	-0.9794	0.0039	GO:0020033	Antigenic variation
PF10_0003	Rifin	-1.6312	0.0002	GO:0020033	Antigenic variation
PF10_0268	Merozoite capping protein 1	-1.2360	0.0024	GO:0030260	Entry into host cell
PF10_0345	Merozoite Surface Protein 3, MSP3	-0.8357	0.0070	GO:0030260	Entry into host cell
PF10_0346	Merozoite Surface protein 6, MSP6	-1.4551	0.0001	GO:0030260	Entry into host cell
PF10_0348	Erythrocyte membrane protein putative	-1.0047	0.0163	GO:0009405	Pathogenesis
PF11_0007	Erythrocyte membrane protein 1 (PfEMP1)	-1.1511	0.0023	GO:0020033	Antigenic variation
PF11_0111	Asparagine-rich antigen	-0.7652	0.0366		Null
PF13_0197	Merozoite Surface Protein 7 precursor, MSP7	-1.2074	0.0026	GO:0030260	Entry into host cell
PF14_0006	Rifin	-0.9203	0.0076	GO:0020033	Antigenic variation
PF14_0138	Hypothetical protein	-1.1509	0.0050	GO:0007155	Cell adhesion
PF14_0773	Erythrocyte membrane protein 1 (PfEMP1) pseudogene	-1.0146	0.0066	GO:0009405	Pathogenesis
PFA0040	Rifin	-1.5605	0.0003		Null
PFA0625w	SURFIN, surface-associated interspersed gene	-0.7778	0.0059		Null
PFB0035c	Rifin	-0.9720	0.0283	GO:0020033	Antigenic variation
PFB0935w	Cytoadherence linked asexual protein 2	-1.6759	0.0007	GO:0020035	Cytoadherence to microvasculature, mediated by parasite protein
PFC0110w	Cytoadherence linked asexual protein, CLAG	-1.1843	0.0030	GO:0020035	Cytoadherence to microvasculature, mediated by parasite protein

PFC0115c	Erythrocyte membrane protein 1 (PfEMP1) pseudogene	-0.8342	0.0126	GO:0009405	Pathogenesis
PFC0120w	Cytoadherence linked asexual protein, CLAG	-2.9282	0.0000	GO:0020035	Cytoadherence to microvasculature, mediated by parasite protein
PFC1115w	Rifin (3D7-rifT3-7)	-0.7908	0.0264		Null
PFD0070c	Rifin	1.3592	0.0019	GO:0008150	Biological process
PFD0135w	Erythrocyte membrane protein 1 (PfEMP1) pseudogene	-1.1015	0.0147	GO:0009405	Pathogenesis
PFD1015c	Erythrocyte membrane protein 1 (PfEMP1)	-0.8224	0.0072	GO:0020033	Antigenic variation
PFD1240	Rifin	-0.8430	0.0302		Null
PFE0070w	Interspersed repeat antigen, putative	-0.7715	0.0476		Null
PFF1580c	Erythrocyte membrane protein 1 (PfEMP1)	-0.8155	0.0082	GO:0020033	Antigenic variation
PFF1590	Rifin	-0.9213	0.0030		Null
PFI0030c	Rifin	-0.8720	0.0072	GO:0020033	Antigenic variation
PFI1475w	Merozoite surface protein 1, precursor	-1.8460	0.0000	GO:0009405	Pathogenesis
PFL0025	Rifin	-1.0036	0.0055		Null
PFL2625	Rifin	-0.9955	0.0027		Null
PFL2640c	Rifin	-0.9908	0.0028	GO:0020033	Antigenic variation
Post-translational modification					
MAL13P1.114	Hypothetical protein	-2.0935	0.0000	GO:0006468	Protein aminull acid phosphorylation
MAL13P1.278	Ser/Thr protein kinase	-1.8277	0.0000	GO:0006468	Protein aminull acid phosphorylation
MAL13P1.297	ADP-ribosylation factor, putative	-0.9679	0.0085	GO:0006471	Protein aminull acid ADP-ribosylation
MAL7P1.147	Ubiquitin carboxyl-terminal hydrolase, putative	-1.0976	0.0038	GO:0016579	Protein deubiquitination
MAL7P1.18	Erythrocyte membrane protein1 (PfEMP1)	-1.1405	0.0073	GO:0006468	Protein aminull acid phosphorylation
MAL7P1.19	Hypothetical protein	-1.1681	0.0022	GO:0006464	Protein modification pocess
MAL7P1.91	Exported serine/threonine protein kinase	-1.2113	0.0004	GO:0006468	Protein aminull acid phosphorylation
MAL8P1.142	Proteasome beta-subunit	-1.7387	0.0001	GO:0006511	Ubiquitin-dependent protein catabolic process
MAL8P1.42	Hypothetical protein	-0.8911	0.0040	GO:0006468	Protein aminull acid phosphorylation
PF08_0044	Protein kinase	-0.8148	0.0139	GO:0006468	Protein aminull acid phosphorylation
PF08_0129	Protein phosphatase, putative	-1.0704	0.0092	GO:0006470	Protein aminull acid dephosphorylation
PF10_0094	Tubulin-tyrosine ligase putative	-2.1475	0.0000	GO:0006464	Protein modification pocess
PF11_0177	Ubiquitin C-terminal hydrolase, family 1, putative	-0.9104	0.0046	GO:0006511	Ubiquitin-dependent protein catabolic process

PF11_0201	Hypothetical protein	-1.2476	0.0007	GO:0006464	Protein modification pocess
PF11_0257	Ethanolamine kinase, putative	-0.9378	0.0104	GO:0006646	Phosphatidylethanulllamine biosynthetic process
PF11_0464	Serine/threonine protein kinase	-2.6785	0.0000	GO:0006468	Protein aminull acid phosphorylation
PF13_0166	Protein kinase, putative	-1.2255	0.0003	GO:0006468	Protein aminull acid phosphorylation
PF13_0211	Calcium-dependent protein kinase	-1.4590	0.0000	GO:0006468	Protein aminull acid phosphorylation
PF13_0258	Sexual stage-specific protein kinase	-0.8562	0.0181	GO:0006468	Protein aminull acid phosphorylation
PF13_0301	Ubiquitin-conjugating enzyme, putative	-0.8789	0.0313	GO:0006464	Protein modification pocess
PF14_0063	ATP-dependent Clp protease, putative	-0.9118	0.0085	GO:0019538	Protein metabolic process
PF14_0142	Serine/threonine protein phosphatase, putative	-0.7891	0.0237	GO:0006470	Protein aminull acid dephosphorylation
PF14_0224	PP1-like protein serine/threonine phosphatase	-2.4132	0.0000	GO:0006470	Protein aminull acid dephosphorylation
PF14_0392	Ser/Thr protein kinase, putative	-1.3650	0.0019	GO:0006468	Protein aminull acid phosphorylation
PF14_0492	Protein phosphatase 2b regulatory subunit, putative	-1.1966	0.0023	GO:0006470	Protein aminull acid dephosphorylation
PF14_0632	26S proteasome subunit, putative	-1.4105	0.0019	GO:0006511	Ubiquitin-dependent protein catabolic process
PF14_0694	Protein disulfide isomerase, putative	-1.6054	0.0000	GO:0006457	Protein folding
PFE0895c	Zinc finger protein, putative	-1.2159	0.0050	GO:0006471	Protein aminull acid ADP-ribosylation
PFF1370w	*P. falciparum* PK4 protein kinase	-1.1607	0.0020	GO:0006468	Protein aminull acid phosphorylation
PFI0160w	Hypothetical protein	-1.2563	0.0026	GO:0006468	Protein aminull acid phosphorylation
PFI1685w	cAMP-dependent protein kinase catalytic subunit	-1.6531	0.0014	GO:0006468	Protein aminull acid phosphorylation
PFL1415w	Hypothetical protein	-1.1644	0.0003	GO:0006457	Protein folding
MAL13P1.185	CDK-related protein kinase 6	1.1192	0.0023	GO:0006468	Protein aminull acid phosphorylation
MAL13P1.64	Ubiquitin-like protein nedd8 homologue, putative	0.8805	0.0182	GO:0006464	Protein modification pocess
MAL7P1.130	3-demethylubiquinone-9 3-methyltransferase-like protein, putative	0.7725	0.0093	GO:0006744	Ubiquinullne biosynthetic process
MAL8P1.108	Protein phosphatase, putative	1.0902	0.0004	GO:0006470	Protein aminull acid dephosphorylation
PF08_0085	Ubiquitin-conjugating enzyme, putative	0.8313	0.0100	GO:0006464	Protein modification pocess
PF08_0121	Peptidyl-prolyl cis-trans isomerase precursor	0.7643	0.0043	GO:0006457	Protein folding
PF10_0141	Cdk7, putative	0.8360	0.0191	GO:0006468	Protein aminull acid phosphorylation
PF10_0203	ADP-ribosylation factor	0.7863	0.0361	GO:0006471	Protein aminull acid ADP-ribosylation
PF10_0298	26S proteasome subunit, putative	0.7563	0.0405	GO:0006511	Ubiquitin-dependent protein catabolic process
PF11_0079	Hypothetical protein	0.9357	0.0219	GO:0006468	Protein aminull acid phosphorylation

PF11_0188	Heat shock protein 90, putative	1.1074	0.0006	GO:0006457	Protein folding
PF11_0258	Co-chaperone GrpE, putative	0.9644	0.0106	GO:0030150	Protein import into mitochondrial matrix
PF11_0281	Hypothetical protein	0.8411	0.0211	GO:0016311	Dephosphorylation
PF11_0510	Ser/Thr protein kinase, putative	0.9708	0.0047	GO:0006468	Protein aminull acid phosphorylation
PF13_0180	Chaperonin, putative	0.8905	0.0327	GO:0006457	Protein folding
PF13_0182	Hypothetical protein	0.8112	0.0136	GO:0006464	Protein modification pocess
PF13_0282	Proteasome subunit, putative	0.9470	0.0103	GO:0006511	Ubiquitin-dependent protein catabolic process
PF14_0145	Hypothetical protein	0.7670	0.0320	GO:0006511	Ubiquitin-dependent protein catabolic process
PF14_0167	Hypothetical protein	1.3617	0.0001	GO:0006457	Protein folding
PF14_0309	Protein-L-isoaspartate O-methyltransferase beta-aspartate Methyltransferase, putative	0.8656	0.0369	GO:0030091	Protein repair
PF14_0716	Proteosome subunit alpha type 1, putative	0.8061	0.0052	GO:0006511	Ubiquitin-dependent protein catabolic process
PFA0460c	Tubulin-specific chaperone a, putative	1.0239	0.0020	GO:0007021	Tubulin protein folding
PFD0975w	ROI kinase-like protein	0.7547	0.0139	GO:0006468	Protein aminull acid phosphorylation
PFD1175w	*Plasmodium falciparum* trophozoite antigen r45-like protein	0.7868	0.0358	GO:0006468	Protein aminull acid phosphorylation
PFE0915c	Proteasome subunit beta type 1	1.0627	0.0002	GO:0006511	Ubiquitin-dependent protein catabolic process
PFF0155w	bcs1-like protein, putative	1.0010	0.0026	GO:0006461	Protein complex assembly
PFF0360w	Uroporphyrinogen decarboxylase, putative	0.9953	0.0182	GO:0006779	Porphyrin biosynthetic process
PFI0095c	Protein kinase, putative	1.1704	0.0003	GO:0006468	Protein aminull acid phosphorylation
PFI0960w	Dolichyl-diphosphooligosaccharide--protein-glycotransferase,putative	0.9829	0.0004	GO:0018279	Protein aminull acid N-linked glycosylation via asparagine
PFL1885c	Calcium/calmodulin-dependent protein kinase 2, putative	0.7565	0.0172	GO:0006468	Protein aminull acid phosphorylation
PFL2550w	Hypothetical protein, conserved in *P. falciparum*	1.1100	0.0016	GO:0006457	Protein folding
Primary Metabolic Process					
MAL13P1.218	UDP-N-acetylglucosamine pyrophosphorylase, putative	0.8095	0.0306	GO:0006047	UDP-N-acetylglucosamine metabolic process
MAL13P1.221	Aspartate carbamoyltransferase	0.9613	0.0013	GO:0006520	Aminull acid metabolic process
MAL13P1.283	TCP-1/cpn60 chaperonin family, putative	1.0749	0.0040	GO:0044267	Cellular protein metabolic process
MAL13P1.326	Ferrochelatase, putative	1.0484	0.0023	GO:0006783	Heme biosynthetic process
MAL8P1.156	Mannose-6-phosphate isomerase, putative	1.0712	0.0027	GO:0005975	Carbohydrate metabolic process
PF07_0047	Cell division cycle ATPase, putative	1.1080	0.0043	GO:0000074	Regulation of progression through cell cycle
PF08_0034	Histone acetyltransferase Gcn5, putative	0.9456	0.0020	GO:0008152	Metabolic process

PF08_0066	Lipoamide dehydrogenase, putative	1.1545	0.0023	GO:0006086	Acetyl-coa biosynthetic process from pyruvate
PF08_0095	Dihydropteroate synthetase	1.3051	0.0004	GO:0006761	Dihydrofolate biosynthetic process
PF10_0026	Tryptophan-rich antigen 3, putative	0.9590	0.0036	GO:0006777	Mo-molybdopterin cofactor biosynthetic process
PF10_0225	Orotidine-monophosphate-decarboxylase, putative	0.7526	0.0061	GO:0006221	Pyrimidine nucleotide biosynthetic process
PF10_0325	Haloacid dehalogenase-like hydrolase, putative	1.0840	0.0009	GO:0008152	Metabolic process
PF10_0363	Pyruvate kinase, putative	1.3988	0.0003	GO:0006096	Glycolysis
PF10_0407	Dihydrolipoamide acetyltransferase, putative	1.0908	0.0036	GO:0008152	Metabolic process
PF11_0145	Glyoxalase I, putative	0.9478	0.0076	GO:0009438	Methylglyoxal metabolic process
PF11_0295	Farnesyl pyrophosphate synthase, putative	0.7969	0.0066	GO:0008299	Isoprenullid biosynthetic process
PF11_0311	N-acetyl glucosamine phosphate mutase, putative	0.8203	0.0073	GO:0005975	Carbohydrate metabolic process
PF11_0331	T-complex protein 1, alpha subunit, putative	1.3016	0.0002	GO:0044267	Cellular protein metabolic process
PF13_0121	Dihydrolipoamide succinyltransferase, putative	0.7610	0.0080	GO:0008152	Metabolic process
PF13_0234	Phosphoenolpyruvate carboxykinase	0.7899	0.0086	GO:0006094	Gluconeogenesis
PF13_0322	Falcilysin	0.7829	0.0124	GO:0020027	Hemoglobin metabolic process
PF13_0349	Nucleoside diphosphate kinase b; putative	0.7767	0.0301	GO:0006241	Pyrimidine ribonucleoside triphosphate biosynthetic process
PF14_0286	Glutamate dehydrogenase, putative	0.8870	0.0113	GO:0006520	Aminull acid metabolic process
PF14_0534	Serine hydroxymethyltransferase	0.9367	0.0187	GO:0006563	L-serine metabolic process
PFC0395w	Asparagine synthetase, putative	0.7799	0.0163	GO:0006529	Asparagine biosynthetic process
PFF0230c	Glyoxalase I, putative	0.9032	0.0136	GO:0009438	Methylglyoxal metabolic process
PFF0430w	Chaperone, putative	1.1381	0.0017	GO:0044267	Cellular protein metabolic process
PFF0775w	Pyridoxal kinase-like protein, putative	0.8641	0.0062	GO:0008614	Pyridoxine metabolic process
PFF1025c	Pyridoxine biosynthetic enzyme pdx1 homologue, putative	1.3008	0.0000	GO:0008615	Pyridoxine biosynthetic process
PFF1105c	Chorismate synthase	0.9951	0.0022	GO:0009073	Aromatic aminull acid family biosynthetic process
PFF1265w	Oxidoreductase, short-chain dehydrogenase family, putative	0.8277	0.0131	GO:0008152	Metabolic process
PFI1105w	Phosphoglycerate kinase	0.7885	0.0115	GO:0006096	Glycolysis
PFL1155w	GTP cyclohydrolase I	0.7539	0.0063	GO:0019438	Aromatic compound biosynthetic process
PFL1270w	cof-like hydrolase, had-superfamily, subfamily iib	1.0312	0.0010	GO:0008152	Metabolic process
PFL1425w	t-complex protein 1, gamma subunit, putative	0.9501	0.0117	GO:0044267	Cellular protein metabolic process

PFL1475w	Sun-family protein, putative	1.0209	0.0057	GO:0008152	Metabolic process
MAL13P1.324	Aldo-keto reductase, putative	-1.0136	0.0058	GO:0008152	Metabolic process
MAL7P1.108	Hypothetical protein	-1.3873	0.0014	GO:0007154	Cell communication
PF08_0094	Cullin-like protein, putative	-1.3244	0.0024	GO:0007049	Cell cycle
PF08_0132	Glutamate dehydrogenase, putative	-0.9944	0.0179	GO:0006520	Aminull acid metabolic process
PF10_0135	Hypothetical protein	-1.8255	0.0000	GO:0044267	Cellular protein metabolic process
PF11_0190	Hypothetical protein	-1.4482	0.0029	GO:0008152	Metabolic process
PF11_0338	Aquaglyceroporin	-1.1885	0.0047	GO:0009247	Glycolipid biosynthetic process
PF11_0410	Hypothetical protein	-1.8063	0.0000	GO:0006730	One-carbon compound metabolic process
PF14_0200	Hypothetical protein	-1.0465	0.0170	GO:0015937	Coenzyme A biosynthetic process
PF14_0350	Hypothetical protein	-1.2812	0.0006	GO:0008152	Metabolic process
PF14_0511	Glucose-6-phosphatedehydrogenase-6-phosphogluconolactonase	-1.3281	0.0011	GO:0006010	Glucose 6-phosphate utilization
PFF0940c	Cell division cycle protein 48 homologue, putative	-0.7837	0.0402	GO:0000074	Regulation of progression through cell cycle
Proteolysis					
MAL13P1.184	Endopeptidase, putative	-1.8816	0.0042	GO:0006508	Proteolysis
MAL13P1.25	Hypothetical protein	1.0111	0.0130	GO:0006508	Proteolysis
MAL13P1.310	Cysteine protease, calpain family	-0.8604	0.0069	GO:0006508	Proteolysis
MAL8P1.126	Serine protease, putative	-1.3819	0.0000	GO:0006508	Proteolysis
MAL8P1.139	Folate/biopterin transporter	-1.6996	0.0001	GO:0006508	Proteolysis
PF08_0020	Ubiquitination-mediated degradation component, putative	-0.8641	0.0016	GO:0016567	Protein ubiquitination
PF08_0108	Pepsinogen, putative	-0.8517	0.0043	GO:0006508	Proteolysis
PF10_0058	Dnaj protein, putative	0.9074	0.0027	GO:0006508	Proteolysis
PF10_0150	Methionine aminopeptidase, putative	1.1106	0.0011	GO:0006508	Proteolysis
PF10_0374	Gene 11-1 protein precursor	-0.9811	0.0029	GO:0006508	Proteolysis
PF11_0161	Falcipain-2 precursor, putative	-0.8589	0.0018	GO:0006508	Proteolysis
PF11_0165	Falcipain 2 precursor	1.6752	0.0001	GO:0006508	Proteolysis
PF11_0203	Peptidase	-0.9804	0.0020	GO:0006508	Proteolysis
PF11_0226	Peptidase, M16 family	-0.9503	0.0066		Null
PF11_0298	GPI8p transamidase	-0.9252	0.0061	GO:0006508	Proteolysis
PF11_0528	Hypothetical protein	-1.5495	0.0063	GO:0006508	Proteolysis

PF14_0075	Plasmepsin, putative	1.0789	0.0005	GO:0006508	Proteolysis
PF14_0077	Plasmepsin 2 precursor	1.2204	0.0015	GO:0006508	Proteolysis
PF14_0078	HAP protein	1.1557	0.0018	GO:0006508	Proteolysis
PF14_0084	Hypothetical protein	-1.0882	0.0008	GO:0006508	Proteolysis
PF14_0160	Hypothetical protein	-1.0863	0.0045	GO:0006508	Proteolysis
PF14_0252	Hypothetical protein	-0.9629	0.0075	GO:0006508	Proteolysis
PF14_0281	Aspartyl protease, putative	-1.4667	0.0000	GO:0006508	Proteolysis
PF14_0363	Metacaspase-like protein	-1.5542	0.0001	GO:0006508	Proteolysis
PF14_0648	Hypothetical protein	1.1745	0.0010	GO:0006508	Proteolysis
PFB0340c	Cysteine protease, putative	-0.9990	0.0423	GO:0006508	Proteolysis
PFD0230c	Protease, putative	-2.1569	0.0001	GO:0006508	Proteolysis
PFE0355c	Serine protease belonging to subtilisin family, putative	-1.7142	0.0001	GO:0006508	Proteolysis
PFE0570w	Hypothetical protein	-0.7872	0.0394	GO:0006508	Proteolysis
PFE1120w	Hypothetical protein	-0.8397	0.0137	GO:0006508	Proteolysis
PFI0135c	Papain family cysteine protease, putative	0.8877	0.0058	GO:0006508	Proteolysis
PFI1570c	Aminopeptidase, putative	1.0156	0.0005	GO:0006508	Proteolysis
RNA metabolic process					
MAL7P1.81	Eukaryotic translation initiation factor 3 37.28 kda subunit, putative	-1.3291	0.0020	GO:0006446	Regulation of translational initiation
PF07_0091	Cell cycle control protein cwf15 homologue	-0.7690	0.0142	GO:0008380	RNA splicing
PF10_0071	Rhogap protein	-2.1673	0.0002	GO:0007266	Rho proteinsignal transduction
PF10_0143	ADA2-like protein	-1.0832	0.0037	GO:0006355	Regulation of transcription, DNA-dependent
PF11_0300	Hypothetical protein	-1.3432	0.0003	GO:0006396	RNA processing
PF11_0477	CCAAT-box DNA binding protein subunit B	-1.3793	0.0002	GO:0006355	Regulation of transcription, DNA-dependent
PF13_0152	Transcriptional regulatory protein sir2 homologue, putative	-1.0388	0.0014	GO:0006355	Regulation of transcription, DNA-dependent
PF13_0229	IRP-like protein	-0.8751	0.0179	GO:0006447	Regulation of translational initiation by iron
PF14_0608	Hypothetical protein	-1.1109	0.0015	GO:0045449	Regulation of transcription
PFD0700c	RNA binding protein, putative	-1.0024	0.0125	GO:0016070	RNA metabolic process
MAL13P1.253	Small nuclear ribonucleoprotein, putative	0.8979	0.0085	GO:0016071	mRNA metabolic process
MAL13P1.294	GTP-binding protein, putative	0.7538	0.0078	GO:0007165	Signal transduction
MAL7P1.69	Calmodulin, putative	1.2267	0.0014	GO:0007165	Signal transduction

MAL8P1.23	Ubiquitin-protein ligase 1, putative	-1.1209	0.0035	GO:0051028	mRNA transport
MAL8P1.48	Small nuclear ribonucleoprotein, putative	0.8966	0.0132	GO:0016071	mRNA metabolic process
PF07_0057	Transcription elongation factor s-ii, putative	1.0043	0.0014	GO:0045449	Regulation of transcription
PF07_0071	Queuine tRNA-ribosyltransferase; putative	-1.1177	0.0024	GO:0006400	tRNA modification
PF07_0075	Hypothetical protein, expressed	0.8749	0.0104	GO:0006350	Transcription
PF07_0123	mRNA (N6-adenosine)-methyltransferase, putative	0.7946	0.0095	GO:0009451	RNA modification
PF10_0085	Nucleolar protein NOP5, putative	1.0606	0.0066	GO:0006364	rRNA processing
PF10_0164	Early transcribed membrane protein10.3, ETRAMP 10.3	1.0653	0.0049	GO:0008150	Biological process
PF10_0269	DNA-directed RNA polymerase II, putative	0.7837	0.0077	GO:0006366	transcription from RNA polymerase II Promoter
PF11_0200	U2 snRNP auxiliary factor, small subunit, putative	-0.9115	0.0056	GO:0000398	Nuclear mRNA splicing
PF11_0255	Hypothetical protein	-1.5704	0.0003	GO:0016071	mRNA metabolic process
PF11_0259	Hypothetical protein	1.5492	0.0001	GO:0042254	Ribosome biogenesis and assembly
PF11_0264	DNA-dependent RNA polymerase	0.7522	0.0372	GO:0006350	Transcription
PF11_0270	Threonine -- tRNA ligase, putative	1.2129	0.0011	GO:0006435	Threonyl-tRNA aminullacylation
PF11_0445	DNA-directed RNA polymerase I, putative	0.9862	0.0041	GO:0006350	Transcription
PF13_0023	DNA-directed RNA polymerase 2, putative	1.1350	0.0021	GO:0006366	transcription from RNA polymerase II Promoter
PF13_0109	N2,N2-dimethylguanosine tRNA methyltransferase, putative	1.6630	0.0003	GO:0008033	tRNA processing
PF13_0142	u6 snRNA-associated sm-like protein, putative	1.0655	0.0034	GO:0016071	mRNA metabolic process
PF13_0150	DNA-directed RNA polymerase 3 largest subunit	0.7525	0.0241	GO:0006383	Transcription from RNA polymerase III Promoter
PF13_0205	Tryptophan--trna ligase, putative	0.8021	0.0094	GO:0006436	Tryptophanyl-tRNA aminullacylation
PF13_0209	Hypothetical protein	0.9239	0.0206	GO:0045449	Regulation of transcription
PF13_0286	Methyltransferase, putative	0.7994	0.0451	GO:0006364	rRNA processing
PF13_0340	Exosome complex exonuclease, putative	0.8260	0.0076	GO:0006396	RNA processing
PF13_0341	DNA-directed RNA polymerase 2, putative	1.0028	0.0022	GO:0006366	transcription from RNA polymerase II Promoter
PF14_0057	RNA binding protein, putative	0.9331	0.0088	GO:0006396	RNA processing
PF14_0241	Basic transcription factor 3b, putative	0.9684	0.0057	GO:0008150	Biological process
PF14_0603	Hypothetical protein	1.0762	0.0030	GO:0006383	Transcription from RNA polymerase III Promoter

PF14_0695	DNA-directed RNA polymerase, alpha subunit, truncated, putative	1.1921	0.0009	GO:0006351	Transcription, DNA dependent
PF14_0713	hypothetical protein	0.8095	0.0046	GO:0006396	RNA processing
PFA0505c	DNA-directed RNA polymerase 2 subunit, putative	1.0533	0.0004	GO:0045449	Regulation of transcription
PFB0370c	RNA-binding protein, putative	0.8892	0.0072		null
PFB0860c	RNA helicase, putative	1.3091	0.0029	GO:0008150	Biological process
PFB0890c	Pseudouridine synthetase, putative	1.2205	0.0003	GO:0000154	rRNA modification
PFC0825c	Cleavage and polyadenylation specificity factor protein, putative	-1.1363	0.0196	GO:0006378	mRNA polyadenylation
PFD0180c	CGI-201 protein, short form	1.0202	0.0024	GO:0006396	RNA processing
PFD0565c	RNA helicase, putative	1.2031	0.0129	GO:0016070	RNA metabolic process
PFE1080w	Ribosomal large subunit pseudouridylate synthase, putative	0.8672	0.0079	GO:0006364	rRNA processing
PFE1390w	RNA helicase-1	0.9676	0.0059		Null
PFF0535	Trancription factor, putative	0.9855	0.0011		Null
PFF1140c	ATP-dependent DEAD box helicase, putative	0.7649	0.0415	GO:0016070	RNA metabolic process
PFF1150w	ribonuclease H1 large subunit, putative	0.8730	0.0025	GO:0006401	RNA catabolic process
PFF1335c	4-methyl-5(B-hydroxyethyl)-thiazol monophosphate biosynthesis Enzyme	1.0933	0.0024	GO:0009228	thiamin biosynthetic process
PFI0860	ATP-dependant RNA helicase, putative	0.9422	0.0023		null
PFI1195c	Thiamine pyrophosphokinase	0.9609	0.0011	GO:0006772	thiamin metabolic process
PFL0075w	XPA binding protein 1, putative	0.9635	0.0032	GO:0006614	SRP-dependent cotranslational protein targeting to membrane
PFL0330	DNA-directed RNA polymerase III subunit, putative	0.8867	0.0028		null
PFL0665c	RNA polymerase subunit 8c, putative	1.2050	0.0006	GO:0006352	transcription initiation
PFL1680w	Splicing factor 3b, subunit 3, 130kD, putative	1.0762	0.0012	GO:0008380	RNA splicing
Signal transduction					
MAL13P1.118	cAMP-specific 3',5'-cyclic phosphodiesterase 4D, putative	-1.2950	0.0008	GO:0007165	Signal transduction
MAL13P1.19	Hypothetical protein	-0.7712	0.0140	GO:0032012	Regulation of ARF protein signal transduction
PF14_0407	Hypothetical protein	-0.9452	0.0427	GO:0032012	Regulation of ARF protein signal transduction
PFA0515w	Phosphatidylinositol-4-phosphate 5-kinase, putative	1.0549	0.0015	GO:0048015	Phosphoinullsitide-mediated signaling
Translation					
MAL13P1.209	60S ribosomal subunit porotein L18, putative	0.8845	0.0027	GO:0006412	Translation
MAL7P1.158	Signal recognition particle, putative	0.8317	0.0097	GO:0045900	Negative regulation of translational elongation

MAL7P1.93	Mitochondrial ribosomal protein S8, putative	0.8393	0.0094	GO:0006412	Translation
MAL8P1.27	Hypothetical protein	0.7594	0.0096	GO:0006413	Translational initiation
PF07_0046	50S ribosomal protein L1, putative	-0.9130	0.0415	GO:0006412	Translation
PF07_0088	40S ribosomal protein S5, putative	0.8646	0.0073	GO:0006412	Translation
PF08_0018	Translation initiation factor-like protein	-0.9036	0.0024	GO:0006413	Translational initiation
PF10_0043	Ribosomal protein L13, putative	1.0172	0.0038	GO:0006412	Translation
PF10_0077	Eukaryotic translation initiation factor 3 subunit 7, putative	0.9279	0.0090	GO:0006413	Translational initiation
PF10_0105	Hypothetical protein	1.0147	0.0012	GO:0006412	Translation
PF10_0187	Ribosomal protein L30e, putative	0.8573	0.0124	GO:0006412	Translation
PF10_0264	40S ribosomal protein, putative	0.8368	0.0036	GO:0006412	Translation
PF11_0245	Translation elongation factor EF-1, subunit alpha, putative	-0.8841	0.0280	GO:0006414	Translational elongation
PF11_0382	Ribosomal protein S9, putative	0.8069	0.0099	GO:0006412	Translation
PF11_0438	Ribosomal protein, putative	0.9148	0.0058	GO:0006412	Translation
PF11_0447	Translation initiation factor eIF-1A, putative	1.1372	0.0011	GO:0006413	Translational initiation
PF11_0454	Ribosomal protein, 40S subunit, putative	1.1045	0.0212	GO:0006412	Translation
PF13_0014	40S ribosomal protein S7 homologue, putative	1.3159	0.0007	GO:0006412	Translation
PF13_0045	40S ribosomal protein S27, putative	0.8079	0.0036	GO:0006412	Translation
PF13_0049	60S ribosomal protein L24, putative	1.1194	0.0008	GO:0006412	Translation
PF13_0171	60S ribosomal protein L23, putative	0.8943	0.0074	GO:0006412	Translation
PF13_0213	60S ribosomal subunit protein L6e, putative	1.1647	0.0007	GO:0006412	Translation
PF13_0268	ribosomal protein L17, putative	1.1319	0.0014	GO:0006412	Translation
PF13_0316	40S ribosomal protein S13	1.3676	0.0003	GO:0006412	Translation
PF14_0027	Ribosomal S27a, putative	0.7824	0.0298	GO:0006412	Translation
PF14_0166	Lysine -- tRNA ligase, putative	0.7542	0.0102	GO:0006418	Trna aminullacylation for protein translation
PF14_0276	Ribosomal protein L15, putative	0.7754	0.0158	GO:0006412	Translation
PF14_0391	Ribosomal protein L1, putative	1.0304	0.0009	GO:0006412	Translation
PF14_0584	Ribosomal protein S4, putative	1.0729	0.0086	GO:0006412	Translation
PF14_0658	Translation initiation factor EF-1, putative	0.8402	0.0060	GO:0006413	Translational initiation
PFB0467w	#N/A	0.8206	0.0371	GO:0006412	Translation
PFB0545c	Ribosomal protein L7/L12, putative	1.2851	0.0043	GO:0006412	Translation

PFB0550w	Peptide chain release factor subunit 1, putative	1.1634	0.0039	GO:0006449	Regulation of translational termination
PFB0645c	Ribosomal protein L13, putative	1.5862	0.0000	GO:0006412	Translation
PFC0701w	Hypothetical protein	0.7918	0.0118	GO:0006412	Translation
PFC0870w	Elongation factor 1 (EF-1), putative	1.1948	0.0006	GO:0006414	Translational elongation
PFD1070w	Eukaryotic initiation factor, putative	0.9144	0.0071	GO:0006446	Regulation of translational initiation
PFE0960w	50S ribosomal subunit protein L14, putative	-0.9873	0.0053	GO:0006412	Translation
PFE1005w	40S ribosomal subunit protein S9, putative	1.1366	0.0017	GO:0006412	Translation
PFF0345w	Translation initiation factor IF-2, putative	0.8125	0.0154	GO:0006413	Translational initiation
PFF0885w	60S ribosomal protein l27a, putative	1.1223	0.0026	GO:0006412	Translation
PFI0625c	Hypothetical protein	0.8439	0.0119	GO:0006446	Regulation of translational initiation
PFI1645c	Hypothetical protein	0.9871	0.0108	GO:0006418	Trna aminullacylation for protein translation
PFL1895w	Ribosomal protein L23, putative	0.9645	0.0033	GO:0006412	Translation
Transport					
MAL13P1.163	Er lumen protein retaining receptor 1, putative	-1.1615	0.0019	GO:0006886	Intracellular protein transport
MAL13P1.241	Gtpase, putative	-0.9160	0.0109	GO:0015031	Protein transport
MAL13P1.51	Rab5B protein	-1.9439	0.0000	GO:0015031	Protein transport
PF07_0070	Transporter/permease protein, putative	1.0789	0.0004	GO:0006810	Transport
PF08_0036	Transport protein	-1.2442	0.0007	GO:0006888	ER to Golgi vesicle-mediated transport
PF08_0087	Importin alpha, putative	0.9459	0.0016	GO:0006886	Intracellular protein transport
PF08_0093	Hypothetical protein	-0.9257	0.0261	GO:0006810	Transport
PF08_0110	Rab18 gtpase, putative	0.8238	0.0269	GO:0006886	Intracellular protein transport
PF10_0051	ADP/ATP carrier protein, putative	-1.0662	0.0012	GO:0006810	Transport
PF10_0337	ADP-ribosylation factor-like protein	-1.0050	0.0160	GO:0006886	Intracellular protein transport
PF10_0366	ADP/ATP transporter on adenylate translocase	0.8155	0.0088	GO:0006810	Transport
PF11_0141	UDP-galactose transporter, putative	-1.1842	0.0007	GO:0015785	UDP-galactose transport
PF11_0461	Rab6	-0.9629	0.0030	GO:0006886	Intracellular protein transport
PF13_0019	Sodium/hydrogen exchanger, putative	-0.9831	0.0021	GO:0006814	Rsodium ion transport
PF13_0271	ABC transporter, putative	-1.3172	0.0002	GO:0006810	Transport
PF13_0350	Signal recognition particle receptor alpha subunit, putative	0.8979	0.0056	GO:0006886	Intracellular protein transport
PF14_0277	Coatamer protein, beta subunit, putative	-0.9689	0.0046	GO:0006605	Protein targeting

PF14_0321	ABC transporter, putative	0.8238	0.0039	GO:0006810	Transport
PF14_0455	Multidrug resistance protein 2	1.1427	0.0050	GO:0006810	Transport
PF14_0678	Exported protein 2	0.9600	0.0026	GO:0008150	Biological process
PF14_0679	Sulfate transporter, putative	-1.4787	0.0022	GO:0008272	Sulfate transport
PFA0310	Calcium-transporting atpase	-0.9104	0.0024		Null
PFA0590w	ABC transporter, putative	0.8998	0.0060	GO:0006810	Transport
PFD0895	Bet3 transport protein, putative	-0.7739	0.0294		Null
PFD0930w	CGI-141 protein homolog, putative	-0.9083	0.0141	GO:0016192	Vesicle-mediated transport
PFE1455w	Sugar transporter, putative	-1.1134	0.0010	GO:0008643	Carbohydrate transport
PFF0450c	Transporter protein, putative	-1.1708	0.0033	GO:0006810	Transport
PFI0255c	Mitochondrial carrier protein, putative	0.9723	0.0038	GO:0006810	Transport
PFI0955	Sugar transporter, putative	-0.7820	0.0158		Null
PFL0110c	Pfmpc	-1.1926	0.0005	GO:0006810	Transport
PFL2000w	Mitochondrial carrier protein, putative	0.9334	0.0124	GO:0006810	Transport
PFL2065	Mitochondrial import inner membrane translocase subunit, putative	0.9068	0.0097		Null
PFL2425w	Adaptor-related protein complex 3, sigma 2 subunit, putative	-0.7973	0.0113	GO:0006886	Intracellular protein transport

APPENDIX 2

Unique transcripts specific to the A51B1C1_1 treatment after comparison with other reported perturbations

PlasmoDB ID	PlasmoDB Process Description
PFE0880c	Actin Cytoskeleton Organization
PF07_0138	Antigenic Variation
PF08_0104	Antigenic Variation
PF10_0003	Antigenic Variation
PFB0035c	Antigenic Variation
PFF1545w	Antigenic Variation
MAL7P1.50	Antigenic Variation
MAL13P1.251	Arginyl-Trna Aminoacylation
MAL13P1.246	ATP Biosynthetic Process
PFD0955w	Attachment Of GPI Anchor To Protein
PF10_0061	Base-Excision Repair
PF14_0783	Carbohydrate Metabolic Process
PF14_0251	Cell Redox Homeostasis
PFD1105w	Cell-Cell Adhesion
PF11_0410	Chromatin Modification
PF11_0326	Cytolysis, Pathogenesis
PF10_0225	De Novo' Pyrimidine Base Biosynthetic Process
PF11_0383	DNA-Dependent DNA Replication
PFB0580w	Drug Transmembrane Transport
PFB0680w	Entry Into Host
MAL13P1.326	Heme Biosynthetic Process
PF14_0034	Intracellular Protein Transmembrane Transport
PF10_0216	Ion Transport, Transport, Zinc Ion Transport
MAL13P1.307	Iron-Sulfur Cluster Assembly
PF14_0534	L-Serine Metabolic Process, Glycine Metabolic Process
PF11_0190	Metabolic Process
MAL7P1.161	Microtubule-Based Movement
PF10_0250	Microtubule-Based Movement
MAL13P1.64	Modification-Dependent Protein Catabolic Process
MAL13P1.1	Pathogenesis
PF14_0773	Pathogenesis
PFA0175w	Phosphate Transport
PF11_0340	Potassium Ion Transport
MAL13P1.297	Protein Amino Acid ADP-Ribosylation, Small Gtpase Mediated Signal Transduction
PF08_0129	Protein Amino Acid Dephosphorylation
PF14_0224	Protein Amino Acid Dephosphorylation
PFI0960w	Protein Amino Acid N-Linked Glycosylation Via Asparagine
MAL13P1.114	Protein Amino Acid Phosphorylation
MAL13P1.185	Protein Amino Acid Phosphorylation
PF10_0141	Protein Amino Acid Phosphorylation, Regulation Of Cell Cycle
PF11_0177	Protein Deneddylation, Protein Deubiquitination, Ubiquitin-Dependent Protein Catabolic Process
PF13_0180	Protein Folding

PF13_0358	Protein Import Into Mitochondrial Inner Membrane, Protein Targeting To Mitochondrion
PF10_0094	Protein Modification Process
PFF0810c	Protein Transport, Small Gtpase Mediated Signal Transduction
PF11_0226	Proteolysis
PF14_0281	Proteolysis
PFE0305w	Regulation Of Transcription, DNA-Dependent, Transcription From RNA Polymerase II Promoter, Transcription Initiation From RNA Polymerase II Promoter
PFE0670w	Regulation Of Transcription, DNA-Dependent, Transcription From RNA Polymerase II Promoter, Transcription Initiation From RNA Polymerase II Promoter
PFA0505c	Regulation Of Transcription, Transcription From RNA Polymerase II Promoter
PF13_0015	Response To Heat, Response To Unfolded Protein
PFD0565c	RNA Metabolic Process
PFD0700c	RNA Metabolic Process
MAL7P1.69	Signal Transduction
PFD0325w	Transcription
MAL13P1.272	Translation
PF13_0021	Translation
PFB0467w	Translation
PFB0545c	Translation
PFC0701w	Translation
PFE1005w	Translation
PFL1895w	Translation
MAL8P1.27	Translational Initiation
PF08_0093	Transport
PFA0720w	Transport
PFL2000w	Transport
MAL7P1.130	Ubiquinone Biosynthetic Process

APPENDIX 3

The non-homologues clustering of *Arabidopsis* treated with Galvestine-2 and *P. falciparum* treated with A51B1C1_1, using COCO

Description for *P. falciparum*	**PlasmoDB ID**	***Arabidopsis* ID**
Cluster 1		
BRIX protein, putative	PF07_0122	AT1G52930
Conserved *Plasmodium* protein, unknown function	PF14_0634	AT4G31850
Conserved *Plasmodium falciparum* protein family	PFD0075w	AT1G49670
tRNA pseudouridine synthase, putative	PFE0815w	AT3G06950
Pseudouridylate synthase, putative	PFI0685w	AT5G51140
Cytidine/deoxycytidylate deaminase, putative	PFL0230w	AT5G24670
Small subunit rrna processing factor, putative	PFL1230w	AT3G57000
Cluster 2		
Cysteine desulfurase, putative	MAL7P1.150	AT5G65720
60S ribosomal subunit export protein, putative	PF07_0121	AT2G03820
Nucleolar preribosomal assembly protein, putative	PF08_0065	AT2G19540
Conserved *Plasmodium* protein, unknown function	PF10_0179	AT2G30000
Methyltransferase, putative	PF10_0274	AT1G36310
Cluster 3		
Dnaj protein, putative	MAL13P1.277	AT2G22360
Conserved *Plasmodium* protein, unknown function	MAL8P1.107	AT3G24506
Diphthine synthase	PF10_0087	AT4G31790
RNA methyltransferase, putative	PF10_0300	AT4G15520
60S ribosomal protein P0	PF11_0313	AT3G11250
Glycine cleavage H protein	PF11_0339	AT2G35120
Conserved *Plasmodium* protein, unknown function	PF11_0347	AT5G38840
Conserved *Plasmodium* protein, unknown function	PF13_0055	AT4G33240
Small subunit rrna processing factor, putative	PF14_0494	AT1G42440
Dihydroorotase, putative	PF14_0697	AT4G22930
CGI-201 protein, short form	PFD0180c	AT5G41770
40S ribosomal processing protein, putative	PFD0455w	AT4G28450
Conserved *Plasmodium* protein, unknown function	PFE1145w	AT1G21570
RNA helicase 1	PFE1390w	AT5G51280
Nucleolar preribosomal gtpase, putative	PFE1435c	AT3G07050
Conserved *Plasmodium* protein, unknown function	PFL0675c	AT2G34970
Cluster 4		
Conserved *Plasmodium* protein, unknown function	MAL13P1.150	AT2G20940
Clp1-related protein, putative	PF08_0040	AT3G04680
Small subunit rrna processing stabilizing factor, putative	PF10_0266	AT5G66540
Conserved *Plasmodium* protein, unknown function	PF11_0269	AT4G14240
Leucine-rich repeat protein	PF14_0496	AT5G22320
Conserved protein, unknown function	PFL1290w	PFL1290w
Microtubule associated katanin, putative	PFL2105c	AT5G14530

Cluster 5		
DNA/RNA-binding protein Alba, putative	MAL13P1.233	AT1G20220
RNA binding protein, putative	PF10_0047	AT3G49430
Cysteine proteinase falcipain 1	PF14_0553	AT1G09850
Plasmodium exported protein (hyp15), unknown function	PFB0953w	AT5G26850
Transporter, putative	PFC0530w	AT1G68790
Plasmodium exported protein (phistc), unknown function	PFL0045c	AT5G55660
Cluster 6		
60S ribosomal protein L3, putative	PF10_0272	AT1G43170
Elongation factor 1-gamma, putative	PF13_0214	AT1G09640
Plasmepsin II	PF14_0077	AT1G11910
Cluster 7		
Glideosome associated protein with multiple membrane spans 3, putative	PF14_0065	AT2G32040
Rhoptry-associated protein 2	PFE0080c	AT5G65410
Cluster 8		
Eukaryotic translation initation factor 4 gamma, putative	MAL13P1.63	AT3G60240
Casein kinase II beta chain	PF11_0048	AT4G17640
Translation elongation factor EF-1, subunit alpha, putative	PF11_0245	AT1G18070
Coproporphyrinogen III oxidase	PF11_0436	AT1G03475
Glutamate--trna ligase, putative	PF13_0257	AT5G26710
Eukaryotic translation initiation factor 2 gamma subunit, putative	PF14_0104	AT1G04170
U2 snrnp spliceosome subunit, putative	PFC0375c	AT5G64270
Beta adaptin protein, putative	PFE1400c	AT4G11380
Eukaryotic translation initiation factor 3 subunit 10, putative	PFL0625c	AT4G11420
Cluster 9		
40S ribosomal protein S6, putative	PF13_0228	AT5G10360
60S ribosomal protein L1, putative	PF14_0391	AT2G27530
40S ribosomal protein S3A, putative	PFC1020c	AT4G34670
40S ribosomal protein S14, putative	PFE0810c	AT3G11510
Cluster 10		
Zinc finger protein, putative	PF08_0056	AT4G12040
Phenylalanyl-trna synthetase beta chain, putative	PF11_0051	AT1G72550
Box C/D snornp rrna 2'-O-methylation factor, putative	PF11_0191	AT1G16920
60S ribosomal protein L6, putative	PF13_0129	AT4G10450
Glutaminyl-trna synthetase, putative	PF13_0170	AT1G25350
Glycine-trna ligase, putative	PF14_0198	AT1G29880
RNA binding protein, putative	PFB0370c	AT5G08420
Activator of Hsp90 atpase, putative	PFC0360w	AT3G12050
U6 snrna-associated sm-like protein lsm2, putative	PFE1020w	AT1G03330
Eukaryotic translation initiation factor 3 subunit 5, putative	PFI0895c	AT2G39990

Cluster 11		
60S ribosomal protein L18-2, putative	MAL13P1.209	AT5G27850
60S ribosomal protein L13, putative	PF10_0043	AT3G24830
60S ribosomal protein L30e, putative	PF10_0187	AT3G18740
40S ribosomal protein S2B, putative	PF10_0264	AT1G72370
60S ribosomal protein L10, putative	PF14_0141	AT1G66580
60S ribosomal protein L21e, putative	PF14_0240	AT1G09590
Helicase 45	PF14_0655	AT3G13920
60S ribosomal protein L31, putative	PFE0185c	AT5G56710
Ribose 5-phosphate epimerase, putative	PFE0730c	AT3G04790
Cluster 12		
Picoplast ribosomal protein L36e precursor, putative	PF11_0106	AT2G37600
Small nuclear ribonucleoprotein D1, putative	PF11_0266	AT4G02840
Aspartyl-trna synthetase	PFA0145c	AT4G26870
Plasmodium exported protein (hyp9), unknown function	PFB0930w	AT4G02500
Eukaryotic translation initiation factor, putative	PFE0885w	AT5G25780
Karyopherin beta	PFE1195w	AT5G19820
Small nuclear ribonucleoprotein (snrnp), putative	PFI0475w	AT1G76300
RNA polymerase subunit 8c, putative	PFL0665c	AT1G54250
Cytoplasmic translation machinery associated protein, putative	PFL2150c	AT2G20280
Cluster 13		
SNARE protein, putative	MAL8P1.21	AT5G22360
Conserved *Plasmodium* protein, unknown function	PF08_0124	AT1G03910
Mitochondrial protein import protein TIM13, putative	PF14_0208	AT1G61570
Protein phosphatase, putative	PF14_0524	AT3G06110
ATP-dependent protease la, putative	PF14_0616	AT5G53170
Histone S-adenosyl methyltransferase, putative	PFL1345c	AT5G50320
Cluster 14		
Gamete antigen 27/25	PF13_0011	AT5G22340
Na	PF14_0182	AT5G57800
Macrophage migration inhibitory factor	PFL1420w	AT5G01650
Cluster 15		
Signal peptidase 21 kda subunit	MAL13P1.167	AT3G15710
Protein kinase 5	MAL13P1.279	AT3G48750
Conserved membrane protein, unknown function	PF07_0078	AT1G54320
Conserved *Plasmodium* protein, unknown function	PF07_0087	AT1G70980
Centrin-4	PF11_0066	AT3G50360
Dihydrolipamide succinyltransferase component of 2-oxoglutarate dehydrogenase complex	PF13_0121	AT4G26910
Centrin-1	PFA0345w	AT3G50360
Cluster 16		
Plasmodium exported protein, unknown function	PF13_0275	AT5G46910
Serine/threonine protein kinase, FIKK family	PFD1175w	AT2G04620
Plasmodium exported protein (PHISTb), unknown function	PFI1770w	AT3G27470

Cluster 17		
Histone-arginine methyltransferase, putative	PF08_0092	AT2G19670
RNA methyltransferase, putative	PF11_0305	AT4G26600
U3 snoRNA-associated small subunit rRNA processing protein, putative	PF13_0309	AT4G04940
Conserved *Plasmodium* protein, unknown function	PF14_0707	AT5G37890
Serine/threonine protein kinase, putative	PFC0105w	AT3G44850
Ribosomal RNA methyltransferase, putative	PFI0415c	AT5G01230
Serine/threonine protein kinase, FIKK family	PFL0040c	AT2G46700
Cluster 18		
Ferredoxin, putative	MAL13P1.95	AT1G10960
Fe-superoxide dismutase	PF08_0071	AT4G25100
Organelle ribosomal protein L28 precursor, putative	PFE0145w	AT2G33450
Heat shock protein 70	PFI0875w	AT5G28540
Cluster 19		
RNA-binding protein s1, putative	PF11_0320	AT5G43960
Dihydrofolate synthase/folylpolyglutamate synthase	PF13_0140	AT3G55630
Proteasome subunit beta type 7 precursor, putative	PF13_0156	AT5G40580
ER lumen protein retaining receptor	PF13_0280	AT3G25040
Peptide chain release factor 1, putative	PF14_0265	AT3G62910
Histone H2A variant, putative	PFC0920w	AT3G54560
Leucine-rich repeat protein	PFL2380c	AT1G10510
Cluster 20		
Conserved *Plasmodium* protein, unknown function	PF14_0101	AT3G29075
Non-canonical ubiquitin conjugating enzyme, putative	PF14_0128	AT1G45050
Ferlin, putative	PF14_0530	AT1G30270
Serine/threonine protein kinase, FIKK family	PFE0045c	AT1G59580
Cluster 21		
Large ribosomal subunit processing protein, putative	MAL7P1.24	AT5G06360
N-acetyltransferase, putative	PF10_0036	AT5G13780
Eukaryotic translation initiation factor 3 subunit 7, putative	PF10_0077	AT5G44320
Peptidase, putative	PF11_0203	AT2G29080
60S ribosomal protein l23a, putative	PF13_0132	AT3G55280
6-phosphofructokinase	PFI0755c	AT4G04040
Eukaryotic translation initiation factor 3 subunit 8, putative	PFL0310c	AT3G56150
Cluster 22		
Conserved *Plasmodium* protein, unknown function	MAL8P1.64	AT5G23880
Stevor	PF14_0007	AT3G16810
Conserved *Plasmodium* protein, unknown function	PFC0885c	AT2G19385
Triose or hexose phosphate/phosphate translocator, putative	PFL0890c	AT1G12500

Cluster 23		
Conserved *Plasmodium* protein, unknown function	MAL13P1.15	AT4G00630
DNA helicase, putative	MAL8P1.65	AT3G57300
RNA binding protein, putative	PF10_0028	AT1G07350
Exonuclease, putative	PF11_0074	AT1G54490
Conserved *Plasmodium* protein, unknown function	PF11_0440	AT5G55310
Dnaj protein, putative	PF13_0036	AT1G65280
ATP-dependent RNA helicase, putative	PFC0915w	AT4G00660
Topoisomerase I	PFE0520c	AT5G55310
Cluster 24		
Dolichyl-phosphate-mannose protein mannosyltransferase, putative	PF10_0104	AT2G25110
NOT family protein, putative	PF11_0049	AT4G24550
NOT family protein, putative	PF14_0170	AT1G02080
Stromal-processing peptidase, putative	PF14_0382	AT5G42390
Signal peptide peptidase	PF14_0543	AT2G03120
Histone deacetylase	PFI1260c	AT4G38130
Hydrolase/phosphatase, putative	PFL1260w	AT2G25870
Cluster 25		
U2 snRNA/tRNA pseudouridine synthase, putative	PF08_0123	AT1G76120
Orotidine monophosphate decarboxylase	PF10_0225	AT1G77600
Conserved *Plasmodium* protein, unknown function	PF11_0469	AT1G67690
Polynucleotide kinase, putative	PF13_0334	AT3G14890
Conserved *Plasmodium* protein, unknown function	PF14_0291	AT1G50180
DEAD box ATP-dependent RNA helicase, putative	PFD0565c	AT5G63630
Cluster 26		
Secreted ookinete protein, putative	MAL13P1.203	AT1G42440
Mitotic control protein dis3 homologue, putative	MAL13P1.289	AT2G17510
Conserved *Plasmodium* protein, unknown function	MAL7P1.134	AT1G73960
Conserved *Plasmodium* protein, unknown function	MAL8P1.100	AT4G30825
RNA-binding protein (U1 snRNP-like), putative	PF08_0084	AT4G03120
Conserved *Plasmodium* protein, unknown function	PF10_0129	AT2G21440
Pre-mRNA splicing factor, putative	PF11_0336	AT2G40650
Conserved *Plasmodium* protein, unknown function	PF11_0406	AT1G20570
Mitochondrial ribosomal protein S15 precursor, putative	PF13_0059	AT1G15810
Nonsense-mediated mRNA decay protein Upf3, putative	PF13_0158	AT1G33980
Pre-mRNA splicing factor, putative	PF14_0070	AT5G37370
Conserved *Plasmodium* protein, unknown function	PF14_0713	AT1G14650
Stevor	PF14_0767	AT3G26300
Conserved *Plasmodium* protein, unknown function	PFE0100w	AT2G05170
Conserved *Plasmodium* protein, unknown function	PFE0550w	AT1G15910
Conserved *Plasmodium* protein, unknown function	PFE1040c	AT3G22590

Cluster 27		
U3 small nucleolar ribonucleoprotein protein, putative	PF08_0055	AT1G63780
Conserved *Plasmodium* protein, unknown function	PF10_0180	AT3G23980
Plasmodium exported protein, unknown function	PF13_0076	AT1G77800
Conserved *Plasmodium* protein, unknown function	PF13_0270	AT1G03080
Lysophospholipase, putative	PF14_0017	AT1G18360
Conserved *Plasmodium* protein, unknown function	PF14_0621	AT5G17880
Lipid/sterol:H symporter	PFA0375c	AT4G38350
Conserved *Plasmodium* membrane protein, unknown function	PFB0675w	AT2G43420
DNA-directed RNA polymerase III subunit, putative	PFL0330c	AT5G45140
Nucleolar rRNA processing protein, putative	PFL2295w	AT3G60360
Cluster 28		
Methionine aminopeptidase 1b, putative	PF10_0150	AT2G45240
SNO glutamine amidotransferase family protein	PF11_0169	AT5G60540
Cytidine triphosphate synthetase	PF14_0100	AT1G30820
Small subunit rrna dimethylase, putative	PF14_0156	AT2G47420
Glucose-6-phosphate isomerase	PF14_0341	AT5G42740
Mitochondrial ribosomal protein S4/S9 precursor, putative	PF14_0584	AT5G15750
Conserved *Plasmodium* protein, unknown function	PFD0905w	AT5G41190
Cluster 29		
Lsm3 homologue, putative	PF08_0049	AT1G76860
Phosphatase, putative	PF14_0036	AT2G27190
Structure specific recognition protein, putative	PF14_0393	AT3G28730
ABC transporter, (CT family), putative	PFA0590w	AT2G34660
Sexual stage-specific protein precursor	PFD0310w	AT3G43540
Actin-like protein, putative	PFE0255w	AT1G18450
M18 aspartyl aminopeptidase	PFI1570c	AT5G60160
Splicing factor 3b, subunit 3, 130kd, putative	PFL1680w	AT3G55200
Cluster 30		
Endomembrane protein 70, putative	PF10_0208	AT3G13772
Clathrin assembly protein AP19, putative	PF11_0187	AT2G17380
Lsm4 homologue, putative	PF11_0524	AT5G27720
SNARE protein	PFC0890w	AT1G11890
Bet3 transport protein, putative	PFD0895c	AT5G54750
Transcriptional regulator, putative	PFE0870w	AT4G10710
Dynein light chain 1, putative	PFL0660w	AT4G15930

Cluster 31		
Conserved *Plasmodium* protein, unknown function	MAL7P1.157	AT1G13220
Inositol phosphatase, putative	MAL8P1.151	AT1G17340
Cg3 protein	PF07_0034	AT3G08950
Mitochondrial ribosomal protein L22/L43, putative	PF10_0097	AT3G59650
Transcription factor with AP2 domain(s), putative	PF14_0471	AT4G09630
ERCC1 nucleotide excision repair protein, putative	PFB0160w	AT3G05210
Conserved *Plasmodium* protein, unknown function	PFB0250w	AT4G33920
Serine repeat antigen 2	PFB0355c	AT3G19400
Phospholipase A2, putative	PFB0410c	AT1G61850
Tubulin-tyrosine ligase, putative	PFE0700c	AT1G77550
S-adenosyl-methyltransferase, putative	PFL1775c	AT5G10910
Conserved *Plasmodium* membrane protein, unknown function	PFL2170c	AT2G35330
Cluster 32		
Acyl coa:diacylglycerol acyltransferase, putative	MAL13P1.285	AT1G61850
Lysophospholipase, putative	PF07_0040	AT1G18360
Conserved *Plasmodium* membrane protein, unknown function	PFC0995c	AT2G19450
Patatin-like phospholipase, putative	PFI1560c	AT4G33700
Cluster 33		
Ubiquitin transferase, putative	MAL7P1.19	AT5G02880
Cysteine desulfurase, putative	PF07_0068	AT1G08490
Conserved *Plasmodium* protein, unknown function	PF11_0089	AT3G25840
Conserved protein, unknown function	PF14_0054	AT4G32600
Pantothenate kinase, putative	PF14_0200	AT4G32180
Dynein-associated protein, putative	PF14_0202	AT1G13120
Conserved *Plasmodium* membrane protein, unknown function	PF14_0596	AT5G13560
Stevor	PFB0955w	AT5G16780
ATP-dependent RNA helicase, putative	PFC0955w	AT1G55150
Conserved *Plasmodium* protein, unknown function	PFD0605c	AT4G28760
Plasmodium exported protein (hyp6), unknown function	PFD1200c	AT2G29140
Cell differentiation protein rcd1, putative	PFE0375w	AT3G20800
Plasmodium exported protein (phistb), unknown function	PFI0130c	AT1G13450
Gtpase activator, putative	PFI0345w	AT5G15930
Sec-1 family protein	PFI1700c	AT3G54860
Conserved *Plasmodium* protein, unknown function	PFL1445w	AT4G13730
Cluster 34		
Serine/threonine protein kinase, putative	MAL13P1.196	AT3G63330
Conserved *Plasmodium* protein, unknown function	PF11_0064	AT1G10240
ATP-dependent Clp protease, putative	PF14_0063	AT2G25140
Conserved *Plasmodium* protein, unknown function	PF14_0347	AT4G23920
Syntaxin, Qa-SNARE family	PFL2070w	AT5G26980

APPENDIX 4

The Plasmodial proteins found in only the A51B1C1_1 treated samples analysed with MS

PlasmoDB ID	Annotated Go Process	GO terms	Cluster
PF11_0465	Microtubule-Based Process	GO:0007017	Biological Process
PF14_0615	Vacuolar Acidification	GO:0007035	Biological Process
PF13_0221	Multicellular Organismal Development	GO:0007275	Biological Process
PF10_0186	Biological Process	GO:0008150	Biological Process
PF10_0287	Biological Process	GO:0008150	Biological Process
PF10_0323	Biological Process	GO:0008150	Biological Process
PF10_0371	Biological Process	GO:0008150	Biological Process
PF11_0092	Biological Process	GO:0008150	Biological Process
PF11_0185	Biological Process	GO:0008150	Biological Process
PF11_0213	Biological Process	GO:0008150	Biological Process
PF11_0218	Biological Process	GO:0008150	Biological Process
PF11_0319	Biological Process	GO:0008150	Biological Process
PF11_0324	Biological Process	GO:0008150	Biological Process
PF11_0503	Biological Process	GO:0008150	Biological Process
PFL1345c	Biological Process	GO:0008150	Biological Process
PFL1415w	Biological Process	GO:0008150	Biological Process
PF14_0262	Biological Process	GO:0008150	Biological Process
PF14_0318	Biological Process	GO:0008150	Biological Process
PF14_0342	Biological Process	GO:0008150	Biological Process
PF14_0372	Biological Process	GO:0008150	Biological Process
PF14_0437	Biological Process	GO:0008150	Biological Process
PF14_0495	Biological Process	GO:0008150	Biological Process
PF14_0563	Biological Process	GO:0008150	Biological Process
PF14_0564	Biological Process	GO:0008150	Biological Process
PF14_0668	Biological Process	GO:0008150	Biological Process
PFA0180w	Null		Biological Process
PFB0375w	Embryonic Development, Keratinocyte Differentiation		Biological Process
PFD0900w	Cell Cycle		Biological Process
PF10_0158	Regulation Of Gtpase Activity		Biological Process
PF13_0210	Endocytosis		Biological Process
MAL13P1.258	Carbohydrate Metabolic Process		Biological Process
PF08_0126	Double-Strand Break Repair Via Homologous Recombination	GO:0000724	DNA Metabolism
PF10_0123	Purine Nucleotide Biosynthetic Process	GO:0006164	DNA Metabolism
PF13_0287	Purine Nucleotide Biosynthetic Process	GO:0006164	DNA Metabolism
PFD0590c	DNA Replication	GO:0006260	DNA Metabolism
PF10_0362	DNA Replication	GO:0006260	DNA Metabolism
PFF1470c	DNA-Dependent DNA Replication	GO:0006261	DNA Metabolism
PFD0790c	DNA Replication Initiation	GO:0006270	DNA Metabolism
PFL0150w	DNA Replication Initiation	GO:0006270	DNA Metabolism
PF13_0080	RNA-Dependent DNA Replication	GO:0006278	DNA Metabolism
PFE0675c	DNA Repair	GO:0006281	DNA Metabolism

PFB0730w	DNA Packaging	GO:0006323	DNA Metabolism
PFE0420c	DNA Packaging	GO:0006323	DNA Metabolism
PF11_0418	Chromatin Assembly Or Disassembly	GO:0006333	DNA Metabolism
PFE0450w	Chromosome Organization And Biogenesis	GO:0051276	DNA Metabolism
PFB0405w	Pathogenesis	GO:0009405	Host Parasite Interaction
MAL7P1.212	Pathogenesis	GO:0009405	Host Parasite Interaction
PFA0765c	Rosetting	GO:0020013	Host Parasite Interaction
PFD0020c	Rosetting	GO:0020013	Host Parasite Interaction
PFD0625c	Rosetting	GO:0020013	Host Parasite Interaction
PFD1005c	Rosetting	GO:0020013	Host Parasite Interaction
PFF0010w	Rosetting	GO:0020013	Host Parasite Interaction
MAL7P1.56	Rosetting	GO:0020013	Host Parasite Interaction
MAL7P1.187	Rosetting	GO:0020013	Host Parasite Interaction
PF11_0007	Rosetting	GO:0020013	Host Parasite Interaction
PFL0020w	Rosetting	GO:0020013	Host Parasite Interaction
PF10_0268	Entry Into Host Cell	GO:0030260	Host Parasite Interaction
PFI1180w	Lipid Metabolic Process	GO:0006629	Lipid Metabolism
PF07_0040	Phospholipid Metabolic Process	GO:0006644	Lipid Metabolism
PF11_0257	Phosphatidylethanolamine Biosynthetic Process	GO:0006646	Lipid Metabolism
PFB0150c	Protein Amino Acid Phosphorylation	GO:0006468	Phosphorylation
PFB0520w	Protein Amino Acid Phosphorylation	GO:0006468	Phosphorylation
PFB0665w	Protein Amino Acid Phosphorylation	GO:0006468	Phosphorylation
MAL7P1.127	Protein Amino Acid Phosphorylation	GO:0006468	Phosphorylation
PF10_0160	Protein Amino Acid Phosphorylation	GO:0006468	Phosphorylation
PF11_0060	Protein Amino Acid Phosphorylation	GO:0006468	Phosphorylation
PF11_0079	Protein Amino Acid Phosphorylation	GO:0006468	Phosphorylation
PF11_0242	Protein Amino Acid Phosphorylation	GO:0006468	Phosphorylation
PF11_0464	Protein Amino Acid Phosphorylation	GO:0006468	Phosphorylation
PFL1110c	Protein Amino Acid Phosphorylation	GO:0006468	Phosphorylation
MAL13P1.278	Protein Amino Acid Phosphorylation	GO:0006468	Phosphorylation
PF14_0294	Protein Amino Acid Phosphorylation	GO:0006468	Phosphorylation
PF14_0320	Protein Amino Acid Phosphorylation	GO:0006468	Phosphorylation
PF14_0516	Protein Amino Acid Phosphorylation	GO:0006468	Phosphorylation
PF14_0214	Protein Amino Acid Phosphorylation		Phosphorylation
PF07_0047	Regulation Of Progression Through Cell Cycle	GO:0000074	Primary Metabolism
MAL8P1.156	Carbohydrate Metabolic Process	GO:0005975	Primary Metabolism
PFF1350c	Generation Of Precursor Metabolites And Energy	GO:0006091	Primary Metabolism
PF11_0294	Glycolysis	GO:0006096	Primary Metabolism
PFF0945c	Glyoxylate Cycle	GO:0006097	Primary Metabolism
PFF0530w	Pentose-Phosphate Shunt	GO:0006098	Primary Metabolism

PF13_0242	Isocitrate Metabolic Process	GO:0006102	Primary Metabolism
PF11_0395	Cgmp Biosynthetic Process	GO:0006182	Primary Metabolism
PFF0275c	GTP Biosynthetic Process	GO:0006183	Primary Metabolism
PF14_0334	Glutamate Biosynthetic Process	GO:0006537	Primary Metabolism
PF14_0421	Metabolic Process	GO:0008152	Primary Metabolism
PF11_0327	Steroid Metabolic Process	GO:0008202	Primary Metabolism
PFL0780w	Glycerol-3-Phosphate Catabolic Process	GO:0046168	Primary Metabolism
PFB0595w	Response To Unfolded Protein	GO:0006986	Protein Folding
PFF1415c	Response To Unfolded Protein	GO:0006986	Protein Folding
PF13_0021	Response To Unfolded Protein	GO:0006986	Protein Folding
PFF1050w	Cotranslational Protein Folding	GO:0051083	Protein Folding
PF13_0180	Protein Folding	GO:0006457	Proteolysis
PF11_0142	Protein Modification Process	GO:0006464	Proteolysis
MAL13P1.310	Proteolysis	GO:0006508	Proteolysis
PF14_0692	Proteolysis	GO:0006508	Proteolysis
PFA0220w	Ubiquitin-Dependent Protein Catabolic Process	GO:0006511	Proteolysis
PFE0915c	Ubiquitin-Dependent Protein Catabolic Process	GO:0006511	Proteolysis
MAL8P1.128	Ubiquitin-Dependent Protein Catabolic Process	GO:0006511	Proteolysis
PF10_0111	Ubiquitin-Dependent Protein Catabolic Process	GO:0006511	Proteolysis
PF13_0182	Ubiquitin Cycle	GO:0006512	Proteolysis
PF10_0081	Protein Catabolic Process	GO:0030163	Proteolysis
PFL1925w	Protein Catabolic Process	GO:0030163	Proteolysis
PFD0680c	Ubiquitin-Dependent Protein Catabolic Process		Proteolysis
MAL7P1.77	Proteolysis, Transcription, RNA-Dependent		Proteolysis
PF11_0189	Proteolysis		Proteolysis
PF14_0068	Rrna Processing	GO:0006364	RNA Metabolic Process
PFF0745c	RNA Processing	GO:0006396	RNA Metabolic Process
MAL13P1.120	Mrna Processing	GO:0006397	RNA Metabolic Process
PF14_0146	RNA Splicing	GO:0008380	RNA Metabolic Process
PFA0330w	Ribosome Biogenesis		RNA Metabolic Process
PFD0090c	Rrna Processing, Ribosome Biogenesis		RNA Metabolic Process
PFE0860c	Transcription		RNA Metabolic Process
PF10_0057	Nuclear-Transcribed Mrna Catabolic Process, Nonsense-Mediated Decay		RNA Metabolic Process
PF10_0179	Trna Processing		RNA Metabolic Process
PFL1010c	Regulation Of Transcription, DNA-Dependent, Transcription		RNA Metabolic Process
PFL1190c	Transcription, DNA-Dependent		RNA Metabolic Process
PFL1900w	Regulation Of Transcription, Regulation Of Transcription, DNA-Dependent		RNA Metabolic Process
PF13_0088	Regulation Of Transcription		RNA Metabolic Process
PF13_0235	Regulation Of Transcription, DNA-Dependent		RNA Metabolic Process
PF14_0059	Regulation Of Transcription From RNA		RNA Metabolic

	Polymerase II Promoter, Transcription		Process
MAL7P1.122	Signal Transduction	GO:0007165	Signal Transduction
PFE0690c	Small Gtpase Mediated Signal Transduction	GO:0007264	Signal Transduction
PFA0515w	Phosphoinositide-Mediated Signaling	GO:0048015	Signal Transduction
PF11_0302	Signal Transduction		Signal Transduction
PFC0300c	Translation	GO:0006412	Translation
PFE0845c	Translation	GO:0006412	Translation
PF13_0213	Translation	GO:0006412	Translation
PFE0830c	Translational Initiation	GO:0006413	Translation
PFF0345w	Translational Initiation	GO:0006413	Translation
PF07_0117	Translational Initiation	GO:0006413	Translation
PF08_0018	Translational Initiation	GO:0006413	Translation
PF10_0103	Translational Initiation	GO:0006413	Translation
MAL13P1.351	Translational Elongation	GO:0006414	Translation
MAL8P1.40	Regulation Of Translation	GO:0006417	Translation
PF14_0401	Trna Aminoacylation For Protein Translation	GO:0006418	Translation
PFB0525w	Asparaginyl-Trna Aminoacylation	GO:0006421	Translation
PF13_0170	Glutamyl-Trna Aminoacylation	GO:0006424	Translation
PF07_0073	Seryl-Trna Aminoacylation	GO:0006434	Translation
PFD0525w	Regulation Of Translation		Translation
MAL7P1.17	Translation, Translational Initiation		Translation
PF13_0139	Translation, Translational Initiation		Translation
MAL13P1.156	Translational Initiation		Translation
PF07_0085	Electron Transport	GO:0006118	Transport
PFI0255c	Transport	GO:0006810	Transport
PF11_0466	Transport	GO:0006810	Transport
PFL1410c	Transport	GO:0006810	Transport
PF14_0622	Potassium Ion Transport	GO:0006813	Transport
PFF0825c	Anion Transport	GO:0006820	Transport
PFC0140c	ER To Golgi Vesicle-Mediated Transport	GO:0006888	Transport
PFB0210c	Monosaccharide Transport	GO:0015749	Transport
PFL0950c	Phospholipid Transport	GO:0015914	Transport
PFI1670c	ATP Synthesis Coupled Proton Transport	GO:0015986	Transport
PF08_0113	Proton Transport	GO:0015992	Transport
PFI0240c	Metal Ion Transport	GO:0030001	Transport
PFC0245c	Protein Transport		Transport
PFE0765w	Endocytosis, Intracellular Transport, Phosphoinositide Phosphorylation, Phosphoinositide-Mediated Signaling		Transport
PFI0670w	Phosphate Transport		Transport
PF10_0262	Phosphate Transport		Transport
MAL13P1.246	Proton Transport		Transport

APPENDIX 5

The Plasmodial proteins found in only the control samples analysed with MS

Gene Id	Annotated Go Process	GO term	Cluster
PFB0205c	Biological_Process	GO:0008150	Biological Process
PFB0380c	Biological_Process	GO:0008150	Biological Process
PFB0400w	Biological_Process	GO:0008150	Biological Process
PFB0640c	Biological_Process	GO:0008150	Biological Process
PFB0745w	Biological_Process	GO:0008150	Biological Process
PF10_0037	Biological_Process	GO:0008150	Biological Process
PF10_0075	Biological_Process	GO:0008150	Biological Process
PF10_0110	Biological_Process	GO:0008150	Biological Process
PF10_0140	Biological_Process	GO:0008150	Biological Process
PF10_0173	Biological_Process	GO:0008150	Biological Process
PF11_0333	Biological_Process	GO:0008150	Biological Process
PF11_0384	Biological_Process	GO:0008150	Biological Process
PF11_0420	Biological_Process	GO:0008150	Biological Process
PF11_0435	Biological_Process	GO:0008150	Biological Process
PFL0130c	Biological_Process	GO:0008150	Biological Process
PFL0880c	Biological_Process	GO:0008150	Biological Process
PFL1240c	Biological_Process	GO:0008150	Biological Process
PFL1395c	Biological_Process	GO:0008150	Biological Process
PFL1800w	Biological_Process	GO:0008150	Biological Process
PFL1815c	Biological_Process	GO:0008150	Biological Process
PFL1980c	Biological_Process	GO:0008150	Biological Process
PF14_0245	Biological_Process	GO:0008150	Biological Process
PF14_0329	Biological_Process	GO:0008150	Biological Process
PF14_0404	Biological_Process	GO:0008150	Biological Process
PF14_0515	Biological_Process	GO:0008150	Biological Process
PF14_0543	Biological_Process	GO:0008150	Biological Process
PF14_0654	Biological_Process	GO:0008150	Biological Process
PF14_0708	Biological_Process	GO:0008150	Biological Process
PF14_0714	Biological_Process	GO:0008150	Biological Process
MAL13P1.324	Metabolic Process	GO:0008152	Biological Process
PFD0880w	Proteasome Assembly		Biological Process
PF11_0053	Chromatin Remodeling	GO:0006338	DNA Metabolism
PFD0685c	Chromosome Organization	GO:0007001	DNA Metabolism
PF11_0061	Chromosome Organization	GO:0007001	DNA Metabolism
MAL13P1.22	DNA Ligation	GO:0006266	DNA Metabolism
PF11_0249	DNA Metabolic Process	GO:0006259	DNA Metabolism
PFI0510c	DNA Repair	GO:0006281	DNA Metabolism
PFB0895c	DNA Replication	GO:0006260	DNA Metabolism
PF10_0154	DNA Replication	GO:0006260	DNA Metabolism
PFL2005w	DNA Replication	GO:0006260	DNA Metabolism
PFF0285c	Double-Strand Break Repair	GO:0006302	DNA Metabolism
PFL2440w	Nucleotide-Excision Repair	GO:0006289	DNA Metabolism
PFD0795w	DNA Repair, Chromatin Modification, Response To DNA Damage Stimulus		DNA Metabolism
PFA0665w	Pathogenesis	GO:0009405	Host Parasite

			Interaction
PFC0005w	Pathogenesis	GO:0009405	Host Parasite Interaction
MAL8P1.220	Pathogenesis	GO:0009405	Host Parasite Interaction
PFD0005w	Rosetting	GO:0020013	Host Parasite Interaction
PFF0845c	Rosetting	GO:0020013	Host Parasite Interaction
PF11_0521	Rosetting	GO:0020013	Host Parasite Interaction
PFL1950w	Rosetting	GO:0020013	Host Parasite Interaction
PFL1960w	Rosetting	GO:0020014	Host Parasite Interaction
PF14_0101	Cell Adhesion		Host Parasite Interaction
PF14_0664	Fatty Acid Biosynthetic Process	GO:0006633	Lipid Metabolism
PF14_0250	Lipid Metabolic Process	GO:0006629	Lipid Metabolism
PFF0410w	Lipid A Biosynthetic Process, Lipid Biosynthetic Process		Lipid Metabolism
PFA0380w	Protein Amino Acid Phosphorylation	GO:0006468	Phosphorylation
PFF1145c	Protein Amino Acid Phosphorylation	GO:0006468	Phosphorylation
PF14_0392	Protein Amino Acid Phosphorylation	GO:0006468	Phosphorylation
PF14_0408	Protein Amino Acid Phosphorylation	GO:0006468	Phosphorylation
PFB0755w	Protein Amino Acid Phosphorylation		Phosphorylation
PFC0560c	Intracellular Signaling Pathway, Protein Amino Acid Phosphorylation		Phosphorylation
PF10_0363	Glycolysis	GO:0006096	Primary Metabolism
PF11_0416	Actin Filament-Based Movement	GO:0030048	Primary Metabolism
PFI1590c	Apoptosis	GO:0006915	Primary Metabolism
PFL1725w	ATP Biosynthetic Process	GO:0006754	Primary Metabolism
PF08_0132	Glutamate Metabolic Process	GO:0006536	Primary Metabolism
PFC0275w	Glycerophosphate Shuttle	GO:0006127	Primary Metabolism
PF10_0026	Mo-Molybdopterin Cofactor Biosynthetic Process	GO:0006777	Primary Metabolism
PFC1030w	Regulation Of Rab Gtpase Activity	GO:0032313	Primary Metabolism
PFL0575w	Thiamin Biosynthetic Process	GO:0009228	Primary Metabolism
PF07_0120	Allantoin Catabolic Process, Purine Base Metabolic Process		Primary Metabolism
PFL0975w	Cell Cycle, Cell Division, Mitosis		Primary Metabolism
PFC0975c	Protein Folding	GO:0006457	Protein Folding
MAL8P1.204	Protein Folding	GO:0006457	Protein Folding
PFI0935w	Protein Folding	GO:0006457	Protein Folding
PFL0055c	Protein Folding	GO:0006457	Protein Folding
PF11_0433	Protein Folding		Protein Folding
PF14_0147	ATP-Dependent Proteolysis	GO:0006510	Proteolysis
PF14_0616	Protein Catabolic Process, Proteolysis	GO:0030163	Proteolysis
PF14_0063	Protein Metabolic Process	GO:0019538	Proteolysis
PFB0355c	Proteolysis	GO:0006508	Proteolysis
PF14_0160	Proteolysis	GO:0006508	Proteolysis
PF11_0201	Ubiquitin Cycle	GO:0006512	Proteolysis
PFI1545c	Ubiquitin-Dependent Protein Catabolic Process	GO:0006511	Proteolysis

PFC0590c	ER-Associated Protein Catabolic Process, Regulation Of Cell Cycle Process		Proteolysis
PFE0395c	Attachment Of GPI Anchor To Protein		Proteolysis
PFE1155c	Proteolysis		Proteolysis
PFE0715w	Aspartyl-Trna Aminoacylation	GO:0006422	RNA Metabolic Process
PF14_0231	Ribosome Biogenesis And Assembly	GO:0042254	RNA Metabolic Process
PFD0265w	RNA Splicing	GO:0008380	RNA Metabolic Process
PFB0715w	Transcription	GO:0006350	RNA Metabolic Process
PFE0870w	Transcription	GO:0006350	RNA Metabolic Process
PF11_0264	Transcription	GO:0006350	RNA Metabolic Process
PF14_0695	Transcription, DNA-Dependent	GO:0006351	RNA Metabolic Process
PFL1210w	Trna Aminoacylation For Protein Translation, Translation	GO:0006418	RNA Metabolic Process
PF11_0282	Trna Metabolic Process	GO:0006399	RNA Metabolic Process
PFD0555c	ATP Biosynthetic Process, Trna Modification, Translation		RNA Metabolic Process
PF07_0012	Transcription, DNA-Dependent		RNA Metabolic Process
PF11_0279	Mrna Processing, Mrna Transport, Regulation Of Translation		RNA Metabolic Process
PFL1085w	Regulation Of Transcription, DNA-Dependent		RNA Metabolic Process
PF13_0097	Regulation Of Transcription, DNA-Dependent		RNA Metabolic Process
PF14_0550	Regulation Of Transcription, DNA-Dependent, Transcription		RNA Metabolic Process
MAL7P1.108	Cell Communication	GO:0007154	Signal Transduction
PFA0335w	Small Gtpase Mediated Signal Transduction	GO:0007264	Signal Transduction
PFD0810w	Small Gtpase Mediated Signal Transduction	GO:0007264	Signal Transduction
PF13_0119	Small Gtpase Mediated Signal Transduction	GO:0007264	Signal Transduction
PFE0850c	Translation	GO:0006412	Translation
PF07_0088	Translation	GO:0006412	Translation
PF14_0240	Translation	GO:0006412	Translation
PFC0225c	Translational Elongation	GO:0006414	Translation
PFL0210c	Translational Initiation	GO:0006413	Translation
PF11_0480	Regulation Of Gene Expression, Translation, Translational Initiation		Translation
PFE0195w	Cation Transport	GO:0006812	Transport
MAL7P1.202	Intracellular Protein Transport	GO:0006886	Transport
PFL0885w	Intracellular Protein Transport	GO:0006886	Transport
PF14_0455	Multidrug Transport	GO:0006855	Transport
PF14_0361	Protein Transport	GO:0015031	Transport
PFC0725c	Transport	GO:0006810	Transport
PFE1400c	Vesicle-Mediated Transport	GO:0016192	Transport
PFF0165c	Vesicle-Mediated Transport	GO:0016192	Transport

PFF0830w	Vesicle-Mediated Transport	GO:0016192	Transport
PFC0435w	Phosphate Transport		Transport
PFF0655c	Intracellular Protein Transport, Vesicle-Mediated Transport		Transport
MAL8P1.123	Endocytosis, Intracellular Protein Transport, Protein Complex Assembly		Transport
PFI0210c	Intracellular Receptor Mediated Signaling Pathway, Intracellular Transport		Transport